

DOTTORATO DI RICERCA IN CHIMICA INDUSTRIALE

Ciclo XXV

**Settore Concorsuale di afferenza:** 03/B2

**Settore Scientifico disciplinare:** CHIM/07

***Novel etheroatom containing aliphatic polyesters  
for biomedical and environmental applications***

Presentata da: Matteo Gigli

Coordinatore Dottorato:  
Chiar.mo Prof. Fabrizio Cavani

Relatore:  
Chiar.ma Prof.ssa Nadia Lotti  
Correlatore:  
Chiar.mo Prof. Andrea Munari

## Abstract

Biodegradable polymers for short time applications have attracted much interest all over the world. The reason behind this growing interest is the incompatibility of the polymeric wastes with the environment where they are disposed after usage. Synthetic aliphatic polyesters represent one of the most economically competitive biodegradable polymers. In addition, they gained considerable attention as they combine biodegradability and biocompatibility with interesting physical and chemical properties.

In this framework, the present research work focused on the modification by reactive blending and polycondensation of two different aliphatic polyesters, namely poly(butylene succinate) (PBS) and poly(butylene 1,4-cyclohexanedicarboxylate) (PBCE). Both are characterized by good thermal properties, but their mechanical characteristics do not fit the requirements for applications in which high flexibility is requested and, moreover, both show slow biodegradation rate. With the aim of developing new materials with improved characteristics with respect to the parent homopolymers, novel etheroatom containing PBS and PBCE-based fully aliphatic polyesters and copolyesters have been therefore synthesized and carefully characterized.

The introduction of oxygen or sulphur atoms along the polymer chains, by acting on chemical composition or molecular architecture, tailored solid-state properties and biodegradation rate: type and amount of comonomeric units and sequence distribution deeply affected the material final properties owing, among all, to the hydrophobic/hydrophilic ratio and to the different ability of the polymer to crystallize.

The versatility of the synthesized copolymers has been well proved: as a matter of fact these polymers can be exploited both for biomedical and ecological applications.

Feasibility of 3D electrospun scaffolds has been investigated, biocompatibility studies and controlled release of a model molecule showed good responses. As regards ecological applications, barrier properties and eco-toxicological assessments have been conducted with outstanding results. Finally, the ability of the novel polyesters to undergo both hydrolytic and enzymatic degradation has been demonstrated under physiological and environmental conditions.

# Table of Contents

<b>1. Introduction</b>	<b>1</b>
1.1 Aliphatic polyesters	5
1.1.1 Synthesis	6
1.1.1.1 Polycondensation	7
1.1.1.2 Ring-opening polymerization	12
1.1.2 Blending	15
1.1.2.1 Reactive blending	18
1.1.3 Physical properties	19
1.1.4 Degradation	20
1.1.4.1 Chemical hydrolysis	21
1.1.4.2 Enzymatic hydrolysis	23
1.1.4.3 Factors influencing hydrolysis	24
1.2 Copolymers	26
1.2.1 Random copolymers	27
1.2.2 Block copolymers	30
1.3 Biomedical applications	32
1.3.1 Tissue engineering	33
1.3.1.1 Electrospinning	37
1.3.2 Controlled drug release	39
1.3.3 Polymers used in biomedical applications	44
1.4 Environmental applications	47
1.4.1 Packaging	49
1.4.1.1 Starch-based polymers	51
1.4.1.2 Polyesters	51
1.4.2 Agricultural applications	55
<b>2. Aim of the work</b>	<b>59</b>
<b>3. Materials and Methods</b>	<b>63</b>
3.1 Materials	64
3.2 Synthesis of homopolymers	64
3.3 Synthesis of copolymers	66
3.3.1 Polycondensation	66

3.3.2	Reactive blending	67
3.4	Film preparation	69
3.5	Scaffold fabrication	69
3.6	Molecular characterization	70
3.6.1	Nuclear magnetic resonance (NMR)	70
3.6.2	Gel permeation chromatography (GPC)	71
3.7	Thermal characterization	71
3.7.1	Thermogravimetric analysis (TGA)	71
3.7.2	Differential scanning calorimetry (DSC)	72
3.8	Wide-angle X-ray measurements (WAXD)	72
3.9	Mechanical characterization	73
3.10	Surface wettability	73
3.11	Hydrolytic degradation tests	73
3.12	Enzymatic degradation tests	73
3.12.1	Opacity assay	74
3.12.2	Attenuated total reflectance infrared spectroscopy (ATRIR)	75
3.13	Soil burial experiments	75
3.14	Composting	76
3.15	Film/scaffold weight loss analyses	76
3.16	Scanning electron microscopy (SEM)	76
3.17	Barrier properties evaluation	77
3.18	Ecotoxicity assessment	77
3.19	Biocompatibility evaluation	78
3.19.1	P(BCEmBDGn) biocompatibility studies	78
3.19.1.1	Cell culture	78
3.19.1.2	Cell viability to materials	79
3.19.1.3	Confocal Laser Scanning Microscopy (CLSM)	79
3.19.2	P(BCEmTECEn) biocompatibility studies	79
3.19.2.1	Cell culture	79
3.19.2.2	MTT assay	80
3.19.3	PBS and P(BS80BDG20) biocompatibility studies	80
3.19.3.1	Cell culture	80
3.19.3.2	Cell Viability Assay	80
3.20	<i>In vitro</i> FITC release experiment	80
<b>4.</b>	<b>Results and discussion</b>	<b>83</b>

4.1 Enzymatic hydrolysis studies on $PBS_mPDGS_n$ and $PBS_mPTDGS_n$ block copolymers	84
4.1.1 Synthesis and characterization of the polymers	84
4.1.2 Screening of the degrading hydrolytic enzymes	88
4.1.3 Optimization and selection of the biodegradation test conditions	89
4.1.4 Biodegradation studies	90
4.1.5 Conclusions	97
4.2 Environmentally friendly PBS-based copolyesters containing PEG-like subunit: effect of block length on solid-state properties and enzymatic degradation	97
4.2.1 Synthesis and molecular characterization of the polymers	98
4.2.2 Thermal properties and crystallization ability	100
4.2.3 Mechanical characterization and wettability behaviour	107
4.2.3 Enzymatic degradation	109
4.2.4 Comparison between PBSTES and PBSPDGS copolymers	113
4.2.5 Conclusions	114
4.3 Synthesis and characterization of novel PBS-based copolyesters designed as potential candidates for soft tissue engineering	115
4.3.1 PBS and PBDG homopolymers characterization	115
4.3.2 PBSPBDGt copolymers synthesis and molecular characterization	117
4.3.3 PBSPBDGt copolymers thermal characterization	120
4.3.4 PBSPBDGt copolymers mechanical characterization	129
4.3.4 Conclusions	130
4.4 Macromolecular design of novel sulphur-containing copolyesters with promising mechanical properties for soft tissue engineering	131
4.4.1 PBTDG homopolymer characterization	131
4.4.2 Solution cast blends	132
4.4.3 PBSPBTDGt block copolymer synthesis and molecular characterization	134
4.4.4 PBSPBTDGt copolymers thermal characterization	137
4.4.5 PBSPBTDGt copolymers mechanical characterization	143
4.4.6 Electrospinning of PBSPBDG and PBSPBTDG copolymers	145
4.4.7 Hydrolytic degradation	147
4.4.8 Cell morphology and viability	152

4.5 Novel random copolyesters of poly(butylene succinate) containing ether-linkages	154
4.5.1 P(BSxBDGy) synthesis and molecular characterization	154
4.5.2 P(BSxBDGy) thermal characterization	155
4.5.3 P(BSxBDGy) copolymers mechanical characterization	163
4.5.4 Electrospinning of PBS and P(BS80BDG20)	164
4.5.5 Characterization of PBS and P(BS80BDG20) scaffolds	165
4.5.6 Hydrolytic degradation	167
4.5.7 Biocompatibility assay	169
4.6 Random copolyesters based on poly(butylene 1,4-cyclohexanedicarboxylate) containing ether-oxygen atoms	170
4.6.1 Synthesis, molecular and thermal characterization	171
4.6.2 Mechanical characterization	181
4.6.3 Barrier properties	182
4.6.4 Enzymatic and hydrolytic degradation studies	185
4.6.5 <i>In vitro</i> fluorescein isothiocyanate (FITC) release	189
4.6.6 Biocompatibility assay	191
4.7 Random PBCE-based copolyesters containing PEG-like subunit	194
4.7.1 Synthesis, molecular and thermal characterization	194
4.7.2 Mechanical characterization	201
4.7.3 Barrier properties	202
4.7.4 Soil burial and composting studies	205
4.7.5 Ecotoxicity assessment	207
4.7.6 Electrospinning of P(BCEmTECEn) copolymers	208
4.7.7 Hydrolytic degradation	209
4.7.8 Biocompatibility	210
<b>5. Conclusions</b>	<b>213</b>
<b>References</b>	<b>a</b>
<b>Publications</b>	<b>g</b>
<b>Scientific contributions to national and international congresses</b>	<b>h</b>

## List of Abbreviations

2-CE: 2-chloroethane

$A_c$ : crystalline area of the diffraction pattern

$A_i$ : initial activity

$A_t$ : total area of the diffraction profile

ATRIR: attenuated total reflectance infrared spectroscopy

$b$ : degree of randomness

BD: 1,4-butanediol

BL:  $\gamma$ -butyrolactone

CI: crystallinity index

CL:  $\epsilon$ -caprolactone

CLSM: confocal laser scanning microscopy

$D$ : diffusion coefficient

$D$ : distance between collector plate and syringe in the electrospinning apparatus

DCM: dichloromethane

DDS: drug delivery system

DEG: diethylene glycol

DGA: diglycolic acid

DMAC: dimethylacetamide

DMCED: dimethylcyclohexane-1,4-dicarboxylate

DMEM: dulbecco's modified eagle medium

DMS: dimethylsuccinate

$DP_n$  : number average polymerization degree

$DP_w$ : weight average polymerization degree

DSC: differential scanning calorimetry

ECM: extracellular matrix

EEE: electrical and electronic equipment

ES: electrospinning; electrospun

FBS: fetal bovine serum

FITC: fluorescein isothiocyanate

GA: glycolic acid

GI: germination index

GPC: gel permeation chromatography

GTR: gas transmission rate

HEPES: 4-(2-hydroxyethyl)-1-piperazineethanesulfonic acid

HFIP: hexafluoro-2-propanol

$k$ : kinetic constant

$K_C$ : equilibrium constant of condensation

LA: lactic acid

LDPE: low density polyethylene

LLA: L,L-dilactide

MD: microdomains

$M_n$ : average number molecular weight

MTT: 3-(4,5-dimethylthiazole-2-yl)-2,5-diphenyl tetrazolium bromide

$M_w$ : average mass molecular weight

$n_i$ : molar fraction

NMR: nuclear magnetic resonance

PA: polyamide

PBCE: poly(butylene cyclohexanedicarboxylate)

P(BCE<sub>x</sub>BDG<sub>y</sub>): poly(butylene cyclohexanedicarboxylate/diglycolate)s

P(BCE<sub>x</sub>TECE<sub>y</sub>): poly(butylene/triethylene cyclohexanedicarboxylate)s

PBDG: poly(butylene diglycolate)

PBS: poly(butylene succinate)

PBSA: poly(butylene succinate/adipate)

P(BS<sub>x</sub>BDG<sub>y</sub>): poly(butylene succinate/diglycolate)s

PBT: poly(butylene terephthalate)  
PBTDG: poly(butylene thiodiglicolate)  
PCL: poly( $\epsilon$ -caprolactone)  
PDGS: poly(diethyleneglycol succinate)  
PDI: polydispersity index  
PDLA: poly(D-lactic acid)  
PDLLA: poly(D,L-lactic acid)  
PE: polyethylene  
PEG: poly(ethylene glycol)  
PET: poly(ethylene terephthalate)  
PGA: poly(glycolic acid)  
PHAs: polyhydroxyalkanoates  
PHB: poly(3-hydroxybutyrate)  
PLA: poly (lactic acid)  
PLGA: poly(lactide-*co*-glycolide)  
PLLA: poly(L-lactic acid)  
PP: polypropylene  
PS: polystyrene  
PTDGS: poly(thiodiethyleneglycol succinate)  
PTECE: poly(triethyleneglycol cyclohexanedicarboxylate)  
PTES: poly(triethyleneglycol succinate)  
PVC: polyvinylchloride  
 $R_{\text{diff}}$ : solvent (or drug) diffusion rate  
 $R_p$ : polyesterification rate  
 $R_{\text{relax}}$ : polymer chain relaxation rate  
RH: relative humidity  
ROP: ring-opening polymerization  
S: solubility

SEM: scanning electron microscopy  
TDEG: thiodiethylene glycol  
TDGA: thiodiglycolic acid  
TEG: triethylene glycol  
TFE: 2,2,2-trifluoroethanol  
TGA: thermogravimetric analysis  
TRITC: tetramethylrhodamine isothiocyanate  
 $T_{5\%}$ : temperature corresponding to 5% weight loss  
 $T_c$ : crystallization temperature  
 $T_{cc}$ : cold crystallization temperature  
 $T_g$ : glass transition temperature  
 $T_m$ : melting temperature  
 $T_{max}$ : max weight loss rate temperature  
TMS: tetramethylsilane  
 $t_L$ : time lag  
 $T_{ODT}$ : order-disorder transition temperature  
WAXD: wide angle X-ray diffraction  
WCA: water contact angle  
 $w_i$ : weight fraction  
 $X_c$ : crystallinity degree  
 $\Delta C_p$ : specific heat increment  
 $\Delta H_c$ : heat of crystallization  
 $\Delta H_m$ : heat of fusion  
 $\rho$ : density

1.

Introduction

Over the last 60 years, plastics have brought economic, environmental and social advantages; synthetic polymeric materials have found wide applications in every aspect of life and industries. This success is mainly due to their low cost, their reproducibility, and their resistance to physical aging and biological attacks (Vert, 2005).

In 2011, around 280 Mt of plastics have been produced worldwide (Figure 1.1), but within a short period of time almost half of them are disposed to the environment.

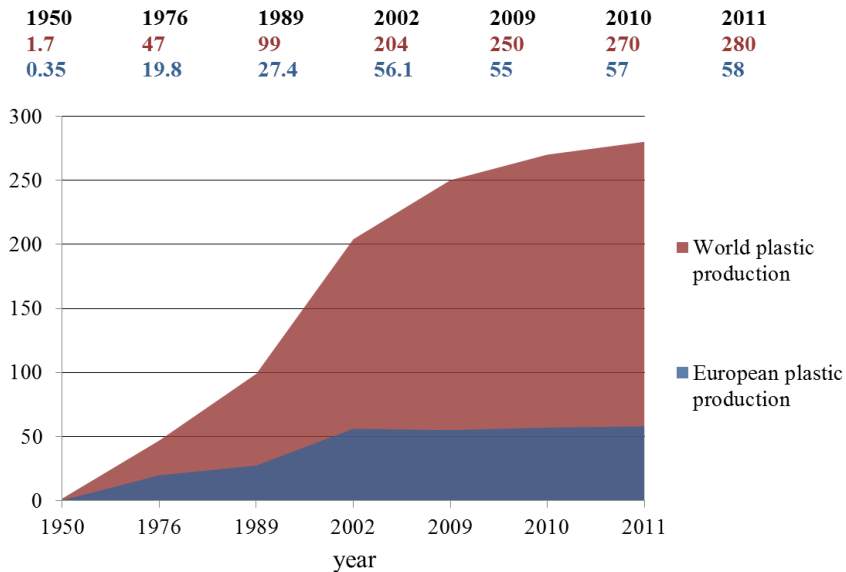


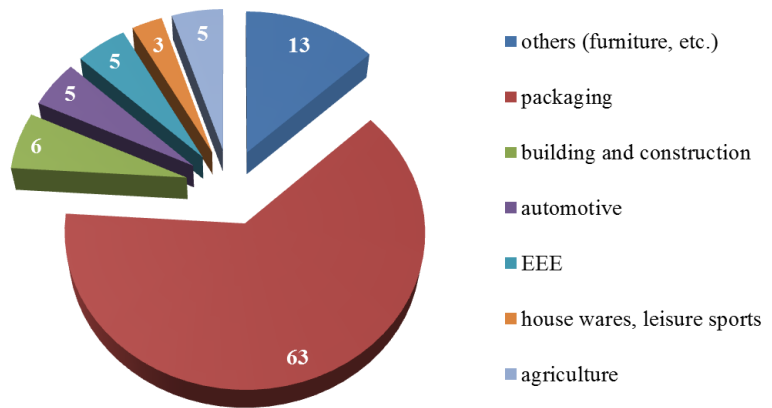
**Figure 1.1**  
Worldwide plastic production 1950-2011 (source: Plastics Europe).

Only in Europe, over 25 Mt of plastics ended up in the waste stream during 2011 (PlasticsEurope).

The main sources of plastic waste are typically the fields which represent the highest plastic consumption. Figure 1.2 shows the contribution of the different sectors to the plastic waste stream in the EU-27, Norway and Switzerland in 2008. Packaging is the largest contributor to plastic waste at 63%, well ahead of “Others” (13%), which includes furniture, medical waste, etc. The remaining sectors include: automotive (5%), electrical and electronic equipment (EEE, 5%), building & construction (6%) and agriculture (5%). In this framework, the resistance of synthetic polymers to the degrading action of living systems is becoming highly problematic particularly in those domains where they are used for a limited period of time before becoming wastes. It is the case in surgery, in pharmacology, in agriculture, and in the packaging as well. In these fields, time-resistant polymeric wastes are no longer acceptable. The use of polymeric materials satisfying the conditions of biodegradability, biocompatibility and release of low-toxicity degradation

products, as an alternative to conventional non-biodegradable ones, is therefore clear (Tserki *et al.*, 2006).

**Figure 1.2**  
Proportions of post-consumer plastic waste in EU-27, Norway and Switzerland by application, 2008 (source: BioIntelligence Service).



Today, a fast-growing industrial and academic competition is established for the production of a great variety of controlled life span materials; optimally designed compounds must be resistant during their use and must have biodegradable properties at the end of their useful life (Lucas *et al.*, 2008).

Biodegradable plastics can be broadly divided into different categories based on the origin of the raw materials (petroleum-based or renewable, Figure 1.3) and on the processes used in their manufacture.

Four main routes have been identified for the design of biodegradable polymers.

The easiest route is to use cheap synthetic polymers and add a biodegradable or photooxidizable component. A more expensive solution is to change the chemical structure by introducing hydrolysable or oxidizable groups in the main chain of non-degradable synthetic polymers. The third way to degradable polymers is to use biopolymers, such as starch, chitosan, chitin or their derivatives, and last, but not least, is to tailor new hydrolysable structures such as polyesters, polyanhydrides, polyurethanes, polyamides and polyureas (Luckachan & Pillai, 2011).

The use of renewable resources in the polymer synthesis is currently being actively researched, mainly because they can complement the limited amount of fossil fuels to some degree, but if the quantity of oil on Earth is finite, renewable resources are not limitless either. On one hand, they must grow again and on the other hand, wheat, corn, sugar cane and rice are first and foremost foodstuffs.

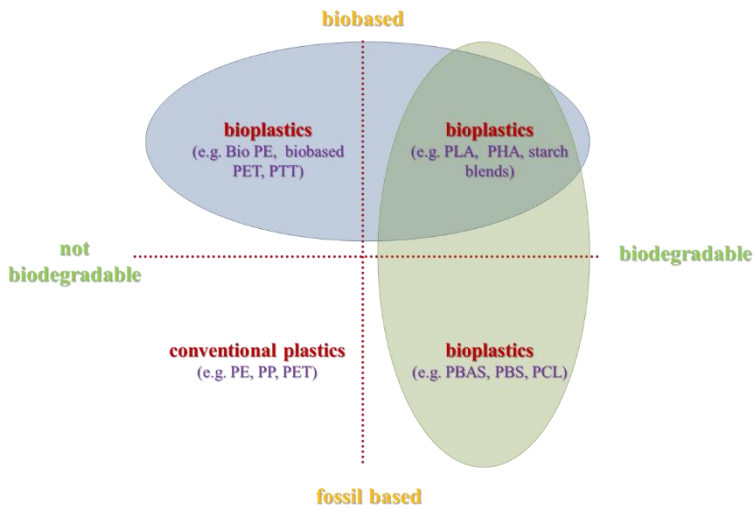


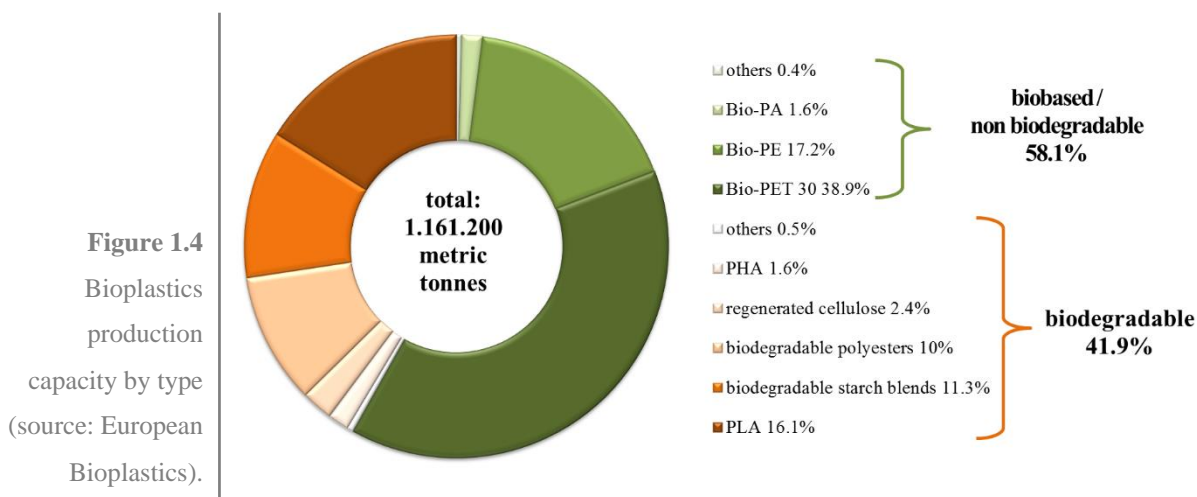
**Figure 1.3**  
Bioplastics categories (source: European Bioplastics).

Life cycle assessments (LCAs) must be evaluated very carefully and many aspects must be taken into consideration; a biomass based product is not per se ecologically more efficient than a petrochemical-based one. As an example, if large amount of forest must be cleared or processes that consume high quantities of energy are needed to refine the biomass, the ecological benefit can easily be reversed. On the economic side, the costs for growing and refining the biomass have to be compared with the price of oil, which is a crucial factor in this respect: bioplastics become more competitive if the price of oil increases, even though the cost of bioplastic production itself is also linked to the oil price (Baker & Safford, 2009).

Taking all these considerations into due account, aliphatic polyesters are therefore expected to be one of the most economically competitive biodegradable polymers (Tserki *et al.*, 2006). In addition, they have attracted considerable attention as they combine the features of biodegradability and biocompatibility with physical and chemical properties comparable with some of the most extensively used polymers, like LDPE, PP, etc.

It is also worth remembering that some of the commonly used monomers for the production of aliphatic polyesters, such as succinic acid, adipic acid, 1,3-propanediol, 1,4-butanediol, lactic acid and  $\gamma$ -butyrolactone can be either obtained from fossil fuels and from renewable resources (Luckachan & Pillai, 2011). Unfortunately, the degradable polymers available up to now usually don't possess optimal physic-mechanical properties and most of them are still very expensive and technically difficult to process. As a result, many attempts are necessary to solve these issues through appropriate modification of their structure.

In this view, copolymerization probably represents the most interesting tool for tailoring materials which display the right combination of properties for the desired application. Moreover, copolymerization permits to prepare novel materials possessing unique properties in that they combine the inherent nature of the parent homopolymers, improving their non-suitable characteristics without compromising those already satisfying. Finally, through this strategy, it is possible to synthesize a new class of polymers with a broad range of properties just varying the mutual amount of the comonomeric units.

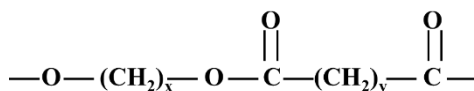


In conclusion, even if the global market is currently dominated by conventional plastics, the challenge is to widen the range of biodegradable polymer types and possible applications so that they become functionally equivalent to petroplastics. Indeed, according to European Bioplastics, the global production capacity of bioplastics will increase from 1.1 Mt in 2011 (Figure 1.4) to 5.8 Mt in 2016, probably not only due to the intense academic and industrial research, but also to the growing interest of governments and public opinion on this crucial topic.

## 1.1 Aliphatic polyesters

The aliphatic polyesters are a class of polymers which contain the ester functional group along the main chain (Figure 1.5).

**Figure 1.5**  
Chemical structure of linear aliphatic polyesters.



Linear polyesters were first synthesized by Carothers and coworkers in the early 1930s. Their pioneering studies on polycondensation (including polyesterification) which were commenced at DuPont in 1928, established a firm base for systematic studies of mechanisms of aliphatic polyester formation (Mark & Whitby, 1940). In particular, these included proof of the high molecular weight nature of the polyesterification products, determination of the so called Carothers equation relating the conversion degree of functional groups with the number average degree of polymerization of the resulting linear polyester, and the importance of ring-chain equilibria in the polyester synthesis.

Further studies by Flory (a former assistant of Carothers) at Cornell University (Flory, 1936, 1939, 1942, 1953) led to the development of the principles of kinetics of polyesterification and of polyester molar mass distribution. Some properties of the aliphatic polyesters, such as hydrolytic instability, low melting temperatures, and solubility in common organic solvents were considered at that time as being detrimental from the practical applications point of view, and this led to a delay in further studies on the synthesis of these polymers.

More recently, as the environmental concerns together with the necessity of controlled life span materials are attracting growing interest, aliphatic polyesters are spotlighted because of their peculiar biodegradability; indeed their application as both biomedical and commodity degradable materials is being intensively studied. Effective techniques have been developed to produce high molecular weight polyesters applicable for practical purposes and aliphatic polyesters such as poly(butylene succinate) (PBS), poly(butylene succinate/adipate) (PBSA) and poly(lactic acid) (PLA) have been commercialized as biodegradable plastics (Okada, 2002).

### 1.1.1 Synthesis

Aliphatic polyesters are synthesized by the polycondensation of difunctional monomers such as the self-condensation of hydroxy acids, diacids with diols, diacid chlorides with diols or by the ester interchange reaction of diesters and diols, or by ring-opening polymerization (ROP) of lactones and lactides (Nair & Laurencin, 2007).

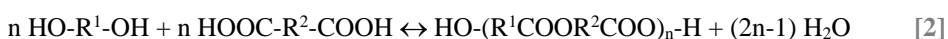
The early studies of polycondensation revealed the formation, in addition to the desired high molar mass linear polymers, also of low molar mass cyclic side products. Some of these, for example  $\epsilon$ -caprolactone, were then isolated, purified, and used by Carothers (Van Natta *et al.*, 1934) as monomers in the ROP, eventually providing linear aliphatic polyesters. However, it was necessary to wait for another 40 years before the methods of controlled polymerization of cyclic esters were elaborated.

Nowadays, commercially available biodegradable polyesters are produced by both these methods. Polycondensation can be applicable for a variety of combinations of diols and diacids, but it requires, in general, higher temperature, longer reaction time and removal of reaction byproducts to obtain high molecular weight polymers. In addition, polymers obtained do not have controlled chain lengths and polydispersity index (PDI) is usually around two. In contrast, ring-opening polymerization has a restriction on monomers, but it can be carried out under milder conditions to produce high molecular weight polymers in shorter time. Furthermore, recent progress in catalyst and initiators for living polymerization has enabled us to gain polyesters of controlled chain lengths (Okada, 2002).

Recently, the use of enzymes as catalysts in organic syntheses has been deeply investigated. In general, enzymatic reactions can be carried out under moderate conditions. More important, enzymes can easily realize high regiospecificity as well as high stereospecificity that conventional catalysts never achieve (Okada, 2002). For polymer synthesis, *in vitro* enzyme-catalyzed polymerization has been developed as an effective method to synthesize environmentally benign polymers. Lipases catalyze the ring-opening polymerization of lactones (small to large rings) and cyclic diesters (lactides) to produce polyesters. The condensation polymerization of hydroxy acid and diacids with diols is also catalyzed by lipase. Lipase catalyzed polymerization is an eco-friendly technique for the preparation of useful polyesters by polycondensation as well as polyaddition (ring-opening) reactions (Varma *et al.*, 2005; Albertsson, 2008; Gross *et al.*, 2010).

#### 1.1.1.1 Polycondensation

Polycondensation is still the major technological method of production of the aliphatic-aromatic polyesters, such as poly(alkylene terephthalate)s, but some fully aliphatic polyesters, such as PBS or PBSA (under the trade name BIONOLLE®), are industrially synthesized at large scale by polycondensation too. Moreover, this synthetic route is used in the alternative method of polylactic acid (PLA) industrial production. Therefore, polycondensation as a method of synthesis of aliphatic polyesters is not only of historical importance. Polyesterification may be based on homo-polycondensation of hydroxycarboxylic acid (Eqn. [1]) or hetero-polycondensation of a diol with a dicarboxylic acid (Eqn. [2]):



where R, R<sup>1</sup>, and R<sup>2</sup> denote alkylene groups. This is a reversible process, and in order to prepare a high molar mass polymer the equilibrium constant of condensation ( $K_C$ ) has to

be high enough. If, as is generally the case for polycondensation of alcohols with carboxylic acids, the equilibrium constant is not sufficiently high (typically  $K_C \leq 10$ ), the condensation side products (usually water) must be removed from the reaction mixture in order to obtain a reasonably high degree of polymerization.

The number average degree of polymerization ( $DP_n$ ) is related to  $K_C$  by a simple equation, which can be derived starting from the expression defining  $K_C$ :

$$DP_n = K_C^{0.5} + 1 \quad [3]$$

Since  $K_C \approx 10$  for a majority of condensations of simple aliphatic alcohols with carboxylic acids, the number average degree of polymerization  $DP_n \approx 4$  would result in the equilibrium polymerization. On the other hand:

$$DP_n = 1 / (1 - p) \quad [4]$$

where  $p$  is a degree of conversion of the reactive groups (Carothers, 1936). This means that for  $K_C = 10$ , only 76% of hydroxyl and carboxylic group would react until an equilibrium is reached. For majority of polyesters,  $DP_n \geq 100$  is needed in order to obtain the required physical properties; this corresponds to degree of conversion not less than 0.99 and in turn would require  $K_C \geq 10^4$ .  $K_C$  of this level are observed when acid chlorides (Schotten-Baumann reaction), acid anhydrides or activated carboxylic acids are used. One of the known ways of activation is based on formation of a highly reactive intermediates such as acyl derivative of imidazole (Staab, 1957), which then reacts in an almost irreversible manner (i.e., with very high  $K_C$ ) with alcohols. In this type of activation, however, for every one ester bond formed one molecule of activator must be used. Another possibility for direct, high molar mass polyester formation provides solid-state polycondensation of the pertinent  $\alpha$ -chloro- $\omega$ -sodium salt derivatives, such as in a case of the recently reported polyglycolide synthesis (Schwarz and Epple, 1999).

Shifting the equilibrium to the side of a high molar mass polyester is realized, as mentioned above, by removing from the reaction mixture the low molar mass byproduct of esterification. Eqn. [5], which is derived from Eqn. [3] by assuming  $K_C \gg 1$ , provides a dependence of the degree of polymerization on the extent of removal of the byproduct ( $q$ ):

$$DP_n = (K_C / q)^{0.5} \quad [5]$$

where  $q = N_e/N_0$ , i.e., the ratio of the concentration of the byproduct at a given equilibrium to its hypothetical concentration resulting from reactive groups conversion degree related to the required  $DP_n$ . For example, in order to prepare polyester having  $DP_n = 10^2$ , it is necessary to keep  $K_C/q$  above  $10^4$ . If  $K_C = 10$ , then  $q$  should be below  $10^{-3}$ . This means that only 0.1% of the byproduct of its “normal” equilibrium concentration is allowed to be

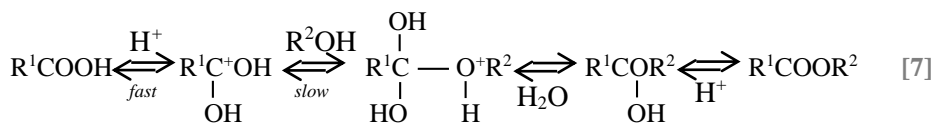
left in the reacting mixture. Such a situation creates one of the practical limitations in the syntheses of various polyesters, including PLA, directly by polycondensation. In addition, high viscosity of the system at higher degrees of conversion hampers removal of the low molar mass byproduct, such as water. Another important factor is related to the stoichiometry of the substrates. Dependence of the number average degree of polymerization of the polyester formed in hetero-polycondensation on the stoichiometric imbalance parameter  $r$  is given by Eqn. [6]:

$$DP_n = (1 + r) / (1 + r - 2p) \quad [6]$$

where  $r = N_{OH}/N_{COOH}$  for  $N_{OH} < N_{COOH}$  or  $N_{COOH}/N_{OH}$  for  $N_{OH} > N_{COOH}$  ( $N_{OH}$  and  $N_{COOH}$  stand for the concentrations of hydroxyl and carboxylic groups, respectively). Thus, for example at  $p = 0.99$ , and  $DP_n = 100$  for the exactly equimolar reacting mixture ( $r = 1$ ), it is sufficient to introduce only 1.0 mol% of imbalance ( $r = 0.99$ ) to reduce  $DP_n$  to the value of 67. Even if in the feed the 1:1 stoichiometry is secured, one of the components may be partially lost during the polycondensation process, either because of volatilization, since high reaction temperatures are often used, or reactant losses by side reactions. Therefore, even in the case of homo-polycondensation the internally supplied equimolar stoichiometry may be distorted. In order to minimize this type of difficulty, modification of polycondensation was introduced based on transesterification. At least in one known instance transesterification is at the basis of the large-scale industrial process, i.e. the two-step synthesis of poly(ethylene terephthalate).

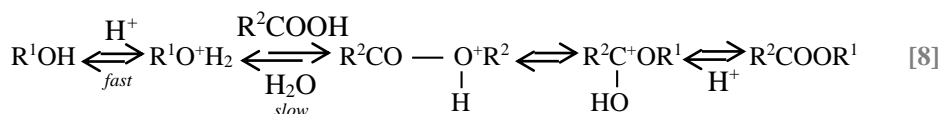
The rate of polycondensation only very seldom agrees with simple kinetic expressions throughout the entire polycondensation process. Changes in the reaction mixture properties, such as viscosity or dielectric constant, influence the course of the reaction, even if the most fundamental assumption of equal reactivities of functional groups, independently on the material chain length is obeyed. It is mostly obeyed indeed, because even if at high viscosities the “diffusion in” is slowed down, it is believed to be compensated by equally slowing down of the “diffusion out” (Rabinovitch, 1937). The major kinetic dependencies reflect basic mechanisms of esterification as formulated by C.K. Ingold (1969). For the catalyzed esterification there are two general mechanisms involving (as in ROP) either acyloxygen or alkyl-oxygen bond cleavage. Both types can be either acid- or base-catalyzed.

From the two acid-catalyzed mechanisms involving acyl-oxygen bond cleavage (namely  $S_N1$  and tetrahedral), the latter is more frequently accepted and reads schematically as follows in Eqn. [7]:



This A<sub>AC</sub>2 mechanism, known also as an addition-elimination mechanism, assumes that the rate-determining step is an alcohol addition to the protonated acid molecule.

In the acid-catalyzed mechanism, involving alkyl-oxygen bond cleavage, esterification can proceed by either S<sub>N</sub>1 (A<sub>AL</sub>1) or S<sub>N</sub>2 (A<sub>AL</sub>2) mechanisms. The latter can be visualized as follows in Eqn. [8]:



Besides simple strong protonic acids and bases being used as catalyst, covalent metal alkoxides are also used (for example, derivatives of Sn(IV) or Ti(IV)). In this case the esterification process proceeds according to the B<sub>AC</sub>2 mechanism and involves ligand exchange, as in the ROP of cyclic esters initiated with multivalent metal alkoxides. This mechanism will be discussed in chapter 1.1.1.2. The mechanisms presented above are compatible with kinetic results of polycondensation with restrictions described at the beginning of this paragraph. As indicated in the preceding section, in order to prepare a high molar mass polyester it is necessary to remove the low molar mass byproduct. Therefore, in spite of the reversibility of the elementary reactions in polyesterification, under the conditions of continuous removal of water for the noncatalyzed reaction of diol with diacid, it is possible to write the following expression for the polyesterification rate ( $R_p$ ):

$$R_p = -d[X] / dt = -d[Y] / dt = k[X][Y] = k[X]^2 \quad [9]$$

Where X and Y stand for -COOH and -OH groups, t is the polyesterification time and k the pertinent rate constant; it is also assumed that at t = 0 : [X]<sub>0</sub> = [Y]<sub>0</sub>, and also that [X] = [Y] throughout the entire kinetic measurement. Integrating this second order equation gives:

$$1/[X] + 1/[Y] = kt \quad \text{or} \quad 1/(1-p) = DP_n = kt + 1 \quad [10]$$

Usually, however, polyesterification is acid-catalyzed, either self-catalyzed or by the addition of a strong protonic acid. In the former:

$$R_p = k[X]^2[Y] = k[X]^3 \quad [11]$$

and in the integrated form:

$$1/[X] + 1/[X]_0 = k't \quad \text{or} \quad 1/(1-p) = DP_n = k't + 1 \quad [12]$$

On the other hand, if the strong protonic acid is added:

$$R_p = k[X]^2[H^+] = k' [X]^2 \quad [13]$$

and:

$$1/[X]^2 + 1/[X]_0^2 = 2kt \text{ or } 1/(1-p)^2 = DP_n^2 = 2[X]_0^2 kt + 1 \quad [14]$$

where  $k' = k[H^+]$ . The resulting equations have similar forms as for the uncatalyzed polyesterification. The only difference is that concentration of catalyst ( $[H^+]$ ), is introduced into the apparent rate constant  $k'$ .

Thus, depending on the catalysis mode, either second or third-order kinetic dependencies (Eqns. [10], [12], [14]) are expected to be linear, providing that all assumptions discussed above are fulfilled. In fact, the available experimental data typically exhibit deviation from linearity in the low conversion range, showing an acceleration effect (up to 80 – 90%, i.e. at  $DP_n = 5 - 10$ ). Flory was the first to explain this kinetic behavior by large changes of polarity during chemical conversions of the polar carboxylic acid and hydroxyl groups into the much less polar ester linkages. Also, hetero or homo-association of the reactive groups, degreasing with conversion, may be responsible for the observed acceleration effect. A slight inhibitory effect (which is sometimes seen at higher conversions) may be related to the losses if the equimolar stoichiometry between the reacting groups.

Expressions describing the molar mass distribution (or polymerization degree) of linear polyester macromolecules formed in polycondensation have been set forth by Flory (1936). The number and weight fractions ( $n_i$  and  $w_i$ , respectively) of macromolecules having a degree of polymerization equal to  $i$  at a given degree of conversion  $p$ , reads:

$$n_i = p^{i-1}(1-p) \quad [15]$$

$$w_i = ip^{i-1}(1-p)^2 \quad [16]$$

These functions are usually called the “most probable” of Flory-Schultz distributions. The number and weight average polymerization degrees ( $DP_n$  and  $DP_w$ , respectively) are given by:

$$DP_n = 1 / (1-p) \quad [17]$$

$$DP_w = (1+p) / (1-p) \quad [18]$$

and finally the polydispersity index:

$$DP_w / DP_n = 1 + p = 2 - DP_n^{-1} \quad [19]$$

Thus for the conversion ( $p = 1$ ) and the infinite molar mass  $DP_w / DP_n = 2$ . The value of this parameter is related to one of the basic differences between polyesters prepared by polycondensation or by ROP. For the latter, in which molar mass distribution is usually more narrow due to the kinetic control of the entire polymerization process,  $DP_w / DP_n$  is not much higher than 1.



systems termination can be excluded; there are, however, two well-documented chain transfer reactions, both of which are based on transesterification and take place also in polycondensation: back and/or end-to-end biting and chain transfer to foreign macromolecules followed by chain rupture.

In ROP, conducted at constant pressure, the change of enthalpy is mostly due to the monomer ring strain energy, if specific interactions monomer-polymer-solvent can be neglected (Duda & Penczek, 2002). The major contributions to the ring strain come from: deviation from the nondistorted bond angle values (e.g., for cyclic esters: 110.5° (C–C–C), 109.5° (C–O–C(O)) or 110° (O–C(O)–C)), bond stretching and/or compression, repulsion between eclipsed hydrogen atoms, and nonbonding interactions between substituents (angular, conformational, and transannular strain, respectively) (Duda & Penczek, 2002).

Moreover, polymerization of the majority of monomers is accompanied by an entropy decrease. Polymerization is permitted thermodynamically when the enthalpic contribution into free energy prevails (thus when  $\Delta H_p < 0$  and  $\Delta S_p < 0$ , the inequality  $|\Delta H_p| > -T\Delta S_p$  is required). Therefore the higher the ring strain, the lower the resulting monomer concentration at equilibrium:

$$\Delta G_p = \Delta H_p - T\Delta S_p \quad [24]$$

$$\ln[M]_{\text{eq}} = \Delta H_p / RT - \Delta S_p^\circ / R \quad [25]$$

where T is the absolute temperature and R the gas constant.

The four-membered  $\beta$ -propiolactone belongs to the most strained cyclic monomers, and its equilibrium monomer concentration is immeasurably low, namely  $\sim 10^{-10}$  mol/l at room temperature.

On the other hand, the six and seven-membered monomers, such as L,L-dilactide (LLA) and  $\epsilon$ -caprolactone (CL) have relatively high equilibrium monomer concentrations, that cannot be neglected in the practical considerations: in handling of the final polymer and in studies of polymerization, particularly at elevated temperatures.

Standard thermodynamic parameters for polymerization of LA are:  $\Delta H_p = -22.9$  kJ/mol and  $\Delta S_p = -25.0$  J/(mol K). Its equilibrium concentration appeared considerably high, particularly at elevated temperatures (at which LA is usually polymerized). Thus, for a temperature range from 80 to 133°C,  $[LA]_{\text{eq}}$  changes from 0.058 to 0.151 mol/l.  $[LA]$  in bulk equals 8.7 mol/l, and this means that almost 2 mol% of LA is left at equilibrium during its homopolymerization at 133°C. LA assumes irregular skew-boat conformation, in which two ester groups can adopt planar conformation, and has therefore a relatively high enthalpy of polymerization. This is very close to the ring strain of  $\delta$ -valerolactone

and CL, which are  $-27.4$  and  $-28.8$  kJ/mol respectively. In these compounds, strain is derived from C–H bond interactions and from distortion of the bond angles. In contrast, high ring strain in the four-membered  $\beta$ -propiolactone is mostly due to the bond angle distortions and resultant bond stretching.

In the five-membered cyclics, ring strain results almost exclusively from the conformational interactions (Duda & Penczek, 2002). It is known, however, that the five-membered esters are not strained because of the reduced number of the C–H bond oppositions, caused by the presence of the carbonyl group in the monomer ring. Indeed, for  $\gamma$ -butyrolactone (BL) we have  $\Delta H_p = 5.1$  kJ/mol and  $\Delta S_p = -65$  J/(mol K). Then,  $[\text{BL}]_{\text{eq}} \approx 3 \cdot 10^2$  mol/l, whereas the monomer concentration in bulk is equal to 13 mol/l. BL is indeed not able to give a high molar mass homopolymer, but this feature sometimes is incorrectly identified with an inability of BL to undergo the ring-opening reaction at all.

Recently, kinetics of polymerization of the 6-, 7-, 9-, 12-, 13-, 16- and 17-membered lactones, initiated with zinc 2-ethylhexanoate/butyl alcohol system have been investigated (Duda et al., 2002). The following relative rates have been measured: 2500, 330, 21, 0.9, 1, 0.9, 1, respectively (bulk polymerization,  $100^\circ\text{C}$ ). Since active species operating in polymerization of various lactones in this system are structurally identical, the order of the resulting polymerization rates is equivalent to the order of the lactones' reactivities. Comparison of the lactone ring sizes with the relative polymerization rates shows that the larger the lactone ring, the lower is its reactivity. It can be expected that in the transition state of propagation the ring strain is partially released and the resulting enthalpy of activation ( $\Delta H_p^\ddagger$ ) is lower for strained monomers in comparison with the nonstrained ones. This is most likely the main reason why the reactivity of lactones decreases as their size increased, with a constant value eventually being reached for larger rings. Other factors, such as electrophilicity of the monomeracyl atom or steric hindrance, hampering approach of the active species to the lactone ester group, probably play a minor role.

A broad range of anionic, cationic and coordinative initiators or catalysts have been reported for the ROP. Generally speaking, ionic initiators are much reactive and, in case of polyesters, are responsible for detrimental inter- and intra-molecular transesterification reactions lowering the molecular weight and broadening the molecular weight distribution of the polymer. Many organometallic derivatives of metals with d-orbitals of a favorable energy, such as Al, Sn, Nd, Y, Yb, Sm, La, Fe, Zn, Zr, Ca, Ti and Mg, are imparting control to the polymerization in contrast to their anionic counterpart. In the more favorable cases, the ring-opening polymerization of lactones and lactides is a living/controlled process that leads to polyesters of narrow molecular weight distribution with a molecular

weight predetermined by the monomer-to-initiator molar ratio. The ROP proceeds mainly via two major polymerization mechanisms depending on the used organometallics. Some of them act as catalysts, and activate the monomer by complexation with the carbonyl group. Polymerization is then initiated by any nucleophile, e.g., water or alcohol, present in the polymerization medium as impurities or as compound added on purpose. In the second mechanism, the organometallic plays the role of initiator and the polymerization proceeds through an ‘insertion–coordination’ mechanism. Metal alkoxides are typical initiators, which first coordinates the carbonyl of the monomer, followed by the cleavage of the acyl–oxygen bond of the monomer and simultaneous insertion into the metal alkoxide bond. For the time being, tin octoate and alkoxides were the most widely used organometallic mediators for the ring-opening polymerization of lactones even if novel powerful and interesting metal free catalytic systems are emerging as valuable alternatives.

Probably the most popular polymerization initiator for ROP of aliphatic polyester is tin(II) bis-(2-ethylhexanoate) also referred as tin octoate ( $\text{Sn}(\text{Oct})_2$ ). It is accepted as a food additive by the US Food and Drug Administration (FDA) and thus no purification of the polymers is needed for applications such as food packaging. In the most likely proposed polymerization mechanism,  $\text{Sn}(\text{Oct})_2$  is converted into tin alkoxide, the actual initiator, by reaction with alcohols (Eqns. [26] and [27]) or other protic impurities.



As a consequence, the polymerization involves a coordination–insertion mechanism. Again, the deliberate addition of a predetermined amount of alcohol to the polymerization medium is an effective way to control the molecular weight by the monomer-to-alcohol molar ratio. Tin octoate is also efficient in copolymerization of various lactones. Playing on the composition of such copolymers allows tailoring their properties.

High volumes of PLA are produced via ROP under the name Natureworks™ by the joint venture between Dow and Cargill in a plant built in North America with a capacity of 0.14 million tones/year, mainly for commodity market (Jerome, 2008).

### 1.1.2 Blending

The practice of blending polymers is as old as the polymer industry itself with early examples involving natural rubber.

Through the first half of the 1900s the greatest progress in the industry was in the development of a wide range of different polymers. However, by the 1970s, most of the economically convenient monomers had already been exploited, therefore over the last forty years two additional directions have evolved in the polymer industry. First is the development of significant new polymerization processes to manufacture both homopolymers and copolymers based on the monomers used much earlier. Meanwhile, a separate technique has flourished, namely polymer blending. It was gradually recognized that new, cheap monomers were less likely but rather a range of new materials could be obtained by combining different, existing polymers. While most monomers cannot be easily copolymerized to gain intermediate properties, their polymers could be economically melt blended.

There is intense commercial interest in polymer blends because of the potential opportunities for combining the attractive features of several materials into one, or improve deficient characteristics of a particular material including recycled plastics.

There are two widely useful types of polymer blends: miscible and immiscible. Miscible blends involve thermodynamic solubility and are characterized by the presence of one phase and a single glass transition temperature. Their properties can often be predicted from the composition weighted average of the properties of the individual components. On the other hand, immiscible blends are phase separated, exhibiting the glass transition temperatures and/or the melting temperatures of each blend component. Their overall performance depends on the properties of the individual components, but significantly also on the morphology of the blends and the interfacial properties between the blend phases. Performance is not easy predictable.

Only few polymer pairs form miscible blends, while most blends are immiscible and have poor physical properties compared to their components. This problem is rooted in the lack of favorable interactions between blend phases. This leads to a large interfacial tension between the components in the blend melt which makes it difficult to deform the dispersed phase of a blend during mixing and to resist phase coalescence during subsequent processing. It also leads to poor interfacial adhesion in the solid state which frequently causes premature mechanical failure, depending on the nature of the applied stress.

The key to make successful blends of this kind is the use of compatibilization to control morphology. Compatibilization is the result of a process or technique for improving blend performance by making blend components less immiscible. Compatibilized blends are characterized by the presence of a finely dispersed phase, good adhesion between blend phases, strong resistance to phase coalescence and technologically desirable properties.

Compatible blends constitute the majority of commercially important blends. The compatibility of these blends may vary widely from one system to another.

There are several methods of compatibilizing immiscible blends, such as: compatibilization by the introduction of non-reactive graft or block copolymers, non-bonding specific interactions, low molecular weight coupling agents and reactive polymers.

Suitable block and graft copolymers can be used as compatibilizer for polymer blends. A suitable block or graft copolymer contains a segment miscible with one blend component and another segment with the other blend component. The copolymer segments are not necessarily identical with the respective blend components. Significant amounts of the copolymer are expected to locate at the interface between immiscible blend phases, reducing the interfacial tension between blend components, reducing the resistance to minor phase breakup during melt mixing thus reducing the size of the dispersed phase, and stabilizing the dispersion against coalescence. The finer morphology and the increased interfacial adhesion usually result in improved physical properties.

Non-bonding specific interactions like hydrogen bonding, ion-dipole, dipole-dipole, donor-acceptor, and  $\pi$ -electron interactions are useful for enhancing the compatibility of polymer blends. Generally, however, these specific interactions are weak and high concentrations, e.g. one interacting group per repeating unit, are often required for effective compatibilization.

Addition of low molecular weight reactive compound may serve the purpose of compatibilization of polymer blends through copolymer formation.

Graft or block polymers acting as compatibilizers for polymer blends can be formed *in situ* through covalent or ionic bonding during the melt blending of suitably functionalized polymers. *In situ* reactive compatibilization has already been implemented in a number of commercial products and, in many instances, appears to be the method of choice for compatibilization.

A required reactive group can be incorporated into a polymer by:

- a. incorporation into the backbone, side chain, and at chain ends as a natural result of polymerization;
- b. copolymerization of monomers contained the desired reactive groups;
- c. chemical modification of a preformed polymer through a variety of chemical reactions.

### *1.1.2.1 Reactive blending*

In reactive blending the compatibilization of immiscible polymers is ensured by a chemical reaction initiated during the process of melt mixing.

As far as the economic aspect are concerned, reactive blending is a very cost-effective process that allows the formulation of new multiphase polymeric materials.

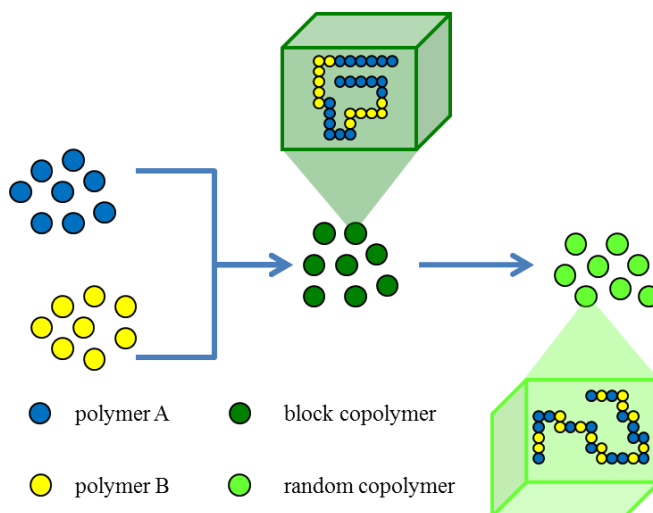
If physical blending requires an additional step for the synthesis and the design of the compatibilizing agent, reactive blending is a straightforward method.

This technique can be carried out in solution, in the melt, or even in the solid state; however, the melt processing step has several advantages. First of all, a solution process is eliminated, thus reducing costs associated with solvent removal, recovery, and losses. Moreover, on account of recent ecological issues and restrictions, the use of organic solvents is rather undesirable. Their substitution by solvent-free processing strategies has thus become increasingly important. Secondly, melt processing reduces the likelihood of contamination of final products. Also, polymer processors can use in-place equipment. Furthermore, the use of an extruder as continuous reaction vessels for the modification of polymers offers additional advantages including good temperature control and pumping efficiency over a wide viscosity range and the economic savings achieved by integrating several discrete operations within a single processing device.

Chemical reactions used must be able to occur in the melt at high temperatures and in absence of solvent. The thermal stability of the reacting groups as well as of the formed chemical bonds is another important limiting factor. Unless a pre-blending stage is employed, the reactive processing has to be a fast industrial operation for cost effectiveness.

As a consequence of these restrictive conditions, only a few types of chemical reactions are commonly employed in reactive blending. These last can be grouped into imidization, ring opening and amidation reactions, and interchange reactions between polycondensates.

**Figure 1.6**  
Polymer structure  
evolution during  
reactive blending.



In this framework, copolyesters formation through this technique appear to be not only feasible, but a particularly interesting solution.

In the case of polyesters, the interchange reactions mainly involved in the process are intermolecular alcoholysis (Eqn. [28]), intermolecular acidolysis (Eqn. [29]) and esterolysis (Eqn. [30]):



During the process, with the increase of the reaction time, there is a progressive evolution in the chemical structure of the formed copolymers from a long block structure to a random one (Figure 1.6).

### 1.1.3 Physical properties

The physical properties of aliphatic polyesters depend on several factors, such as the composition of the repeating units, flexibility of the chain, presence of polar groups, molecular mass, degree of branching, crystallinity, orientation, etc. Short chain branches reduce the degree of crystallinity of polymers while long chain branches lower the melt viscosity and impart elongational viscosity with tension-stiffening behavior.

Aliphatic polyesters showing  $x, y \geq 2$  (Figure 1.5) are characterized by a high crystallinity degree,  $T_m$  usually in the range 40-90°C (in most cases it is well below 100°C) and  $T_g$  between -70 and -30°C. In general, the lower the ratio between methylene and carboxylic groups in the polymer chain, the higher the melting temperature: e.g. poly(butylene

adipate)  $T_m$  is equal to  $47^\circ\text{C}$ , while poly(butylene succinate) shows  $T_m = 116^\circ\text{C}$  (Albertsson & Varma, 2002).

As far as mechanical properties are concerned, polyesters containing ether-linkages display enhanced flexibility, e.g. poly(1,4-dioxan-2-one) properties are similar to those of the human tissues (Albertsson & Varma, 2002)

The properties of these materials can further be tailored by blending and copolymerization or by changing the macromolecular architecture (e.g. hyper-branched polymers, star-shaped or dendrimers, etc.).

### *1.1.4 Degradation*

Polymer degradation and erosion play a crucial role for all plastics. The distinction between degradable and non-degradable polymers is, therefore, not clean-cut and is in fact arbitrary, as all polymers degrade. It is the relation between the time-scale of degradation and the time-scale of the application that seems to make the difference between degradable and non-degradable polymers. We usually assign the attribute “degradable” to materials which degrade during their application, or immediately after it. Non-degradable polymers are those that require a substantially longer time to degrade than the duration of their application (Gopferich, 1996).

Polymer degradation takes place mostly through scission of the main chains or side-chains of polymer molecules, induced by their thermal or mechanical activation, oxidation, photolysis, radiolysis, or hydrolysis. Some polymers undergo degradation in biological environments when living cells or microorganisms are present around the polymers. Such environments include soils, seas, rivers, and lakes on the earth as well as the body of human beings and animals. These latter are called biodegradable polymers.

Concerning the solid environments under which the biodegradable polymers biodegrade, the two main categories considered in the technical literature, in the norms and in the market are: (a) the materials that biodegrade under composting conditions (compostable materials; the composting conditions may vary though) and (b) the materials which biodegrade in soil (biodegradable in soil materials). Some compostable materials are also biodegradable in soil, but in many cases compostable materials do not biodegrade in soil (Briassoulis & Dejean, 2010).

Biodegradation catalyzed by microorganisms, which can occur in the presence of oxygen (aerobically) or in its absence (anaerobically), ultimately leads to the formation of carbon dioxide, water and new biomass (Figure 1.7).

The chemical process can be summarized by the following equations:

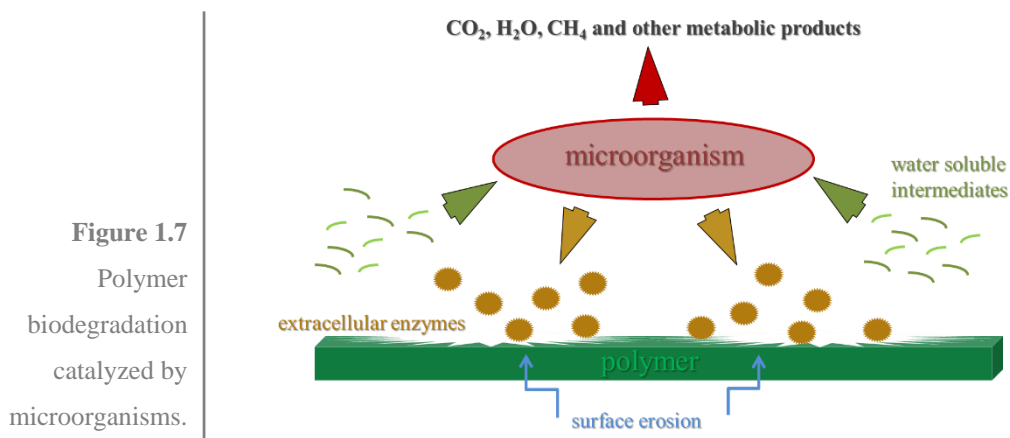
Aerobic conditions (C = carbon):



Anaerobic conditions:



Complete biodegradation (or mineralization) occurs when no residue remains, i.e. when the original product is completely converted into gaseous products and salts (Grima, 2002).



Biodegradable polymers are therefore defined as those which are degraded in these biological environments not through thermal oxidation, photolysis, or radiolysis but through non-enzymatic (or chemical) or enzymatic hydrolysis.

In a strict sense, a polymer that loses its weight over time in a living body should be called absorbable, resorbable or bioabsorbable, regardless of its degradation mode, in other words, for both chemical and enzymatic hydrolysis; while the term biodegradable should be used only for such ecological polymers that have been developed aiming at the protection of earth environments from plastic wastes (Ikada, 2000).

In the following, however, the term “biodegradable” is used in spite of this confusion since it has been widely utilized in the biomaterial world for both biomedical and environmental polymers.

The processes involved in the biodegradation of a polymer, and specifically in the case of polyesters, are complicated. As mentioned, they can be divided into chemical and enzymatic hydrolysis, in both cases being water involved in the process.

#### 1.1.4.1 Chemical hydrolysis

To be degraded by H<sub>2</sub>O, the polymer must contain hydrolysable covalent bonds such as esters, orthoesters, ethers, anhydrides, amides, carbamides (ureas), ester amides (urethanes) and so forth (Lucas, 2008).

It is mainly the type of bond within the polymer backbone that determines the rate of hydrolysis. Several classifications for ranking the reactivity exist which are either based on hydrolysis kinetics data for polymers or are extrapolated from low-molecular weight compounds containing the same functional group. Anhydride and orthoester bonds are the most reactive ones, followed by esters and amides. Such rankings must be viewed, however, with circumspection. Reactivities can change tremendously upon catalysis or by altering the chemical neighborhood of the functional group through steric and electronic effects (Gopferich, 1996).

There are two principal pathways by which polymer bonds can be cleaved: if the diffusion of water into the polymer is faster than the degradation of polymer bonds, the polymer will undergo bulk erosion, because degradation is not confined to the polymer surface. If, however, the degradation of the polymer bonds is faster than the diffusion of water, it will be consumed by the hydrolysis of bonds on the polymer surface and will thus be prevented from diffusion into the bulk. Degradation processes are then strictly confined to the matrix surface and we have, in an ideal case, i.e. when the degradation products are reasonably water soluble, a surface eroding polymer (Von Burkersroda, 2002).

The hydrolytic degradation of aliphatic polyesters occurs in bulk and involves several phenomena, namely water absorption, ester bond cleavage, neutralization of carboxyl endgroups at the surface, autocatalysis inside, and the diffusion and solubilization of soluble oligomers (Li, 2006).

Water enters the polymer bulk, which might be accompanied by swelling. The intrusion of water triggers the chemical polymer degradation, leading to the creation of oligomers and monomers (Gopferich, 1996).

The reaction is:



The chemical hydrolysis reaction is catalyzed by acid or basic compounds. The byproduct, RCOOH, is an acid and is able to accelerate the hydrolysis by autocatalysis. From a macroscopic point of view, this hydrolysis occurs in two steps.

The first step results in random cleavage of polymer chain backbone with a concomitant substantial decrease in molecular weight, leading to a decrease in mechanical properties such as tensile strength, ultimate elongation and impact strength, while weight losses are negligible (Mochizuki, 1997). In the intermediate to the last stage of degradation, the molecular fragments are solubilized and the matter disappears (Grima 2002).

### 1.1.4.2 Enzymatic hydrolysis

The reaction products of an enzymatic hydrolysis or a chemical hydrolysis are the same. The only difference is the catalyst involved in the reaction. Unlike the chemical hydrolysis, the biological hydrolysis reaction is catalyzed by enzymes. A large number of different enzymes are involved, depending of the type of bond to be hydrolyzed. In general, they are called depolymerases. Glycosidic bonds, peptide bonds, and ester bonds are affected by this kind of reaction. It is well known that the ester bond of aliphatic polyesters is cleaved by lipases and PHA-depolymerases (Mochizuki, 1997).

It is generally accepted that to be effective in biodegradation, an enzyme should fit into the stereochemical conformation of the substrate molecule. This action is described as analogous to a key fitting into a lock (Figure 1.8). That is, in general in a biological system, each enzyme performs one chemical function.

It is important to note that Michaelis–Menten kinetics are applicable to homogeneous enzymatic reactions and cannot be applied to heterogeneous enzymatic reactions such as enzymatic hydrolysis of water-insoluble substrates. In the heterogeneous system, it has been reported that the enzymes have a hydrophobic domain as a binding site to adhere hydrophobic substrates in addition to a catalytic domain as an active site. The binding domains have been found in other enzymes such as cellulase and chitinase capable of depolymerizing water-insoluble substrates.

A new kinetic model applicable to heterogeneous enzymatic reactions has been proposed and its usefulness has been confirmed experimentally (Mukai *et al.*, 1993). The heterogeneous enzymatic degradation takes place via two steps of adsorption and hydrolysis. The hydrophobic domains of enzymes adhere to solid substrates by hydrophobic interactions before hydrolysis by catalytic domains.

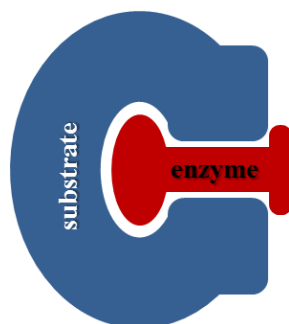


**Figure 1.8** Key-lock mechanism of enzyme-substrate fitting.

Enzymatic degradation proceeds only on the surface of the solid substrate accompanying both the surface erosion and weight loss, because the enzyme cannot penetrate polymer matrix. Thus, with an enzymatic hydrolysis, the polymer weight decreases and molar mass and molecular weight distribution barely changes, unlike in chemical hydrolysis (Grima, 2002). The low molecular weight degradation products are removed from the substrate by solubilization in the surrounding aqueous medium.

There are two types of degradation process, in that cleavage occurs either at random points along the polymer chain (the process by an endo-type degradation) or at the ends of the polymer chain (the process by an exo-type degradation). The degradation process of lipases or PHA depolymerases are primarily based on the endo-type scissions, and thus are not dependent on the molecular weight and molecular weight distribution.

A very common feature of depolymerases is a reaction mechanism that uses three aminoacids residues: aspartate, histidine and serine. Aspartate interacts with the histidine ring to form a hydrogen bond. The ring of histidine is thus oriented to interact with serine. Histidine acts as a base, deprotonating the serine to generate a very nucleophilic alkoxide group (-O<sup>-</sup>). Actually, it is this group that attacks the ester bond (the alkoxide group is a stronger nucleophile than an alcohol group) leading to the formation of an alcohol end group and an acyl-enzyme complex. Subsequently, water attacks the acyl-enzyme bond to produce a carboxyl end group and the free enzyme. This arrangement of serine, histidine and aspartate is termed as catalytic triad (Lucas, 2008).

### *1.1.4.3 Factors influencing hydrolysis*

The degradation process is controlled by a wide variety of compositional and property variables, e.g., matrix morphology, chain orientation, chemical composition, stereochemical structure, sequence distribution, molecular weight and molecular weight distribution, the presence of residual monomers, oligomers and other low molecular weight products, size and shape of specimen, and the degradation environment, e.g. presence of moisture, oxygen, microorganisms, enzymes, pH, temperature and so on. Which degradation mechanisms dominates depends on both the structure of the polyester and the environment it is subjected to (Albertsson & Varma, 2002).

Crystallinity is the most important factor of solid-state morphology that affects the rate of degradation of solid polymers such as fibers or films. Both enzymatic and non-enzymatic degradations proceed through selective processes with easier degradations of amorphous regions, which allow water and enzymes to diffuse into the substrate, than the crystalline regions, although the crystallites are eventually degraded from the edges inward (Mochizuki & Hiram, 1997).

Chain orientation in both crystalline and amorphous regions could also play an important role in the degradation of polymers. In the case of melt-spun fibers, for example, alternative crystalline and amorphous regions arrange in the direction of the fiber axis. Chain orientation along the fiber axis impedes water penetration and enhances the resistance to hydrolytic attack. It is also worthwhile to note that the presence of imperfections and defective crystalline regions has got an effect on degradation rate. When the spherulitic crystallization develops within a matrix containing impurities, monomers or oligomers, these noncrystallizable species are often concentrated at the inter-spherulitic boundaries. These defects are generally preferentially degraded with the amorphous regions (Li, 2006). Due to the faster erosion of amorphous compared to crystalline polymer regions, the overall crystallinity of samples increases (Gopferich, 1996).

The porosity of polymer matrix is also an important factor. A faster degradation is observed in the case of nonporous films as compared with porous ones. This can be assigned to the fact that in the case of porous films, no internal autocatalysis occurred to the ionic exchange facilitated by the porous structure (Li, 2006). On the contrary, when a porous surface is exposed to enzymes, the degradation rate increases due to the enhanced surface/volume ratio, thus higher availability for the enzymatic attack.

As far as the molecular weight is concerned, generally the lower the  $M_w$ , the faster the degradation rate, in agreement with the presence of more carboxylic acid catalyzing groups (Li, 2006).

The effect of pH on degradation has been investigated carefully for many biodegradable polymers. It is well known that the hydrolysis of esters is affected tremendously by pH variations (Von Burkensroda, 2002). Ester hydrolysis can be either acid or base catalyzed. After shifts in pH, reaction rates of esters may thereby change some orders of magnitude due to catalysis (Gopferich, 1996). In the case of enzymatic hydrolysis, the pH plays even a greater role, due to the strict and well-known relationship between enzymatic activity and pH.

Among the degradable aliphatic polyesters, a polymer having a lower melting point,  $T_m$ , is generally more susceptible to biodegradation than one having a higher melting point.

In order to a synthetic polymer to be degraded by an enzyme catalyst, the polymer chain must be flexible enough to fit into the active site of the enzyme. This accounts for the above-mentioned fact that the flexible aliphatic polyesters, having also generally lower  $T_m$ , are readily degraded by lipases, while the more rigid aromatic polyesters are bioinert (Mochizuki, 1997).

As to the relationship between biodegradability and primary structure of aliphatic polyesters, it is generally accepted that enzymatic and microbial degradations of various analogous synthetic polymer series proceed better with balanced hydrophobicity–hydrophilicity ratio in the polymer structure (Mochizuki, 1997).

Finally, the composition of polymer chains greatly determines the degradation rates of aliphatic polyesters (Li, 2006). By introducing a second monomer into the polymer chain, many properties of the original polymer can be influenced, such as crystallinity degree, melting point and glass transition temperature. These factors can have additional indirect effects on degradation rates (Gopferich, 1996).

## 1.2 Copolymers

Copolymers are macromolecules derived from more than one species of monomer. The copolymerization process continues to attract much attention both academically and industrially because of the possibility to tailor the properties of the final material. Most commercial copolymers are designed to present synergistic improvements with respect to their parent homopolymers, including better processability, higher mechanical properties and better chemical resistance, to cite only some examples. In fact, the final properties of the copolymers can be favorably modified, depending on the kind, relative amount and distribution of the comonomeric units along the polymeric chain.

To better comprehend the structure of a copolymer, different parameters have to be taken into due account and calculated on the basis of different kinetic and statistical models. These latter permit to describe the comonomeric units linking process and their distribution along the polymer chain.

Copolymers classification can be made based on the monomeric units (in the following called A and B) arrangement along the polymeric chain. There are:

- **alternating copolymers** with regular alternating of A and B units:



- **periodic copolymers** with A and B units arranged in a repeating sequence:



- **statistical or random copolymers** in which the sequence distribution of monomeric units follows Bernoullian statistics:



- **block copolymers** with two or more homopolymer subunits linked by covalent bonds. Block copolymers with two or three distinct blocks are called diblock copolymers and triblock copolymers, respectively:



Copolymers may also be described in terms of the existence of or arrangement of branches in the polymer structure. **Linear copolymers** consist of a single main chain whereas **branched copolymers** consist of a single main chain with one or more polymeric side chains. **Graft copolymers** are a special type of branched copolymers in which the side chains are structurally distinct from the main chain: usually main chain and side chains are composed of two distinct homopolymers. However, the individual chains of a graft copolymer may be homopolymers or copolymers; moreover, different copolymer sequencing is sufficient to define a structural difference, thus an **A-B** diblock copolymer with **A-B** alternating copolymer side chains is properly called a graft copolymer. Other special types of branched copolymers include **star copolymers**, **brush copolymers**, and **comb copolymers**.

In the following, the present work will focus on random and block copolymers, i.e. the two copolymer types synthesized during the experimental research.

### 1.2.1 Random copolymers

In amorphous random copolymers,  $T_g$  is usually a monotonic function of composition and the most common relationship used to predict  $T_g$  as a function of comonomer content is the Fox equation (Fox, 1956):

$$1/T_g = \omega_A/T_{g,A} + \omega_B/T_{g,B} \quad [34]$$

where  $T_{g,A}$  and  $T_{g,B}$  are the glass transition temperatures of the pure homopolymers and  $\omega_A$  and  $\omega_B$  the respective weight fractions.

Among the other various equations proposed to describe the composition dependence of the glass transition temperature in random copolymers, essentially two basic concepts are discussed. Gordon and Taylor (Gordon & Taylor, 1952) assumed volume additivity of the repeating units in copolymers, analogous to the interpretation of packing phenomena in ideal solutions of small molecules.

Di Marzio and Gibbs (Di Marzio & Gibbs, 1959), on the other hand, based on the idea that chain stiffness is the main determinant of the glass transition, supposed additivity of “rotatable” (“flexible”) bonds, i.e. of those simple bonds which by rotation contribute to conformational changes of the molecule. Incidentally, the resulting expression of both models are formally of the same “Gordon-Taylor” type:

$$T_g = (\omega_A T_{g,A} - k \omega_B T_{g,B}) / (\omega_A + k \omega_B) \quad [35]$$

The parameter  $k$  is, however, model specific, i.e.:

$$k_{GT} = (\rho_A / \rho_B) (\Delta\alpha_A / \Delta\alpha_B) \quad [36]$$

for the Gordon-Taylor volume additivity model and:

$$k_{DMG} = (\mu_A / \gamma_A) / (\mu_B / \gamma_B) \quad [37]$$

for the Di Marzio-Gibbs 'flexible' bond additivity model.  $\rho_i$  are the densities and

$$\Delta\alpha_i = (\alpha_{melt} - \alpha_{glass})_{T_g} \quad [38]$$

the increments of the expansion coefficients at  $T_g$ , whereas  $\mu_i$  and  $\gamma_i$  are the masses and the numbers of "flexible" bonds, respectively, of the monomeric units.

In the assumption of validity of the Simha-Boyer rule,  $\Delta\alpha T_g = 0.113$  (Simha & Boyer, 1962) and neglecting in a first approximation the differences between the mostly very similar densities of polymers, i.e. supposing  $\rho_A / \rho_B = 1$ , the constant  $k_{GT}$  for volume additivity can be substituted in a first approximation by  $k_f = T_{g,A} / T_{g,B}$ . Accordingly, the Gordon-Taylor equation can be reformulated:

$$1/T_g = \omega_A/T_{g,A} + \omega_B/T_{g,B}$$

the result being the well-known Fox relation.

A random copolymer can potentially crystallize in two extreme ways. It can form a two-phase system in which the crystalline phase is composed entirely of A units and is in equilibrium with a mixed amorphous phase of A units and non crystallizable comonomer B units (comonomer exclusion). Alternatively, the copolymer may form a two phase system in which the crystalline phase is a solid solution of A and B units; the comonomer B units produce defects in the crystalline A lattice and both phases have the same composition (comonomer inclusion). Real copolymer crystals may exhibit a morphology intermediate to the two extremes (Sanchez & Eby, 1973).

The case of comonomer exclusion in thermodynamic equilibrium was first described by Flory (Flory, 1947), who calculated the upper bound of the copolymer melting temperature, i.e., the melting temperature of crystals built up from "infinitely long" homopolymer sequences of units A in the copolymer. Starting with the general equation:

$$\Delta G = \Delta G^\circ + RT \ln(\alpha) \quad [39]$$

where  $\alpha$  is the activity of the crystallizing copolymer, Flory found the melting temperature equation:

$$1/T_m^\circ - 1/(T_m(X_B)) = (R/H_m^\circ) \ln(1-X_B) \quad [40]$$

where  $X_B$  is the concentration of B units in the polymer and  $\ln(1-X_B)$  equals the collective activities of A sequences in the limit of the upper bound of the melting temperature.  $T_m^\circ$

and  $H_m^\circ$  denote the homopolymer equilibrium melting temperature and heat of fusion and  $R$  is the gas constant.

The drawback of this model is Flory's assumption that these homopolymer sequences of infinite length build up unfolded crystals of the length of A sequences, an assumption that is unrealistic for polymers.

Attempts to overcome this drawback treat copolymer crystals as a "pseudo-eutectic" system, where the homopolymer sequences of length  $\xi$  may only be included into crystals of lamellar thickness corresponding to that length. The activity of a sequence of length  $\xi$  is then related to the mean sequence length  $\langle \xi \rangle$  as follows:

$$\Delta G = \Delta G^\circ + (RT / \xi) \ln(X_{A\xi} / f_{A\xi}) \quad [41]$$

$X_{A\xi}$  is the concentration and  $f_{A\xi}$  is the activity coefficient for crystallizing sequences of length  $\xi$ . Baur (Baur, 1966) used the activity coefficient:

$$f_{A\xi} = (\xi / \langle \xi \rangle) e^{-[\xi / \langle \xi \rangle - 1]} \quad [42]$$

The melting point of infinitely long homopolymer sequences is then given by:

$$1 / T_m^\circ - 1 / (T_m(X_B)) = (R / H_m^\circ) [\ln(1 - X_B) - \langle \xi \rangle^{-1}] \quad [43]$$

where  $\langle \xi \rangle = [2X_B(1 - X_B)]^{-1}$  is the average length of homopolymer sequences in the melt. This model, while incorporating finite crystal thickness and concomitant depression in the melting point, still neglects the fact that the homopolymer sequences are invariably fixed in chains due to bond connectivity; the eutectic equilibrium, which requires total separation into the "components" (the homopolymer sequences of same length  $\xi$ ) is unrealistic. However, it was shown by several investigations (Baur, 1966; Helfland & Lauritzen, 1973; Sanchez & Eby, 1975; Windle *et al.*, 1985; Allegra *et al.*, 1992; Yoshie *et al.*, 1994; Wendling & Suter, 1998) that the Baur model fits experimental data much better than the Flory equation. Inspection of experimental data shows readily that comonomer exclusion alone cannot account for the observed melting point depression in many cases; hence, comonomer inclusion is to be considered in the melting point prediction.

The case of comonomers B that are included into the crystal of A where they act as defects was considered by Helfand and Lauritzen (Helfland & Lauritzen, 1973) and later in a more general way by Sanchez and Eby (Sanchez & Eby, 1975). In this model, the melting temperature is then given by:

$$1 / (T_m(X_B)) - 1 / T_m^\circ = (R / H_m^\circ) \{ (\epsilon X_{CB}) / (RT_m) + (1 - X_{CB}) \ln[(1 - X_{CB}) / (1 - X_B)] + X_{CB} \ln(X_{CB} / X_B) \} \quad [44]$$

This equation (Eqn. [44]) holds for any concentration  $X_{CB}$ , including two limits: when  $X_{CB} = X_B$ , uniform inclusion takes place and Eqn. [44] reduces to:

$$T_m(X_B) = T_m^\circ [1 - \varepsilon X_B / H_m^\circ] \quad [45]$$

For the equilibrium state, the concentration of B units in the cocrystal is given by:

$$X_{CB}^{eq} = (X_B e^{-\varepsilon/RT}) / (1 - X_B + X_B e^{-\varepsilon/RT}) \quad [46]$$

and the equilibrium melting point is derived from Eqn. [44] as:

$$1/T_m^\circ - 1/(T_m(X_B)) = (R/H_m^\circ) \ln(1 - X_B + X_B e^{-\varepsilon/RT}) \quad [47]$$

This equation is similar to the Flory equation (Eqn. [40]) but includes the equilibrium fraction  $X_B e^{-\varepsilon/RT}$  of repeat units B that are able to crystallize. It is obvious that Eqn. [47] reduces to the Flory model for the case of high defect free energies, and one might not be surprised that it also overestimates the melting temperatures for  $\varepsilon \gg 0$  or, in the general application of this model, underestimates the defect free energy. The temperatures derived by Eqn. [47] can be taken as an upper bound of the melting temperature. The behavior at  $\varepsilon \gg 0$  is the principal shortcoming of the Sanchez-Eby model: when  $\varepsilon$  is too high to allow cocrystallization, Eqn. [47] reduces to the Flory model (Eqn. [40]), but it should preferentially converge to the Baur model, (Eqn. [43]).

The model recently proposed by Wendling and Suter (Wendling & Suter, 1998), equals Eqn. [47] and Eqn. [41] in the limits of high and low defect free energies.

Accordingly to this method, the melting temperature is given by:

$$1/(T_m(X_B)) - 1/T_m^\circ = (R/H_m^\circ) \{ (\varepsilon X_{CB}) / (RT_m) + (1 - X_{CB}) \ln[(1 - X_{CB}) / (1 - X_B)] + X_{CB} \ln(X_{CB} / X_B) + \langle \xi \rangle^{-1} \} \quad [48]$$

Assuming equilibrium comonomer inclusion, Eqn. [47], Eqn. [48] reduces to:

$$1/T_m^\circ - 1/(T_m(X_B)) = (R/H_m^\circ) \{ \ln(1 - X_B + X_B e^{-\varepsilon/RT}) - \langle \xi \rangle^{-1} \} \quad [49]$$

where:

$$\langle \xi \rangle^{-1} = 2(X_B - X_B e^{-\varepsilon/RT}) / ((1 - X_B + X_B e^{-\varepsilon/RT})) \quad [50]$$

Both the inclusion and exclusion models predict a depression of the crystalline melting point. For the inclusion model the melting point depression is caused by a defective heat of fusion that accompanies the crystallization, whereas for the exclusion model, the depression is caused by the fact that preferential ordering of the copolymer chains is required for crystallization which raises the entropy of fusion. However, careful crystallinity studies combined with calorimetric determinations of heats of fusion can ascertain which model is more appropriate for a given random copolymer system.

### 1.2.2 Block copolymers

Crystallization within block copolymer microdomains (MDs) is an important issue since it can completely change the block copolymer morphology. The structure development in semicrystalline block copolymers depends on two competing self-organizing mechanisms:

microphase separation and crystallization. The most commonly studies of the semicrystalline block copolymer systems in the literature are the AB block copolymers or the ABA triblock copolymers, where one block is amorphous and the other semicrystalline. It is generally accepted that the changes of state as a function of temperature can determine the final morphology according to three key transition temperatures: the order-disorder transition (ODT) temperature,  $T_{ODT}$ , the crystallization temperature,  $T_c$ , of the crystallizable block and the glass-transition temperature of the amorphous block ( $T_g$ ). Five general cases have been described for AB diblocks with one crystallizable block (Muller *et al.*, 2005):

- *Homogeneous melt*,  $T_{ODT} < T_c < T_g$ . In diblock copolymers exhibiting homogeneous melts, microphase separation is driven by crystallization if  $T_g$  of the amorphous block is lower than  $T_c$  of the crystallizable block. This generally results in a lamellar morphology where crystalline lamellae are sandwiched by the amorphous block layers and spherulite formation can be observed depending on the composition.
- *Weakly segregated systems*,  $T_{ODT} > T_c > T_g$  with soft confinement. In this case, crystallization often occurs with little morphological constraint, enabling a “breakout” from the ordered melt MD structure and the crystallization overwrites any previous melt structure, usually forming lamellar structures and, in many cases, spherulites depending on the composition.
- *Weakly segregated systems*,  $T_{ODT} > T_c < T_g$  with hard confinement. In this case, the crystallization of the semicrystalline block can overwhelm the microphase segregation of the MD structures even though the amorphous block is glassy at the crystallization temperature, because of the weak segregation strength.
- *Strongly segregated systems*,  $T_{ODT} > T_c > T_g$  with soft confinement. If the segregation strength is sufficiently strong, the crystallization can be confined within spherical, cylindrical or lamellar MDs in strongly segregated systems with a rubbery block.
- *Strongly segregated systems*,  $T_{ODT} > T_c < T_g$  with hard confinement. A strictly confined crystallization within MDs has been observed for strongly segregated diblock copolymers with a glassy amorphous block.

A distinct situation arises in block copolymers where both blocks within a diblock copolymer, or more than one block (typically two) within triblock terpolymers can crystallize. As it is expected, the crystallization behavior of crystalline-crystalline block copolymers is more complicated; for instance, when the copolymers are quenched from a

microphase-separated melt into various temperatures below the melting temperatures of the corresponding blocks, various situations can be observed. When the melting temperatures of both blocks are close enough, a coincident crystallization of both blocks can be obtained by quenching. On the other hand, when the melting temperature of one block is far from the other, one block crystallizes in advance and produces a specific morphology, which can or cannot be modified upon crystallization of the other block. Such modification depends, among other controlling parameters, on segregation strength, crystallization temperature and molecular weight of the block components (Muller *et al.*, 2007).

### 1.3 Biomedical applications

For the last forty years, increasing attention has been paid to the so-called biodegradable or absorbable therapeutic systems in order to replace currently used biostable (or long lasting) metals, alloys and ceramics or to provide novel therapeutic solutions, anytime a therapeutic function is required for a limited period of time.

Polymers certainly possess significant potential because of their flexibility which gives rise to materials with great diversity of physical and mechanical properties (Ulery *et al.*, 2011). Degradable polymers are of utmost interest because these biomaterials are able to be broken down and excreted or resorbed without removal or surgical revision. Although natural polymers such as collagen have been used biomedically for thousands of years, research into biomedical applications of synthetic degradable polymers is relatively new, starting in the 1960s.

In surgery, degradable sutures, bone fracture fixation devices, stents, dental reconstruction, tissue engineering, etc., are attractive targets, some having already received commercial applications.

In pharmacology, sustained release from degradable polymeric matrices is exploited in human, especially in birth control and cancer therapy. However, other applications that require degradation are still at the research level. It is the case of polymer-based functions like targeting of receptors, cells or organs, promoting intracellular penetration of recalcitrant drugs, transfecting genes and releasing drugs at the right place and the right dose. Tissue engineering is largely based on cell cultures onto polymer surfaces or into porous polymer scaffolds that should be eliminated also at the end of their useful life. Until now, attention has been primarily paid to cell behaviors (adhesion and proliferation, less

frequently phenotype) and much less to the fate of the scaffolds designed to support correct tissue formation.

Like any biomaterial, a polymeric system aimed at serving for a limited period of time before degradation and elimination from the body, must first fulfill severe criteria (Vert, 2009).

The host response depends on the chemical, physical, and biological properties of the material used. When these materials are also biodegradable, there exists the additional issue of continuing changes in the material properties induced by degradation over time. These changes can cause long-term host responses to these biomaterials to be greatly different than the initial response. In the design of biodegradable biomaterials, many important properties must be considered. These materials must (Lloyd, 2002):

- not evoke a sustained inflammatory response;
- possess a degradation time coinciding with their function;
- have appropriate mechanical properties for their intended use;
- produce nontoxic degradation products that can be readily resorbed or excreted;
- include appropriate permeability and processability for designed application.

These properties are greatly affected by a number of features of degradable polymeric biomaterials including, but not limited to: material chemistry, molecular weight, hydrophobicity, surface charge, water adsorption, degradation and erosion mechanism. Given the complexity and the range of applications polymeric biomaterials are currently used, there is not just one polymeric system available that could be considered as an ideal biomaterial (Nair & Laurencin, 2007). This underlines the need for developing a wide range of biodegradable materials available that can appropriately match the specific and unique requirements of each individual medical application.

Indeed, the selection and design of a polymer is a challenging task because of the inherent diversity of structures and requires a thorough understanding of the surface and bulk properties of the polymer that can give the desired chemical, interfacial, mechanical and biological functions. The choice of a specific polymer, in addition to its physico-chemical properties, is dependent on the need for extensive biochemical characterization and specific preclinical tests to prove its safety (Hoffman, 2008).

### *1.3.1 Tissue engineering*

Disease, injury and trauma can lead to damage and degeneration of tissues in the human body, which necessitates treatments to facilitate their repair, replacement or regeneration.

Treatment typically focuses on transplanting tissue from one site to another in the same patient (an autograft) or from one individual to another (a transplant or allograft). While these treatments have been revolutionary and lifesaving, major problems exist with both techniques. Harvesting autografts is expensive, painful, constrained by anatomical limitations and associated with donor site morbidity due to infection and hematoma. Similarly, allografts and transplants also have serious constraints due to problems with accessing enough tissue for all of the patients who require them and the fact that there are risks of rejection by the patient's immune system and the possibility of introducing infection or disease from the donor to the patient. Alternatively, the field of tissue engineering aims to regenerate damaged tissues, instead of replacing them, by developing biological substitutes that restore, maintain or improve tissue function (Bonassar & Vacanti, 1998; Langer, 2000; Atala, 2004). The term 'tissue engineering' was officially coined at a National Science Foundation workshop in 1988 to mean "the application of principles and methods of engineering and life sciences toward the fundamental understanding of structure-function relationships in normal and pathological mammalian tissues and the development of biological substitutes to restore, maintain or improve tissue function". However, while the field of tissue engineering may be relatively new, the idea of replacing tissue with another goes as far back as then 16th century. Gasparo Tagliacozzi (1546-99), Professor of Surgery and Anatomy at the University of Bologna, described a nose replacement that he had constructed from a forearm flap in his work "De Custorum Chirurgia per Insitionem" (The Surgery of Defects by Implantation) which was published in 1597. The field of tissue engineering is highly multidisciplinary and draws on experts from clinical medicine, mechanical engineering, materials science, genetics, and related disciplines from both engineering and the life sciences. It relies extensively on the use of porous 3D-scaffolds to provide the appropriate environment for the regeneration of tissues and organs. These scaffolds essentially act as a template for tissue formation and are typically seeded with cells and occasionally growth factors, or subjected to biophysical stimuli in the form of a bioreactor, a device or system which applies different types of mechanical or chemical stimuli to cells (Martin *et al.*, 2004). These cell-seeded scaffolds are either cultured *in vitro* to synthesize tissues which can then be implanted into an injured site, or are implanted directly into the injured site, using the body's own systems, where regeneration of tissues or organs is induced *in vivo*. This combination of cells, signals and scaffold is often referred to as a tissue engineering triad (Figure 1.9). Numerous scaffolds, produced from a variety of biomaterials and manufactured using a plethora of fabrication techniques, have been used in the field in attempts to regenerate

different tissues and organs in the body. Regardless of the tissue type, a number of key considerations are important when designing or determining the suitability of a scaffold for use in tissue engineering.

**Figure 1.9** Tissue engineering triad of cells, signals and the scaffold.



*Biocompatibility.* The very first criterion of any scaffold for tissue engineering is that it must be biocompatible; cells must adhere, function normally, and migrate onto the surface and eventually through the scaffold and begin to proliferate before laying down new matrix. After implantation, the scaffold or tissue engineered construct must elicit a negligible immune reaction in order to prevent it causing such a severe inflammatory response that it might reduce healing or cause rejection by the body.

*Biodegradability.* The objective of tissue engineering is to allow the body's own cells, over time, to eventually replace the implanted scaffold or tissue engineered construct. Scaffolds and constructs, are not intended as permanent implants. The scaffold must therefore be biodegradable so as to allow cells to produce their own extracellular matrix (Babensee *et al.*, 1998). The by-products of this degradation should also be non-toxic and able to exit the body without interference with other organs. In order to allow degradation to occur in tandem with tissue formation, an inflammatory response combined with controlled infusion of cells such as macrophages is required. Now that tissue engineering strategies are entering clinical practice more routinely, the field of immunology is playing a role of increasing prominence in the research area (Brown *et al.*, 2009; Lyons *et al.*, 2010).

*Mechanical properties.* Ideally, the scaffold should have mechanical properties consistent with the anatomical site into which it is to be implanted and, from a practical perspective,

it must be strong enough to allow surgical handling during implantation. While this is important in all tissues, it provides some challenges for cardiovascular and orthopedic applications specifically. Producing scaffolds with adequate mechanical properties is one of the great challenges in attempting to engineer bone or cartilage. For these tissues, the implanted scaffold must have sufficient mechanical integrity to function from the time of implantation to the completion of the remodeling process (Hutmacher *et al.*, 2000). A further challenge is that healing rates vary with age; for example, in young individuals, fractures normally heal to the point of weight-bearing in about six weeks, with complete mechanical integrity not returning until approximately one year after fracture, but in the elderly the rate of repair slows down. This must be taken into account too when designing scaffolds for orthopedic applications.

Many materials have been produced with good mechanical properties, but with detriment of retaining a high porosity and many materials, which have demonstrated potential *in vitro*, have failed when implanted *in vivo* due to insufficient capacity for vascularization. It is clear that a balance between mechanical properties and porous architecture to allow cell infiltration and vascularization is the key to the success of any scaffold.

*Scaffold architecture.* The architecture of scaffolds used for tissue engineering is of critical importance. Scaffolds should have an interconnected pore structure and high porosity to ensure cellular penetration and adequate diffusion of nutrients to cells within the construct and to the extra-cellular matrix formed by these cells. Furthermore, a porous interconnected structure is required to allow diffusion of waste products out of the scaffold, and the products of scaffold degradation should be able to exit the body without interference with other organs and surrounding tissues. The issue of core degradation, arising from lack of vascularization and waste removal from the center of tissue engineered constructs, is of major concern in the field of tissue engineering (Ko *et al.*, 2007; Phelps *et al.*, 2009). Another key component is the mean pore size of the scaffold. Cells primarily interact with scaffolds via chemical groups (ligands) on the material surface. Scaffolds synthesized from natural extracellular materials (e.g. collagen) naturally possess these ligands in the form of Arg-Gly-Asp (RGD) binding sequences, whereas scaffolds made from synthetic materials may require deliberate incorporation of these ligands through, for example, protein adsorption. The ligand density is influenced by the specific surface area, i.e. the available surface within a pore to which cells can adhere. This depends on the mean pore size in the scaffold. The pores thus need to be large enough to allow cells to migrate into the structure, where they eventually become bound to the ligands within the scaffold, but small enough to establish a sufficiently high specific

surface, leading to a minimal ligand density to allow efficient binding of a critical number of cells to the scaffold (Yannas *et al.*, 1989; O'Brien *et al.*, 2005). Therefore, for any scaffold, a critical range of pore sizes exists (Murphy *et al.*, 2010a, 2010b) which may vary depending on the cell type used and tissue being engineered.

*Manufacturing technology.* In order for a particular scaffold or tissue engineered construct to become clinically and commercially viable, it should be cost effective and it should be possible to scale-up from making one at a time in a research laboratory to small batch production. The development of scalable manufacturing processes to good manufacturing practice standard is critically important in ensuring successful translation of tissue engineering strategies to the clinic (Hollister, 2009). Another key factor is determining how a product will be delivered and made available to the clinician. This will determine how either the scaffold or the tissue engineered construct will be stored. Clinicians typically prefer off-the shelf availability without the requirement for extra surgical procedures in order to harvest cells prior to a number of weeks of *in vitro* culture before implantation. However, for some tissue types, this is not possible and *in vitro* engineering prior to implantation is required.

The final criterion for scaffolds in tissue engineering, and the one which all of the criteria listed above are dependent upon, is the choice of biomaterial from which the scaffold should be fabricated.

#### 1.3.1.1 Electrospinning

Among various processing techniques, electrospinning (ES) is the only method capable of producing continuous polymer nanofibres (Jiang *et al.*, 2004). Electrospinning is a unique technology that can produce non-woven fibrous articles with fiber diameters ranging from tens of nanometers to microns, a size range that is otherwise difficult to access by conventional nonwoven fiber fabrication techniques (Reneker & Chun, 1996; Li & Xia, 2004).

The electrospinning technology is well suited to process natural biomaterials and synthetic biocompatible or bioabsorbable nanofibers for biomedical applications. Interest in the electrospinning process has increased in recent years, and this technology has been exploited for a wide range of applications. The emphasis of current research is focused on determining appropriate conditions for electrospinning various polymers and biopolymers. The most important processing parameters of nanofibers are: applied voltage, solution flow rate, polymer concentration, molecular weight and distance between the syringe needle tip to ground collection plate (Theron *et al.*, 2004). Solution viscosity has been found to influence fiber diameter, initiating droplet shape, and the jet trajectory.

Increasing solution viscosity has been associated with the production of larger diameter fibers (Reneker *et al.*, 2000).

The advantages of the electrospinning process are its technical simplicity and its easy adaptability.

The apparatus used for electrospinning is quite simple in construction. Basically an electrospinning system consists of three major components which are (Figure 1.10):

- a high voltage power supply with positive or negative polarity;
  - a syringe pump with capillaries or tubes to carry the solution from the syringe or pipette to the spinnerets;
  - a grounded collecting plate (usually a metal screen, plate, or rotating mandrel).
- The collector can be made of any shape according to the requirements, like a flat plate, rotating drum, etc.

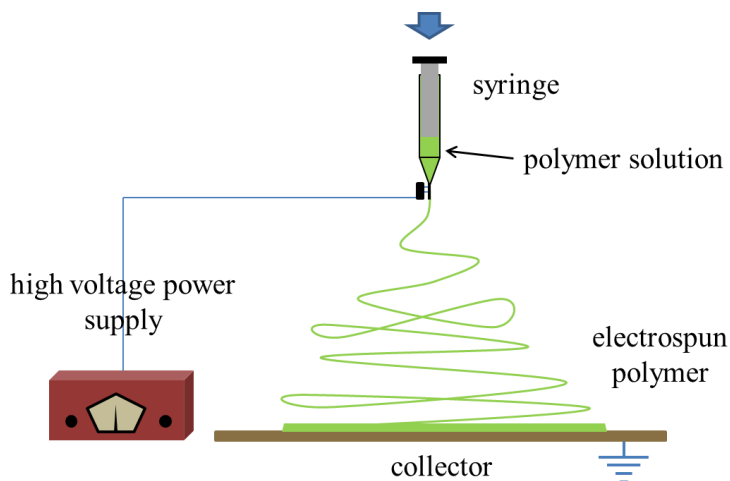


**Figure 1.10**  
Schematic illustration of electrospinning apparatus.

The solution or the melt that has to be spun is forced through a syringe pump. At the end of the capillary, the polymer solution held by its surface tension, which is subjected to an electric field and an electric charge, is induced on the liquid surface due to this electric field.

The pendant hemispherical polymer drop takes a cone like projection in the presence of an electric field at the end. When the applied potential reaches a critical value, the repulsive electrical forces overcome the surface tension forces. Eventually, a charged jet of the solution is ejected from the tip of the Taylor cone and an unstable and a rapid whipping of the jet occurs in the space between the capillary tip and collector which leads to evaporation of the solvent, leaving the polymer behind (Taylor, 1969; Yarin *et al.*, 2001; Adomaviciute & Rimvydas, 2007). For instance, the polymer solution must have a

concentration high enough to cause polymer entanglements, but not too high that the viscosity prevents polymer motion induced by the electric field. The solution must also have a surface tension low enough, a charge density and a viscosity high enough to prevent the jet from collapsing into droplets before the solvent has evaporated. Morphological changes can occur upon decreasing the distance between the syringe needle and the substrate. Increasing the distance or decreasing the electrical field decreases the bead density, regardless of the concentration of the polymer in the solution (Reneker *et al.*, 2000).

Another advantage of the electrospinning technique is the simplicity of the process: in fact, it does not require any sophisticated and expensive equipment and it can be easily scaled-up for mass production. Besides the aforementioned benefits, its power arises from the morphological features of the products obtained. Indeed, electrospun fiber dimensions and spatial organization resemble the fibrous component of extracellular matrix (ECM), making ES a technology for the production of morphologically biomimetic scaffolds. As a consequence, this kind of scaffolds can be used to elicit different responses from the same cell phenotype only thanks to their particular topography. Indeed, it is well-established that, besides being influenced by external chemical signals coming both from ECM and from nearby cells, cell behavior is manipulated also by the morphological features of their environment that control cell adhesion, orientation, motility, gene expression, etc. (Webster *et al.*, 2001). A comprehensive review about the effect of surface topography on cells is available in the literature (Stevens & George, 2005). The authors describe cell behavior interacting with differently structured scaffolds and conclude that nanoscaled architectures promote better spreading and attachment when compared with microscaled scaffolds. Their model was supported by several studies reporting that cells are able to better adhere and spread when cultured on sub-micrometric fibres with respect to micrometric ones (Kwon *et al.*, 2005; Noh *et al.*, 2006).

### *1.3.2 Controlled drug release*

Conventional oral drug administration does not usually provide rate-controlled release or target specificity. In many cases, conventional drug delivery implies sharp increases of drug concentration at potentially toxic levels. Following a relatively short period at the therapeutic level, drug concentration eventually drops off until re-administration.

Today new methods of drug delivery are possible: desired drug release can be provided in a controlled way through different mechanism and profiles.

Controlled drug delivery can be used to achieve (Bajpai *et al.*, 2008):

- sustained constant concentration of therapeutically active compounds in the blood with minimum fluctuations;
- predictable and reproducible release rates over a long period of time;
- protection of bioactive compounds having a very short half-life;
- elimination of side-effects, waste of drug and frequent dosing;
- optimized therapy and better patient compliance;
- solution of the drug stability problem.

Five controlled release profiles (Figure 1.11) are possible (Bajpai *et al.*, 2008):

*Profile I:* conventional delayed, but not constant release.

*Profile II:* constant or zero order release. Synthetic polymers or pumps deliver drugs at a constant rate so that the drug concentration in the blood stream is maintained at an optimal level of therapeutic effectiveness. These are often referred to as zero order drug delivery systems and many have been or are being commercialized to deliver a number of drugs. Profiles I and II are now common in commercial systems.

*Profile III:* substantial delayed release followed by a constant release of active agent. Such systems will be most useful for the delivery of active agents commencing at some period during the night.

*Profile IV:* delay followed by a tight pulse of drug release. This again allows for nocturnal delivery or for the delivery of a hormone, which often requires pulsed rather than constant delivery.

*Profile V:* multiple pulses at specified periods.

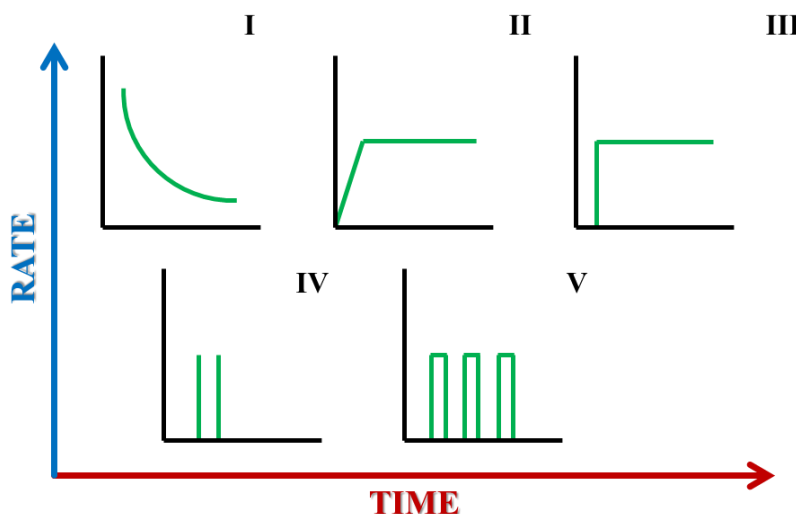


**Figure 1.11**  
Different release profiles of drugs.

Taking all the possibilities described above into due account, to gain successful pharmacotherapy intervention, a strict control over the spatial and temporal characteristics of drug delivery is required. This could only be achieved through the development of well-designed drug carriers that would be able to meet the specific delivery challenges that each particular disease poses, and to overcome the physiological barriers (extra- and intra-cellular degradation, unfavorable tissue distribution and poor penetration through cell membranes), allowing the drug molecules to reach the intra-cellular sites of action at the required quantities and for the required period of time.

Today, polymers are the most used materials to construct carriers with controlled drug delivery properties, that is, carriers which could perform one or more of the following:

- increase drug availability to the target cells;
- increase selectivity towards the target cells;
- release their drug load only at the site of drug action (or nearby) in response to internal or external stimuli (e.g. pH or temperature changes);
- release drug only when it is required in response to biological signals (e.g. an increase in glucose levels in blood).

The idea of controlled release from polymers dates back to the 1960s through the employment of silicone rubber (Folkman & Long, 1964) and polyethylene. The well-known lack of degradability in these systems implies the requirement of eventual surgical removal and limited their applicability. In the 1970s, biodegradable polymers were suggested as appropriate drug delivery materials circumventing the requirement of removal (Jalil & Nixon, 1990).

Since then, various drug delivery systems (DDS) have been investigated and optimized; they can be classified according to the mechanism controlling the drug release (Figure 1.12) (Bajpai *et al.*, 2008):

- diffusion controlled systems
  - reservoir (membrane systems)
  - matrix (monolithic systems);
- chemically controlled systems
  - bioerodible and biodegradable systems
  - pendant chain systems;
- swelling controlled systems;
- modulated release systems.

*Diffusion controlled systems.* In diffusion systems, drugs diffuse through polymer; the polymer may undergo subsequent biodegradation on exhaustion of the drug. Two types of

diffusion-controlled devices have been used in drug delivery. These are reservoir devices and matrix devices. Reservoir systems are hollow devices in which an inner core of dissolved, suspended or neat drug is surrounded by a polymer membrane. In this device, the drug core is encapsulated in a polymeric membrane. Drug diffusion through the membrane is rate limiting and controls the overall drug release rate. A saturated concentration of reservoir of the drug inside the reservoir is essential to maintain a constant concentration gradient across the membrane. The drug transport mechanism through the membrane is usually a solution-diffusion mechanism. Drug transport occurs first by dissolution of the drug in the membrane on one side followed by diffusion through the membrane and desorption from the other side of the membrane.

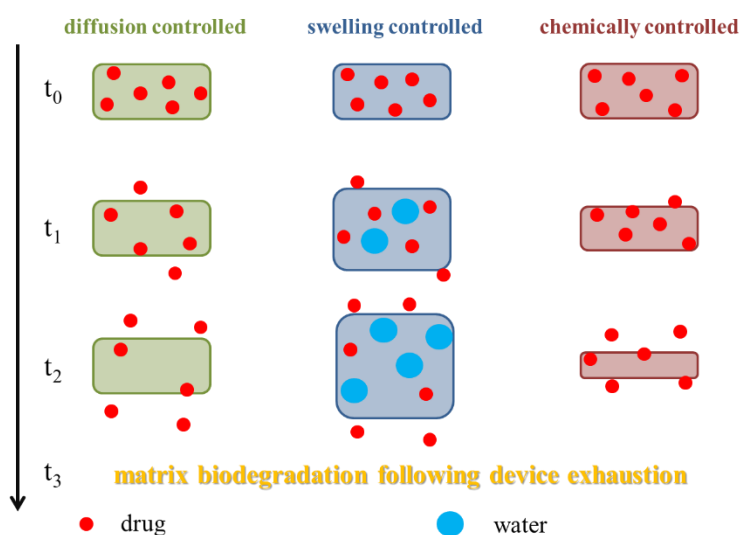


**Figure 1.12**  
Mechanisms for controlled drug release from a polymer matrix.

In matrix systems, the drug is uniformly dissolved or dispersed. An inherent drawback of the matrix systems is their first-order release behavior with continuously decreasing release rate. This is due to the increasing diffusion path length and the decreasing area at the penetrating diffusion front as the matrix release proceeds. A matrix (or monolith) device is easy to formulate and gives a higher initial release rate than a reservoir device and can be made to release at a nearly constant rate.

*Chemically controlled systems.* In chemically controlled drug delivery systems, the release of a pharmacologically active agent usually takes place in the aqueous environment by one or more of the following mechanisms:

- Gradual biodegradation of a drug containing polymer system.

In these systems, the polymer erodes because of the presence of hydrolytically or enzymatically labile bonds. As the polymer erodes, the drug is released to the

surrounding medium. Erosion may be either surface or bulk erosion. The main advantages of such biodegradable systems are the elimination of the need for surgical removal, their small size and potential low cost.

- Biodegradation of unstable bonds by which the drug is coupled to the polymer system.

In these systems, the drug molecule is chemically bonded to a polymer backbone and the drug is released by hydrolytic or enzymatic cleavage. The rate of drug release is controlled by the rate of hydrolysis. This approach provides an opportunity to target the drug to a particular cell type or tissue.

*Swelling controlled systems.* Hydrogels consist of macromolecular chains cross-linked to create a tangled mesh structure, providing a matrix for the entrapment of drugs. When such hydrogels come in contact with a thermodynamically compatible solvent, polymer chains relax (Shukla *et al.*, 2003). This happens when the characteristic glass-rubber transition temperature of the polymer is below the temperature of experiments. Swelling is the macroscopic evidence of this transition. The dissolved drug diffuses into the external receiving medium, crossing the swollen polymeric layer formed around the hydrogel.

When the hydrogel contacts the release medium, the penetrant water molecules invade the hydrogel surface and thus a moving front is observed that clearly separates the unsolvated glassy polymer region ahead of the front from the swollen and rubbery hydrogel phase behind it. Just ahead of the front, the presence of solvent plasticizes the polymer and causes it to undergo a glass-to-rubber transition (Davidson & Peppas, 1986). The following possibilities arise:

- if the glass transition temperature  $T_g$  of polymer is well below the experimental temperature, the polymer will be in the rubbery state and polymer chains will have a high mobility that allows easier penetration of the solvent into the loaded hydrogel and subsequent release of the drug molecules into the release medium (Grinsted *et al.*, 1992). This clearly results in Fickian diffusion which is characterized by a solvent (or drug) diffusion rate  $R_{diff}$  slower than the polymer chain relaxation rate  $R_{relax}$  ( $R_{diff} \ll R_{relax}$ ).
- if the experimental temperature is below  $T_g$ , the polymer chains of hydrogels are not sufficiently mobile to permit immediate penetration of the solvent into the polymer core. The latter situation gives rise to a non-Fickian diffusion process which includes two cases depending on the relative rates of diffusion and chain relaxation ( $R_{diff} \gg R_{relax}$  and  $R_{diff} \sim R_{relax}$ ).

*Modulated release systems.* In these systems, the drug release is controlled by external stimuli such as temperature, pH, ionic strength, electric field, electromagnetic radiation or UV light, etc.

### 1.3.3 Polymers used in biomedical applications

Due to the intense and increasing research activity carried on both industrially and academically on polymers suitable for biomedical applications, it is difficult to identify the number of different systems relevant to time-limited applications in the field of biomaterials. Two main broad categories can be identified: synthetic polymers and naturally occurring polymers.

Among the synthetic polymers, because of the relative ease of their synthesis (via ring-opening or condensation polymerization) and commercial availability, poly( $\alpha$ -esters) have been the most heavily researched degradable biomaterials to date (Coulembier *et al.*, 2006).

*Poly(glycolic acid).* PGA can be considered one of the very first degradable polymers ever investigated for biomedical use. With a melting point ( $T_m$ ) higher than 200 °C, a glass transition temperature ( $T_g$ ) of 35–40 °C, and very high tensile strength (12.5 GPa) (Maurus & Kaeding, 2004), PGA found favor as the degradable suture DEXON<sup>®</sup>, which has been actively used since 1970 (Kats & Turner, 1970). From 1984 to 1996, PGA was marketed as an internal bone pin under the name Biofix<sup>®</sup>, but since 1996 Biofix<sup>®</sup> has been converted to a poly(L-lactide) base for better longterm stability (Burns, 1995; Reed, 1999). Because of PGA's rapid degradation and insolubility in many common solvents, limited research has been conducted with PGA-based drug delivery devices. Instead, most recent research has focused on short-term tissue engineering scaffolds and the utilization of PGA as a filler material coupled with other degradable polymer networks. Although there has been research conducted into a wide range of applications, there exists significant issues with PGA. Rapid degradation leads to the loss of mechanical strength and significant local production of glycolic acid. Although glycolic acid is bioresorbable by cells via the citric acid cycle (Gunatillake *et al.*, 2006), high level of glycolic acid have been linked to a strong, undesired inflammatory response.

*Poly(lactic acid).* As PLA possesses chiral molecules, PLAs exists in four forms: poly(L-lactic acid) (PLLA), poly(D-lactic acid) (PDLA), poly(D,L-lactic acid) (PDLLA), a racemic mixture of PLLA and PDLA, and meso-poly(lactic acid). As far as use in biomedical research, only PLLA and PDLLA have shown promise and have been extensively studied. PLLA has a  $T_g$  of 60–65 °C, a melting temperature of around 175 °C

and a mechanical strength of 4.8 GPa (Middleton & Tipton, 2000). The additional methyl group in PLA causes the polymer to be much more hydrophobic and stable against hydrolysis than PGA. High molecular weight PLLA has been shown to take greater than 5 years to be completely resorbed *in vivo* (Suuronen *et al.*, 1998). Because of the slow degradation rate, limited research has been recently conducted into drug delivery by PLLA systems alone (Zielhuis *et al.*, 2007; Lensen *et al.*, 2010). To reduce degradation time, investigators have either developed modification techniques or have blended or copolymerized PLLA with other degradable polymers.

Under the product name Fixsorb<sup>®</sup>, PLLA has been used as a bone fixator (Ueda & Tabata, 2003). PLLA has also been extensively utilized in tissue engineering applications ranging from scaffolds for bone, cartilage, tendon, neural, and vascular regeneration (Ulery *et al.*, 2011). Composite materials include PLLA combined with PDLLA, poly(lactide-co-glycolide) (PLGA), poly( $\epsilon$ -caprolactone), poly(ethylene glycol) (PEG), collagen, and chitosan (Ulery *et al.*, 2011).

PDLLA is an amorphous polymer due to the random positions of its two isomeric monomers within the polymer chain yielding a slightly lower  $T_g$  of 55–60 °C and lower mechanical strength of 1.9 GPa (Maurus & Kaeding, 2004). Although possessing more desirable degradation properties than PLLA, PDLLA still takes over a year to properly erode which has kept it from being researched as a particle-based delivery vehicle. Instead PDLLA has been commonly used as a drug delivery film for inorganic implants, or as a tissue engineering scaffold (Ulery *et al.*, 2011).

Like PLLA, PDLLA has been often combined with other degradable polymers such as PLGA, PEG, and chitosan to create composites with desirable material properties (Ulery *et al.*, 2011).

*Poly(lactide-co-glycolide)*. Random copolymerization of PLA (both L- and D,L-lactide forms) and PGA, known as PLGA, is the most investigated degradable polymer for biomedical applications and has been used in sutures, drug delivery devices, and tissue engineering scaffolds.

PLGA has been used as a suture material since 1974 (Conn *et al.*, 1974) under the product name Vicryl<sup>®</sup> (Ethicon), a 10:90 (LA/GA ratio) PLGA braided construct. More recently a modified version, Vicryl Rapide<sup>®</sup>, has come to market. Panacryl<sup>®</sup> (Ethicon) is another product which has a higher LA/GA ratio (90:10) than Vicryl<sup>®</sup> causing it to undergo less rapid degradation. Unfortunately, Panacryl<sup>®</sup> has seen a significant drop in recent use due to public concern that it induces significant inflammation after implantation even though a recent report refutes this argument (Ulery *et al.*, 2011). Although Ethicon produces the

most widely used PLGA sutures, Polysorb<sup>®</sup> (Syneture) and Purasorb<sup>®</sup> (Purac Biomaterials) are also commonly used suture materials composed of PLGA.

With rapid degradation compared to other polyesters, PLGA has been utilized extensively in drug delivery applications. PLGA has been used to deliver chemotherapeutics, proteins, vaccines, antibiotics, analgesics, anti-inflammatory drugs and siRNA (Ulery *et al.*, 2011). Most often PLGA is fabricated into microspheres, microcapsules, nanospheres, or nanofibers, to facilitate controlled delivery of encapsulated or adsorbed payloads (Ulery *et al.*, 2011). Depending on the composition of the PLGA used and the interactions between payload and polymer, drug or protein release profiles can vary (Ulery *et al.*, 2011). Unfortunately, bulk erosion of the polymer prevents significant modulation of the release rate.

PLGA demonstrates great cell adhesion and proliferation properties making it an excellent candidate for application in tissue engineering. PLGA has been fabricated into scaffolds by a number of different techniques including gas foaming, microsphere sintering, porogen leaching, electrospinning, polymer printing, or a combination of these techniques, to create unique nanostructured and microstructured materials that can facilitate tissue development (Ulery *et al.*, 2011).

*Polyhydroxyalkanoates.* Polyhydroxyalkanoates are biodegradable polyesters that can be produced by both bacterial and synthetic routes. The most common polymer in this family is poly(3-hydroxybutyrate) (PHB), a semicrystalline isotactic polymer that undergoes surface erosion due to the hydrophobicity of its backbone and its crystallinity (Abe & Doi, 1999). PHB has a  $T_g$  around 5 °C and a melting temperature from 160 to 180 °C (Zhijiang & Zhihong, 2007). Hydrolytic degradation of PHB results in the formation of D-(–)-3-hydroxybutyric acid, a normal blood constituent (Laeger *et al.*, 2010). The biocompatibility, processibility, and degradability of PHB make it an excellent candidate for use in long-term tissue engineering applications (Ulery *et al.*, 2011). Unfortunately, the stability of PHB makes it a poor candidate for controlled delivery applications.

*Poly( $\epsilon$ -caprolactone).* PCL is a semicrystalline polyester with great organic solvent solubility, a melting temperature of 55 – 60 °C and  $T_g$  -54 °C (Patlolla *et al.*, 2010). Because of PCL's very low *in vivo* degradation rate and high drug permeability, it has found favor as a long-term implant delivery device. Capronor<sup>®</sup> is a commercial contraceptive PCL product that is able to deliver levonorgestrel *in vivo* for over a year and has been on the market for over 25 years (Darney *et al.*, 1989). Current research is being conducted into the development of microsized and nanosized drug delivery vehicles, but the degradation rate (2–3 years) is a significant issue for pure PCL products to be FDA

approved for this use. Instead PCL is often blended or copolymerized with other polymers such as PLLA, PDLLA, PLGA and polyethers to expedite overall polymer erosion (Ulery *et al.*, 2011). Although somewhat limited in drug delivery applications, tissue engineering implications of PCL are numerous. PCL has low tensile strength (~ 23 MPa), but very high elongation at breakage (4700%) making it a very good elastic biomaterial (Gunatillake *et al.*, 2006). PCL's processability allows the formation of scaffolds composed of adhered microspheres, electrospun fibers, or through porous networks created by porogen leaching (Ulery *et al.*, 2011). PCL and PCL composites have been used as tissue engineering scaffolds for the regeneration of bone, ligament, cartilage, skin, nerve and vascular tissues (Ulery *et al.*, 2011).

Other interesting classes of synthetic polymers used in medicine are: polyanhydrides, polyacetals, poly(ortho esters), polycarbonates, polyurethanes, polyphosphazenes, polyphosphoesters and polyethers, among all poly(ethylene glycol) (Ulery *et al.*, 2011).

As far as the natural occurring polymers are concerned, proteins and poly(amino acids), collagen, elastin and elastin-like polypeptides, fibrin, albumin and polysaccharides of human and non-human origin, such as chitin and chitosan, have been extensively studied for biomedical applications, in some cases reaching also the global market (Ulery *et al.*, 2011).

There currently exists a wide range of degradable polymers that hold potential as biomaterials. With advancements in polymer synthesis techniques, the paradigm of utilizing a few well-characterized polymers (e.g., PLGA and collagen) for all biomedical applications has shifted to using polymers, both heavily researched and newly developed, that can fit certain niches (e.g., DNA and RNA association with phosphoesters and inherent bioactivity of chitosan) (Ulery *et al.*, 2011). In addition, the emergence of combination polymers holds promise for the creation of novel materials that possess desired properties for highly specific applications.

## 1.4 Environmental applications

Conventional polymers such as polyethylene and polypropylene persist for many years after disposal. Built for the long haul, these polymers seem inappropriate for applications in which plastics are used for short time periods and then disposed. As a matter of fact, around 10% by weight of the municipal waste stream is plastic (Barnes *et al.*, 2009).

In recent years, the recycling of plastic materials has increased, but the recycling rates for most plastics remain low (Davis & Song, 2006; Hopewell *et al.*, 2009). A large number of

different types of polymers, each of which may contain different processing additives such as fillers, colorants and plasticizers, are used for all kind of applications. These composition complexities together with contamination by food and other biological substances during use, often render recycling uneconomic, impractical and generally undesirable compared with disposal in landfill (Gross & Kalra, 2002; Song *et al.*, 2009).

There are other technologies available for the treatment of conventional plastic waste including: integrated collection and incineration with energy recovery, selective combustion of plastics with high calorific value (e.g. in cement kilns) and use as a reducing agent in blast furnaces or as feedstock for polymer synthesis (Song *et al.*, 2009).

Energy generation by incineration of plastic waste is in principle a viable use for recovered waste polymers since hydrocarbon polymers replace fossil fuels and thus reduce the CO<sub>2</sub> burden on the environment. The calorific value of polyethylene (PE) is similar to that of fuel oil and the thermal energy produced by incineration of polyethylene is of the same order as that used in its manufacture (Scott, 2000).

Incineration is the preferred energy recovery option of local authorities because they can gain financially by selling waste plastics as fuel. However, in most developed countries public distrust of incineration limits the potential of waste-to-energy technologies.

An alternative to direct incineration is to convert polymer wastes by pyrolysis or by hydrogenation to low molecular weight hydrocarbons for use either as portable fuels or as polymer feedstock. This is a highly specialized fluid-bed operation which is not appropriate for municipal waste disposal.

As a result, substantial quantities of plastic have accumulated in the natural environment and in landfills. Discarded plastic also contaminates a wide range of natural terrestrial, freshwater and marine habitats, with newspaper accounts of plastic debris on even some of the highest mountains (Thompson *et al.*, 2009).

The growing environmental awareness imposes to plastic materials both user-friendly and eco-friendly attributes. As a consequence, biodegradability is not only a functional requirement, but also an important environmental attribute.

Biodegradable polymers disposed in bioactive environments degrade by the enzymatic action of microorganisms such as bacteria, fungi, and algae. Their polymer chains may also be broken down by non-enzymatic processes such as chemical hydrolysis. Biodegradation converts them to CO<sub>2</sub>, CH<sub>4</sub>, water, biomass, humic matter, and other natural substances. Biodegradable plastics are thus naturally recycled by biological processes (section 1.1.4).

The use of biodegradable plastics is of interest specially if the products can provide economical and/or ecological benefits beyond simply “disappearing from view” by being buried in soil or incorporated into the organic waste stream.

For example, if conventional plastic garbage bags for organic waste are not to be separated from their contents in a time-consuming process, then incineration remains the only possibility for disposing of the filled bags. This makes no sense from the energy standpoint, since organic waste is about two-thirds water. If, however, a biodegradable garbage bag is used, separation is not necessary, and the organic waste together with the bag undergoes organic disposal. There are various possibilities for this approach: first of all, composting, secondly, anaerobic fermentation during which the biomass is converted into biogas (methane), providing a source of energy. In this way, biodegradable plastics represent not only a cost-effective disposal solution, but can also make an important contribution to efficient management of organic waste.

Target markets for biodegradable plastics include packaging materials (trash bags, wrappings, loose-fill foam, food containers, film wrapping, laminated paper), hygiene products (diaper back sheets, cotton swabs), consumer goods (fast-food tableware, containers, egg cartons, razor handles, toys), and agricultural tools (mulch films, pots) (Gross & Kalra, 2002).

#### *1.4.1 Packaging*

Packaging represents the largest plastic application segment covering alone almost 40% of the European converter demand (Plastics Europe, 2012).

Total plastic packaging waste generation in 2008 for the EU-27, Norway and Switzerland was approximately 15.6 Mt, with a per capita average generation of about 30.6 kg (BioIntelligence Service, 2011).

Till now, petrochemical-based plastics such as polyethylene terephthalate (PET), polyvinylchloride (PVC), polyethylene, polypropylene (PP), polystyrene (PS) and polyamide (PA) have been increasingly used as packaging materials because their large availability at relatively low cost and because their good mechanical performance such as tensile and tear strength, good barrier to oxygen, carbon dioxide, anhydride and aroma compound, heat sealability, and so on (Siracusa *et al.*, 2008). But nowadays their use has been restricted because they are not totally recyclable and/or not biodegradable so they pose serious ecological problems.

Particularly in food packaging applications, the performance expected from plastic materials is containing the food and protecting it from the environment and maintaining

food quality (Arvanitoyannis, 1999). It is obvious that to perform these functions is important to control and modify polymer mechanical and barrier properties (Figure 1.13), that consequently depend on the structure of the polymeric packaging material.

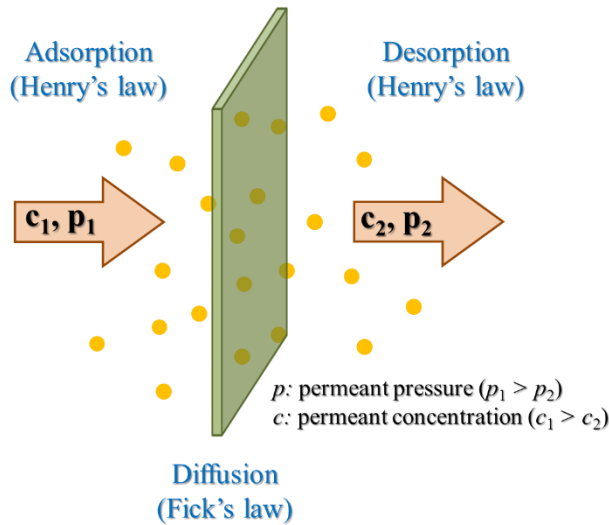


**Figure 1.13** General mechanism of gas or vapor permeation through a plastic film.

In addition, it is important to study the change that can occur on the characteristics of the plastics during the time of interaction with the food (Scott, 2000). Last but not least, the compatibility with the food plays a crucial role in this kind of application; as a matter of fact, it has been recognized as a potential source of loss in food quality properties (Halek, 1988).

The field of application of biodegradable polymers in food-contact articles includes disposable cutlery, drinking cups, salad cups, plates, overwrap and lamination film, straws, stirrers, lids and cups, plates and containers for food dispensed at delicatessen and fast-food establishments. These articles will be in contact with aqueous, acidic and fatty foods that are dispensed or maintained at or below room temperature, or dispensed at temperatures as high as 60°C and then allowed to cool to room temperature or below (Conn *et al.*, 1995).

For all these reasons, up to now, only a limited amount of biodegradable polymers have suitable properties and can be used for food packaging application. More solutions have been found for other packaging types.

Depending on the production process and on the source, biopolymers can have properties similar to traditional ones. They are generally divided into two main groups: starch-based polymer and polyesters.

#### 1.4.1.1 Starch-based polymers

Starch is an inexpensive, annually renewable material derived from corn and other crops. The biodegradation of starch products recycles atmospheric CO<sub>2</sub> trapped by starch-producing plants. All starches contain amylose and amylopectin, at ratios that vary with the starch source. This variation provides a natural mechanism for regulating starch material properties. Depending on the type of the thermoplastic starch materials, they can degrade in 5 days in aqueous aerobic environment, in 45 days in controlled compost and in water (Siracusa *et al.*, 2008).

Starch-based bioplastics can be produced by blending or mixing them with synthetic polymers. By varying the synthetic blend component and its miscibility with starch, the morphology and hence the properties can be regulated easily and efficiently. Blends containing thermoplastic starch (destructured starch that is noncrystalline, produced by the application of heat and work) may be blended or grafted with biodegradable polyesters, such as poly( $\epsilon$ -caprolactone), to increase flexibility and resistance to moisture. This approach has been successfully implemented: first attempt was successful in 1993, when LDPE-starch blends were commercialized under the trade name Ecostar<sup>®</sup>. Other commercial trade names are Bioplast<sup>®</sup> (from Biotec GmbH), NOVON<sup>®</sup> (from NOVON International) and Mater-Bi<sup>®</sup> (from Novamont). All these materials are mainly formed into films and sheets. Blends with more than 85% starch are used for foaming and injection molding. The foams can be used as loose-fill in place of polystyrene; the starch-based loose fills have an average density of 6 to 8 kg/m<sup>3</sup>, compared with 4 kg/m<sup>3</sup> for expanded polystyrene loose fill. The commercial trade names are Biopur<sup>®</sup> (from Biotec GmbH), Eco-Foam<sup>®</sup> (from National Starch & Chemical) and Envirofill<sup>®</sup> (from Norel).

Loose-fill materials from starch are generally water sensitive. This is a problem if the packaging material is exposed to water, but an advantage when down-the-drain disposal is desired.

By mixing thermoplastic starch with cellulose derivatives, rigid and dimensionally stable injection-molded articles result.

Chemically modified plant cellulose is used in a remarkably diverse set of applications. For example, cellulose acetate is used in many common applications, including toothbrush handles and adhesive tape backing. Eastman Chemical Company has developed very promising fully biodegradable cellulose acetates.

#### 1.4.1.2 Polyesters

As early as 1973, it was shown that PCL degrades when disposed in bioactive environments such as soil (Potts *et al.*, 1973; Tokiwa *et al.*, 1976; Cook *et al.*, 1981). This

and related polyesters are water resistant and may be melt-extruded into sheets, bottles, and various shaped articles, marking these plastics as primary targets for use as bioplastics. Several biodegradable polyesters are now in the market or at an advanced stage of development.

*Polyhydroxylalkanoates (PHAs)*. These polymers are produced directly from renewable resources by microbes. They can be accumulated to high levels in bacteria (about 95% of the cellular dry weight), and their structures can be manipulated by genetic or physiological strategies (Doi, 1990; Steinbuchel, 1991). The physical properties and biodegradability of PHAs can be regulated by blending with synthetic or natural polymers. The widespread synthesis of PHAs by microbes is matched by a corresponding abundance of microbes that produce PHA-degrading enzymes. PHAs with short side chains behave similarly to polypropylene, whereas PHAs with longer side chains are elastomeric.

In the late 1980s, ICI Zeneca commercialized PHAs produced by microbial fermentation under the trade name Biopol<sup>®</sup>. Wella AG used the polymer to make shampoo bottles. Biopol<sup>®</sup> was expensive, but customers accepted the price as part of an all-natural high-end cosmetic product. Such consumer behavior is unusual; in most cases, consumers are not willing to pay more for a product that is natural and/or biodegradable. Metabolix (Cambridge, MA) and Bio-on (S. Giorgio di Piano, Italy) continue to pursue the commercialization of PHAs both in plant crops and by fermentation processes.

*Poly(lactic acid) (PLA)*. The manufacture of polyester from lactic acid was pioneered by Carothers in 1932 and further developed by Dupont and Ethicon (Gross & Kalra, 2002). Prohibitive production costs restricted the applicability of these polymers outside the medical field until the late 1980s. Since then, major breakthroughs in process technology, coupled with decreased costs of biologically produced lactic acid, have led to the commercial-scale production of plastics from lactic acid for nonmedical applications. This integration of biotechnology and chemistry is an important strategy that will be critical to improvements in many other chemical processes in future years.

Two chemical routes have been developed to convert lactic acid to high molecular weight PLA. Cargill Dow LLC uses a solvent-free continuous process and a novel distillation method (Lunt, 1998). In contrast, Mitsui Toatsu (Lunt, 1998) converts lactic acid directly to high molecular weight PLA by a solvent based process with the azeotropic (where vapor and liquid have the same composition at some point in distillation) removal of water by distillation.

Upon disposal, PLA degrades primarily by hydrolysis, not microbial attack (Gross & Kalra, 2002). Hence, even at high humidity, it is uncommon to encounter contamination

of high molecular weight PLA by fungi, mold, or other microbes. This unusual characteristic of a bioplastic is attractive for applications in which they are in direct contact with foods for extended time periods. PLA can be converted into compost in municipal compost facilities. It can be thermally processed with minimal changes to standard machinery.

PLA is currently used in packaging (film, thermoformed containers, and short-shelflife bottles). Cargill Dow LLC uses conventional melt-spinning processes to form fibers for clothing and other uses (Woodings, 2001). Fabrics produced from PLA provide a silky feel, durability, and moisture-management properties (moisture is quickly wicked away from the body, keeping the wearer dry and comfortable).

*PCL and poly(alkylene succinate)s.* PCL is a thermoplastic biodegradable polyester synthesized by chemical conversion of crude oil, followed by ring-opening polymerization. PCL has good water, oil, solvent, and chlorine resistance, a low melting point, and low viscosity, and is easily processed thermally. To reduce manufacturing costs, PCL may be blended with starch for example, to make trash bags. By blending PCL with fiber-forming polymers (such as cellulose), hydro-entangled nonwovens (in which bonding of a fiber web into a sheet is accomplished by entangling the fibers by water jets), scrub-suits, incontinence products, and bandage holders have been produced (Woodings, 2001).

The rate of hydrolysis and biodegradation of PCL depends of course on its molecular weight and degree of crystallinity. However, many microbes in nature produce enzymes capable of complete PCL biodegradation.

In contrast to PCL, PLA from lactide, and PHAs, a series of biodegradable aliphatic polyesters have been developed on the basis of traditional polycondensation reactions. Most notable are the poly(alkylene succinate)s manufactured by Showa Denko, trademarked Bionolle®.

These polyesters have properties that mimic those of traditional plastics such as low-density poly(ethylene) (LDPE). Their physical properties and biodegradation kinetics depend on the choice and composition of the diol/diacid building blocks. Current uses of Bionolle® are fibers, films, bottles, and cutlery. Bionolle® plastics have been found to biodegrade in compost, moist soil, fresh water, activated sludge, and sea water.

*Aliphatic-aromatic polyesters and other copolymers.* The strength of aliphatic polymers may be increased by substituting a fraction of the ester links by amide groups, which increase interchain hydrogen bonding and, therefore, material strength. Bayer had introduced an injection-moldable grade of poly(ester amide), BAK 2195, built from

hexamethylene diamine, adipic acid, butanediol, and diethylene glycol (Grigat *et al.*, 1998), but in 2001 the company withdrew from the production and sale of this product. The strength of aliphatic polyesters can also be increased by substituting some aliphatic diacid building blocks with more rigid aromatic diacids. Eastman Chemical Company (Yamamoto *et al.*, 2002) and BASF (Witt *et al.*, 1999) have developed such aliphatic/aromatic resins that retain their biodegradability. BASF projects a double-digit growth figure for its aliphatic/aromatic resin, Ecoflex<sup>®</sup>, which is used mainly as an additive to plastics from renewable resources (for example, blended with thermoplastic starch) and as a primary component of films and laminates. Ecoflex<sup>®</sup> – PLA blends are commercialized by BASF under the trade mark Ecovio<sup>®</sup>. They are suitable for carrier and organic waste bags.

Some of the physical properties of the described polyesters are listed in Table 1.1.

At present, unfortunately, biopolymers must compete head-to-head in cost and performance with existing familiar and inexpensive products. This is extremely difficult because new processes require intensive research and large capital expenses and must be scaled-up to be economically competitive.

**Table 1.1** Physical properties of various commercial biodegradable plastics: melting temperature ( $T_m$ ), tensile stress at break ( $\sigma_b$ ), elongation at break ( $\epsilon_b$ ), tensile modulus (E) and density ( $\delta$ ).

property	PHB (Biopol)	PHB-V (Biopol)	PCL (Tone787)	PLA (Ecopia)	PBSA (Bionolle 3000)	PBS (Bionolle 1000)
$T_m$ (°C)	177	135	60	177-180	94	114
$\sigma_b$ (Mpa)	40	25	4	45	40	60
$\epsilon_b$ (%)	6	25	800-1000	3	600	800
E (Mpa)	4000	1000	386	2800	300	500
$\delta$ (g/cm <sup>3</sup> )	1.25	1.25	1.15	1.21	1.23	1.26
property	PEA (BAK1095)	Ecoflex	Ecovio C2224	EastarBio	Mater-Bi Y101U	Mater-Bi ZF 03U/A
$T_m$ (°C)	125	110-115		108		64
$\sigma_b$ (Mpa)	25	36	27-35	22	26	31
$\epsilon_b$ (%)	400	820	250-320	700	27	900
E (Mpa)	180	80	520-750	100	1700	180
$\delta$ (g/cm <sup>3</sup> )	1.07	1.25	1.25	1.22	1.35	1.23

In conclusion, on the basis of both economic and environmental considerations, the commercialization of biodegradable plastics will continue to increase especially in those markets where products have a relatively short-use lifetime.

#### *1.4.2 Agricultural applications*

In agriculture, plastics have largely replaced glass in greenhouses and cloches and they have gained a unique position in the growing of soft fruits and vegetables over very thin polymers (mulching films).

The current intensive and semi-intensive agricultural practices used throughout Europe require indeed the use of large quantities of plastics. In 2004, the consumption of plastic materials for agricultural applications reached 615000 t/year. Most recent data suggest that agriculture and horticulture are responsible for a consumption of about 1500000 t/year of all polymers in Europe. Concerning the category of thin films, more than 130000 t/year mulching films are consumed per year in Europe and 2600000 t/year worldwide (2003–2005 data). The consumption of direct cover and low tunnel films in Europe are 72000 and 75000 t/year, respectively (Briassoulis & Dejean, 2010).

This extensive use of plastics, usually polyethylene, whose lack in biodegradability is well-known, results in increased accumulation of plastic waste in rural areas.

Part of this plastic waste may be recycled, especially the greenhouse films, silage films and fertilizer sacks, pipes and other plastic products. Another part of the agricultural plastic waste is difficult to recycle for technical and/or financial reasons.

The most common current disposal practices for the non-recyclable, but in many cases also for recyclable agricultural plastic wastes, is burying in the soil (mulching films), burning, or disposing them at the open fields or in landfills (Briassoulis & Dejean, 2010). These practices are of course illegal and have serious negative consequences for the environment, for the health of the farmers and consumers and the quality and the market value of the agricultural products.

However, the process of recovering and recycling those plastics, following the end of the cultivation period, is very difficult as approximately 80% of the weight of the recovered waste mulching film is foreign materials (e.g. soil, sand etc.) (Briassoulis & Dejean, 2010). Also the cost of removing from the soil and cleaning this material is prohibitively high (Hiskakis & Briassoulis, 2006).

Specifically for the case of agricultural plastic wastes that cannot be easily collected and recycled, a very attractive alternative is biodegradation. This refers to the replacement of

conventional agricultural plastics, which cannot be recovered from the field, with biodegradable ones, which will biodegrade in the soil after the end of their useful lifetime. To this purpose, partially biodegradable films or even films of controlled photodegradation followed by a questionable fate in the soil (Kyrikou & Briassoulis, 2007; Feuilloley, 2004; Fritz, 2003; Scott & Gilead, 1995) have been introduced and used in agricultural applications. The addition of pro-oxidants in polyethylene films accelerates the breakdown of polyethylene to very small fragments (this is why these materials are also known as fragmentable).

Three major photodegradable products available on the market were Plastigone<sup>®</sup>, an ultraviolet-activated, time-controlled degradable plastic; Biolan<sup>®</sup>, an agricultural mulch film designed to photodegrade according to a predetermined schedule into harmless particles, which then biodegrade into carbon dioxide; and Agplast<sup>®</sup>, a photodegradable material made by Lecofilms (Lamont & Marr 1990; Clough & Reed 1989; Sanders *et al.* 1989; Kostewicz & Stall 1989; Johnson 1989).

All photodegradable polyethylene films can be degraded to stage V, which means that almost no film exists on the surface of the ridges 2–3 months after the induction periods (Kasirajan & Ngouajio, 2012), but biodegradability of such materials is still strongly disputed (Briassoulis & Dejean, 2010).

The controversy over these materials is based on the following considerations: degradation/fragmentation represent only the first (preliminary) stage of the biodegradation process. Heat, moisture, sunlight and/or enzymes shorten polymer chains in this stage, resulting in fragmentation residues and cross-linking to create more intractable persistent residues. On the other hand, biodegradation is the second stage of this process and it is considered to occur only if the fragmented residues are totally consumed by microorganisms as a food and energy source and if this happens in an acceptable rate. Biodegradation of the fragments of photodegradable polymers based on polyethylene with pro-oxidants, remains however an open question as it has not been proven beyond any doubt (Briassoulis & Dejean, 2010; Feuilloley *et al.*, 2005).

For example, Feuilloley *et al.* (2005) studied the biodegradability of three different commercial mulch films: a 50 µm thick Mater-Bi<sup>®</sup> film, a PCL/starch blend (60:40, w/w), a 60 µm thick Ecoflex<sup>®</sup> film, an aliphatic-aromatic copolyester, and a 36 µm thick Actimais<sup>®</sup> film (from SMS Trioplast), which is made of polyethylene containing prooxidant additives. The study concludes that a very low degree of biodegradation of the commercial polyethylene films is achieved under those experimental conditions and that

cross-linked polyethylene micro-fragments are remaining in soil for a very long period of time.

Therefore, photodegradable plastic mulches even if effective, have proven to be unreliable as well as expensive to use (Greer & Dole, 2003).

Also oxodegradable materials (polymer to which small amount of salt has been added to speed up the oxidative process) do not solve the pollution problem; as a matter of fact they behave similarly to photodegradable materials, i.e., the buried part does not suffer degradation and needs to be exposed to light and air because the degradation of oxobiodegradable plastics is a result of oxidative and cell-mediated phenomena, either simultaneously or successively. Oxodegradable polymers do break down into small fragments over time, but cannot be considered biodegradable since they do not meet the degradation rate or the residual-free content specified in the ASTM D6400 standards (Kasirajan & Ngouajio, 2012).

In conclusion, fully biodegradable and compostable plastics remain the only real choice and ultimate solution.

Polyesters and starch-based polymers play a predominant role also in this field of application. Nowadays, materials such as PLA, PBS, PCL, or poly(butylene adipate/terephthalate) (Ecoflex<sup>®</sup>) are being adopted as biodegradable mulch sheets (Kyrikou & Briassoulis, 2007; Shah *et al.*, 2008). A particular formulation of Ecovio<sup>®</sup> is also used for agricultural mulching films.

Starch-based mulch films have become quite popular too, because starch is an inexpensive and abundant natural polymer that can produce a film structure (Liu, 2005; Guilbert & Gontard, 2005); in fact it can readily be cast into films via a process called gelatinization (Kasirajan & Ngouajio, 2012).

PLA is often blended with starch to increase biodegradability and reduce costs. However, the brittleness of the starch-PLA blends is a major drawback in many applications. To remedy this limitation, a number of low molecular weight plasticizers such as glycerol, sorbitol, and triethyl citrate are used (Kasirajan & Ngouajio, 2012). Also polyvinyl alcohol showed excellent compatibility with starch, therefore several such blends have been developed and tested for biodegradable packaging applications and appear to have potential for use as agricultural mulch film (Tudorachi *et al.*, 2000).

Other more environmentally friendly alternatives for mulching, like the use of materials of plant origin (e.g., straw), or paper, carry associated disadvantages (Martin-Closas *et al.*, 2003) and have poorer agronomical properties.

Unfortunately, while some progress has been made with the expansion of the use of bio-based and biodegradable (compostable) packaging materials, the development, use and expansion of bio-based and biodegradable materials and products in the European Agriculture is very much limited; the current use of biodegradable, mainly bio-based, plastics in agricultural applications in Europe is in fact about 2000 t/year (Briassoulis & Dejean, 2010). The two main reasons for this hysteresis are (a) the current cost of the bio-based and biodegradable plastics compared to the conventional ones in certain applications, and (b) the still open discussion with regard to testing agricultural biodegradable plastics for biodegradation in soil and under farm composting. The second one hinders the development of a relevant certification and labeling scheme which could be implemented, for example, in synergy with the recently developed labeling scheme for agricultural plastic wastes (Briassoulis & Dejean, 2010). As a matter of fact, no European standard is available today concerning the testing of a biodegradable polymer for biodegradation in soil.

However, the use of biodegradable polymers for agricultural plastics is increasing for specific applications in the agricultural sector (Nayak, 1999; Gross & Kalra, 2002; Wang *et al.*, 2003). Such applications mainly concern mulching films, but also plant pots, guide strings/nets for climbing plants, nets for agriculture and forestry (including animal nets), compost bags etc. (Briassoulis, 2004).

2.

Aim of the work

Biodegradable polymers for short time applications in different fields such as surgery, pharmacology, agriculture and the environment have attracted much interest all over the world. The reason behind this growing interest is the incompatibility of the polymeric wastes with the environment where they are disposed after usage. The recovery of the wastes as a solution to this problem is not easy or feasible, like in surgery for obvious reasons, or in the environment in the case of litter. The development of novel biodegradable polymers satisfying the requirement of degradability, compatibility with the disposed environment and release of low-toxicity degradation products is the ultimate solution to these issues. The recent technological advances offer great promise towards achieving biodegradability with less pollutants and greenhouse emissions. Linking performance with cost is a tremendous task which needs imaginative steps in the selection of materials, processes, product structures and production schedules.

To date, synthetic aliphatic polyesters represent one of the most economically competitive biodegradable polymers (Tserki *et al.*, 2006). In addition, they have attracted considerable attention as they combine the afore mentioned features with interesting physical and chemical properties.

Among aliphatic polyesters, poly(butylene succinate) (PBS) is one of the most representative, generally acknowledged and extensively used polymers. Moreover, it is characterized by good mechanical properties and thermal stability, even though it exhibits a slow biodegradation rate mainly due to its high crystallinity degree (Papageorgiou & Bikiaris, 2007).

It is also worth remembering that PBS and poly(butylene succinate adipate) copolymers are commercialized by Showa Denko, under the trademark Bionolle®.

Poly(butylene 1,4-cyclohexanedicarboxylate) (PBCE) is another very interesting member of aliphatic polyesters, since it contains an aliphatic ring in the monomeric unit, whose stereochemistry strongly influences the final properties of the material. In particular, the *trans* stereoisomer is less flexible and more symmetrical than the *cis* one and tends to improve chain packing, capacity to crystallize and crystal perfection (Berti *et al.*, 2008a; 2008b). The presence of the aliphatic ring along the polymer backbone enables the material to have high melting point, good thermal stability, even higher than poly(butylene terephthalate) (PBT) (Berti *et al.*, 2008b), to show interesting mechanical properties and to maintain biodegradability (Berti *et al.*, 2010). Moreover, aliphatic ring containing polyesters are characterized by good resistance to weather, heat, light and moisture (Berti *et al.*, 2008a).

Biodegradable polymers available today on the market lack in versatility, do not fulfilling all the requirements for a wide range of possible uses. In this view, copolymerization is the most interesting tool to tailor materials which display the right combination of properties for the desired application.

A simple copolymerization strategy to synthesize new biodegradable polymers is undoubtedly the reactive blending approach. It consists of simply mixing two or more homopolymers in the molten state in the presence of a catalyst. In this economic and solvent-free synthetic route, exchange reactions among functional groups belonging to the different homopolymers lead to the formation of multiblock copolymers.

Through reactive blending, and more generally through copolymerization, it is possible to obtain a new class of polymers with a broad range of properties depending on the kind, relative amount and distribution of the comonomeric units along the polymer chain.

Lastly, copolymerization represents also an efficacious way of promoting the biodegradability of a polymer and this is basically attributed to the limited copolymer crystallinity (Rizzarelli *et al.*, 2004).

In this framework, the present research work focused on the synthesis and characterization of novel PBS and PBCE-based fully aliphatic polyesters and copolyesters, whose syntheses have been conducted through reactive blending or copolycondensation. In particular, ether-oxygen and sulphur atoms have been introduced along the polymeric chain.

By varying the mutual ratio of comonomeric units, random copolymers of different compositions have been obtained through copolycondensation, while a modulation of the reaction time during reactive blending allowed the formation of block copolymers with fixed molar composition, but different and tailored molecular architectures.

The presence along the polymer chains of etheroatoms can have different effects:

- the glass transition temperature can vary depending on which of the two following effects prevails:
  - the polymer chain becomes more flexible ( $T_g$  decreases);
  - the polymer chain mobility decreases, because of the stronger interchain interactions ( $T_g$  increases).

As reported in literature (Korshak & Vinogradova, 1965), usually the first effect prevails when etheroatoms are introduced along the polymeric chain of aromatic polyesters, and probably more generally in the presence of rigid rings. On the contrary, the second effect is predominant in the case of aliphatic polymers.

- the melting point and the ability to crystallize decrease, due to a reduction of the chain symmetry;
- the hydrophilic character of the polymer increases due to the higher electronegativity of O and S with respect to C atoms, which give rise to the formation of C-O and C-S polar bonds.

Moreover, a comparison between oxygen or sulphur-containing polyesters can be made:

- the larger dimensions of sulphur atoms with respect to the oxygen ones, thus S-C bonds longer than the O-C ones, make the polymer chains more flexible;
- the lower electronegativity of sulphur atoms with respect to the oxygen ones, gives rise to less polar C-S bonds and therefore to weaker interchain interactions.

All these characteristics significantly influence the final properties of the investigated polyesters such as tensile strength, barrier properties, biodegradability and biocompatibility.

The research activity here presented consisted of the following steps:

- careful bibliographic research to get the state of the art on the subject;
- screening and optimization of the reaction conditions;
- molecular, physico-chemical and mechanical characterization of the synthesized polymers;
- analysis of the biodegradability under various environments and conditions.

Moreover, in the case of environmental applications, analysis of the barrier properties and eco-toxicological assessments have been conducted, while for biomedical applications studies of biocompatibility and of release of a model molecule have been carried out.

3.

Materials  
& Methods

### 3.1 Materials

All the reagents (Figure 3.1) were purchased from Sigma Aldrich (Milan, Italy). Dimethylsuccinate (DMS), dimethyl *trans*-cyclohexane-1,4-dicarboxylate (DMCED), diglycolic acid (DGA), thiodiglycolic acid (TDGA), 1,4-butanediol (BD), diethylene glycol (DEG), thiodiethylene glycol (TDEG) and triethylene glycol (TEG) were reagent grade products and were used without any further purification. The catalyst employed for all the syntheses, titanium tetrabutoxide ( $\text{Ti}(\text{OBu})_4$ ) (Sigma-Aldrich), was on the contrary distilled before use.

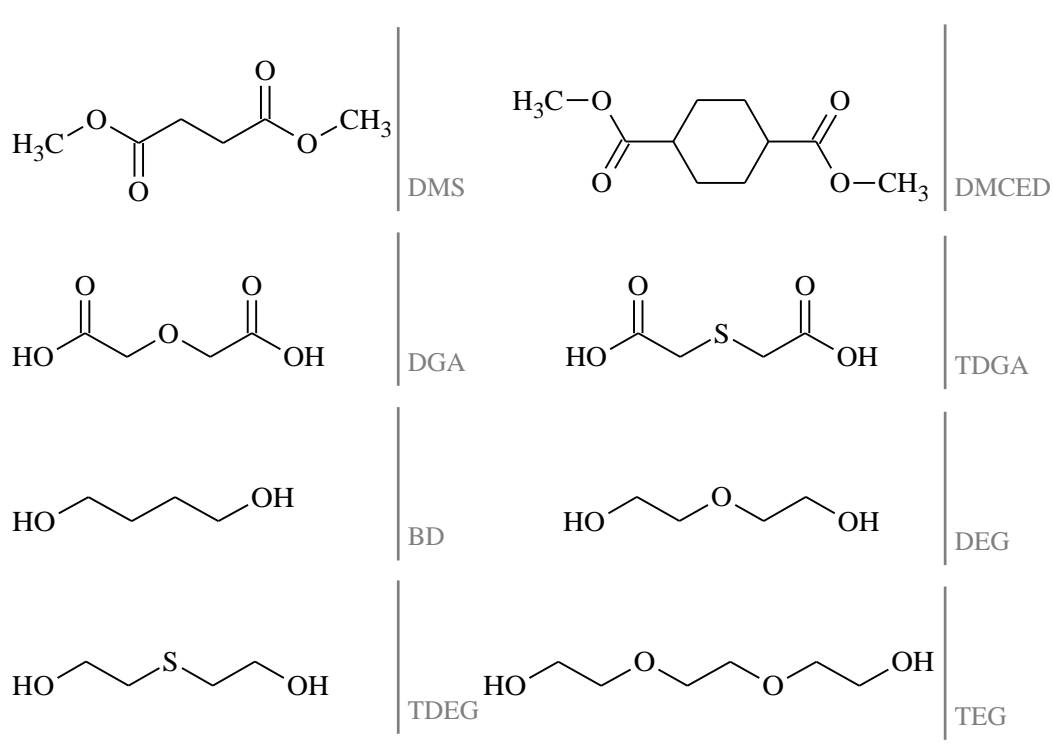


**Figure 3.1**  
Reagents employed in the polymer syntheses.

### 3.2 Synthesis of homopolymers

Homopolymers were synthesized in bulk starting from the appropriate monomers (using 20% mol excess of the glycol with respect to dimethylester/dicarboxylic acid), employing  $\text{Ti}(\text{OBu})_4$  as catalyst (about 150 ppm of Ti/g of theoretical polymer). The syntheses were carried out in a 250 mL stirred glass reactor, with a thermostatted silicon oil bath; temperature and torque were continuously recorded during the polymerization (Figure 3.2).

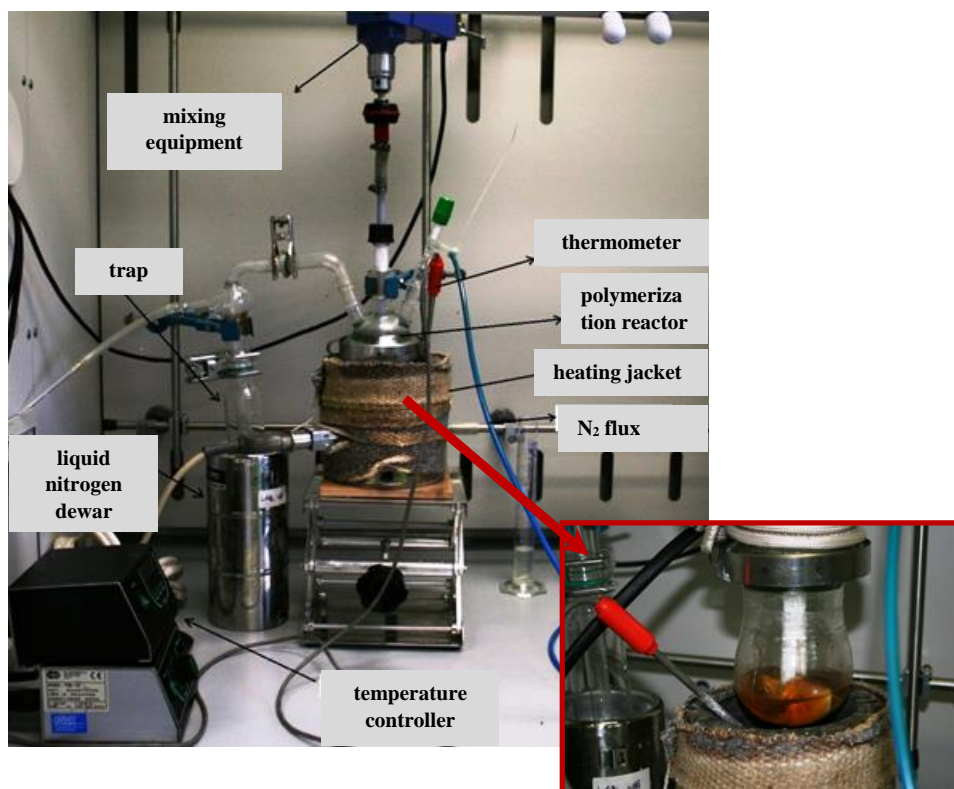


**Figure 3.2**  
Polycondensation  
equipment.

**Table 3.1** Reagents and operating conditions employed for homopolymer syntheses.

polymer	dimethylester / dicarboxylic acid	glycol	T <sub>1</sub> <sup>st</sup> stage (°C)	T <sub>2</sub> <sup>nd</sup> stage (°C)
<i>poly(butylene succinate) (PBS)</i>	DMS	BD	180	230
<i>poly(diethyleneglycol succinate) (PDGS)</i>	DMS	DEG	180	230
<i>poly(thiodiethyleneglycol succinate) (PTDGS)</i>	DMS	TDEG	180	230
<i>poly(triethyleneglycol succinate) (PTES)</i>	DMS	TEG	180	230
<i>poly(butylene cyclohexanedicarboxylate) (PBCE)</i>	DMCED	BD	180	250
<i>poly(triethyleneglycol cyclohexanedicarboxylate) (PTECE)</i>	DMCED	TEG	180	250
<i>poly(butylene diglicolate) (PBDG)</i>	DGA	BD	180	200
<i>poly(butylene thiodiglicolate) (PBTDG)</i>	TDGA	BD	180	200

The polymers were prepared according to the usual two-stage polymerization procedure. In the first stage, under pure nitrogen flow, the temperature was raised to 180°C and maintained there for until more than 90% of the theoretical amount of methanol was distilled off (about 2 hours). In the second stage the pressure was reduced to about 0.1 mbar, in order to facilitate the removal of the glycol in excess and the temperature was risen to 200-250°C (Table 3.1); the polymerizations were carried out until a torque constant value was measured.

### 3.3 Synthesis of copolymers

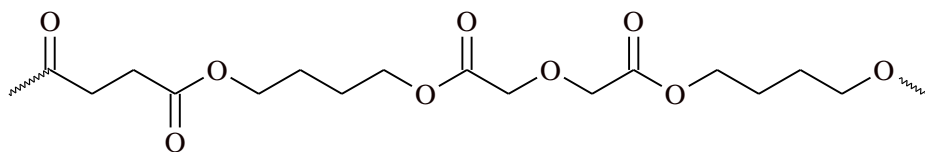
#### 3.3.1 Polycondensation

Random copolymers were synthesized in bulk starting from the appropriate monomers (using 20% mol excess of the glycol with respect to dimethylester/dicarboxylic acid), employing  $\text{Ti}(\text{O}i\text{Bu})_4$  as catalyst (about 150 ppm of Ti/g of theoretical polymer). The syntheses were carried according to the procedure described above for homopolymers (Chapter 3.2). Depending on the synthesized copolymers, different ratios of the two diols or dimethylesters / dicarboxylic acids have been employed in order to obtain copolymers of variable compositions.

Three different classes of random copolymers were synthesized by polycondensation:

- poly(butylene succinate/diglycolate)s  
(P(BS $x$ BDG $y$ ))
- poly(butylene cyclohexanedicarboxylate/diglycolate)s  
(P(BCE $x$ BDG $y$ ))
- poly(butylene/triethylene cyclohexanedicarboxylate)s  
(P(BCE $x$ TECE $y$ ))

where  $x$  and  $y$  represent the mol% of the two different comonomeric units. The chemical structures of copolymers are reported in Figure 3.3, while details on operative conditions are reported in Table 3.2.



P(BS $x$ BDG $y$ )

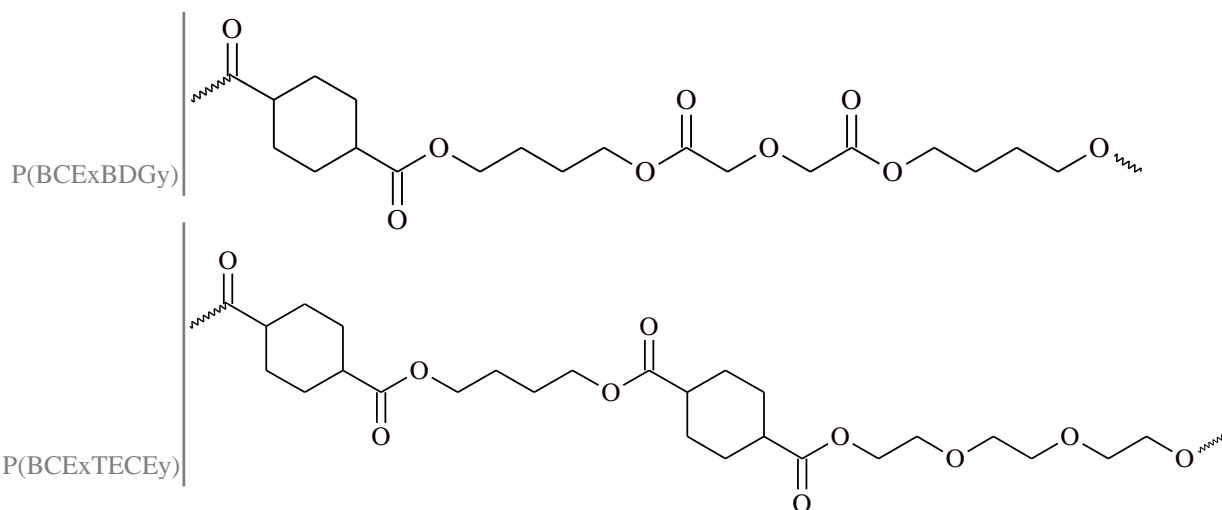


**Figure 3.3** Chemical structure of P(BSxBDGy), P(BCExBDGy) and P(BCExTECEy) random copolymers.

**Table 3.2** Reagents and operating conditions employed for the syntheses of random copolymers.

copolymer	dimethylester / dicarboxylic acid		glycol		T <sub>1</sub> <sup>st</sup> stage (°C)	T <sub>2</sub> <sup>nd</sup> stage (°C)
	1	2	1	2		
P(BSxBDGy)	DMS	DGA	BD	/	180	220
P(BCExBDGy)	DMCED	DGA	BD	/	180	220
P(BCExTECEy)	DMCED	/	BD	TEG	180	250

### 3.3.2 Reactive blending

Various multiblock copolyesters (Figure 3.4) were obtained by melt mixing of two parent homopolymers (Table 3.3). These latter were mixed in a 1:1 molar ratio in a 200-mL glass reactor, with mixing rate of 100 rpm, at 225-235°C under dry nitrogen atmosphere to prevent thermal degradation. During the process, samples were taken from the reactor at different reaction times and cooled in air. Copolymer formation was catalysed by the residual catalyst (Ti(OBu)<sub>4</sub>) present in the two parent homopolymers. In Figure 3.3 the chemical structures of copolymers under investigation are reported; m and n represent the average block length of the two comonomeric units.

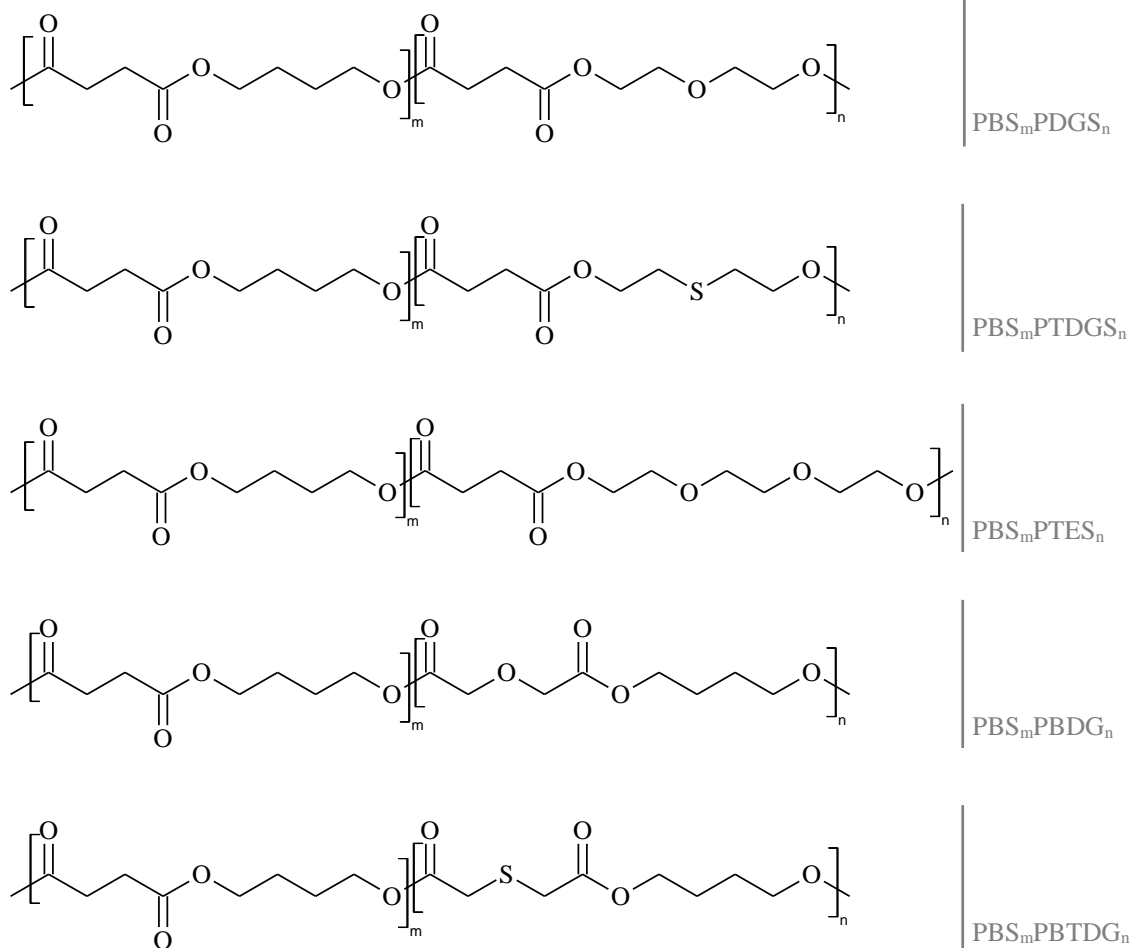


**Figure 3.4** Chemical structure of the synthesized block copolymers.

**Table 3.3** Operating conditions employed for the syntheses of block copolymers.

copolymer	homopolymer 1	homopolymer 2	$T_{\text{mix}}$ (°C)
<i>PBS<sub>m</sub>PDGS<sub>n</sub></i>	PBS	PDGS	225
<i>PBS<sub>m</sub>PTDGS<sub>n</sub></i>	PBS	PTDGS	225
<i>PBS<sub>m</sub>PTES<sub>n</sub></i>	PBS	PTES	225
<i>PBS<sub>m</sub>PBDG<sub>n</sub></i>	PBS	PBDG	225
<i>PBS<sub>m</sub>PBTDG<sub>n</sub></i>	PBS	PBTDG	225

### 3.4 Film preparation

Films (0.2 mm thick) of the various semicrystalline polymers were obtained by compression moulding. The polymeric powders were placed between thin Teflon plates (0.3 mm thick), with an appropriate spacer, and heated at  $T = T_m + 40^\circ\text{C}$  for 2 min under a pressure of 2 ton/m<sup>2</sup>. Hot-pressed films were cooled down to room temperature by cooling water.

Prior to characterization and degradation tests, films were kept under ambient temperature for at least 2 weeks in order to attain equilibrium crystallinity.

### 3.5 Scaffold fabrication

Some of the synthesized polymers were subjected to electrospinning in order to realize 3D-scaffolds to be employed in tissue engineering (Table 3.4).

**Table 3.4** Electrospinning operating conditions.

<i>polymer</i>	<b>Fiber size and layout</b>	<b>voltage</b> (kV)	<b>solvent (conc.)</b>	<b>flowrate</b> (ml/h)	<b>D (cm)</b>
<i>PBS</i>	random sub-microfibers	14	DCM:2-CE (80:20) (23%)	0.6	15
<i>PBSPBDG5</i>	random microfibers	20	HFIP (25%)	0.3	15
<i>PBSPBTDG10</i>	random microfibers	19	HFIP (25%)	0.5	15
<i>PBSPBDG20</i>	random microfibers	17	DCM:2-CE (90:10) (35%)	0.6	20
<i>PBSPBDG20</i>	random sub-microfibers	22	HFIP (25%)	0.5	15
<i>PBSPBTDG45</i>	random sub-microfibers	23	HFIP (25%)	0.5	15
<i>PBS</i>	random sub-microfibers	18	HFIP (15%)	0.3	15
<i>P(BS80BDG20)</i>	random sub-microfibers	18	HFIP (16%)	2.0	15
<i>PBCE</i>	random sub-microfibers	14	TFE (20%)	1.2	20
<i>PBCE</i>	aligned sub-microfibers	14	TFE (20%)	1.2	20
<i>PBCE</i>	aligned microfibers	15	TFE (30%)	1.2	20
<i>P(BCE80TECE20)</i>	random sub-microfibers	16	TFE:DMAC (90:10) (22%)	0.6	20
<i>P(BCE80TECE20)</i>	aligned sub-microfibers	16	TFE:DMAC (90:10) (22%)	0.6	20
<i>P(BCE80TECE20)</i>	aligned microfibers	13	TFE (22%)	1.2	20
<i>P(BCE70TECE30)</i>	random sub-microfibers	18	TFE (21%)	0.6	20
<i>P(BCE70TECE30)</i>	aligned sub-microfibers	18	TFE (20%)	0.6	20
<i>P(BCE70TECE30)</i>	aligned microfibers	14	TFE (24%)	2.4	15

Electrospun mats were fabricated in the labs of Ciamician Department, University of Bologna and of Institute for Biomedical Technology and Technical Medicine, University of Twente, thanks to the scientific collaborations with Dr. Maria Letizia Focarete and Dr. Lorenzo Moroni, respectively.

In particular, the following copolymeric systems have been taken into consideration:

- a. PBS, PBSPBDG and PBSPBTDG blends and long block copolymers
- b. PBS and PBS80PBDG20 random copolymer
- c. PBCE, P(BCE80TECE20) and P(BCE70TECE30) random copolymers

3D-scaffolds were produced by means of an handmade electrospinning apparatus, comprised of a high-voltage power supply (SL 50 P 10/CE/230; Spellman), a syringe pump (KD Scientific 200 series), a glass syringe, and a stainless steel blunt-ended needle (inner diameter = 0.84 mm) connected with the power supply electrode and a grounded alluminium plate-type collector (7 cm x 7 cm). Polymer solution was dispensed through a Teflon tube to the needle which was placed vertically on the collecting plate at a measured distance ( $D$ ). The scaffolds were produced at room temperature and a relative humidity of  $40\% \pm 5\%$ . Operating conditions for each polymer are reported in Table 3.4. Electrospun mats were kept under vacuum over  $P_2O_5$  at room temperature overnight to remove residual solvents.

## 3.6 Molecular characterization

### 3.6.1 Nuclear magnetic resonance (NMR)

The polymer structure and actual copolymer composition were determined by means of  $^1H$ -NMR spectroscopy, whereas the distribution of the comonomeric sequences along the polymer chain was evaluated by means of  $^{13}C$ -NMR spectroscopy. The samples were dissolved in chloroform- $d$  solvent with 0.03% (v/v) tetramethylsilane (TMS) added as an internal standard.  $^1H$ -NMR spectra were recorded at room temperature for solutions with a polymer concentration of 0.5 wt% (a relaxation delay of 1 s, an acquisition time of 1 s and up to 64 repetitions).  $^{13}C$ -NMR spectra were obtained using 5 wt% solutions and a full decoupling mode with a NOE effect (a relaxation delay of 2 s, an acquisition time of 1 s and up to 512 repetitions). A Varian INOVA 400 MHz instrument was employed for the measurements.

Information on the arrangement of the comonomeric units in the main chain of copolymers can be deduced by the degree of randomness  $b$ , which has been determined by  $^{13}C$ -NMR spectroscopy. It has to be emphasized that  $b$  is equal to 1 for random copolymers, equal to

2 for alternate copolymers, closed to zero for physical blends and between 0 and 1 for block copolymers.

The calculation of  $b$  has been carried out taking into consideration the resonance peaks of the carbon atoms of the common subunit between the two comonomeric units (X and Y), so it can be expressed:

$$b = P_{X-Y} + P_{Y-X} \quad [51]$$

where  $P_{X-Y}$  and  $P_{Y-X}$  are the probability of finding a X unit next to a Y unit and the probability of finding a Y unit next to a X unit, respectively.

The two probabilities can be expressed as:

$$P_{X-Y} = \frac{(I_{X-Y} + I_{Y-X})/2}{(I_{X-Y} + I_{Y-X})/2 + I_{X-X}} \quad [52]$$

$$P_{Y-X} = \frac{(I_{Y-X} + I_{X-Y})/2}{(I_{Y-X} + I_{X-Y})/2 + I_{Y-Y}} \quad [53]$$

where  $I_{X-Y}$ ,  $I_{Y-X}$ ,  $I_{X-X}$  and  $I_{Y-Y}$  represent the integrated intensities of the resonance signals of X-Y, Y-X, X-X, and Y-Y sequences, respectively.

Additionally, the average length of the sequences of the two different comonomeric units are defined as:

$$L_X = 1/P_{X-Y} \quad [54]$$

$$L_Y = 1/P_{Y-X} \quad [55]$$

### 3.6.2 Gel permeation chromatography (GPC)

Molecular weight data were obtained by gel-permeation chromatography (GPC) at 30°C using a 1100 Hewlett Packard system equipped with a PL gel 5m MiniMIX-C column (250 mm/4.6 mm length/i.d.) and a refractive index detector. In all cases, chloroform was used as eluent with a 0.3 mL min<sup>-1</sup> flow and sample concentrations of about 2 mg mL<sup>-1</sup> were applied. Polystyrene standards in the range of molecular weight 2000–100000 were used.

## 3.7 Thermal characterization

### 3.7.1 Thermogravimetric analysis (TGA)

Thermogravimetric analysis was carried out both in air and under nitrogen atmosphere using a Perkin Elmer TGA7 apparatus (gas flow: 30 mL/min) at 10°C/min heating rate up to 900 °C. The procedure suggested by the supplier was followed for the temperature calibration of equipment. This method is based on the change of the magnetic properties

of two metal samples (Nickel and Perkalloy) at their Curie points (354.0 and 596.0°C, respectively).

### 3.7.2 Differential scanning calorimetry (DSC)

Calorimetric measurements were carried out by means of a Perkin Elmer DSC7 instrument equipped with a liquid sub ambient accessory and calibrated with high purity standards (indium and cyclohexane). With the aim of measuring the glass transition and the melting temperatures of the polymers under investigation, the external block temperature control was set at -120°C and weighed samples of c.a. 10 mg were encapsulated in aluminium pans and heated up to 40°C above fusion temperature at a rate of 20°C/min (first scan), held there for 3 min, and then rapidly quenched (about 100°C/min) to -80°C. Finally, they were reheated from -80°C to a temperature well above the melting point of the sample at a heating rate of 20°C/min (second scan). The glass-transition temperature  $T_g$  was taken as the midpoint of the heat capacity increment  $\Delta c_p$  associated with the glass-to-rubber transition. The melting temperature ( $T_m$ ) and the crystallization temperature ( $T_c$ ) were determined as the peak value of the endothermal and the exothermal phenomena in the DSC curve, respectively. When multiple endotherms were observed, the highest peak temperature was taken as  $T_m$ . The specific heat increment  $\Delta c_p$ , associated with the glass transition of the amorphous phase, was calculated from the vertical distance between the two extrapolated baselines at the glass transition temperature. The heat of fusion ( $\Delta H_m$ ) and the heat of crystallization ( $\Delta H_c$ ) of the crystal phase were calculated from the total areas of the DSC endotherm and exotherm, respectively. In order to determine the crystallization rate under non-isothermal conditions, the samples were heated at 20°C/min to about 40°C above fusion temperature, kept there for 3 min and then cooled at 5°C/min. The temperature corresponding to the maximum of the exothermic peak in the DSC cooling-curve ( $T_{cc}$ ) has been correlated to the crystallization rate.

## 3.8 Wide-angle X-ray diffraction (WAXD)

X-ray diffraction (XRD) patterns of polymeric films were carried out by using a PANalytical X'PertPro diffractometer equipped with a fast solid state X'Celerator detector and a copper target ( $\lambda = 1.5418 \text{ \AA}$ ). Data were acquired in the 5-60°  $2\theta$  interval, by collecting 100 s at each 0.10° step. The indices of crystallinity ( $X_c$ ) were evaluated from the XRD profiles by the ratio between the crystalline diffraction area ( $A_c$ ) and the total area of the diffraction profile ( $A_t$ ),  $X_c = A_c/A_t$ . The crystalline diffraction area has been

obtained from the total area of the diffraction profile by subtracting the amorphous halo. The amorphous portion was modelled as bell shaped peak baseline. The non-coherent scattering was taken into consideration.

The crystal sizes were calculated by using the Scherrer method from the broadening at half the maximum intensity of an appropriate peak for each crystalline phase under investigation. The shape factor was chosen 1.0 and the instrumental broadening was taken in the due account.

### **3.9 Mechanical characterization**

Stress-strain measurements were performed using an Instron 4465 tensile testing machine equipped with a 100N load cell, on rectangular films (5 mm wide and 0.2 mm thick). The gauge length was 20 mm and the cross-head speed was 5.0 mm/min. Load-displacement curves were obtained and converted to stress-strain curves. Tensile elastic modulus was determined from the initial linear slope of the stress-strain curve. At least six replicate specimens were run for each sample and the results were provided as the average value  $\pm$  standard deviation.

### **3.10 Surface wettability**

Static contact angle measurements were performed on polymer films by using a KSV CAM101 instrument at ambient conditions by recording the side profiles of deionized water drops for image analysis. Five drops were observed on different area for each film and contact angles were reported as the average value  $\pm$  standard deviation.

### **3.11 Hydrolytic degradation tests**

Hydrolytic degradation studies were carried out in duplicate on rectangular hot-pressed polymer films (5 x 40 mm, 200  $\mu\text{m}$  thick). Films were individually immersed in phosphate buffered solution (0.1 M, pH = 7.4) and incubated in a SW22 Julabo shaking water bath at 37°C and 50 rpm. The buffer solution was periodically changed to keep the pH constant during the entire time scale of the degradation experiments.

### **3.12 Enzymatic degradation tests**

Enzymatic hydrolysis tests were performed in duplicate on rectangular hot-pressed polymer films (10 x 35 mm, 200  $\mu\text{m}$  thick) by incubating them under sterile conditions in

5 mL of 0.1 M phosphate buffer solution in the presence and absence (negative control) of the enzyme. Incubation was performed in 10 mL screw-cap glass vials secured horizontally on an orbital lab-shaker at 80 rpm. Films were periodically removed from the incubation solution for film opacity measurement, weight loss determination and/or molecular and thermal characterization. When film opacity measurements only were performed, films were placed back into the incubation solution; in the other cases sacrificial samples were used.

To optimize the biodegradation test conditions, different incubation temperatures (25°C, 30°C, 37°C), enzyme concentrations (25, 50 or 100 U/mL in 0.1M phosphate buffer at pH 7.4) and pH values (from 6.3 to 7.4) were considered. Enzyme solutions were prepared according to the unit amount per mg of solid declared by the enzyme provider.

During long lasting incubations, enzyme solutions were replaced periodically according to the stability of the enzyme, to avoid incubation in the presence of residual enzyme activity lower than 70%. To determine the stability of lipase, the enzyme was incubated under the conditions used in the film enzymatic degradation test and its residual activity in time was measured by the titrimetric method (Peled and Krenz). The test used a CO<sub>2</sub>-free substrate solution containing 4 g/l glyceryl trioleate, Triton X-100 (12% v/v) and 0.86 M NaCl; enzyme activity was expressed against a reagent blank as the rate of 0.01 N NaOH addition (µl per minute per mg of solid added to the reaction mixture) required to maintain pH constant at 7.7, as described elsewhere. Half-life of enzyme was calculated according to a 2<sup>nd</sup> order kinetic ( $r^2=0.95$ ) as  $t_{1/2} = 1/(A_i \times k)$ , where  $A_i$  is the initial activity and  $k$  the kinetic constant.

#### 3.12.1 Opacity assay

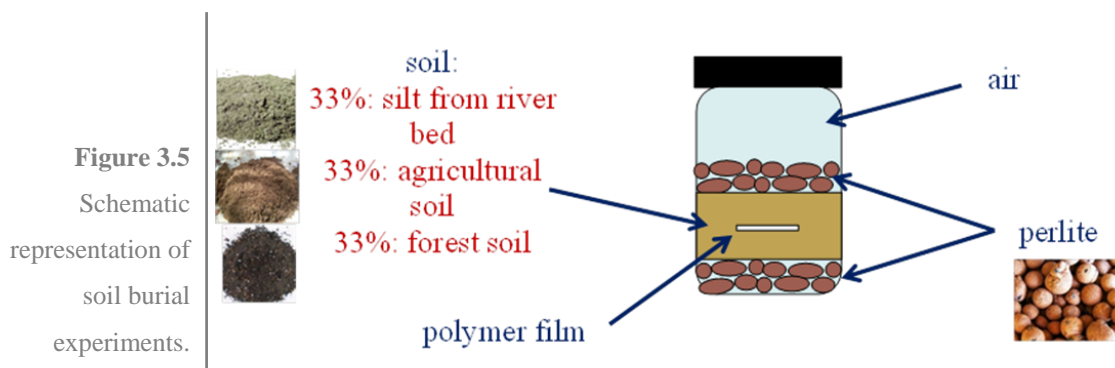
Films periodically removed from an incubation solution, rinsed with deionized water and dried on filter paper were placed in a 1 cm light path cuvettes and their optical density at 475 nm ( $OD_{475}$ ) was taken at four positions on the film; the  $OD_{475}$  values were then averaged. It was imperative that the film lied flat and still against the side of the cuvette to ensure a proper reading of the optical density. Determinations of  $OD_{475}$  were made relatively to the empty cuvette and the increment of  $OD_{475}$  in time was recorded. The biodegradation rate was defined as increment of absorbance units  $\times 10^{-3} \text{ min}^{-1}$  and calculated with linear fitting, according to a first-order kinetic.

### 3.12.2 Attenuated total reflectance infrared spectroscopy (ATRIR)

ATRIR was used to measure surface crystallinity of films under investigation. This assay permits a relative measure of the surface crystallinity degree by normalizing the better resolved band which displays the largest difference in intensity between the crystalline and the amorphous states to that which appears insensitive to the degree of crystallinity. The results are expressed in terms of crystallinity index (CI), i.e. the ratio of a crystalline-sensitive absorbance to a crystalline insensitive absorbance. This index is not an absolute determination of crystallinity, being however a simple and useful semi-quantitative indicator. Experimental ATR modified absorbance spectra were collected on a Perkin Elmer FTIR in the range 400 – 4000  $\text{cm}^{-1}$ . CI was determined from the average of three replicate measurements of a given sample.

### 3.13 Soil burial experiments

Tests were carried out at room temperature ( $21 \pm 1^\circ\text{C}$ ). Each polyester film was placed in a darkened vessels containing a multi-layer substrate (Figure 3.5). The films (diameter of 16 mm) were sandwiched between two layer of soil (20 g each). Soil used in the test was a mixture 1:1:1 by weight of forest soil, agricultural soil and silt from a river bed. Before use, each soil was sieved at 1 mm and dried for 72 h under vacuum at room temperature to remove the residual water.



The bottom and top layers were filled with 8 g of perlite moistened with 10 ml of distilled water. Perlite was added to increase aeration of the soil and the amount of water retained. 10 ml of distilled water were supplied from the top of each vessel every 6 weeks. Experiments were run in duplicate.

### 3.14 Composting

The biodegradation of some of the copolyesters under study was investigated in real composting facilities treating the organic fraction of municipal solid waste of Bologna (Figure 3.6).

Films of 35 x 35 mm, about 0.2 mm thick, were placed inside the organic matter at 50 cm depth. Dry weight of each sample was measured prior to incubation. Temperature and air supply were continuously recorded throughout the test.

After 14 and 37 days of incubation, specimen were recovered, gently washed with deionized water, and dried over  $P_2O_5$  under vacuum for 2 days to constant weight prior to further characterization.



**Figure 3.6**  
Biotunnel for the treatment of municipal organic waste. In the inset an enlarged image of the organic waste.

### 3.15 Film/scaffold weight loss analyses

Prior to degradation experiments each specimen was dried over  $P_2O_5$  under vacuum at room temperature to constant weight, and weighed to obtain the sample initial mass. At different time intervals, duplicate sacrificial specimens for each sample were repeatedly washed with deionized water and dried over  $P_2O_5$  under vacuum for 2 days to constant weight. The mass loss was determined gravimetrically by comparing the dry weight remaining at a specific time with the initial weight.

### 3.16 Scanning electron microscopy (SEM)

SEM images were acquired on a desktop Phenom microscope directly on film samples glued with carbon tape on aluminium stabs. The samples were not submitted to metal sputter coatings.

### 3.17 Barrier properties evaluation

Barrier properties evaluation of the polymers investigated in the present work has been conducted in the labs of Agri-food Science and Technology Department, University of Bologna, thanks to the scientific cooperation with Prof. Valentina Siracusa.

The permeability determination was performed by a manometric method using a Permeance Testing Device, type GDP-C (Brugger Feinmechanik GmbH), according to ASTM 1434-82 (Standard test Method for Determining Gas Permeability Characteristics of Plastic Film and Sheeting), DIN 53 536 in compliance with ISO/DIS 15 105-1 and according to Gas Permeability Testing Manual, Registergericht München HRB 77020, Brugger Feinmechanik GmbH.

The equipment consists of two chambers between which the film is placed. The chamber on the film is filled with the gas used in the test ( $\text{CO}_2$  or  $\text{O}_2$ ), at a pressure of 1 atm. A pressure transducer, set in the chamber below the film, records the increasing of gas pressure as a function of time. From pressure/time plot the software automatically calculates permeation which, known the film thickness, can be converted in permeability. The film sample was placed between the top and the bottom of the permeation cell. The gas transmission rate (GTR), i.e. the value of the film permeability to gas, was determined considering the increase in pressure in relation to the time and the volume of the device. Time lag ( $t_L$ ), Diffusion coefficient ( $D$ ) and Solubility ( $S$ ) of the test gases were measured according to the mathematical relations reported in literature (Mrkic *et al.*, 2006).

Fluctuation of the ambient temperature during the test was controlled by special software with an automatic temperature compensation, which minimizes gas transmission rate deviations.

All the measurements have been carried out at 23°C, with a relative humidity (RH) of 26%. The operative conditions were: gas stream of 100  $\text{cm}^3 \cdot \text{min}^{-1}$ ; 0% of gas RH; sample area of 11.34  $\text{cm}^2$ . The sample temperature was set by an external thermostat HAAKE-Circulator DC10-K15 type. Permeability measurements were performed at least in triplicate and the mean value is presented.

### 3.18 Ecotoxicity assessment

In order to assess the ecological risks associated with soil contamination due to the release of monomers during the biodegradation process of copolyesters under study, the *Lepidium sativum* ecotoxicity test was performed in duplicate on dilutions of three stock solutions containing different ratios of the comonomeric units for a total amount of 2000 ppm,

according to the procedures described in literature (Kreysa and Wiesner,1995) and in UNI 11357:2010 guidance, with minor modifications.

A total amount of 10 *Lepidium sativum* seeds were placed on filter paper into glass Petri dishes and exposed to serial dilutions (dilution factor 2) of the three stock solutions, over a fixed germination period of five days, in the dark at room temperature. The root length of the germinated seeds, and their number, was recorded and compared with the root growth of the seeds in an appropriate control containing deionized water. These data were analyzed by calculating the Germination Index (GI), according to the following formula:

$$GI = ((Gs*Ls) / (Gc*Lc))*100 \quad [56]$$

where  $G_s$  and  $G_c$  are the average number of germinated seeds in the sample dishes and in the blank ones.  $L_s$  and  $L_c$  are the average root length measured for the sample solution and the blank, respectively.

The EC50 index, defined as the toxicant concentration where the 50% of the organisms are died, was deduced by the graph plotting the GI, or the relative Inhibitory Effect, against the toxic concentration.

### 3.19 Biocompatibility evaluation

Biocompatibility studies have been conducted in the laboratories of Molecular Medicine Department of the University of Pavia, thanks to the fruitful collaboration with Dr. Livia Visai.

#### 3.19.1 *P(BCEmBDGn)* biocompatibility studies

##### 3.19.1.1 Cell culture

Murine fibroblast cell line L929 (ECACC 85011425) were cultured in Dulbecco's Modified Eagle Medium (DMEM, Sigma), supplemented with 10% fetal bovine serum (FBS), 1% nonessential amino acids, 1% antibiotic. Cell line INS-1 (Asfari *et al.*, 1992) were cultured in a humidified atmosphere containing 5% CO<sub>2</sub> in complete medium composed of RPMI 1640 supplemented with 5% heat-inactivated fetal calf serum, 1 mM sodium pyruvate, 50 µg 2-mercaptoethanol, 2 mM glutamine, 10 mM 4-(2-hydroxyethyl)-1-piperazineethanesulfonic acid (HEPES), 100 U/ml penicillin, and 100 µg/ml streptomycin.

Both cell cultures were cultured at 37 °C with 5% CO<sub>2</sub>, routinely trypsinized after confluence, counted, and seeded onto each film. The polymeric films were placed inside standard 96-well-plates, sterilized with a solution of ethanol 70% for 20 minutes, washed

several times with a solution containing 1% antibiotics and at the end with cell culture medium in order to remove possible chemical residues. A cell suspension of  $2 \times 10^4$  cells (0.1 ml) was added onto the top of each sample and, after 1h, 0.1 ml of culture medium was added to cover the samples. The culture medium was changed every three days. The culture were further incubated for 24h and 7 days.

#### *3.19.1.2 Cell viability to materials*

To determine the number of viable cells adherent to each type of material, a 0.4% trypan blue solution was used. Briefly, at the end of each incubation time, the adherent cells were washed with phosphate buffer, treated with trypsin to detach them and finally a 1:1 ratio of trypan blue solution was added. Then cells were counted at the optical microscope using a burker chamber. The control sample was represented by cells adherent to culture tissue plastic and treated as indicated for the other materials after 24 h and 7 days. The data were expressed as percent of the control (set as 100%).

#### *3.19.1.3 Confocal Laser Scanning Microscopy (CLSM)*

After 24 h and 7 days incubation, L929 or INS-1 cells attached to each material were fixed with 4% (w/v) paraformaldehyde solution in 0.1 M phosphate buffer (pH 7.4) for 30 minutes at room temperature, washed extensively with phosphate buffer solution and then permeabilized with 10% Triton X-100 in phosphate buffer solution for 20 min. After phosphate buffer solution washing, cell were stained with for 30 minutes at RT (to visualize F-actin), followed by incubation with FITC-conjugated  $\alpha$ - phalloidin–tetramethylrhodamine isothiocyanate (TRITC)tubulin antibody (to visualize tubulin). The samples were then treated with DAPI for 15 min at RT and washed extensively with phosphate buffer. Positive controls were represented by cells seeded on glass coverslips and stained as indicated above. Negative controls were represented by unseeded materials incubate with all the previous indicated fluorescent probes. The images were taken with a BX51 Olympus fluorescence microscope equipped with a digital image capture system (Olympus) at 40x (L929) and 63x (INS-1) magnification. The fluorescence background of the negative controls was almost negligible.

### *3.19.2 P(BCEmTECEn) scaffolds biocompatibility studies*

#### *3.19.2.1 Cell culture*

The murine myoblast cell line C2C12 (ATCC CRL-1772™) was routinely cultured in complete DMEM, supplemented with 10% fetal bovine serum (FBS), 1% penicillin/streptomycin, 1% L-glutamine and 1% sodium pyruvate (Life Technologies).

For the experiments C2C12 cells were seeded onto the polymeric scaffolds at a density of  $3 \times 10^4$  and incubated at 37°C with a 5% CO<sub>2</sub> atmosphere.

#### 3.19.2.2 MTT assay

To evaluate the cell viability onto scaffolds, a test with 3-(4,5-dimethylthiazole-2-yl)-2,5-diphenyl tetrazolium bromide (MTT, Sigma-Aldrich), was performed (Saino *et al.*, 2010). The culture medium was replaced by 500 µL DMEM with 50 µL of a 5mg/mL solution of MTT in phosphate buffered saline (137mM NaCl, 2.7mM KCl, 4.3mM Na<sub>2</sub>HPO<sub>4</sub>, 1.4mM KH<sub>2</sub>PO<sub>4</sub>, pH 7.4), and the cell cultures were incubated for 3 h. Viable cells are able to reduce MTT into formazan crystals. After incubation time, 500 µL of Solution C (2-propanol and HCl 0.04%) were added, aliquots of 100 µL were sampled, and the related absorbance values were measured at 595nm by a microplate reader (BioRad Laboratories). A standard curve of cell viability was used to express the results as percentage of cell seeded onto different scaffolds.

#### 3.19.3 PBS and P(BS80BDG20) scaffolds biocompatibility studies

##### 3.19.3.1 Cell culture

The murine myoblast cell line C2C12 (ATCC CRL-1772™) was cultured as described above (3.19.2.1).

##### 3.19.3.2 Cell Viability Assay

The cell viability was evaluate by Cell Counting Kit 8 assay after 24h and 7 days from seeding according to manufacturer's instructions (Sigma-Aldrich). Briefly, the culture medium was replaced by 200 µL DMEM and 20 µL of CCK-8 solution was added onto each scaffolds. After incubation at 37°C for 2 h, aliquots of 100 µL were sampled and analyzed by an ELISA reader (BioRad Laboratories, Hercules, CA) at 450 nm. A standard curve of cell viability was used to express the results as percentage.

### 3.20 *In vitro* FITC release experiment

Polymeric films containing 0.3 wt% of fluorescein isothiocyanate (FITC) were prepared by solvent casting, dissolving the appropriate amounts of FITC and polymer in DCM. The solutions were cast on circular Teflon molds and the solvent was allowed to evaporate overnight at room temperature. Complete solvent evaporation was verified through TGA analysis. The obtained polymeric films were hot-pressed between Teflon plates (section 3.3), in order to obtain films with a regular thickness.

About 70 mg of FITC-loaded polymeric films were immersed in 15 mL of phosphate buffered solution (0.1 M, pH = 7.4) and incubated in a SW22 Julabo shaking water bath at 37°C and 50 rpm under dark conditions. At predetermined time intervals, phosphate buffer aliquots (300 mL) were taken out and FITC release was monitored by measuring UV absorbance at 494 nm with a Cary 1E (Varian) spectrophotometer and converted to FITC concentration through a calibration curve of FITC in the same buffer. Measurements were performed on three specimens for each polymer sample and the cumulative release was provided as average.



4.

Results &  
discussion

## 4.1 Enzymatic hydrolysis studies on $\text{PBS}_m\text{PDGS}_n$ and $\text{PBS}_m\text{PTDGS}_n$ block copolymers

In the present study, copolymers of PBS containing diethylene succinate (PBSPDGS) and tiodiethylene succinate (PBSPTDGS) sequences with different molecular architecture have been prepared in our laboratories via reactive blending to modulate PBS biodegradation rate through a targeted modification of its hydrophilicity, flexibility, and crystallinity degree.

Optimization on the synthesis and solid-state characterization of the copolyester classes involved in this study have been carried out by the research group in which was conducted the present PhD Thesis and are reported elsewhere (Soccio *et al.*, 2008; Soccio *et al.*, 2012).

Two different molecular architectures have been considered: long block sequences, obtained after 20 min of melt mixing (in the following those copolymers are named *block*) and random distribution of sequences obtained after 240 min of melt mixing (in the following those copolymers are named *random*).

It has to be emphasized that PDGS and PTDGS respectively differ from PBS for the presence of an ether-oxygen atom and sulphur atom in the glycol sub-unit. On the basis of the chemical structure of PDGS and PTDGS, it is expected that PDGS sequences impart to the final material a higher hydrophilicity than PTDGS ones, but in the meantime PBSPTDGS copolymeric chains are expected to display a higher flexibility and mobility with respect to PBSPDGS ones.

The solid-state properties and wettability of the polymers under investigation were correlated to their enzymatic degradability. Lastly, the biodegradation rate of these copolymers has been compared in order to evaluate the effect of the presence of ether-oxygen instead of sulphur atoms in the PBS polymeric chain.

### 4.1.1 Synthesis and characterization of the polymers

At room temperature the as-prepared polyesters are slightly opaque and light yellow coloured, except PDGS which is a rubber. The chemical structure of the copolymers are previously reported (Figure 3.4).

The data concerning molecular characterization of PBS, PDGS, PTDGS, and their copolymers are reported in the following (Table 4.1).

Table 4.1 Molecular characterization data.

polymer	$M_n^{a)}$	$PDI^{b)}$	$BS$ (mol %) <sup>b)</sup> ( <sup>1</sup> H-NMR)	$L_{BS}^{c)}$	$L_{DGs}$ or $L_{TDGS}^{d)}$	$b^{e)}$	$WCA^{g)}$ (°)
PBS	38300	2.1	100	-	-	-	96 ± 3
PDGS	28200	2.3	0	-	-	-	-
PBSPDGS $_{block}$	28200	2.2	52	23	23	0.12	66 ± 3
PBSPDGS $_{random}$	27000	2.3	50	2	2	1.02	72 ± 3
PTDGS	25000	2.2	0	-	-	-	78 ± 3
PBSPTDGS $_{block}$	22100	2.3	51	19	19	0.15	74 ± 4
PBSPTDGS $_{random}$	23900	2.3	50	2	2	1.02	77 ± 1

a) average molecular weight calculated by GPC analysis (section 3.6.2)

b) polydispersity index calculated by GPC analysis (section 3.6.1)

c) actual composition calculated by <sup>1</sup>H-NMR (section 3.6.1)

d) butylene succinate block length calculated by <sup>1</sup>H-NMR (section 3.6.1)

e) thiodiethylene succinate block length calculated by <sup>1</sup>H-NMR (section 3.6.1)

f) degree of randomness calculated by <sup>1</sup>H-NMR (section 3.6.1)

g) by observation of six water drops for each sample (section 3.10).

All the homopolymers (PBS, PDGS and PTDGS), as well as the synthesized copolyesters, were characterized by relatively high molecular weights. This indicated that during syntheses, no appreciable thermal degradation occurred. <sup>1</sup>H-NMR spectra of the homopolymers were found to be consistent with the expected structure and for the copolymers the actual molar composition was close to the feed one (data not shown).

The average block length ( $L_{BS}$  and  $L_{DGs}$  or  $L_{TDGS}$ ) and the degree of randomness ( $b$ ) of *block* and *random* copolymers (Table 4.1) indicated that the copolymers under investigation were characterized by different molecular architecture. The copolymers obtained after short mixing time were characterized by a block distribution of long sequences ( $b = 0.12$  and  $b = 0.12$  respectively), whereas PBSPDGS $_{random}$  and PBSPTDGS $_{random}$  had a random distribution of sequences ( $b = 1.02$ ) which, on the contrary, are very short.

In order to investigate the relative hydrophilicity of the synthesized polymers, water contact angle (WCA) measurements were performed on hot-pressed films (section 3.4). It has to be pointed out that surface wettability reflects surface hydrophilicity but, in the present case, it cannot be directly correlated with bulk material hydrophilicity. Indeed, given the identical chemical composition of the investigated copolymers (section 3.3.2),

material hydrophilicity is expected to be the same in all cases. Table 4.1 reports the contact angle values for each polymer.

The data showed that PBS was the most hydrophobic material. For each copolymer system, as expected, practically same WCA values were found. Therefore, copolymerization of PBS with PDGS or PTDGS permitted to obtain two new classes of copolymers which resulted more hydrophilic than PBS, due to the presence along the polymer chain of polar ether-oxygen or sulphur atoms. PBSPDGS copolymers resulted slightly more hydrophilic than PBSPTDGS, due to the higher electronegativity of oxygen with respect to sulphur atom.

All the polymers under investigation were afterwards subjected to DSC analysis (Table 4.2).

With the exception of PDGS, which is completely amorphous, all the polyesters under investigation were semicrystalline: in the case of copolymers, a significant decrease of melting temperature and level of crystallinity, as compared to PBS was observed.

The higher crystallinity degree of *block* copolymers with respect to *random* ones can be explained on the basis of their higher crystallizing ability, which is normally lower for shorter crystallizing blocks (BS blocks). In fact, the work of chain folding increases with decreasing block length, considering that in the copolymers characterized by very short crystallizable blocks, the segmental mobility of these last is strongly hindered by the presence of the non-crystallizable ones (DGS and TDGS blocks) (Soccio *et al.*, 2008).

In PBSPDGS copolymers, X-ray analysis (section 3.8) demonstrated the only presence of the PBS crystal phase. PBS is a semicrystalline material with a well-defined set of crystalline diffraction peaks: two intense reflections at  $19.6^\circ$  and at  $22.5^\circ$ , a shoulder at  $21.7^\circ$  and some weak reflections between  $25^\circ$  and  $45^\circ$  (data not shown). WAXS patterns of copolymers displayed the same reflections of PBS with different intensities, indicating that in all the copolymers the BS units were able to develop a crystal phase (data not shown). As far as the crystallinity degree is concerned, it decreased with decreasing BS block length in agreement with the calorimetric results (Table 4.2).

A more complex situation arose in PBSPTDGS samples. PTDGS X-ray pattern is reported elsewhere (Soccio *et al.*, 2012). PBSPTDGS<sub>random</sub> was characterized by an X-ray spectrum which closely match that of PBS, proving that the developed crystal structure corresponds to the characteristic lattice of  $\alpha$ -PBS; in the case of PBSPTDGS<sub>block</sub> several partially overlapped peaks at the same angular positions of those characteristic of PBS and PTDGS were observed, which is a clear evidence of the simultaneous presence of the crystalline phases of the two homopolymers. As far as the crystallinity degree is

concerned, PBS homopolymer displayed the highest content of crystal phase (average value 41%), whereas in both copolymers, where a lower amount of rigid crystal phase was dispersed in a much higher quantity of mobile amorphous phase, crystallinity degree was found to regularly decrease as crystallisable block length was decreased (Table 4.2). The DSC analysis, in agreement with the WAXS results, showed a single melting endothermic peak in the case of PBSPTDGS*random*, whereas two separate melting phenomena were present in PBSPTDGS*block*, further confirming the simultaneous presence of both the crystalline phases of PBS and PTDGS.

**Table 4.2** Thermal characterization data (1<sup>st</sup> scan, heating rate 20°C/min).

polymer	T <sub>g</sub> (°C)	T <sub>m,TDGS</sub> (°C)	T <sub>m,BS</sub> (°C)	ΔH <sub>m,TDGS</sub> (J/g)	ΔH <sub>m,BS</sub> (J/g)	χ <sub>c</sub> <sup>a)</sup> (%)
PBS	-36	-	114	-	82	41
PBSPDGS <i>block</i>	-30	-	112	-	44	27
PBSPDGS <i>random</i>	-32	-	51	-	29	18
PBSPTDGS <i>block</i>	-36	41	112	20	34	29
PBSPTDGS <i>random</i>	-38	-	59	-	36	24

<sup>a)</sup> crystallinity degree from WAXS analysis (section 3.8)

The presence of a single T<sub>g</sub>, below room temperature, indicated that all copolymers were miscible in the amorphous phase. They were characterized by a “soft” amorphous mobile phase (T<sub>g</sub> < room temperature) and by a crystalline “hard” phase. The ratio between “hard” and “soft” phases was high in the case of PBS and significantly decreased with copolymerization; moreover, it could be further modulated by changing the molecular distribution of the sequences (*block* or *random*).

Tensile mechanical properties of the investigated polymers are reported in Table 4.3, where elastic modulus E, stress at break σ<sub>b</sub>, and deformation at break ε<sub>b</sub> are listed. PBS homopolymer displayed the highest elastic modulus and the stiffest behavior among the synthesized polymers, with a relatively low deformation at break (ε<sub>b</sub>=31%).

Overall, mechanical characterization demonstrated that the introduction of comonomeric units into PBS chains resulted in a significant change in the copolymer mechanical properties. All copolymers displayed elastic moduli and stresses at break significantly lower than those of PBS, but the *block* copolymers had a deformation at break comparable to PBS. Interestingly, *random* copolymers were characterized by an elastomeric behavior, with an extremely high deformation at break that reached a value of about 600%.

**Table 4.3** Mechanical characterization data.

polymer	E(MPa)	$\sigma_b$ (MPa)	$\varepsilon_b$ (%)
PBS	337 $\pm$ 26	24 $\pm$ 4	31 $\pm$ 2
PBSPDGS <i>block</i>	238 $\pm$ 9	23 $\pm$ 3	21 $\pm$ 2
PBSPDGS <i>random</i>	56 $\pm$ 3	7 $\pm$ 1	605 $\pm$ 22
PBSPTDGS <i>block</i>	153 $\pm$ 2	10 $\pm$ 1	21 $\pm$ 1
PBSPTDGS <i>random</i>	67 $\pm$ 3	8 $\pm$ 1	630 $\pm$ 60

Since the investigated polymers displayed a soft amorphous phase and a rigid hard crystal phase, the observed trend can be explained on the basis of polymer crystallinity degree (Table 4.2): in fact, PBS, the most rigid material, displayed the highest amount of crystal phase; the lowest amount of rigid crystal phase present in *random* copolymers resulted on the contrary in their elastomeric behaviour.

#### 4.1.2 Screening of the degrading hydrolytic enzymes

Four different lipases (from *Candida rugosa*, *Candida cylindracea*, *Aspergillus niveus* and hog pancreas) and a serine protease ( $\alpha$ -Chymotrypsin from bovine pancreas) were screened for their polymer degradation capability by using the film opacity assay. The following conditions (48 h incubation) were initially selected since previously used in similar enzymatic degradation studies of poly(butylene succinate) copolymers (Rizzarelli & Impallomeni, 2004): 0.1 M phosphate buffer, pH 7.4, 37°C, mixing on a rotary shaker at 80 rpm. Enzyme concentration of 50 U/ml was chosen being the highest used in previous studies on polyester enzymatic degradation (Walter *et al.*, 1995).

As reported in the literature (Timmins *at al.*, 1997), the film opacity assay is well suited for studying the very early stages of enzymatic degradation of a polymer, when meaningful reliable weight loss measurements are difficult to obtain (section 3.12.1). In fact, when a polymer film is exposed to a depolymerase, its surface roughens and becomes visibly opaque. Such increase in opacity is correlated to the preferential removal of amorphous material from the surface and to the scattering of light by the exposed crystalline domains.

No significant OD<sub>475</sub> increment was observed in PBS, PBSPDGS*block* and in PBSPTDGS copolymers throughout incubation with any of the enzymes tested. Under the experimental conditions adopted, only lipase from *Candida cylindracea* induced a rapid OD<sub>475</sub> increment in PBSPDGS*random* which reached a maximum (0.55 $\pm$ 0.03mAU) after 4h.

Therefore, lipase from *Candida cylindracea* was the enzyme selected for further investigations.

#### 4.1.3 Optimization and selection of the biodegradation test conditions

To optimize the experimental conditions for the polymer biodegradation assays, lipase from *Candida cylindracea* and PBSPDGs<sub>random</sub> were used. The opacity assay was employed for measuring the polymer biodegradation rate in the presence of different enzyme concentrations, temperatures and pH.

At increasing enzyme concentrations, increasing initial degradation rates were detected (Table 4.4). Such an increase was proportional to enzyme concentrations up to 50 U/mL, thus indicating that for higher enzymes concentrations (100 U/mL) the substrate concentration (intended as the amount of ester bonds available on the film surface for enzymatic attack) was not far exceeding the enzyme concentration.

**Table 4.4** Optimization of the biodegradation assay with *Candida cylindracea* lipase and PBSPDGs<sub>random</sub>. (a) Condition used as reference.

enzyme concentration (U/ml)	T (°C)	pH	degradation rate ( $\Delta$ mAU min <sup>-1</sup> )	std. dev.	Error (%)
50 <sup>(a)</sup>	37 <sup>(a)</sup>	7.4 <sup>(a)</sup>	29.4	0.5	1.5
25	37	7.4	16.0	2.5	15.4
100	37	7.4	50.9	1.3	2.6
50	25	7.4	14.4	1.8	12.5
50	30	7.4	15.7	1.1	6.7
50	37	7.0	41.2	5.3	12.8

For this reason, 50 U/mL seemed to be the most appropriate enzyme concentration to properly follow the biodegradation process, i.e., the conditions for a zero order reaction. No significant difference in the initial degradation rates were observed between 25°C and 30°C, while a double initial rate was detected at 37°C. Therefore, the selected temperature was 30°C, since it represented a trade-off between mild operating conditions (it is close to ambient temperature) and a reasonable sample biodegradation rate. As to pH effect, as expected, biodegradation rate was found to be affected by pH, showing the highest value at pH 7.0 (Figure 4.1). Consequently, the biodegradation tests were carried out at such pH.

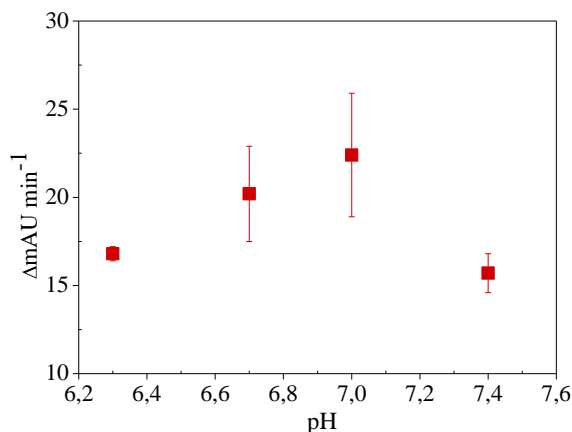


**Figure 4.1**  
Enzymatic degradation of PBSPDGS<sub>random</sub> by lipase from *Candida cylindracea* (50 U/ml, 30°C) at different pH values.

Lastly, the stability of the enzyme under the selected conditions was investigated in order to evaluate the possible need to replace the enzyme solution during long-lasting incubations (Figure 4.2).

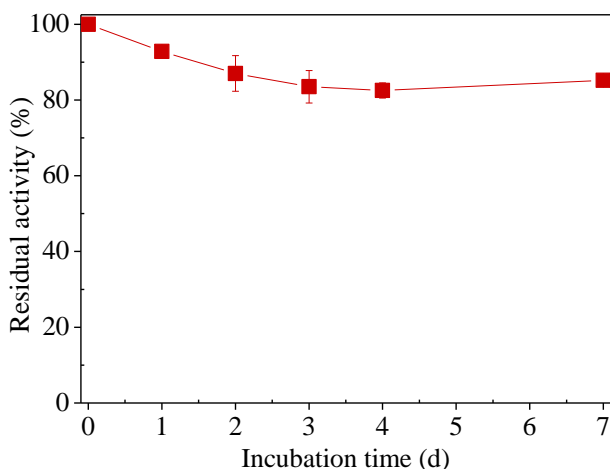


**Figure 4.2**  
Residual activity as a function of incubation time for lipase from *Candida cylindracea* at T=30°C, pH=7.0. Standard deviations are reported as error bars.

Enzyme activity was reduced by 20% in the first four days of incubation according to a second order kinetic which corresponded to an enzyme half-life of 17 days. Based on this observation the enzyme solution was replaced weekly in order to avoid incubation in the presence of residual enzyme activity lower than 70% of the initial one.

#### 4.1.4 Biodegradation studies

Figure 4.3 shows the release of biodegradation products, measured as absorbance increment at 475 nm, as a function of incubation time for PBSPDGS<sub>random</sub> incubated in *Candida cylindracea* lipase (Enzyme 50 U/ml, 30°C, pH 7.0). Data obtained from the biodegradation experiments of other polymers are shown in Table 4.5.

As expected, initially the OD<sub>475</sub> increased linearly with time, then the OD increment slowed down and lastly a plateau was reached. The opacity ceased to increase because of the completion of a “roughness fringe” or layer of etched material, which formed at the surface of the degrading films. Formation of this roughness fringe proceeded rapidly, and thus opacity reached a maximum OD<sub>475</sub> rather quickly.

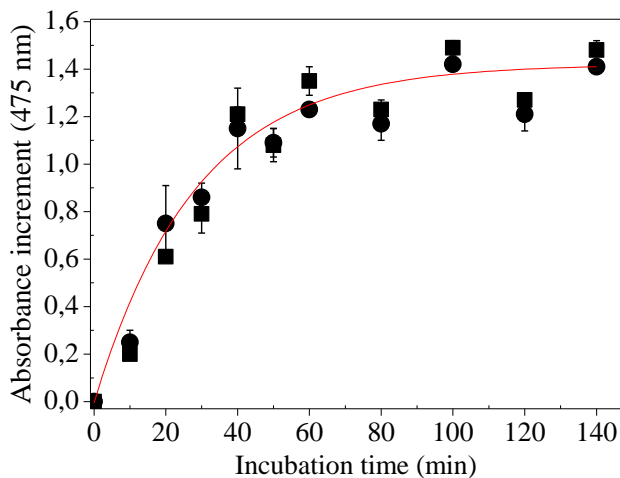


**Figure 4.3** Increase of film opacity (measured as OD<sub>475</sub>) as a function of incubation time for PBSPDGS<sub>random</sub> in the presence of lipase from *Candida cylindracea* (50 U/ml, 30°C, pH 7.0). (●) I replicate; (■) II replicate; (—) guide for the eyes of the experimental data. Standard deviations are reported as error bars.

The biodegradation rate at longer enzyme exposition times was investigated by weight loss measurements (section 3.15).

**Table 4.5** Biodegradation rate of PBS, PBSPDGS and PBSPTDGS copolymers in the early stage of the enzymatic treatment with lipase from *Candida cylindracea*.

polymer	$v_i$ ( $\Delta$ AmU $\text{min}^{-1}$ )	Std. Dev.	err. (%)
PBS	-	-	-
PBSPTDGS <sub>block</sub>	0.8	0.1	8.8
PBSPDGS <sub>block</sub>	0.2	0.1	25.0
PBSPTDGS <sub>random</sub>	15.8	4.1	26.3
PBSPDGS <sub>random</sub>	22.4	3.5	15.4

As far as PBS is concerned, both analysis came to the same result: as it can be seen from Table 4.5, no data for homopolymer PBS are reported as no appreciable increments of  $OD_{475}$  were observed along the test, thus indicating that PBS degraded much slower than PBSPDGS and PBSPTDGS copolymers, probably for its higher crystallinity degree and crystal dimensions. Similarly, after 1 year of incubation, PBS practically did not lose weight (data not shown), whereas all copolymers appreciably degraded (Figure 4.4).

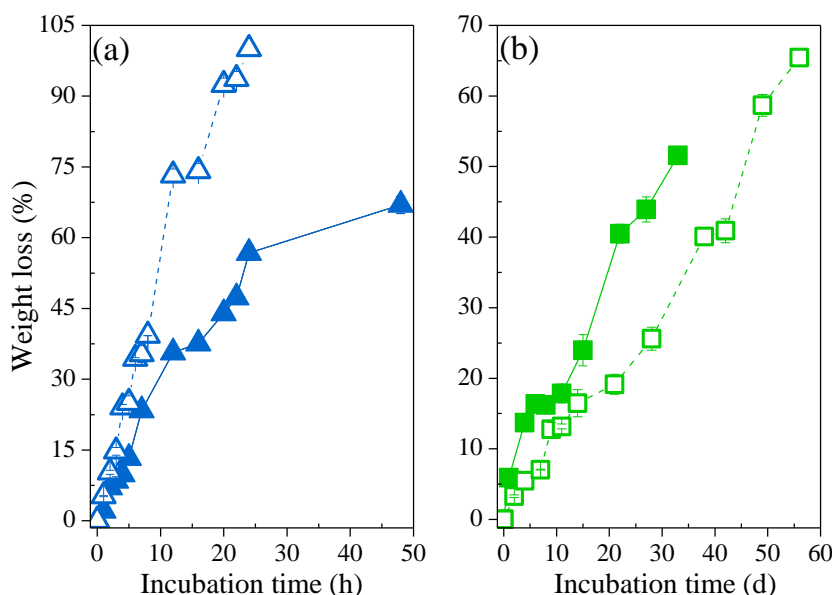


**Figure 4.4** Weight loss data as a function of incubation time for (a) *random* copolymers: (▲) PBSPTDGS<sub>random</sub>, (△) PBSPDGS<sub>random</sub>; (b) *block* copolymers: (■) PBSPTDGS<sub>block</sub>, (□) PBSPDGS<sub>block</sub>.

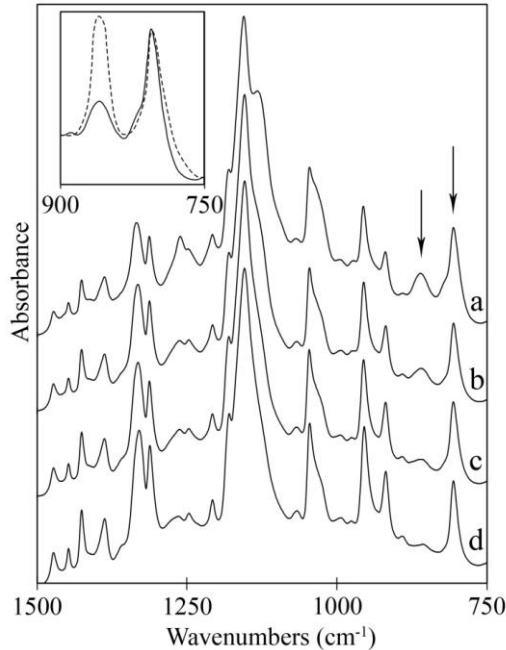
As regards copolymers, both turbidimetric assay and weight losses indicated that PBSPTDGS<sub>block</sub> degrades faster than PBSPDGS<sub>block</sub> (Figure 4.4b). Both copolymers were characterized by: i) very long sequences,  $L_{DGS} = 23$  and  $L_{TDGS} = 19$  respectively, ii) same  $T_m$  (112°C), iii) comparable degree of crystallinity,  $\chi_c \approx 27\%$  and  $29\%$ , respectively and iv) similar hydrophilicity,  $WCA \approx 66^\circ$  and  $74^\circ$ , respectively. Taking into account all these factors, the trend observed can be ascribed to the presence of PTDGS crystalline phase beside the PBS crystalline one in PBSPTDGS<sub>block</sub>. In fact, as shown below, PTDGS crystalline phase was attacked by the lipase simultaneously to the amorphous phase and therefore degraded significantly faster than PBS one.

The opposite trend was observed in the case of random copolymers: PBSPDGS<sub>random</sub> biodegradation rate was higher than that of PBSPTDGS<sub>random</sub> (Figure 4.4a): this is due

to the higher crystallinity degree of the latter ( $\chi_c \approx 18\%$  and  $\chi_c \approx 24\%$  respectively), in spite of the similar melting temperature and hydrophylicity of the two copolymers.

We hypothesized that an amorphous skin is first removed from the polymer surface so that the crystallinity of the film surface increases. To confirm this, films degraded to different extents were analyzed by attenuated total reflectance infrared spectroscopy, employing an ATR-modified version of the assay described by Bloembergen and co-workers (Bloembergen & Marchessault, 1986).

**Figure 4.5** FTIR spectrum of PBSPDGS $block$  copolymer degraded at different extent: a 0 h; b 8 h; c 24 h; d 72 h. In the inset the two bands used to calculate the C.I. index are shown in an enlarged scale.



The assay permitted to measure the surface crystallinity degree by normalizing the better resolved band at  $858\text{ cm}^{-1}$  (and  $991\text{ cm}^{-1}$ ), which displays the largest difference in intensity between the crystalline and the amorphous states to that which appears insensitive to the degree of crystallinity at  $810\text{ cm}^{-1}$  (and  $956\text{ cm}^{-1}$ ) for PBSPDGS (and PBSPTDGS) copolymers. For the samples under investigation, these two bands were identified comparing the FTIR spectra of the completely amorphous and the not-degraded crystalline block copolymer (insert of Figure 4.5).

As an example, changes in the surface crystallinity index (C.I.) of PBSPDGS $block$  and PBSPTDGS $block$  as a function of enzyme incubation time are reported in Figure 4.6 (part a and part b, respectively). As it can be seen, the surface total crystallinity increased significantly during the very early stages of biodegradation, confirming that amorphous material was being preferentially degraded.

A further confirmation that the amorphous regions of the polymer were degraded more quickly than the crystalline ones was obtained by subjecting the partially degraded samples of both copolymers to a heating calorimetric scan (1<sup>st</sup> scan at 20°C/min). All the calorimetric traces were found to be characterized by an endothermic peak associated with the fusion process of crystalline portion of the material (data not shown). The corresponding heat of fusion was normalized respect to the heat of fusion of non-degraded sample ( $\Delta H_t/\Delta H_0$ ). The results obtained are reported in Figure 4.7 and figure 4.8 for *random* and *block* copolymers, respectively.

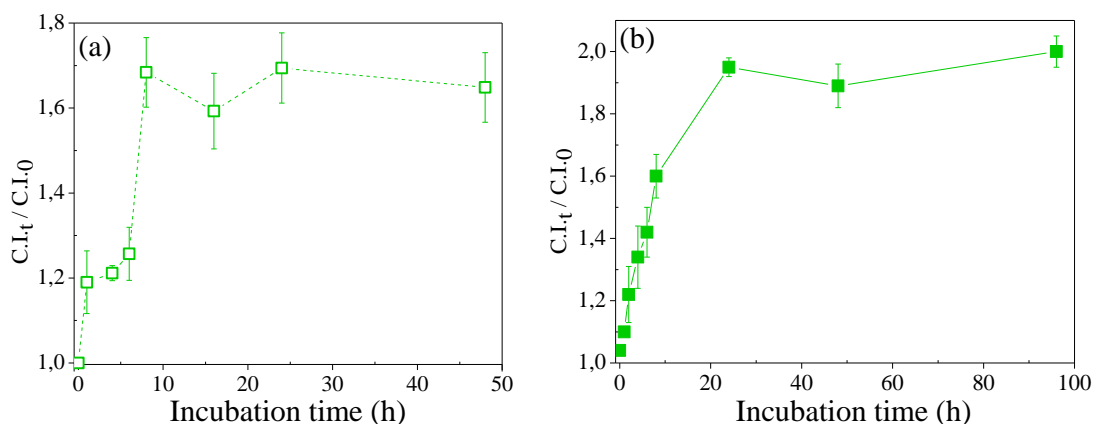


**Figure 4.6** ATRIR-determined crystallinity index of: (a) PBSPDGS*block* and (b) PBSPTDGS*block* films degraded to various extents.

In all the copolymers, with the exception of PBSPTDGS*block* (Figure 4.8 b), initially the normalized heat of fusion regularly increased with incubation time up to a maximum value, then decreased. The observed trend confirmed that the amorphous regions of a polymer are preferentially degraded. The decrement of  $\Delta H_t/\Delta H_0$  at longer incubation time indicated that when the amorphous portion of the polymer has been almost completely degraded, the enzyme attacks the crystalline region.

Interestingly, in the case of PBSPTDGS*block*, two different trends can be highlighted: while the PBS crystalline phase follows the same behavior displayed by the other copolymers, the PTDGS crystalline phase is on the contrary attacked by the enzyme together with the amorphous one, being almost completely degraded after 33 days of incubation (Figure 4.8b): this phenomenon can be explained on the basis of the lower packing density and degree of perfection of the PTDGS crystalline lamellae with respect to the PBS ones, which permitted an easier access of enzyme to the polymer chain and higher diffusion rate of water.

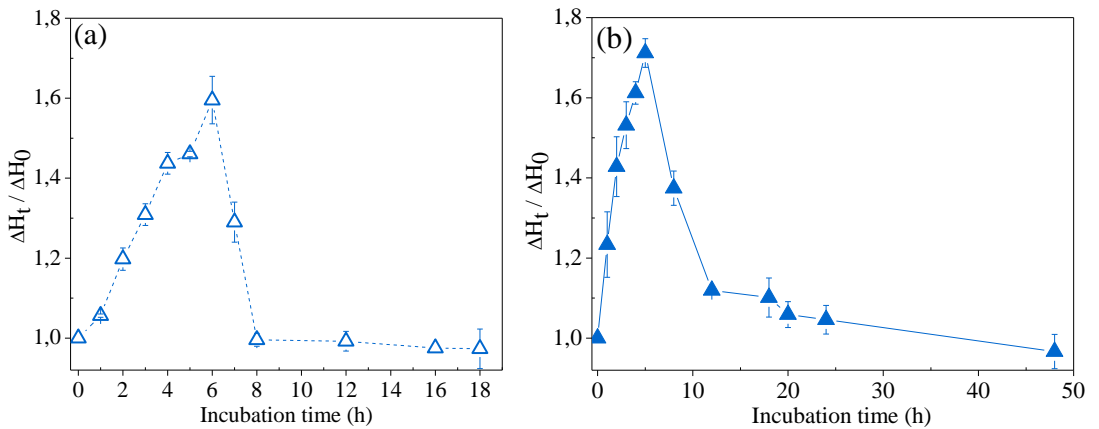


**Figure 4.7** Normalized heat of fusion as a function of incubation time for (a) PBDPDGS<sub>random</sub> and (b) PBSPTDGS<sub>random</sub>

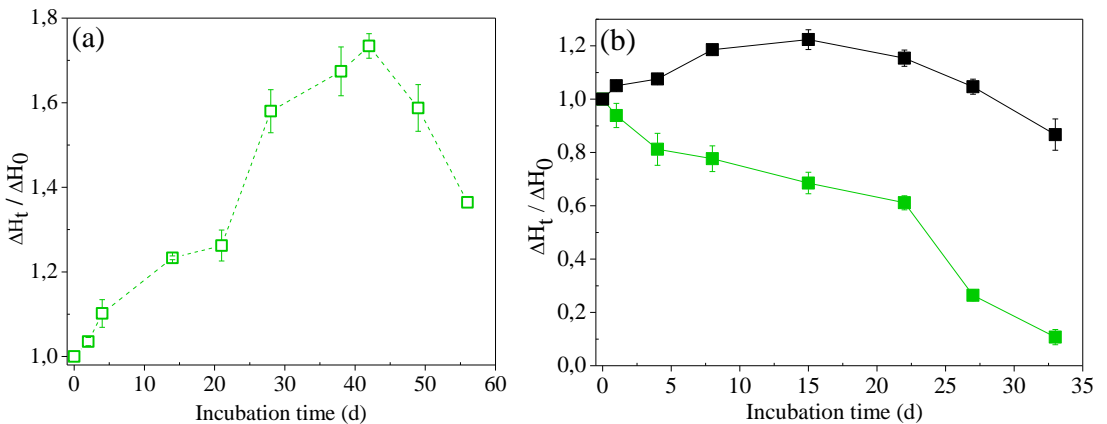


**Figure 4.8** Normalized heat of fusion as a function of incubation time for (a) PBSPDGS<sub>block</sub> and (b) PBSPTDGS<sub>block</sub>: (■) PBS crystalline phase, (■) PTDGS crystalline phase.

To hypothesize the mechanism of enzymatic biodegradation and therefore understand the reason why copolymers degraded much faster than the parent homopolymer PBS, partially degraded samples of both copolymers were subjected to NMR spectroscopy in order to verify if etheroatom containing sequences, more hydrophilic and therefore more susceptible of enzyme catalysed hydrolytic attack of water, were preferentially hydrolysed. If this is the case, copolymer composition changes have to be observed during biodegradation.

Indeed, as shown in Figure 4.9, the mol% of BS units increased with the incubation time, thus confirming that DGS and TDGS sequences were preferentially hydrolysed, due to their hydrophilic nature which favoured their solubilisation in water. On the contrary, the

long highly hydrophobic BS blocks were much more resilient to hydrolytic biodegradation.

It is noteworthy that the *random* copolymers underwent no composition change. In our opinion, the etheroatom containing sequences were still preferentially attacked by the enzyme, but in this case the BS blocks were so short to be solubilised in water, even though they are more hydrophobic than DGS and TDGS moieties.

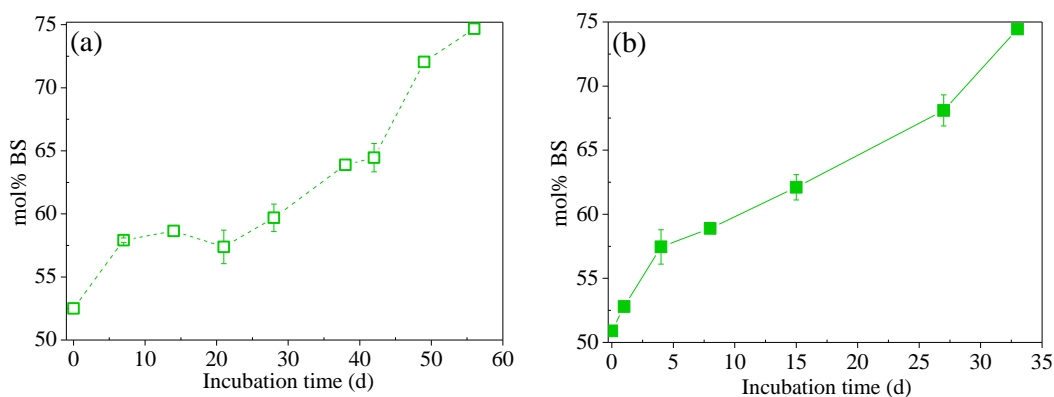


**Figure 4.9** Copolymer composition (expressed as mol% of BS units) as a function of incubation time for: (a) PBSPDGS*block*, (b) PBSPTDGS*block*.

The morphology of the polymer films was analysed using SEM. As an example, micrographs of PBSPTDGS*random* films taken before and after enzymatic hydrolysis are presented in Figure 4.10.

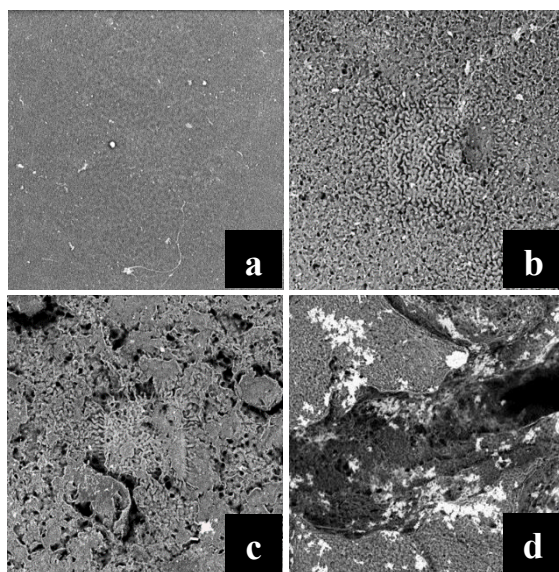


**Figure 4.10** SEM micrographs of PBSPTDGS*random* during enzymatic hydrolysis at (a) 0, (b) 2, (c) 8, (d) 20 hours of incubation, 5000 $\times$  magnification.

The micrograph of both samples under investigation prior to enzyme exposure revealed a homogeneous and smooth surface. On the contrary, after enzyme exposure, especially in the case of *random* copolymers, surface irregularities appeared and progressively deeper damaged areas began to appear with increasing exposure time. Holes and channels showed remarkable mass loss even since the first 2 hours of enzymatic hydrolysis, leading to large portions of the film surface broken up after 20 hours of incubation.

#### 4.1.5 Conclusions

The results obtained in the present study demonstrated that the introduction of ether-oxygen or sulphur atoms along poly(butylene succinate) polymer chain is a winning strategy to increase PBS biodegradability as it allowed to tailor both the crystallinity degree and the hydrophilicity of the final polymer. In fact, the resulting more hydrophilic DGS and TDGS sequences, with respect to the BS ones, were preferentially hydrolyzed by lipase. The biodegradation rate could be further enhanced acting on the molecular architecture: sequence distribution deeply affected biodegradation rate owing to the different ability of the polymer to crystallize. As a matter of fact, the *random* copolymers investigated in the present work biodegraded much faster than the *block* ones, being characterized by a lower melting point and crystallinity degree, this latter being strictly correlated to the crystallizable block length.

Lastly, the nature of the crystalline phase, in addition to the crystallinity degree, significantly contributed to the final biodegradation rate of the polymers investigated.

## 4.2 Environmentally friendly PBS-based copolyesters containing PEG-like subunit: effect of block length on solid-state properties and enzymatic degradation

In the present study, multiblock copolymers containing different butylene succinate (BS) and triethylene succinate (TES) block lengths, obtained by melt mixing PBS and poly(triethylene succinate) (PTES) have been taken into consideration. PTES differs from PBS for the presence of PEG-like subunit (-OCH<sub>2</sub>CH<sub>2</sub>O-) in the macromolecular chain which imparts good hydrophilicity to the final material. The solid-state properties and wettability of these copolyesters have been investigated and correlated to their enzymatic degradation. Lastly, the biodegradation rate of copolymers under investigation has been

compared with the data of PBSPDGS copolymers previously studied in order to evaluate the effect of the replacement of ether-oxygen atoms with PEG-like subunits.

In the following, the synthesized polymers will be named PBSPTES<sub>t</sub>, with *t* equal to the mixing time during reactive blending.

#### 4.2.1 Synthesis and molecular characterization of the polymers

At room temperature the as-prepared polyesters were opaque and light yellow coloured. As far as the two neat homopolymers are concerned, it can be noted from Table 4.6 that both PBS and PTES were characterized by relatively high molecular weights, indicating that appropriate synthesis conditions and a good polymerization control were obtained. In order to have an understanding into their chemical structure, the <sup>1</sup>H-NMR investigation on these two samples was performed. In both cases, the spectra were found to be consistent with the expected structure.

In order to optimize the mixing conditions of copolyester samples, several preliminary runs were carried out at different reaction temperatures (165, 215, 225 and 233°C).

The best temperature turned out to be 225°C: at this temperature transesterification reactions occurred with appreciable rate permitting the preparation of polymers with different block length. These last are listed in Table 4.6 along with some molecular characterizations data. As it can be seen, all the copolyesters were characterized by relatively high and similar molecular weights, comparable to those of parent homopolymers. Looking into more detail the data, a slight increase of molecular weight with the mixing time is observed. This result is not surprising taking into account that transesterification reactions prevail on chain scission reactions at long mixing times, in the range of time employed.

The chemical structure of all copolyesters was determined by <sup>1</sup>H-NMR spectroscopy. As an example, the <sup>1</sup>H-NMR spectrum of PBSPTES<sub>70</sub> is shown in Figure 4.11, together with the chemical shift assignments. In all cases, the spectra were found to be consistent with the expected structures. The copolymer composition was calculated from the relative areas of the <sup>1</sup>H-NMR resonance peak of the **b** aliphatic proton of the butanediol subunit located at 4.11 ppm and of the **d** protons of the methylene groups of the triethylene diol subunit at 4.25 ppm. From the data of Table 4.6, it can be seen that in all cases the actual molar composition is close to the feed one.

**Table 4.6** Molecular characterization data.

polymer	$M_n$	$PDI$	$TES$ (mol %) ( $^1H$ -NMR)	$L_{BS}$	$L_{TES}$	$b$
PBS	40000	2.2	0.0	-	-	-
PTES	27000	3.6	100.0	-	-	-
PBSPTES5	26000	4.0	50.2	33	32	0.06
PBSPTES15	25000	4.1	50.3	10	9	0.21
PBSPTES20	24000	3.9	50.1	6.3	6.7	0.31
PBSPTES30	27000	3.7	50.2	4.5	4.1	0.47
PBSPTES35	27500	3.8	50.1	3.0	3.0	0.66
PBSPTES45	28500	3.8	50.2	2.3	2.4	0.84
PBSPTES60	28500	3.9	50.3	2.2	2.2	0.91
PBSPTES70	31200	3.5	50.4	2.0	2.0	1.10

$^1H$ -NMR spectra can be also used to study the structural changes occurring by transesterification reactions in the blends and the progress of these reactions with the change of reaction conditions such as time and temperature. In particular new peaks appeared in the region between  $\delta = 2.61$  and  $\delta = 2.65$ , as the transesterification reactions between PBS and PTES proceeded (Figure 4.11). The signals of the methylene protons adjacent to the ester group of succinic subunit are shifted respect to those of plain PBS and PTES, because of the presence of different environments. The arrangement of the comonomeric units in the chain was deduced by the degree of randomness  $b$ , calculated from  $^1H$ -NMR data (section 3.6.1).

As it can be seen from Figure 4.11, the resonance peaks due to mixed sequences are partially overlapped. In order to perform an accurate calculation of the two probabilities, a nonlinear fitting was performed with multiple Gaussian curves. The average sequence length for PBS and PTES repeated units and the degree of randomness of PBSPTES copolyesters are collected in Table 4.6. It is confirmed quantitatively from the data that the increment of mixing time increased the extent of transesterification reactions. In fact, as these latter proceeded, the average length of the copolymer sequences decreased and the degree of randomness increased. Therefore, we can conclude that the experimental conditions adopted permitted us to prepare a mechanical mixture of the two polymers, several block copolymers, whose block length decreases with the increment of mixing time ( $5 < t_{mix} < 60$  min), and a random copolymer (PBSPTES70), simply by changing the reaction time.

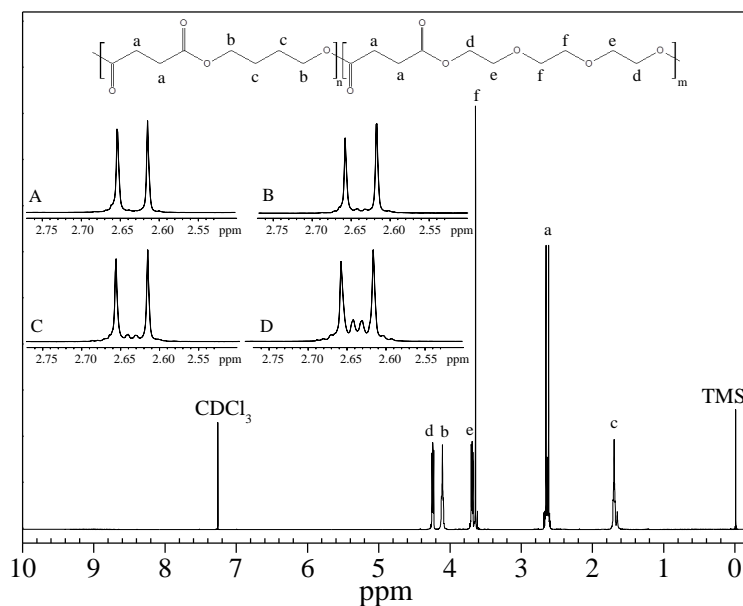


**Figure 4.11** <sup>1</sup>H-NMR spectrum of PBSPTES70 and resonance assignments with expansion of interesting aliphatic region between 2.55 and 2.75 ppm for: A PBSPTES15; B PBSPTES20; C PBSPTES35; D PBSPTES70.

#### 4.2.2 Thermal properties and crystallization ability

The polyesters were examined by thermogravimetric analysis and differential scanning calorimetry. The investigation on the thermal stability was carried out both in air and under nitrogen atmosphere. From the thermogravimetric curves in air of some samples under investigation shown in Figure 4.12,  $T_{onset}$  was determined and collected in Table 4.7. In all cases the weight loss took place practically in one-step and is 100%. From the comparison between the TGA curves of PBS and PTES, one can see that the ether oxygen-containing polyester is thermally less stable than PBS. As a matter of fact, as documented in the literature (Zimmermann, 1984) the introduction of etheroatoms along the polymer chains affects the thermal stability, in particular favoring the thermooxidative processes of decomposition. A confirmation of this hypothesis can be obtained comparing the thermal stability of PTES, characterized by two ether-oxygen atoms per repeat unit, with that of poly(diethylene succinate) (PDGS), previously investigated (Soccio *et al.*, 2008) which contains only one ether-oxygen atom per repeating unit. This latter turned out in fact more thermally stable, being characterized by a  $T_{onset} = 356^{\circ}\text{C}$ , a value higher than that of PTES. As far as PBSPTES copolymers are concerned, their thermal stability was found to be similar and intermediate with respect to those of homopolymers.

**Table 4.7** Thermal characterization data.

polymer	$T_{\text{onset}}$ (°C)	1 <sup>st</sup> scan				2 <sup>nd</sup> scan						
		$T_g$ (°C)	$\Delta C_p$ (J/°C·g)	$T_m$ (°C)	$\Delta H_m$ (J/g)	$T_g$ (°C)	$\Delta C_p$ (J/°C·g)	$T_c$ (°C)	$\Delta H_c$ (J/g)	$T_m$ (°C)	$\Delta H_m$ (J/g)	$T_{cc}$ (°C)
PBS	394	-32	0.182	115	81	-34	0.212	-	-	115	62	92
PTES	348	-33	0.798	-	-	-33	0.798	-	-	-	-	-
PBSPTES5	354	-30	0.665	114	39	-31	0.686	-	-	114	35	88
PBSPTES15	354	-31	0.621	107	37	-32	0.668	-	-	107	34	80
PBSPTES20	355	-32	0.607	99	36	-32	0.606	-	-	99	32	59
PBSPTES30	357	-32	0.601	81	35	-32	0.607	-	-	81	30	50
PBSPTES35	359	-34	0.654	73	32	-37	0.710	29	26	73	27	20
PBSPTES45	362	-33	0.674	67	30	-37	0.706	34	9	63	10	18
PBSPTES60	362	-34	0.665	63	29	-37	0.699	35	5	61	6	14
PBSPTES70	372	-34	0.666	53	25	-37	0.844	-	-	-	-	-

However, it is worth noting that all the samples were characterized by a good thermal stability. Similar trends were obtained by means of TGA measurements carried out under nitrogen atmosphere.

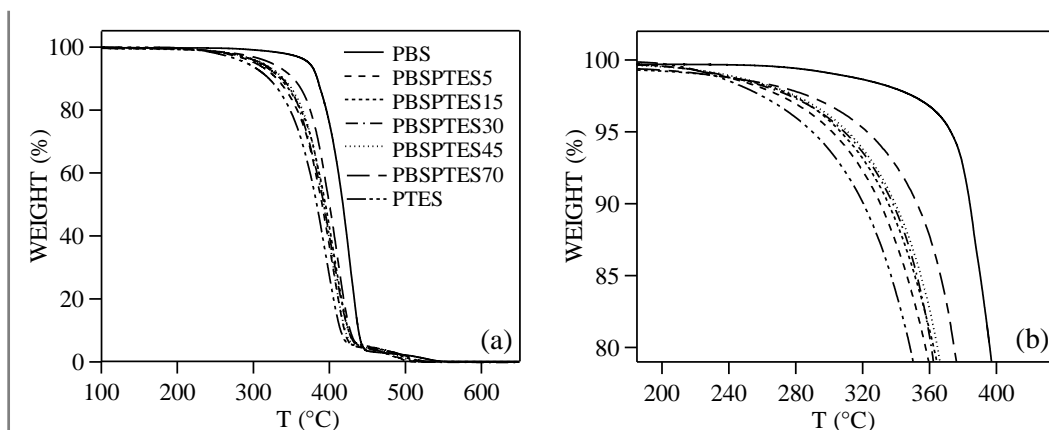


**Figure 4.12.** (a) Thermogravimetric curves of PBS, PTES and of some PBSPTES copolymers in air (heating rate: 10 °C/min). (b) Enlarged view of TGA curves.

As regards calorimetric results, being the samples characterized by high  $M_n$ s, an influence of molecular weight on the glass transition and melting of the polymers synthesized can be excluded.

It is well established that the melting behaviour of a polymer is affected by its previous thermal history and therefore, in order to provide the same heat treatment to all the samples

investigated, as mentioned above, prior to thermal analysis each sample was kept at room temperature for about 4 weeks. The DSC traces of the so-treated samples are reported in Figure 4.13 and the results obtained in Table 4.7.

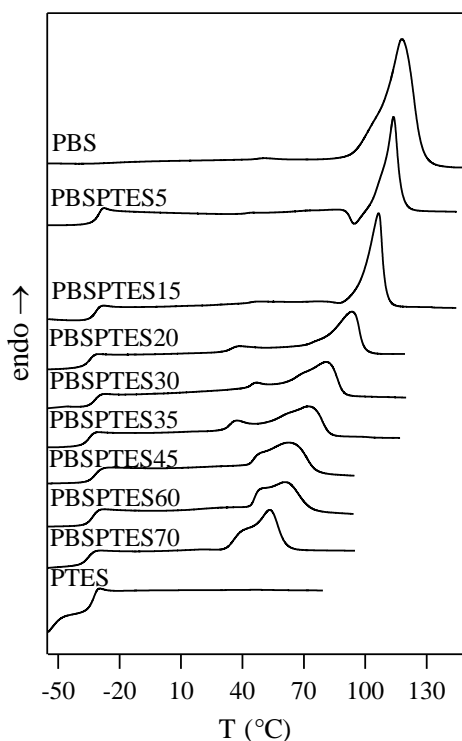


**Figure 4.13**  
Calorimetric curves  
of PBS, PTES and  
their copolymers  
(1<sup>st</sup> scan).

In all cases, a glass transition and a melting endotherm are evident, with exception of PTES, whose DSC trace was characterized only by an endothermal baseline deviation associated with the glass transition phenomenon. First of all, it has to be emphasized that the phase behaviour of the two parent homopolymers is opposite: PBS is semicrystalline, whereas PTES completely amorphous. As is well known, the crystallization capacity of a polymer is correlated to several factors, among these the flexibility and the symmetry of the polymeric chain. This latter is low in PTES, due to the presence of ether-oxygen atoms (whose van der Waals radius ( $1.4 \text{ \AA}$ ) is significantly lower than that of the neighbor  $-\text{CH}_2$  groups ( $2.0 \text{ \AA}$ )). As far as the glass transition phenomenon is concerned, from the data collected in Table 4.7 it can be evinced that the two homopolymers are characterized by similar  $T_g$  values, even though PBS is semicrystalline, whereas PTES is completely amorphous. Such difference can be ascribed to interchain interactions present in PTES, due to the polarity of ether-oxygen atoms. Quite interestingly,  $T_{g,\text{PTES}} < T_{g,\text{PDGS}}$ , even though the former contains two ether-oxygen atoms per repeat unit and the latter only one. Therefore, it is expected that stronger interchain interactions occur in PTES. To explain

this anomalous result, it has to be considered that repeating unit of PTES is characterized by a higher number of methylene groups (two more) than PDGS. Therefore, in order to analyse the influence of chemical structure on glass transition temperature, two effects have to be taken into consideration: i) a higher number of methylene groups made more flexible the polymer chain; ii) a higher number of ether-oxygen atoms per repeat unit caused a decrement of the polymer chain mobility, because of the stronger interchain interactions. In this case, the first effect prevailed on the second one.

As far as the PBSPTES copolymers are concerned, only one glass transition temperature was always clearly evident, independently of block length. However, no consideration can be made on miscibility having the two parent homopolymers very similar  $T_g$  values. Concerning the melting phenomenon, it can be noted that the endothermic process became broader and its peak shifted to lower temperature as the mixing time increased. Being PTES completely amorphous, the melting peaks observed in the copolymers can be attributed to the fusion of the crystalline phase of PBS. Therefore, the decrement of the block length induced the formation of crystals with a low degree of perfection and a wide distribution of dimensions. As far as the heat of fusion is concerned, it was found that it regularly decreased as the block length was decreased, indicating that PBS crystallized in the copolymers in minor percentage as in the pure state.

Moreover, in the case of copolymers with short BS block length (PBSPTES45 and PBSPTES60) and of random copolymer (PBSPTES70), multiple melting endotherms were evident, that can be ascribed to melt-recrystallization processes taking place during the DSC scan, similarly to PBS homopolymer (Yoo & Im, 1999; Yasuniwa *et al.*, 2002). In order to investigate more deeply the nature of the crystalline phase in the polymers under investigation, X-ray analysis was performed. The X-ray diffraction profiles for PBS and some of PBSPTES copolymers are reported in Figure 4.14. As it can be seen, all the patterns of copolymers show intense reflections at the  $2\theta$  values of  $19.6^\circ$ ,  $21.8^\circ$ ,  $22.7^\circ$  and  $29.0^\circ$ . Taking into account the lattice parameters of the crystal phases of PBS, the observed peaks are attributable to the 020, 021, 110 and 111 planes of  $\alpha$ -PBS, respectively. Moreover, a strong similarity between the pattern of  $\alpha$ -PBS homopolymer and those of PBSPTES copolymers is evidenced in Figure 4.14.

The presence of TES units did not alter the kind of the pattern at the shortest reaction times. However, for times longer than 15 min the reflections became broader and the peak 021 was no more visible, even though the crystalline fraction is ordered in the same manner, i.e. the phase is always  $\alpha$ -PBS, independently on the reaction time.

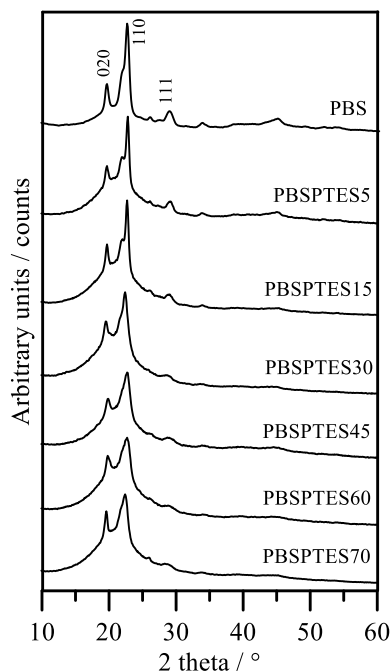


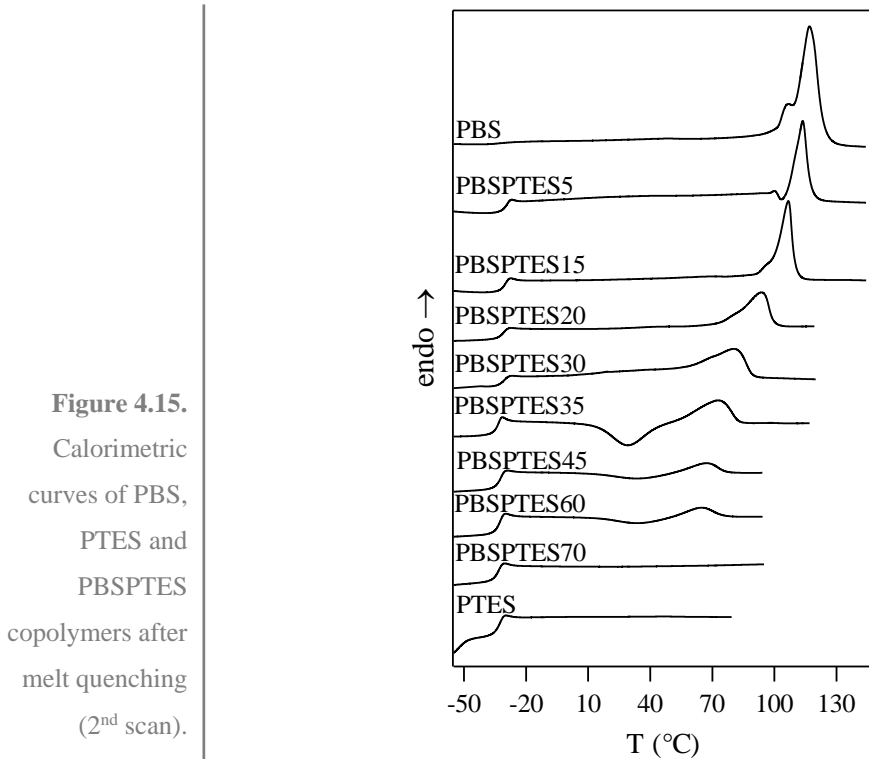
**Figure 4.14** XRD patterns of PBS and PBSPTES copolymers.

The mean crystal sizes and the crystallinity indexes for some of the copolymers investigated are reported in Table 4.8, together with PBS homopolymer for sake of comparison. The crystallinity index and the peak sharpness roughly decreased as the reaction time increased, giving evidence of a general worsening of the order degree and a reduction of the size of the ordered domains as the reaction went on.

**Table 4.8** Crystallinity indexes ( $\chi_c$ ) and coherent domain lengths in the direction perpendicular to 0 2 0 planes ( $L_{020}$ ).

polymers	$\chi_c$ (%)	$L_{020}$ (nm)
PBS	$41 \pm 4$	
PBSPTES5	$32 \pm 3$	18
PBSPTES15	$29 \pm 3$	16
PBSPTES20	$29 \pm 2$	16
PBSPTES30	$24 \pm 4$	14
PBSPTES35	$22 \pm 3$	13
PBSPTES45	$20 \pm 3$	13
PBSPTES60	$20 \pm 3$	13
PBSPTES70	$19 \pm 3$	12

Considerations on the crystallization capacity of the PBSPTES copolymers can be done on the samples quenched from the melt. The corresponding DSC traces are shown in Figure 4.15: as it can be seen, the calorimetric traces of PBS, PBSPTES5, PBSPTES15, PBSPTES20, and PBSPTES30 are characterized by a glass transition followed by a conspicuous melting endotherm.



The DSC curves of PBSPTES $t$  copolymers obtained after a mixing time ranging from 35 to 60 minutes showed a glass transition followed by an exothermal “cold crystallization” peak and a melting endotherm at higher temperature. In all cases, the enthalpy of crystallization well compared with the corresponding heat of fusion, indicating that these polymers are completely amorphous. As regards the calorimetric curve of the pure PTES and random PBSPTES70 copolymer, only an intense endothermal baseline deviation associated with the glass transition was observed. The phase behaviour of PBSPTES $t$  copolymers appeared to depend on the mixing time (therefore on the block length): as a matter of fact, after melt quenching, completely amorphous samples can be exclusively obtained at long mixing times.

Regarding the glass transition phenomenon, in all cases only one glass transition was evident, analogously to the first scan. In particular, the PBSPTES $t$  copolymers obtained at mixing times longer than 30 min, which, as mentioned above, are completely amorphous

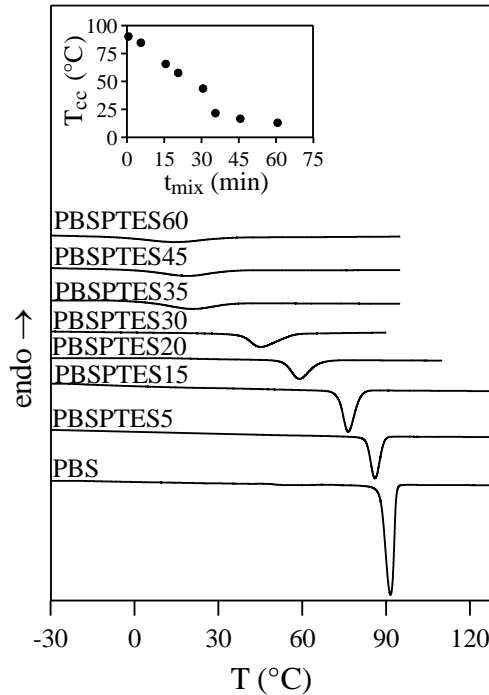
after melt quenching, showed a glass transition of  $-37^{\circ}\text{C}$ , which perfectly agreed with the value predicted by the Fox equation, valid for random copolymers and/or miscible polymer blends (with  $T_g$  values of  $-39^{\circ}\text{C}$  for completely amorphous PBS (Legras *et al.*, 1986) and  $-33^{\circ}\text{C}$  for PTES). In the case of copolymers obtained at  $5 < t_{\text{mix}} < 30$  min slightly higher values of  $T_g$  were found (Table 4.7). This result can be explained on the basis of two effects: i) the crystallinity present in these samples acted like crosslinking and gave rise to a restrictive effect on the segmental motion of amorphous polymer chains; ii) a progressive enrichment of the amorphous phase in triethylene succinate segments took place as crystallinity developed.

As far as the “cold crystallization” peak is concerned, it is worth noting that the  $T_c$  values increased from PBSPTES35 to PBSPTES60, indicating that the rate of crystallization of PBS decreased. This fact can be considered the result of two effects, which became more significant with decreasing the BS block length: the former is an increment of the copolymer  $T_g$  together with a decrease of the copolymer  $T_m$  which reduce the  $T_g/T_m$  window, hindering the crystallization process (the mobilization and the consequent rearrangement of the macromolecules into 3-dimensional order can occur in a narrower temperature range); the latter is a marked decrement of the transport of crystallizable chain segments on the crystal growth surface, due to the TES blocks, which act as defects during the chain folding of BS blocks. As a matter of fact, in PBSPDGS90 block copolymer the tendency of BS sequences to crystallize is completely undone (Soccio *et al.*, 2008). Therefore, we can conclude that PBSPTES copolymeric chains are characterized by a higher flexibility and mobility with respect to PBSPDGS ones, as predictable on the basis of the fact that PTES has a  $T_g$  significantly lower than that of PDGS ( $-23^{\circ}\text{C}$ ).

To confirm that in the copolymers the tendency of PBS to crystallize decreases, non-isothermal experiments were carried out, subjecting the samples to a controlled cooling rate from the melt (section 3.7.2). It is worth remembering that the half-time of primary crystallization in isothermal experiments correlates with the temperature corresponding to the maximum of the crystallization peak in non-isothermal experiments ( $T_{cc}$ ), being this latter more easily obtainable. The exothermic crystallization peaks of the samples under investigation are displayed in Figure 4.16: as it can be seen, the random copolymer is not reported being unable to crystallize even though cooled from the melt at very low rate ( $1^{\circ}\text{C}/\text{min}$ ). From the inset of Figure 4.16, where the  $T_{cc}$  values are reported as a function of mixing time, it can be observed that the temperature corresponding to the maximum of the exothermal crystallization peak regularly decreased as the mixing time was increased.

This result indicates that the crystallization process was more and more difficult as the BS blocks became progressively shorter and the copolymer tended toward a random distribution of the sequences. Such trend is due to the effect of the PTES phase, which limits the transport of the PBS chains on the crystal surface and can act as a defect during chain folding. Therefore, in block copolymers, a decrement of the crystallization rate with a reduction of the block length is evident.

**Figure 4.16.** DSC crystallization exotherms of PBS and PBSPTES copolymers cooled from the melt at 5°C/min. In the inset:  $T_{cc}$  as a function mixing time.



#### 4.2.3 Mechanical characterization and wettability behaviour

Some of the copolymers under study have been subjected to further characterization. In particular, stress-strain measurements, wettability and enzymatic degradation studies have been performed on hot-pressed films of PBSPTES15, PBSPTES20, PBSPTES35, PBSPTES70.

Tensile mechanical properties (section 3.9) of the investigated polymers are reported in Table 4.9, where elastic modulus  $E$ , stress at break  $\sigma_b$ , and deformation at break  $\epsilon_b$  are listed. PBS homopolymer displayed the highest elastic modulus and the stiffest behaviour among the synthesized polymers, with a relatively low deformation at break ( $\epsilon_b=31\%$ ). PBSPTES15 and PBSPTES20 displayed a very similar mechanical behaviour with elastic moduli and stresses at break significantly lower than those of PBS, but a comparable deformation at break. In the case of PBSPTES35 and PBSPTES70, elastic modulus

regularly decreased, whereas deformation at break regularly increased with block length. Interestingly, PBSPTES70 was characterized by an elastomeric behaviour, with an extremely high deformation at break that reached a value of about 700%. Overall, mechanical characterization demonstrated that the introduction of TES units into PBS chains resulted in a significant change in the copolymer mechanical properties.

**Table 4.9** Mechanical characterization and wettability data.

polymer	E (MPa)	$\sigma_b$ (MPa)	$\epsilon_b$ (%)	WCA(°)
PBS	490 ± 30	24 ± 4	31 ± 2	96 ± 3
PBSPTES15	95 ± 12	6.6 ± 0.9	23 ± 5	43 ± 6
PBSPTES20	93 ± 12	6.2 ± 0.4	23 ± 5	53 ± 4
PBSPTES35	59 ± 6	5.9 ± 0.5	225 ± 15	62 ± 4
PBSPTES70	47 ± 4	7.0 ± 0.7	700 ± 70	70 ± 3

However, mechanical behaviour was not directly correlated to BS and TES block length, since PBSPTES15 and PBSPTES20 had similar tensile properties. Moreover, only PBSPTES70 displayed a peculiar elastomeric behaviour. To gain further understanding of this result, mechanical properties were interpreted on the basis of the reported thermal and structural characterization data, that allowed the estimation of the amount of crystal phase in the materials. Since all the investigated polymers displayed a soft amorphous phase ( $T_g$  values are in all cases well below room temperature) and a rigid hard crystal phase, the observed trend can be explained on the basis of polymer crystallinity degree (see Table 4.8): in fact, PBS, the most rigid material, displayed the highest amount of crystal phase, PBSPTES15 and PBSPTES20 had a similar  $\chi_c$ , whereas in PBSPTES35 and PBSPTES70 the lower amount of rigid crystal phase dispersed in a higher amount of mobile amorphous phase decreased with block length.

In order to investigate the relative hydrophilicity of PBS and PBSPTES<sub>t</sub> films, water contact angle (WCA) measurements were performed (section 3.10). Table 4.9 reports the contact angle values for each polymer: PBS was the most hydrophobic material and the presence of TES units along the chain resulted in increasing material hydrophilicity, due to the PEG-like portion. In the copolymers wettability appeared remarkably affected by block length, in particular, longer blocks led to higher wettability.

### 4.2.3 Enzymatic degradation

To evaluate the biodegradability of the copolyesters under investigation in a short time scale, enzymatic degradation was performed in the same optimized conditions utilized in the previous work (section 4.1.3). As reported in the previous paragraph (section 4.1.5) the turbidimetric film assay was used for studying the early stages of biodegradation. No appreciable increments of  $OD_{475}$  were observed for homopolymer PBS and PBSPTES15 and PBSPTES20 in the time scale explored and this indicates that these products degrade much slower than PBSPTES35 and PBSPTES70, which on the contrary showed a relevant increment of optical density at 475 nm. From a comparison between the latter two copolymers, it can be found that PBSPTES70 copolymer is characterized by a biodegradation rate about eight times higher ( $30.3 \pm 0.7 \Delta\text{mAU min}^{-1}$ ) than that of PBSPTES35 ( $4.35 \pm 0.05 \Delta\text{mAU min}^{-1}$ ). The lower biodegradability of PBSPTES35 can be explained on the basis of the higher melting point, amount of crystal phase and larger mean crystal size present in this sample, in spite of its slightly higher hydrophilicity, as compared to the random one.

The higher crystallinity degree of block copolymer can be explained on the basis of its higher crystallizing ability, which is normally lower for shorter crystallizing blocks (BS blocks), as previously reported (section 4.1.1).

The biodegradation process of samples under investigation at longer enzyme exposition times was investigated by carrying out weight loss measurements (Figure 4.17).

As already reported (section 4.1.4), after one year of incubation PBS practically did not lose weight, whereas all copolymers appreciably degraded: in particular, biodegradation rate appeared to be strongly affected by the block length. Interestingly, no regular trend of biodegradation rate with block length was however found: as a matter of fact PBSPTES15 appeared characterized by a higher biodegradation rate as compared to PBSPTES20. Moreover, PBSPTES35 and PBSPTES70 degraded much faster than block copolymers with long sequences. To explain the trend observed, it has to be reminded that the following factors influence the biodegradability of a polymer: crystallinity degree, crystal dimensions and hydrophilicity. It is commonly accepted that low crystallinity degree, small crystal size and high hydrophilicity improve the biodegradability.

Therefore, the higher biodegradation rate of PBSPTES15 with respect to PBSPTES20 can be attributed to its higher hydrophilicity, the crystallinity degree being comparable for the two copolymers. On the contrary, the consistently higher biodegradability of PBSPTES35

and PBSPTES70 with respect to PBSPTES15 and PBSPTES20 has to be ascribed to their lower crystallinity degree and melting point.

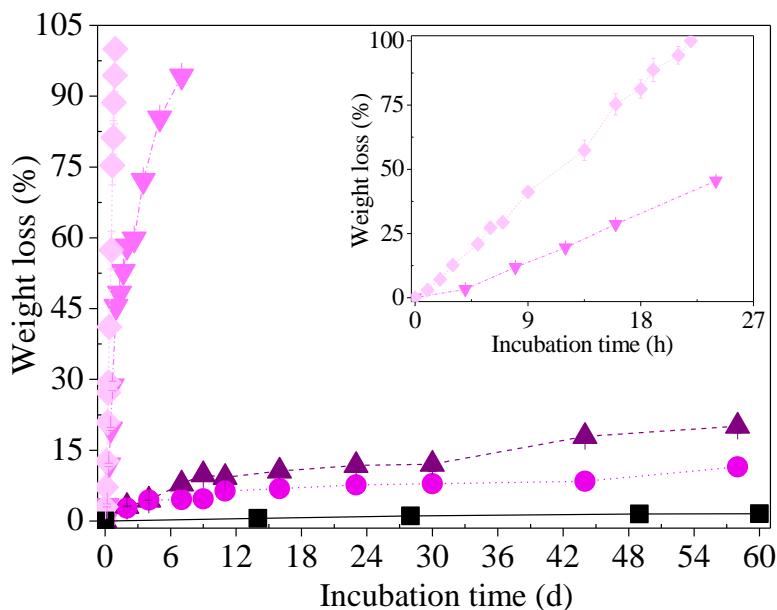


**Figure 4.17** Weight loss (%) as a function of incubation time: (■) PBS; (▲) PBSPTES15; (●) PBSPTES20; (▼) PBSPTES35; (◆) PBSPTES70. In the inset the weight loss of PBSPTES35 and PBSPTES70 are shown in an enlarged scale.

As mentioned above, PBSPTES70 degraded faster than PBSPTES35 because of its further lower degree of crystallinity and melting point. Moreover, as evident in Figure 4.17, in the case of PBSPTES15 and PBSPTES20 a decrement of rate of enzymatic hydrolysis was observed at longer incubation time, in agreement with data reported in the literature for PBS and its copolymers (Yang *et al.*, 2004).

Hydrolytic degradation studies in buffer solution without enzyme addition were also carried out. In the case of PBSPTES35 and PBSPTES70 the weight loss was negligible; for PBSPTES15 and PBSPTES20, over a period of 58 days polymer mass loss was 6 and 4% respectively, confirming the trend found when enzyme was present.

A confirmation that the amorphous regions of a polymer are degraded more quickly than the crystalline ones, as reported in the previous chapter (section 4.1.4) was obtained by subjecting the partially degraded copolymer samples to a heating calorimetric scan (20°C/min). All the calorimetric traces were found to be characterized by an endothermic peak associated with the fusion process of crystalline portion of the material (data not shown). The corresponding heat of fusion was normalized respect to the heat of fusion of

non-degraded sample ( $\Delta H_i/\Delta H_0$ ). As an example, the results obtained for PBSPTES15 and PBSPTES20 are reported in Figure 4.18a.

In both cases, initially the normalized heat of fusion regularly increased with incubation time up to a maximum value, then kept practically constant. The observed trend is in agreement with data reported in the literature indicating that at first crystallinity of the samples increases rapidly, then levels off to a much slower rate (Spyros *et al.*, 1997). Our results confirmed that the mobile amorphous regions of the sample are preferentially degraded, due either to the easier access of enzyme to the polymer chain and to the higher diffusion rate of water. Similar behaviour was shown by PBSPTES35 and PBSPTES70.

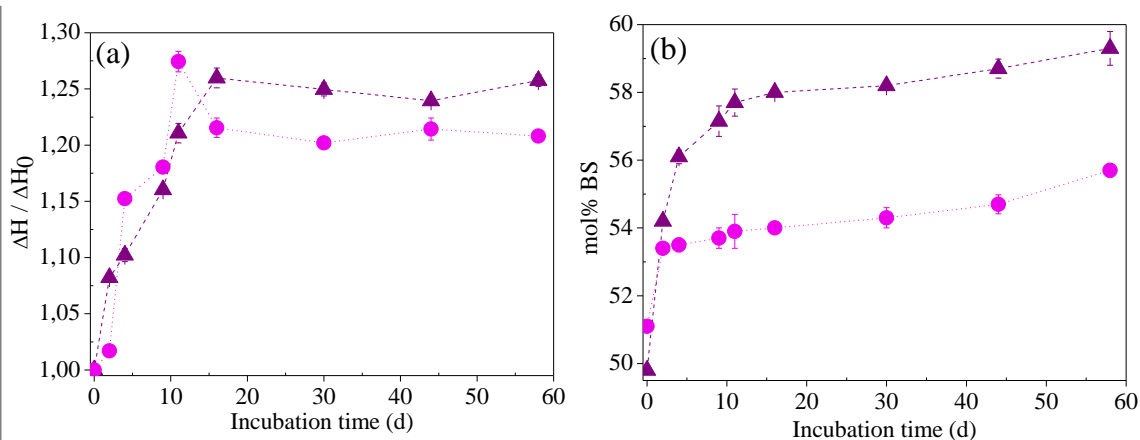


**Figure 4.18** (a) Normalized heat of fusion and (b) copolymer composition (expressed as mol% of BS units) as a function of incubation time for: (▲) PBSPTES15; (●) PBSPTES20.

In order to gain a better understanding of the enzymatic degradation mechanism of the copolymers,  $^1\text{H-NMR}$  measurements were performed on degraded retrieved samples. As an example, Figure 4.18b reports the content of BS units in mol% as a function of degradation time. An evident increase of BS content was observed during degradation, which was more relevant for samples with longer blocks. In particular, after about 60 days of enzyme solution exposure, the amount of BS units increased from the initial 50 mol% of the non-degraded samples up to 59%, and 56%, for PBSPTES15 and PBSPTES20 respectively. The variation of composition during polymer enzyme exposition was more modest in the case of PBSPTES35, whereas the chemical composition of PBSPTES70 remained constant. Copolymer composition change indicates that ester cleavage preferentially occurred on chain segments containing long TES sequences, which, due to their hydrophilic nature, were easily solubilized in water. On the contrary, the long highly hydrophobic BS blocks were much more resilient to hydrolytic biodegradation.

The constancy of composition observed in random copolymer is probably related to the solubilisation in water of the short hydrophobic BS blocks, in spite of the still preferential attack by enzyme of TES sequences.

The morphology of the polymer films was analysed using SEM; micrographs of some of polymer films taken before and after enzymatic hydrolysis are presented in Figure 4.19.

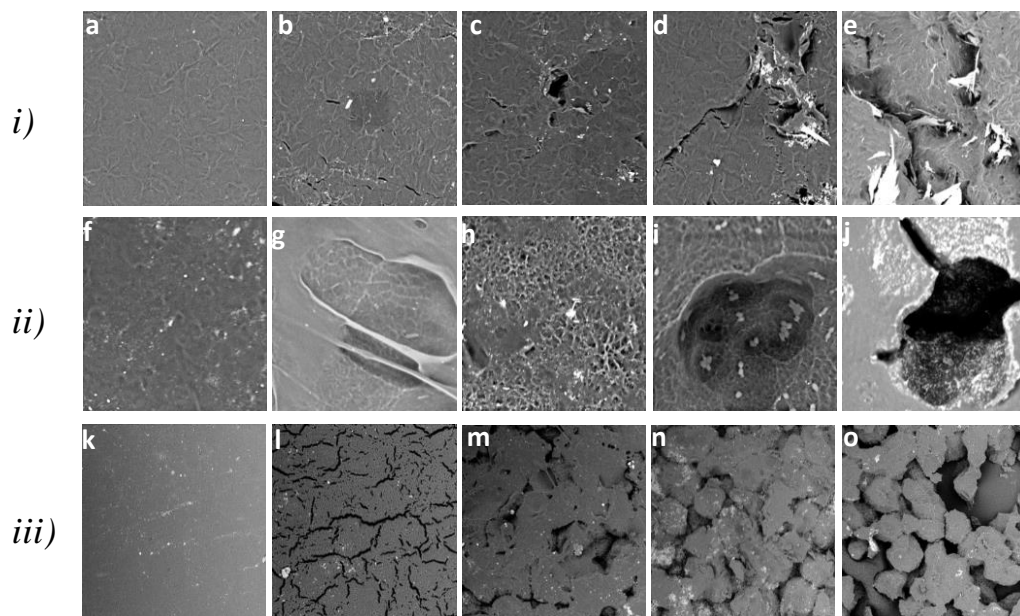


**Figure 4.19** SEM micrographs of PBSTES<sub>t</sub> copolymers during enzymatic hydrolysis at several times: *i*) PBSPTES20 at (a) 0, (b) 2, (c) 7, (d) 16, (e) 58 days, 5000× magnification; *ii*) PBSPTES35 at (f) 0, (g) 12, (h) 24, (i) 48, (j) 88 hours, 10000× magnification; *iii*) PBSPTES70 at (k) 0, (l) 2, (m) 7, (n) 16, (o) 21 hours, 1000× magnification.

The micrograph of all samples under investigation prior to enzyme exposure revealed a homogeneous and smooth surface. On the contrary, after enzyme exposure, surface irregularities appeared, which became deeper by increasing the exposure time. Then holes, cracks and channels formed, whose dimensions increased with enzyme exposure time. Looking into more detail, each copolymer showed different behaviour depending on the block length, as it was also found from weight loss measurements. For PBSPTES70, which showed a large mass loss even from the first 2 hours of enzymatic hydrolysis, large parts of the film surface were removed after 21 hours. On the other hand, only small holes were created on the film surface in PBSPTES20, in agreement with a consistently lower rate of weight loss.

In conclusion, on the basis of biodegradation profiles of the samples under investigation, copolymers with long blocks could be utilized as mulching films for seasonal crops, whereas those characterized by very short blocks proved to be interesting for disposable packaging.

#### 4.2.4 Comparison between PBSTES and PBSPDGS copolymers

In a previous paragraph (section 4.1), copolymers of PBS containing diethylene succinate sequences (PBSPDGS) with different molecular architecture have been described: in particular, a block copolymer with long sequences ( $L_{BS}$ ,  $L_{DGS} = 23$ ) and a random one (with very short sequences,  $L_{BS}$ ,  $L_{DGS} = 2$ ) have been considered.

On the basis of the chemical structure of PDGS and PTES, it is expected that TES sequences impart to the final material a higher hydrophilicity than DGS ones. In order to analyse the effect of different chemical structure on polymer biodegradability, some “ad hoc” comparisons between the two copolymeric systems have been performed. In Figure 4.20a, weight loss measurements as a function of incubation time are reported for PBSPTES15, PBSPTES20 and PBSPDGS $_{block}$  ( $L_{BS} = 23$ ): as it can be seen, PBSPDGS copolymer degraded significantly faster than the others two, in spite of very similar crystallinity degree ( $\chi_{c,PBSPTES15}$  and  $\chi_{c,PBSPTES20} \cong 28\%$ ,  $\chi_{c,PBSPDGS_{block}} \cong 27\%$ ). The marked difference can be explained remembering that surface polymer film must have a balanced hydrophobic/hydrophilic ratio. From the water contact angle values ( $WCA_{PBSPDGS_{block}} = 66^\circ$ ,  $WCA_{PBSPTES15} = 43^\circ$ ), it can be evicted that surface of PBSPTES15 film is markedly more hydrophilic than that of PBSPDGS $_{block}$ .

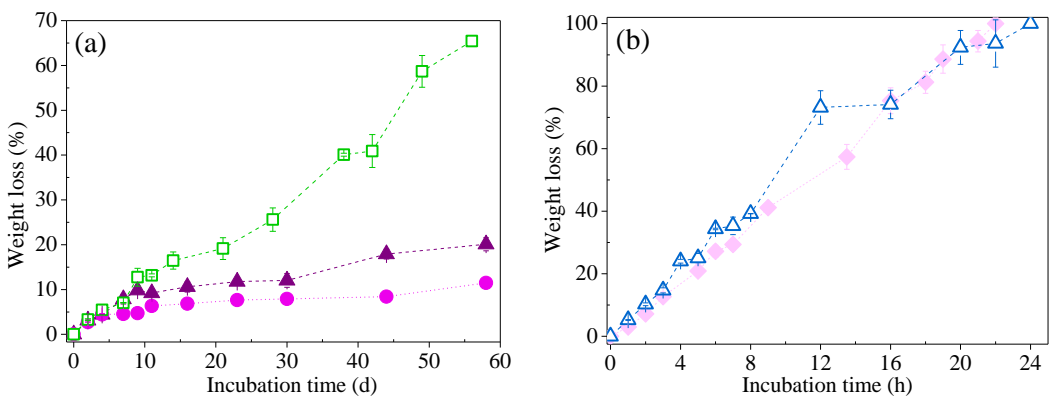


**Figure 4.20** Weight loss data as a function of incubation time for: (a) block copolymers: ( $\square$ ) PBSPDGS $_{block}$ ; ( $\blacktriangle$ ) PBSPTES15; ( $\bullet$ ) PBSPTES20; (b) random copolymers: ( $\triangle$ ) PBSPDGS $_{random}$ ; ( $\blacklozenge$ ) PBSPTES70.

It is long known that extra-cellular hydrolytic enzymes, such as lipases, are water-soluble enzymes acting on non-soluble substrates. Maximum activity occurs only when the enzyme is adsorbed to an oil-water interface. Lipases contain buried catalytic sites whose activation occurs as a result of a conformational change induced upon binding to a lipid interface. In aqueous media, an  $\alpha$ -helical lid covers the active site of the enzyme and blocks the access to the substrate. However, when in contact with a hydrophobic surface, the  $\alpha$ -helical lid rolls back upon the body of the molecule, whereby the active site becomes fully accessible, enhancing substantially the hydrophobicity around the active site, and the enzyme assumes the active conformation (Tokiwa & Suzuki, 1977). On this ground, in the case of PBSPTES15 and PBSPTES20 the more hydrophilic surface film hinders the adhesion of enzyme molecules to polymer film, slowing down the biodegradation process on respect to the more hydrophobic PBSPDGS*block*. Once enzyme molecules were adsorbed on solid substrates through hydrophobic interactions, hydrolysis of ester groups by water catalysed by catalytic enzyme domains took place more easily as the polymer is more hydrophilic and this explained the higher biodegradation rate of PBSPTES15 with respect to PBSPTES20.

In Figure 4.20b, random copolymers of the two copolymeric systems are compared: the two samples biodegraded with the same rate, as expected considering the similar crystallinity degree ( $\chi_c \cong 18\%$ ).

In conclusion, from the comparisons made, it can be pointed out that in the presence of long sequences biodegradation rate of copolymers is determined by hydrophilic/hydrophobic ratio, which has to be balanced; on the contrary, for random copolymers, biodegradability is governed by crystallinity degree.

#### 4.2.5 Conclusions

For this series of copolyesters possessing the same chemical composition, thermal and mechanical properties, surface wettability, and enzymatic biodegradation rate can be tailored by simply varying block length. In terms of mechanical properties, we were able to synthesize polyesters whose stiffness and deformability can be tailored by controlling the crystallinity degree. In particular, PBSPTES70 showed the lowest value of elastic modulus and the highest deformability, and thus this polymer can be used as elastomer. The introduction of ether-oxygen atoms along PBS polymer chain revealed to be a winning strategy to increase the PBS biodegradability, allowing to tailor both crystallinity degree and hydrophobic/hydrophilic ratio. Moreover, it has been observed that block length has a remarkable effect on enzymatic hydrolysis rate. Indeed, in vitro degradation experiments

performed over a period of 58 days showed that polymer mass loss can be tuned from 5 to 100% by simply decreasing block length.

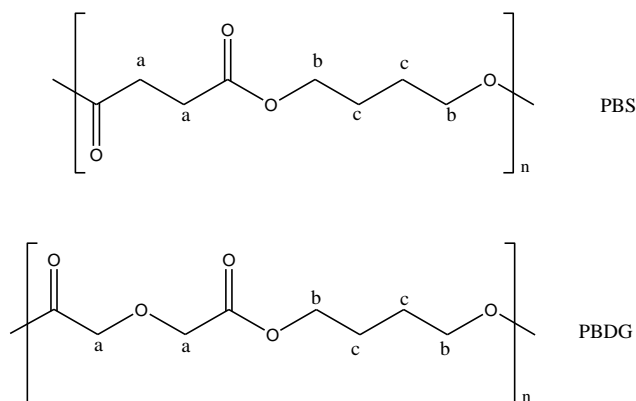
### 4.3 Synthesis and characterization of novel PBS-based copolyesters designed as potential candidates for soft tissue engineering

In the present work, PBS polymer chain has been modified by insertion in the diacid sub-unit of an ether-oxygen atom. At first, PBS and poly(butylene diglycolate) (PBDG) have been prepared by the usual two-stage polycondensation procedure; then block poly(butylene succinate/diglycolate) copolyesters (PBSPBDG) were obtained by reactive blending of PBS and PBDG.

Herein, the results concerning the synthesis and the molecular, thermal and mechanical characterization of PBS, PBDG and PBSPBDG copolymers are described, paying particular attention to structure-properties correlation, that is fundamental to design tailor-made materials for specific applications. In the following, the synthesized polymers will be named PBSPBDG<sub>t</sub>, with *t* equal to the mixing time during reactive blending.

#### 4.3.1 PBS and PBDG homopolymers characterization

At room temperature the as-prepared polyesters were opaque and light yellow coloured. The obtained polymers were carefully purified by dissolution in chloroform and re-precipitation in methanol. The purification procedure was repeated three times. Finally, the samples were kept under vacuum at room temperature (RT) for several days in order to remove the residual solvent. Afterwards, both samples were kept at ambient temperature for further 2 weeks prior to characterization. As it can be noted from Table 4.10 reported below, both PBS and PBDG were characterized by relatively high molecular weights, indicating that appropriate synthesis conditions and a good polymerization control were obtained. In order to have an understanding into their chemical structure, the <sup>1</sup>H-NMR investigation on these two samples was performed. In both cases, the spectra were found to be consistent with the expected structure, the chemical shift assignments ( $\delta$ , ppm) being the following: PBS:  $\delta = 4,099$  (t, H<sup>4b</sup>),  $\delta = 2,605$  (s, H<sup>4a</sup>),  $\delta = 1,689$  (m, H<sup>4c</sup>); PBDG:  $\delta = 4,23$  (s, H<sup>4a</sup>);  $\delta = 4,191$  (t, H<sup>4b</sup>);  $\delta = 1,732$  (m, H<sup>4c</sup>) as from the following chemical structure:



Subsequently, the two polyesters were subjected to thermogravimetric analysis and the temperatures corresponding to 5% weight loss ( $T_{5\%}$ ) and to the maximum weight loss rate ( $T_{\max}$ ) were determined and collected in Table 4.11.

As evidenced in Figure 4.24 reported in the following, in both cases the weight loss took place practically in one-step and the thermogravimetric curves were characterized by a char residue higher for PBDG sample. From the comparison between the two TGA curves of PBS and PBDG, it can be seen that the former is more thermally stable than the latter, except in the low temperature range where the ether oxygen-containing polyester appeared to be more stable (section 4.2.2).

As regards the calorimetric results, the phase behaviour of the two parent homopolymers was similar: as a matter of fact, both were semicrystalline, being the corresponding calorimetric traces characterized by a conspicuous melting endotherm (Table 4.11): PBDG  $T_m$  ( $T_{m,\text{PBDG}} = 66^\circ\text{C}$ ) was anyway significantly lower than that of PBS ( $T_{m,\text{PBS}} = 115^\circ\text{C}$ ). As a matter of fact, the perfection of crystalline phase is correlated to the symmetry of the polymeric chain, this latter being drastically reduced by the introduction of ether-oxygen atoms along the PBS polymer chains. It has to be emphasized that the van der Waals radius of oxygen atom (1.4 Å) is significantly lower than that of the neighbor –  $\text{CH}_2$  groups (2.0 Å).

Furthermore, as evidenced by the calorimetric curve shown in Figure 4.25, the endothermic process of PBDG is broader and characterized by a well-defined shoulder on the low temperature side, confirming the presence in this polyester of a crystalline phase with a low degree of perfection. After melt quenching, the phase behaviour of the two polymers became opposite: PBS was semicrystalline, whereas PBDG was completely amorphous, indicating that the capacity of crystallizing of PBS was significantly higher than that of PBDG.

The higher crystallization rate of PBS can be related to the higher symmetry and the higher flexibility of PBS polymer chain on respect PBDG one. Furthermore glass transition temperature of PBS ( $T_{g,PBS} = -39^{\circ}\text{C}$ ) turned out to be lower than that of PBDG ( $T_{g,PBDG} = -27^{\circ}\text{C}$ ) and this can be explained on the basis of interchain interactions among PBDG macromolecular chains, due to the electronegativity of ether-oxygen atoms. Lastly, as evidenced in Table 4.13, PBDG was characterized by a lower elastic modulus, a similar stress at break and a much higher elongation at break than PBS, indicating that PBS is stronger than PBDG. Since both the investigated polymers displayed a soft amorphous phase, the observed decrease in stiffness might be ascribed to the decrease in crystallinity degree ( $\chi_{c,PBS} = 41\%$  and  $\chi_{c,PBDG} = 34\%$ ).

#### 4.3.2 PBSPBDGt copolymers synthesis and molecular characterization

Several preliminary runs carried out at different reaction temperatures were performed (165, 215, 225 and 233°C), in order to optimize mixing conditions. The best temperature turned out to be 225°C, which was adopted to prepare the copolymers under investigation. At RT the as-prepared copolymers were opaque and light yellow coloured solids, analogously to parent homopolymers. Prior to characterization, the copolymers were also purified according to the procedure described above for the homopolymers.

**Table 4.10** Molecular characterization data of PBS, PBDG and PBSPBDGt copolymers.

polymer	$M_n$	$D$	$BDG$ (mol%) $^1\text{H-NMR}$	$L_{BS}$	$L_{BDG}$	$b$
PBS	51200	2.3	0	/	/	/
PBDG	28100	2.0	100	/	/	/
PBSPBDG5	33200	2.4	51.1	/	/	0
PBSPBDG20	35300	2.1	50.9	11.1	10.9	0.18
PBSPBDG40	34800	2.0	50.9	5.8	5.4	0.36
PBSPBDG60	37500	2.2	50.3	3.8	3.6	0.53
PBSPBDG90	41300	2.0	49.3	2.6	2.5	0.78
PBSPBDG120	49000	2.2	48.5	2.3	2.2	0.88
PBSPBDG180	47300	2.0	48.4	2.0	2.0	1.02

PBSPBDGt samples, together with the parent homopolymers for comparison, are listed in Table 4.10 along with molecular characterizations data. As it can be seen, all the

copolyesters were characterized by relatively high and similar molecular weights, comparable to those of PBS and PBDG. This result indicates that no relevant thermal degradation occurred during the mixing. Looking into more detail the data, a slight increase of molecular weight with the mixing time is observed. This result is not surprising taking into account that transesterification reactions prevail on chain scission reactions at long mixing times, in the range of time employed.

The chemical structure of all copolyesters was determined by  $^1\text{H-NMR}$  spectroscopy. As an example, the  $^1\text{H-NMR}$  spectrum of PBSPBDG60 is shown in Figure 4.21, together with the chemical shift assignments. In all cases, the spectra were found to be consistent with the expected structures. The copolymer composition was calculated from the relative areas of the  $^1\text{H-NMR}$  resonance peak of the **a** aliphatic proton of the succinic subunit located at 2.62 ppm and of the **d** protons of the diglycolic subunit at 4.23 ppm. From the data of Table 4.10, it can be seen that in all cases the actual molar composition is very close to the feed one.

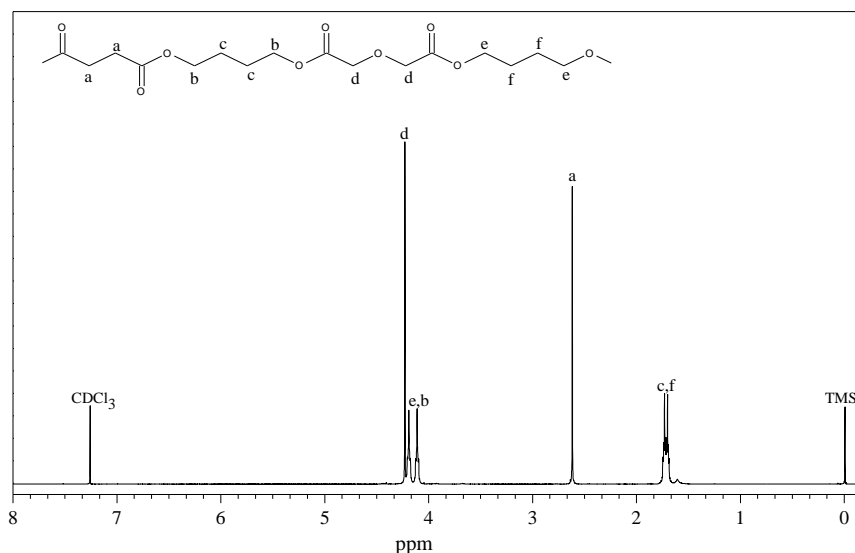


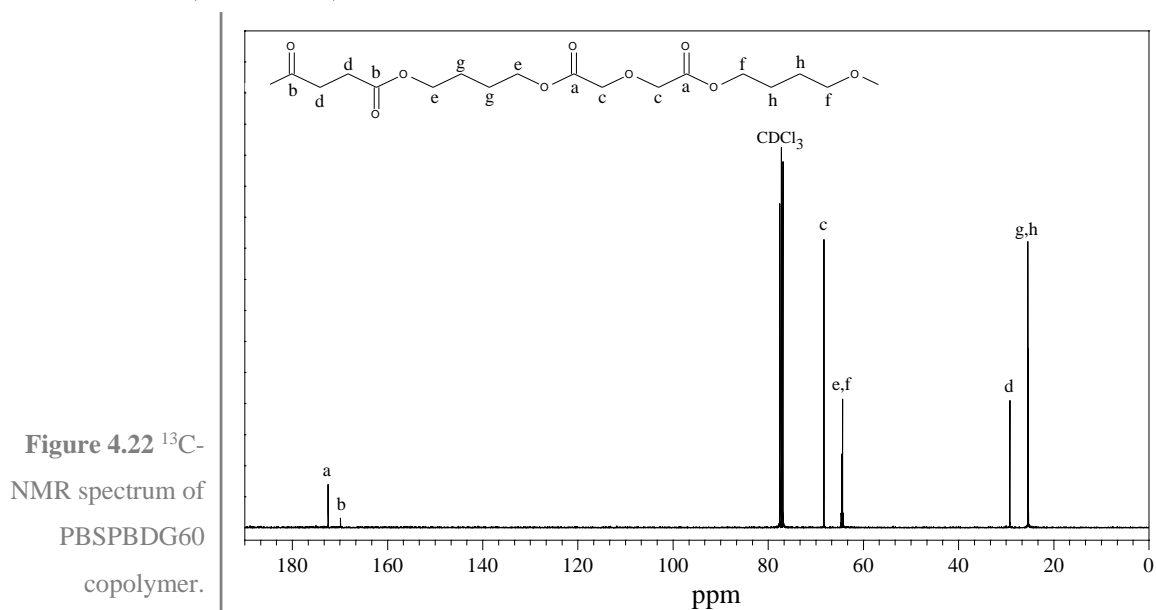
**Figure 4.21**  $^1\text{H-NMR}$  spectrum of PBSPBDG60 copolymer.

Since the  $^1\text{H-NMR}$  resonance peaks of interest (**c** and **f**) in evaluating the progress of transesterification reactions are not sufficiently resolved,  $^{13}\text{C-NMR}$  measurements were performed to study the structural changes. In particular, the region between  $\delta = 64.1$  and  $\delta = 64.9$  ppm (where the signals due to the carbon atoms of the 1,4-butanediol glycol subunit are located) is of special interest to evaluate the extent of the transesterification reactions occurring during the mixing at high temperature between PBS and PBDG (see the peaks labelled as **e** and **f** in Figure 4.22).

As evident from Figure 4.23, where the region between 64.1 and 64.9 ppm is reported for some copolymers, the  $^{13}\text{C}$ -NMR spectrum of PBSPBDG5 (corresponding  $t_{\text{mix}} = 5$  min) is the mere additive spectra of PBS and PBDG homopolymers, indicating that no significant chemical reactions took place during their mixing at  $225^\circ\text{C}$ . In fact, if transesterification reactions between PBS and PBDG occurred, new peaks should appear due to the mixed sequences (Figure 4.23).

As a matter of fact, in the copolymers PBSPBDGt obtained after mixing times longer than 5 min, two new peaks developed. As it can be seen from Figure 4.23, the intensity of these last increases with the mixing time, indicating that the transesterification reactions proceeded.

Information on the arrangement of the comonomeric units in the chain has been deduced by the degree of randomness  $b$ , which can be determined by  $^{13}\text{C}$ -NMR spectroscopy (section 3.6.1).



The average sequence length for PBS and PBDG repeated units and the degree of randomness of PBSPBDGt copolyesters are collected in Table 4.10. These results confirmed that the increment of mixing time increases the extent of transesterification reactions. In fact, as these latter proceed, the average length of the PBS and PBDG sequences decreases and the degree of randomness increases. Therefore, we can conclude that the experimental conditions adopted permitted us to prepare a mechanical mixture of the two polymers (PBSPBDG5), several block copolymers, whose block length decreases

with the increment of mixing time ( $20 < t_{\text{mix}} < 120$  min), and lastly a random copolymer (PBSPTDGS180), simply by increasing the reaction time.

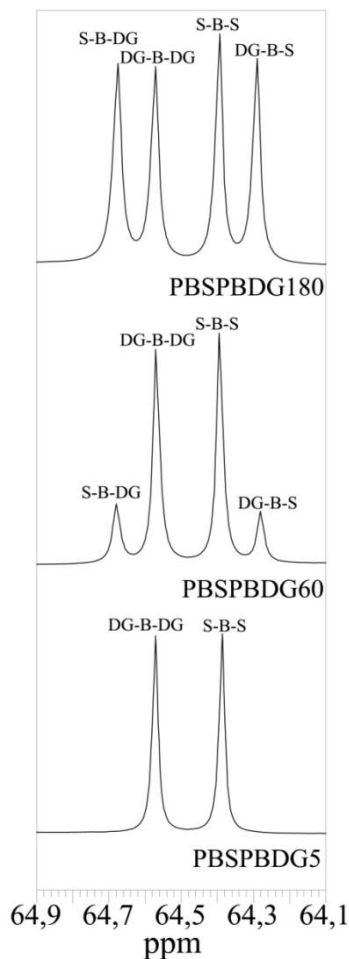


**Figure 4.23**  $^{13}\text{C}$ -NMR spectra of PBSPBDGt copolymers: expansion of the region between 64.1 and 64.9 ppm. Evolution of the spectrum as a function of mixing time.

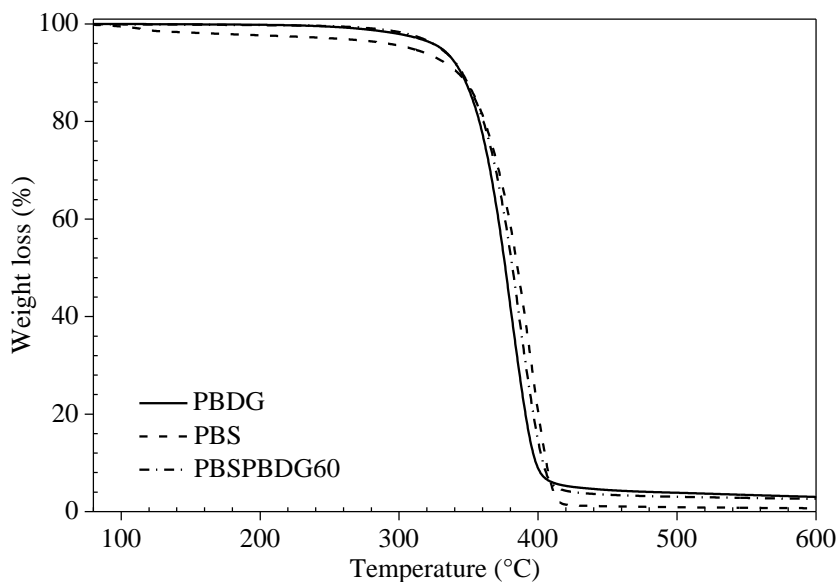
#### 4.3.3 PBSPBDGt copolymers thermal characterization

The polyesters were afterwards examined by thermogravimetric analysis and differential scanning calorimetry. The investigation on the thermal stability was carried out under dry nitrogen atmosphere. Analogously to parent homopolymers, the temperature corresponding to 5% weight loss ( $T_{5\%}$ ) and the temperature corresponding to the maximum weight loss rate ( $T_{\text{max}}$ ) were determined from the thermogravimetric curves and collected in Table 4.11.

In Figure 4.24 as an example, the thermogravimetric curve under nitrogen flow of PBSPBDG60, together with those of the two parent homopolymers are shown: as it can be seen, the weight loss took place practically in one-step for the copolymer too, and the

thermal stability and the char residue of PBSPBDG60 were intermediate between those of parent homopolymers.

**Figure 4.24**  
Thermogravimetric curves of PBS, PBDG and PBSPBDG60 copolymer under nitrogen atmosphere (heating rate: 10 °C/min).



As far as the thermal stability of all the copolymers synthesized is concerned, it was found good and similar for all the copolymers under investigation ( $T_{max}$  ranging from 386 to 389 °C in Table 4.11).

**Table 4.11** Thermal characterization data of PBS, PBDG and PBSPBDGt copolymers.

polymers	1 <sup>st</sup> Scan								2 <sup>nd</sup> Scan					
	$T_{5\%}$ (°C)	$T_{max}$ (°C)	$T_g$ (°C)	$\Delta C_p$ (J/°C g)	$T_{m,BS}$ (°C)	$\Delta H_{m,BS}$ (J/g)	$T_{m,BDG}$ (°C)	$\Delta H_{m,BDG}$ (J/g)	$T_g$ (°C)	$\Delta C_p$ (J/°C g)	$T_c$ (°C)	$\Delta H_c$ (J/g)	$T_m$ (°C)	$\Delta H_m$ (J/g)
PBS	305	395	-32	0.101	115	60	/	/	-39	0.105	/	/	116	64
PBDG	330	380	-23	0.296	/	/	66	55	-27	0.672	/	/	/	/
PBSPBDG5	326	386	-29	0.234	114	33	63	31	-28	0.491	/	/	114	31
PBSPBDG20	323	384	-32	0.367	106	35	46	4	-28	0.377	/	/	107	39
PBSPBDG40	329	389	-33	0.343	90	31	38	2	-31	0.601	28	30	90	41
PBSPBDG60	329	386	-33	0.363	82	42	/	/	-33	0.633	33	26	83	32
PBSPBDG90	335	388	-30	0.380	75	41	/	/	-33	0.689	42	7	76	7
PBSPBDG120	330	388	-34	0.453	64	35	/	/	-33	0.718	/	/	/	/
PBSPBDG180	315	388	-32	0.447	56	28	/	/	-33	0.734	/	/	/	/

In order to provide the same heat treatment to all the samples investigated, as mentioned above, prior to thermal analysis each sample was kept at room temperature for 2 weeks. The DSC traces of the so-treated samples are reported in Figure 4.25 and the results obtained in Table 4.11. In all cases, a glass transition and melting phenomena are evident. As far as the glass transition phenomenon is concerned, only one glass transition temperature is always clearly evident, independently of block length, suggesting the presence of a homogeneous amorphous state. The miscibility of the two components in the amorphous phase will be however more accurately evaluated analysing the thermal behaviour of the samples after melt quenching (see below).

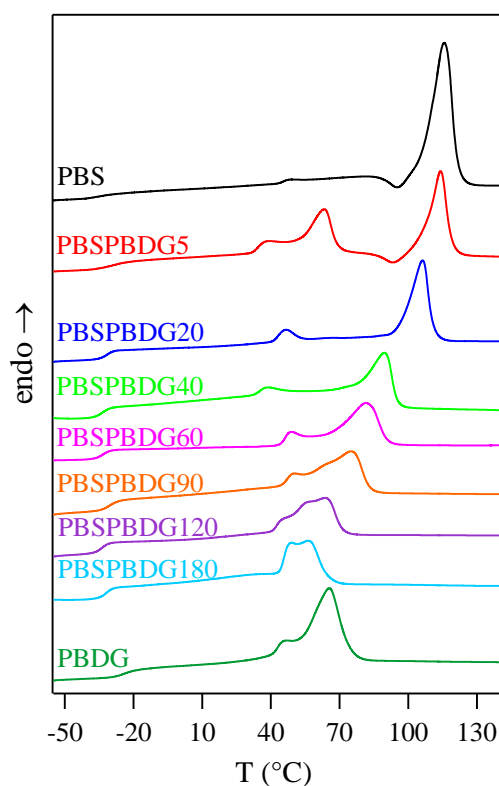


**Figure 4.25**  
Calorimetric curves  
of PBS, PBDG and  
their copolymers  
(1<sup>st</sup> scan).

As far as melting phenomenon is concerned, it appears quite complex in the copolymers under investigation: in the DSC curves of copolymers obtained at  $5 \leq t_{\text{mix}} \leq 40$  min two well distinct melting phenomena are evident. The shape and position of PBSPBDG5 melting peak at lower temperature are similar to those of PBDG, whereas the melting peak at higher temperature practically corresponds to that of PBS. This result suggests the presence in such copolymer of both the crystalline phases of the two homopolymers. In

the case of PBSPBDG20 and PBSPBDG40 both the two melting temperatures decreased as the mixing time was increased, still suggesting the presence in these two samples of PBS and PBDG crystalline phases, but each of them with a lower degree of perfection. In the DSC curves of copolymers obtained at  $t_{\text{mix}} \geq 60$  min multiple overlapped melting peaks are present: the peak at higher temperature shifted to lower values and the melting phenomenon became broader as the mixing time was increased, indicating that the decrement of the block length induced the formation of crystals with a low degree of perfection and a wide distribution of dimensions. Considering the melting peak temperatures and taking into account that PBS crystallizes much more quickly than PBDG, it is reasonable to hypothesize that the complex melting phenomenon that appears in PBSPBDG60-180 copolymers is related to the fusion of PBS crystalline phase. X-ray measurements will confirm this hypothesis, as discussed below. Generally speaking, the possible origin of multiple melting peaks may be due to: (a) the presence of more than one crystal structure and (b) the melt-recrystallization processes occurring during the DSC scan. As it is well known from the literature, the multiple melting phenomenon observed in PBS has been ascribed to a reorganization process taking place during the DSC scan, due to a mechanism based on melting and recrystallization of less perfect crystallites into thicker crystals, which melt at higher temperature (Yoo & Im, 1957; Yasuniwa *et al.*, 2002). It is reasonable to hypothesize that the multiple melting peaks present in the DSC traces of copolymers have the same origin. In the case of PBDG too, it is plausible to ascribe the multiple melting peaks to melt-recrystallization processes occurring during the DSC scan.

As far as the total heat of fusion is concerned, it has been found that it regularly decreased as the block length was decreased, with the exception of PBSPBDG5 whose value corresponds to the sum of heats of fusion of PBS and PBDG after normalization for the BS or BDG unit content.

In order to confirm the origin of multiple melting peaks observed in the DSC scans and investigate more deeply the nature of the crystalline phase in the polymers under investigation, X-ray analysis was performed. The X-ray diffraction profiles for PBS, PBDG and PBSPBDGt copolymers are reported in Figure 4.26a.

The XRD pattern of PBS homopolymer exhibit a well-defined set of crystalline diffraction peaks, attributable to the  $\alpha$ -phase (Ichikawa *et al.*, 2000): the profile, is characterized by two intense reflections at  $19.6^\circ$  ( $2\theta$ , 0 2 0 planes) and at  $22.5^\circ$  (1 1 0 planes), a shoulder at  $21.7^\circ$  (due to 0 2 1 planes) and by some weak reflections between  $25^\circ$  and  $45^\circ$ . The PBDG pattern is dominated by a sharp very intense reflection at  $19.3^\circ$  (100) and shows other

significant peaks at  $13.8^\circ$  (7),  $22.0^\circ$  (12),  $23.9^\circ$  (8),  $25.5^\circ$  (10),  $26.6^\circ$  (5),  $32^\circ$  (2) (draft intensity % based on peaks heights in parentheses). This profile is completely different with respect to the PBS one and can be ascribed to a different crystal structure. All the PBSPBDGt copolymers were characterized by X-ray patterns very similar to that of PBS, proving that the crystal structure present in the copolymers corresponds to the characteristic lattice of  $\alpha$ -PBS, with the exception of PBSPBDG5 and PBSPBDG20. In these samples, as evidenced from the zoomed plot partially shown in Figure 4.26b, a shoulder and a double peak at  $19.5^\circ$ , as well as a broad low intense reflection at  $13.8^\circ$ , a shoulder at  $23.9^\circ$  and a splitting of the small peak at  $25.6^\circ$  were found. This can be considered a proof of the contemporary presence of the crystalline phases of the two homopolymers. In the samples obtained at times longer than 20 min these features were no more detectable, indicating that if there is yet an aliquot of PBDG phase, it is less than the detection limit (about 3-5%). With the increment of mixing time, the 020 and 021 reflections shift towards smaller angles.

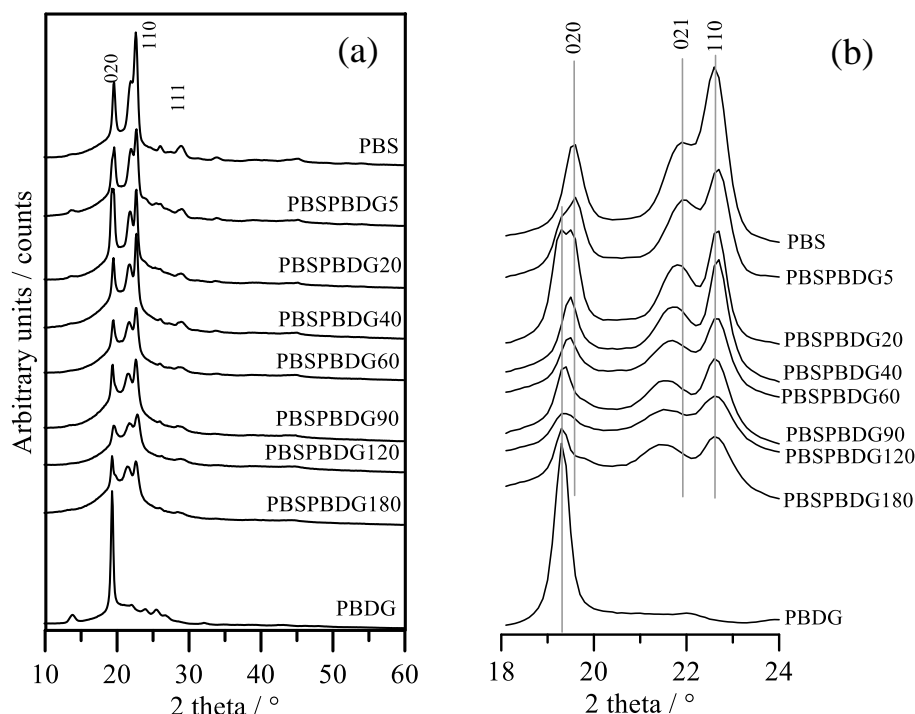
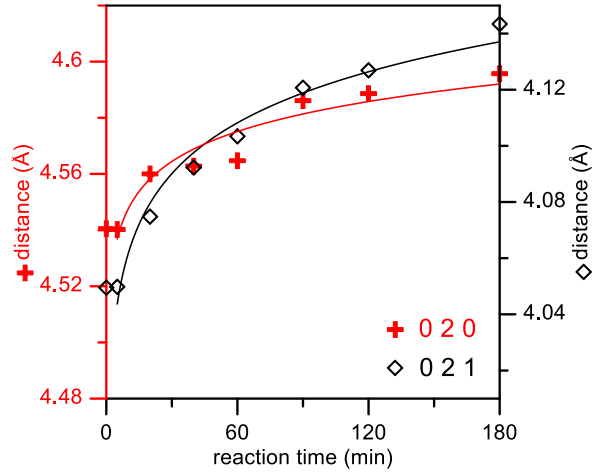


**Figure 4.26** a) X-ray diffraction patterns of PBS, PBDG and PBSPBDGt copolymers; the indexes of the three main peaks of  $\alpha$ -PBS are reported. b) magnification of XRD patterns reported in a); the vertical lines are guidelines at the positions of the main PBDG peak and 020, 021, 110  $\alpha$ -PBS peaks.

The plot of the d-spacings as a function of the reaction time, reported in Figure 4.27, shows that the increase of the 021 distance is almost double respect to the 020. The position of 110 peak seemed on the contrary not be affected by  $t_{\text{mix}}$ .

**Figure 4.27** 020 and 021 interlayer distances as a function of reaction time. The plotted curves are guidelines for the reader.



The significant variation of the interlayer 021 distance, the 020 being on the contrary only marginally affected, indicates a consistent expansion of the c-axis and a modest enlargement of b-one. Taking into account that in the PBS crystal structure the polymeric chains are parallel to c-axis, the observed increase of this axis can be correlated to the comonomer BDG inclusion in PBS crystal phase.

**Table 4.12** Crystal sizes in the direction perpendicular to 110 planes ( $L_{110}$ ), crystallinity indexes ( $\chi_c$ ) and  $T_{cc}$  values for PBS, PBDG and PBSPBDGt copolymers.

polymer	$L_{110}$ (nm)	$\chi_c$ (%)	$T_{cc}$ ( $^{\circ}\text{C}$ )
PBS	$21 \pm 1$	$41 \pm 4$	78
PBSPBDG5	$22 \pm 1$	$34 \pm 3$	/
PBSPBDG20	$22 \pm 1$	$28 \pm 3$	76
PBSPBDG40	$22 \pm 1$	$26 \pm 4$	60
PBSPBDG60	$18 \pm 1$	$24 \pm 3$	37
PBSPBDG90	$18 \pm 1$	$22 \pm 3$	27
PBSPBDG120	$15 \pm 1$	$24 \pm 3$	16
PBSPBDG180	$15 \pm 1$	$21 \pm 3$	/
PBDG	$22 \pm 1$	$34 \pm 3$	/

As a matter of fact, BDG co-units contains one more atom (ether-oxygen) per repeating unit respect to PBS one. On the contrary, the a- and b- unit cell lattice dimensions are only marginally affected since the lateral hindrance of PBDG and PBS are equal.

The overall width of the peaks and the relative area of the halo due the amorphous material increased as the transesterification reactions proceeded. Consequently, the values of the mean crystal size and of the crystallinity degree decreased (Table 4.12).

In conclusion, though it seems reasonable that  $\alpha$ -PBS crystal phase preferentially accept the parent homopolymer, the present results demonstrate the partial inclusion of BDG co-units in PBS crystal lattice, i.e. real occurrence of cocrystallization.

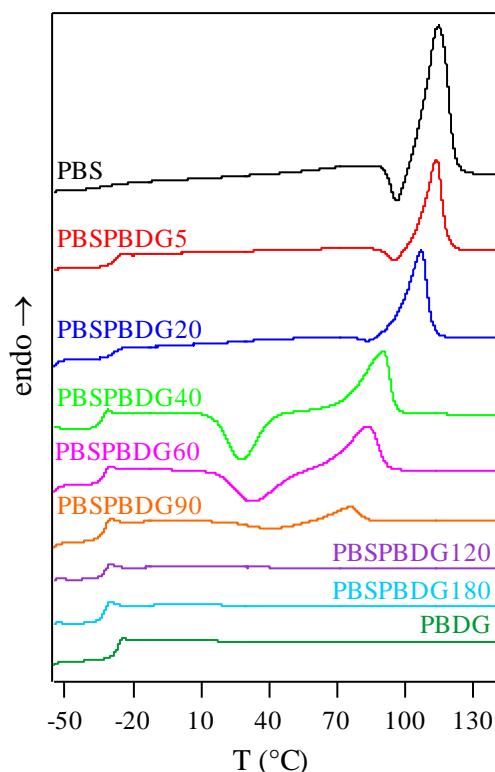


**Figure 4.28**  
Calorimetric curves of PBS, PBDG and PBSPBDGt copolymers after melt quenching (2<sup>nd</sup> scan).

The miscibility of polymer blends is frequently judged by the analysis of the glass transition of the blend. In this latter, as well as in block copolymers, the presence of a single glass transition at a temperature intermediate with respect to the  $T_g$ 's of the pure components, suggests complete miscibility; on the contrary, the appearance of two  $T_g$ 's indicates immiscibility or partial miscibility of the components. In particular, the presence of two glass transitions, at temperatures corresponding to those of the pure homopolymers, is a clear evidence of no miscibility. Lastly, the observation of two glass transition phenomena whose position changes with composition proves the existence of two mixed

phases, each one able to accommodate molecules of the second component (partial miscibility).

Therefore, the miscibility and the crystallization capacity of PBSPBDGt samples can be investigated on the samples quenched from the melt (2<sup>nd</sup> scan). The corresponding DSC traces are shown in Figure 4.28: as it can be seen, the calorimetric traces of PBS, PBSPBDG5 and PBSPBDG20 are characterized by a glass transition followed by a conspicuous melting endotherm.

The DSC curves of PBSPTDGSt copolymers obtained after a mixing time ranging from 40 to 90 minutes showed a glass transition followed by an exothermal “cold crystallization” peak and a melting endotherm at a higher temperature. In particular, as concern PBSPTBDG40 copolymer, the enthalpy associated with the crystallization phenomenon was lower than that of fusion endotherm, indicating that this sample cannot be frozen into a completely amorphous state by quenching. Nevertheless, a portion of amorphous material, once  $T_g$  is exceeded, acquires enough mobility to rearrange and crystallize. In the case of PBSPBDG60 and PBSPBDG90 copolymers, the enthalpy of crystallization well compares with the corresponding heat of fusion, indicating that these polymers are completely amorphous. As regards the calorimetric curves of PBSPBDG120, PBSPBDG180 and pure PBDG, only an intense endothermal baseline deviation associated with the glass transition was observed. Therefore, the phase behaviour of PBSPTBDGt copolymers appears to depend on the mixing time (therefore on the block length): as a matter of fact, after melt quenching, completely amorphous samples can be exclusively obtained at long mixing times.

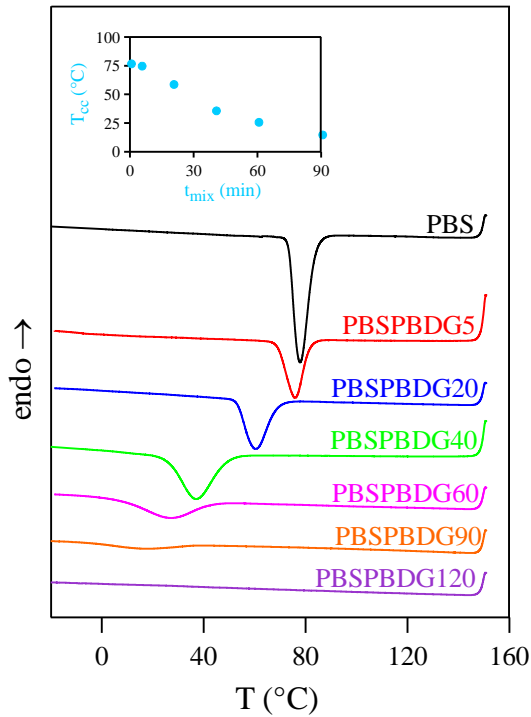
Regarding the glass transition phenomenon, in all cases only one glass transition is evident, analogously to the first scan, confirming the presence of a single homogeneous amorphous phase. In particular, the PBSPBDGt copolymers obtained at mixing times longer than 40 min, which, as mentioned above, are completely amorphous after melt quenching, showed a glass transition ranging from -31 to -33°C, which well agrees with the value of -33°C predicted by the Fox equation, valid for random copolymers and/or miscible polymer blends (with  $T_g$  values of -39 and -27°C for PBS and PBDG, respectively, as reported in Table 4.11). In the case of copolymers obtained at  $5 < t_{\text{mix}} < 40$  min slightly higher values of  $T_g$  were found (Table 4.11). This result can be explained on the basis of two effects: i) the crystallinity present in these samples acts like physical crosslinking and gives rise to a restrictive effect on the segmental motion of amorphous polymer chains; ii) a progressive enrichment of the amorphous phase in butylene diglycolate segments takes place as crystallinity develops.

As far as the “cold crystallization” peak is concerned, it is worth noting that the  $T_c$  values increased from PBSPBDG40 to PBSPBDG90, indicating that the tendency of PBS to crystallize decreases. This fact can be considered the result of two effects, which become more significant with decreasing BS block length: the former is an increment of the copolymer  $T_g$  together with a decrease of the copolymer  $T_m$  which reduce the  $T_g/T_m$  window, hindering the crystallization process (the mobilization and the consequent rearrangement of the macromolecules into 3-dimensional order can occur in a narrower temperature range); the latter is a marked decrement of the transport of crystallizable chain segments on the crystal growth surface, due to the BDG blocks, which act as defects during the chain folding of BS blocks. As far as the melting phenomenon is concerned, an analogous trend to that observed in the first scan was found: the melting point decreased with increasing mixing time, due to the formation of less perfect crystals; moreover the width of the endothermic peak increased as the mixing time was increased because of the presence of a larger distribution of crystallites with different degree of perfection. Lastly, a decrement of the heat of fusion of the copolymers with respect to that of homopolymer PBS was observed.

To confirm that in the copolymers the tendency of PBS to crystallize decreases, non-isothermal experiments were carried out, subjecting the samples to a controlled cooling rate from the melt (section 3.7.2). The exothermic crystallization peaks of the samples under investigation are displayed in Figure 4.29 and the  $T_{cc}$  values are reported in Table 4.12: as it can be seen, the copolymers obtained at mixing times longer than 90 min were not able to crystallize even though cooled from the melt at very low rate ( $1^\circ\text{C}/\text{min}$ ). From the inset of Figure 4.29, where the  $T_{cc}$  values are reported as a function of mixing time, it can be observed that the temperature corresponding to the maximum of the exothermal crystallization peak regularly decreases as the mixing time is increased.

This result indicates that the crystallization process became more and more difficult as the BS blocks became progressively shorter and the copolymer tended toward a random distribution of the sequences. Such trend is due to the effect of the PBDG phase, which limits the transport of the PBS chains on the crystal surface and can act as a defect during chain folding. Therefore, in block copolymers, a decrement of the crystallization rate with a reduction of the block length is evident.

**Figure 4.29** DSC crystallization exotherms of PBS and PBSPBDGt copolymers cooled from the melt at 5°C/min. In the inset:  $T_{cc}$  as a function mixing time.



#### 4.3.4 PBSPBDGt copolymers mechanical characterization

Taking into account that strain affects stem cells biology, the investigation of mechanical properties of the two homopolymers and of PBSPBDGt copolymers, is crucial.

The tensile behavior of the investigated polymers is shown in Figure 4.30 that plots, as an example, the stress as a function of strain for PBSPBDG40. Table 4.13 reports the corresponding mechanical data (elastic modulus,  $E$ ; stress at break,  $\sigma_b$ , and deformation at break,  $\varepsilon_b$ ) of PBS, PBDG and some of the copolymers under investigation.

**Table 4.13** Mechanical data of PBS, PBDG and PBSPBDGt copolymers.

polymer	$E$ (MPa)	$\varepsilon_b$ (%)	$\sigma_b$ (MPa)
PBS	$337 \pm 26$	$24 \pm 4$	$31 \pm 2$
PBSPBDG5	$229 \pm 20$	$17 \pm 1$	$18 \pm 1.5$
PBSPBDG20	$139 \pm 9$	$302 \pm 44$	$16 \pm 0.5$
PBSPBDG40	$136 \pm 19$	$458 \pm 92$	$14 \pm 0.8$
PBSPBDG90	$101 \pm 8$	$773 \pm 24$	$16 \pm 1$
PBSPBDG180	$83 \pm 7$	$883 \pm 72$	$16 \pm 2.5$
PBDG	$148 \pm 21$	$427 \pm 33$	$23 \pm 1.5$

As it can be seen, all the copolymers, except PBSPBDG5, were characterized by a lower elastic modulus and therefore are less strong compared with PBS and PBDG.

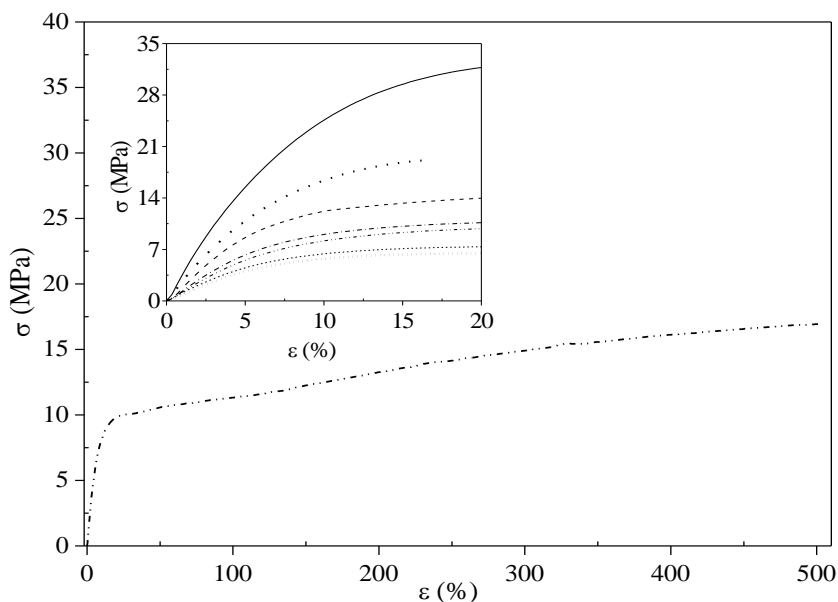


**Figure 4.30** Stress-strain curve of PBSPBDG40. In the inset: enlarged zone of the initial linear portion of the stress-strain curve: solid line PBS; dot PBSPBDG5; dash dot PBSPBDG20; dash dot dot PBSPBDG40; short dash PBSPBDG90; short dot PBSPBDG180; dash PBDG.

Moreover elastic modulus and elongation to break decreased and increased, respectively as the block length decreases. Since all the investigated polymers display a soft amorphous phase ( $T_g$  values are in all cases well below RT), the observed trend can be ascribed to the decrease in crystallinity degree (Table 4.12).

The copolymers obtained at  $t_{\text{mix}} \geq 20$  min were characterized by an elastomeric behaviour, which is particularly important in the context of soft tissue engineering applications.

#### 4.3.4 Conclusions

NMR data and the DSC results indicated that either block copolymers with well-defined length, which decreases with increasing mixing time, or random copolymers can be easily obtained.

A detailed investigation of thermo-mechanical properties of both parent homopolymers and the corresponding copolymers allowed to correlate copolymer properties to its specific

molecular architecture. In particular, it has been demonstrated that the introduction of BDG units into PBS chain had the effect of changing polymer mechanical properties (as a consequence of the depression of polymer crystallinity degree) towards an elastomeric behaviour, which is particularly important in the context of soft tissue engineering applications.

In conclusion, the physical properties of the investigated materials are very interesting in view of their possible application in regenerative medicine of soft tissues.

#### **4.4 Macromolecular design of novel sulphur-containing copolyesters with promising mechanical properties for soft tissue engineering**

The just illustrated polymeric system is represented by poly(butylene succinate/diglycolate) block copolymers, where the butylene diglycolate comonomeric unit differs from that of PBS for the presence in the diacid sub-unit of an ether-oxygen atom (section 4.3). The research activity has been carried on by replacing the ether-oxygen atom with a sulphur one, which, as well known, is characterized by larger dimensions and lower electronegativity. These chemical characteristics should render the resulting sulphur-containing copolymers less rigid. At first, we prepared the poly(butylene thiodiglycolate) (PBTGD) homopolymer by the usual two-stage polycondensation procedure; then block copolyesters were obtained by reactive blending of PBS and PBTGD.

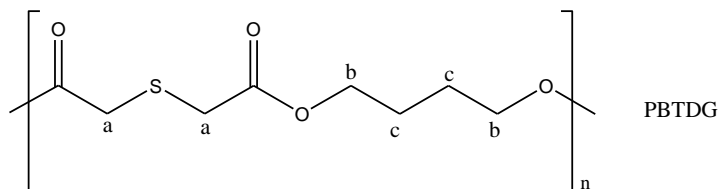
In the following, block copolymers will be named PBSPBTGD<sub>t</sub>, with *t* equal to the mixing time during reactive blending.

In addition, solution cast blends of PBS and PBTGD have been prepared. Throughout this work the resulting blends are denoted as ScbPBS-PBTGD<sub>X</sub>, where *X* is the mol percentage of PBTGD in the blends.

##### *4.4.1 PBTGD homopolymer characterization*

At room temperature the as-prepared polyester is a light brown coloured rubber. The sample was kept at ambient temperature for 2 weeks prior to characterization. As it can be noted from Table 4.15 reported below, PBTGD was characterized by a relatively high molecular weight, indicating that appropriate synthesis conditions and a good polymerization control were obtained. In order to have an understanding into its chemical

structure, the  $^1\text{H-NMR}$  investigation was performed. The spectrum was found to be consistent with the expected structure, the chemical shift assignments ( $\delta$ , ppm) being the following: PBTDG:  $\delta = 4,16$  (t, 4  $\text{H}^b$ );  $\delta = 3,38$  (s, 4  $\text{H}^a$ );  $\delta = 1,75$  (m, 4  $\text{H}^c$ ) according to the following chemical structure:



Subsequently, the polyester was subjected to thermogravimetric analysis and the temperature corresponding to 5% weight loss ( $T_{5\%}$ ) and the temperature corresponding to the maximum weight loss rate ( $T_{\text{max}}$ ) were determined and collected in Table 4.16. As evidenced in Figure 4.31, the weight loss took place practically in one-step and was 100%. From the comparison between the TGA curves of PBTDG and that of PBS added for comparison, it can be seen that the latter is more thermally stable, for the same reasons reported for PBSPTES copolymers (section 4.2.2). Moreover, taking into account that among the various degradation mechanisms proposed to shed light on the thermal degradation reactions occurring in polyesters, the random cleavage of covalent bonds of the polymeric chains can be invoked, the higher stability of PBS with respect to PBTDG can be explained on the basis of the higher energy of the C-C bond with respect to C-S one.

As regards the calorimetric results, the phase behaviour of the two parent homopolymers is opposite: as a matter of fact, PBS is semicrystalline (section 4.3.1) whereas PBTDG is amorphous.  $T_g$  values of the two polymers cannot be easily compared because after melt quenching PBS is still highly semicrystalline and is well known crystallinity acting like crosslinking raises  $T_g$ . Anyway, the high difference between the two  $T_g$ 's values indicates that PBTDG is characterized by a lower glass transition temperature than PBS. To explain this result, the larger dimension of sulphur atoms with respect to the carbon ones has to be taken into consideration: as a matter of fact S-C bonds longer than the C-C ones form, making the polymer chains more flexible.

#### 4.4.2 Solution cast blends

The as-prepared blends of PBS and PBTDG were opaque because of the crystallinity generated during the storage at room temperature (more than two weeks), due to the semicrystalline nature of PBS blend component. Preliminarily, the solution cast blends

were subjected to thermogravimetric analysis in order to evaluate the thermal stability as a function of composition. From the thermogravimetric curves in air, the temperature corresponding to 5% weight loss ( $T_{5\%}$ ) and the temperature corresponding to the maximum weight loss rate ( $T_{\max}$ ) were determined and collected in Table 4.14.

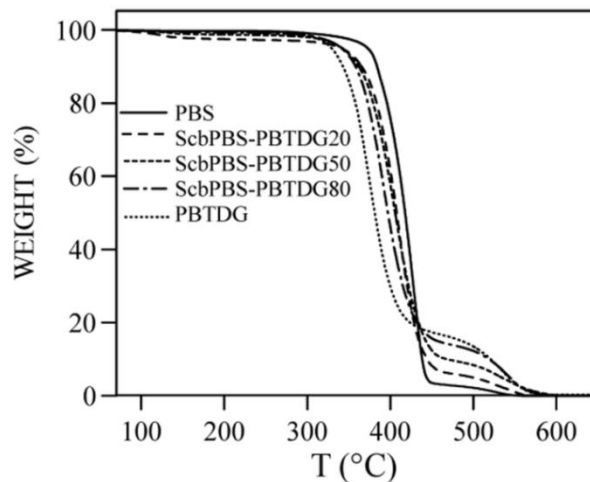
**Table 4.14** Thermal characterization data of PBS, PBTGD and ScbPBS-PBTGD SX solution cast blends.

blend	$T_{5\%}$ (°C)	$T_{\max}$ (°C)	2 <sup>nd</sup> scan					$\chi_c$ (%)
			$T_g$ (°C)	$\Delta C_p$ (J/g°C)		$T_m$ (°C)	$\Delta H_m$ (J/g)	
PBS	393	428	-34	0.104		113	63	32
PBTGD	344	373	-48	0.520		/	/	/
ScbPBS-PBTGD20	357	389	-48 -34	0.14	0.06	115	45.6	29
ScbPBS-PBTGD50	368	402	-48 -35	0.29	0.09	115	29.3	29
ScbPBS-PBTGD80	374	408	-49 -34	0.50	0.08	114	12.1	30

The weight loss was 100%, analogously to the two parent homopolymers (Figure 4.31). As far as the thermal stability is concerned, it was found to depend on composition, being lower as PBTGD content was increased. However, all the samples were characterized by a good thermal stability, the temperature of initial decomposition  $T_{5\% \text{ w.loss}}$  ranging from 357 to 374°C (Table 4.14).

As it is well known, the miscibility of polymer blends is frequently judged by the analysis of their glass transition (see Section 4.3).

**Figure 4.31**  
Thermogravimetric curves of PBS (from Ref. 15), PBTGD and solution cast blends ScbPBS-PBTGD SX in air (heating rate: 10 °C/min).



Therefore, to better evaluate the miscibility in the amorphous phase, the DSC scans after melt quenching have been analysed. As evident from the data collected in Table 4.14, all the blends examined are semicrystalline, being characterized by a conspicuous melting endotherm, the temperature of the melting peak not changing appreciably with respect to that of PBS.

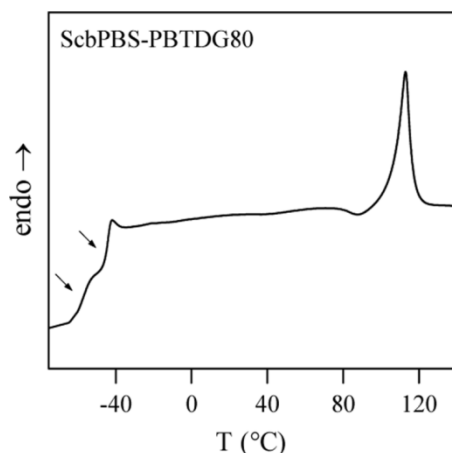


**Figure 4.32.** Calorimetric curve of PBS-PBTDG80 solution cast blend after melt quenching (2<sup>nd</sup> scan).

As far as the glass transition phenomenon is concerned, as evidenced in Figure 4.32, where, as an example, the second calorimetric scan of ScbPBS-PBTDG80 is shown, no evidence of compatibility was obtained by calorimetric measurements: in fact, two distinct glass transitions, with constant temperatures corresponding to those of the pure blend components were evident. In conclusion, in ScbPBS-PBTDGX solution cast blends no miscibility at all was found and therefore the system analyzed formed a biphasic system over the whole composition range, with the phases consisting of the two pure homopolymers.

#### 4.4.3 PBSPBTDGt block copolymer synthesis and molecular characterization

In order to obtain block copolymers, equimolar amounts of PBS and PBTDG were melt mixed at high temperature. In this case too, several preliminary runs were carried out to optimize melt mixing (section 4.3.2). At RT the as-prepared copolymers were opaque and light brown coloured solids.

PBSPBTDGt samples, together with the parent homopolymers for comparison, are listed in Table 4.15 along with molecular characterizations data. As it can be seen, all the copolyesters were characterized by relatively high molecular weights, intermediate between those of the parent homopolymers PBS and PBTDG. This result indicates that no

relevant thermal degradation occurred during the mixing. Looking into more detail the data, a slight increase of molecular weight with the mixing time is observed, analogously to previously discussed block copolymeric systems PBSPTES and PBSPBDGt. The chemical structure of all copolyesters was determined by  $^1\text{H-NMR}$  spectroscopy. As an example, the  $^1\text{H-NMR}$  spectrum of PBSPBTDG120 is shown in Figure 4.33, together with the chemical shift assignments.

**Table 4.15** Molecular characterization data.

<i>polymer</i>	$M_n$	$D$	$BS$ (mol %) $^{13}\text{C-NMR}$	$L_{BS}$	$L_{BTDG}$	$b$
PBS	51200	2.3	100			
PBDTG	40900	2.2	0			
PBSPBTDG10	42000	2.2	50.3	/	/	0.0
PBSPBTDG45	45200	2.1	49.6	10.4	9.9	0.2
PBSPBTDG120	48500	2.4	49.7	4.4	3.8	0.49
PBSPBTDG180	48800	2.5	50.2	3.0	2.6	0.73
PBSPBTDG240	49400	2.1	53.4	2.2	1.8	1.01

In all cases, the spectra were found to be consistent with the expected structures. The copolymer composition was calculated from the relative areas of the  $^1\text{H-NMR}$  resonance peak of the **a** aliphatic proton of the succinic subunit located at 2.61 ppm and of the **b** protons of the thiodiglycolic subunit at 3.38 ppm. From the data of Table 4.15, it can be seen that in all cases the actual molar composition is very close to the feed one.

Since the  $^1\text{H-NMR}$  resonance peaks of interest (**e** and **f**) in evaluating the progress of transesterification reactions were not sufficiently resolved,  $^{13}\text{C-NMR}$  measurements were performed to study the structural changes. In particular, the region between  $\delta = 64.1$  and  $\delta = 65.5$  ppm (where the signals due to the carbon atoms of the 1,4-butanediol glycol subunit are located) is of special interest to evaluate the extent of the transesterification reactions occurring during the mixing at high temperature between PBS and PBDTG (see the peaks labelled as **c** and **h** in Figure 4.34).

As evident from Figure 4.35, where the region between 64.1 and 65.5 ppm is reported for some copolymers, the  $^{13}\text{C-NMR}$  spectrum of PBSPBTDG10 (corresponding  $t_{\text{mix}} = 10$  min) is the mere additive spectra of PBS and PBDTG homopolymers, indicating that no appreciable chemical reactions took place during their mixing at 225°C. In fact, if transesterification reactions between PBS and PBDTG occurred, new peaks should appear due to the mixed sequences (Figure 4.35).

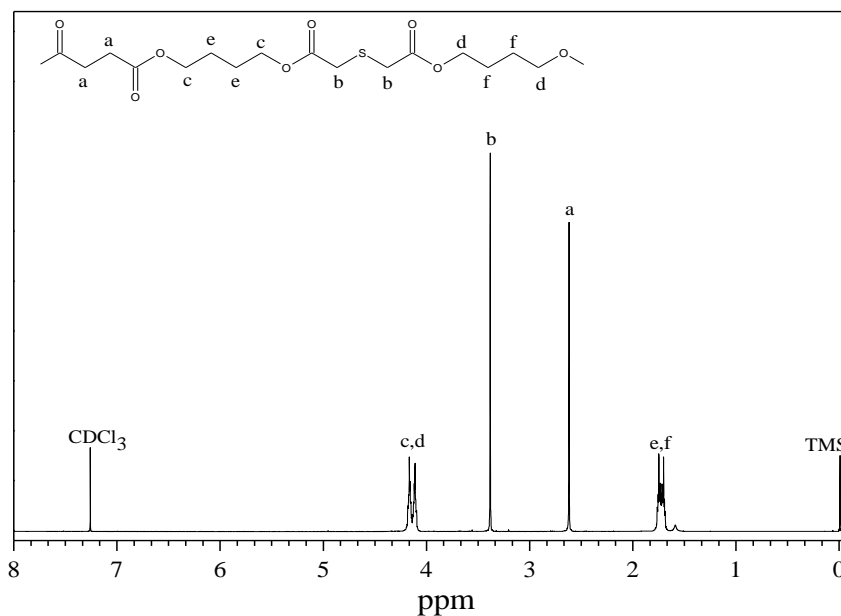


**Figure 4.33**  $^1\text{H}$ -NMR spectrum of PBSPBTDG12 copolymer.

As a matter of fact, in the copolymers PBSPBTDG obtained after mixing times longer than 10 min, two new peaks, due to the mixed sequences, developed. As it can be seen from Figure 4.35, the intensity of these last increases with mixing time, indicating that the transesterification reactions proceeded.

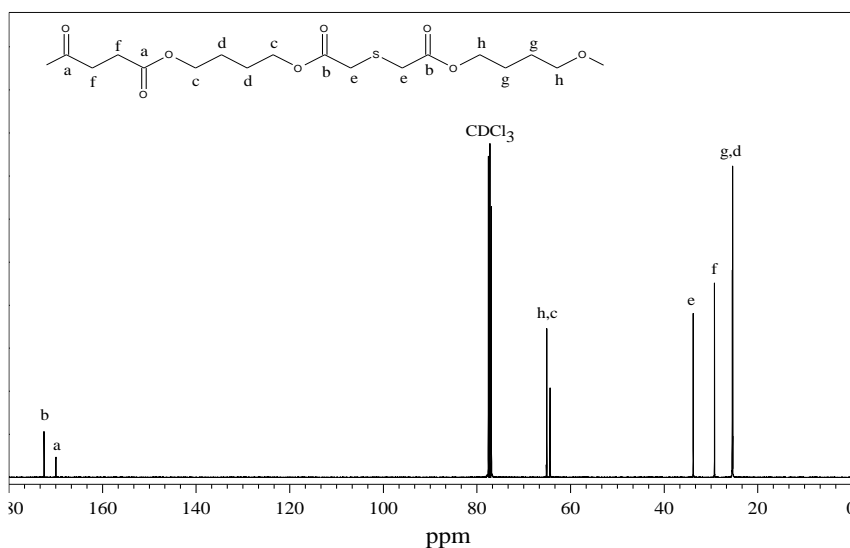


**Figure 4.34**  $^{13}\text{C}$ -NMR spectrum of PBSPBTDG120 copolymer.

Information on the arrangement of the comonomeric units in the chain has been deduced by the degree of randomness  $b$ . The average sequence length for PBS and PBDTG repeated units and the degree of randomness of PBSPBTDG copolyesters are collected in

Table 4.15. These results confirmed that the increment of mixing time increases the extent of transesterification reactions. In fact, as these latter proceeded, the average length of the PBS and PBTDG sequences decreased and the degree of randomness increased. Therefore, we can conclude that the experimental conditions adopted permitted also in this case to prepare several block copolymers, whose block length decreases with the increment of mixing time ( $45 < t_{\text{mix}} < 180$  min), and lastly a random copolymer (PBSPTDGS240), simply by increasing the reaction time.

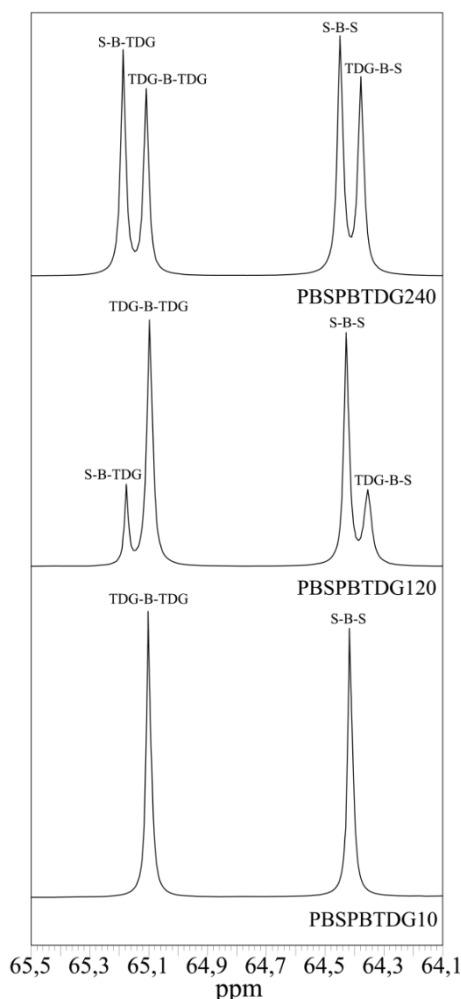


**Figure 4.35**  $^{13}\text{C}$ -NMR spectra: expansion of the region between 64.1 and 65.5 ppm. Evolution of the spectrum as a function of mixing time.

#### 4.4.4 PBSPBTDGt copolymers thermal characterization

The copolyesters were afterwards examined by thermogravimetric analysis and differential scanning calorimetry. The investigation on the thermal stability was carried out under dry nitrogen atmosphere. Analogously to parent homopolymers, the temperature corresponding to 5% weight loss ( $T_{5\%}$ ) and the temperature corresponding to the maximum

weight loss rate ( $T_{\max}$ ) were determined from the thermogravimetric curves and collected in Table 4.16.

As it can be seen, the thermal stability of the copolymers was good and very similar to that of PBTDG ( $T_{5\% \text{ w.loss}}$  ranging from 322 to 331 °C in Table 4.16).

In order to provide the same heat treatment to all the samples investigated, as mentioned above, prior to thermal analysis each sample was kept at room temperature for 2 weeks. The DSC traces of the so-treated samples are reported in Figure 4.36 and the results obtained in Table 4.16. In all cases, a glass transition and a melting phenomenon were evident, with the exception of PBTDG. As far as the glass transition phenomenon is concerned, only one glass transition temperature was always clearly evident, independently of block length, suggesting the presence of a homogeneous amorphous state. Therefore the melt mixing of the two components for short time ( $t_{\text{mix}} = 10 \text{ min}$ ) favoured the miscibility in the amorphous phase even though no significant transesterification reactions took place. The miscibility of the two components in the amorphous phase will be however more accurately evaluated analysing the thermal behaviour of the samples after melt quenching (see below).

**Table 4.16** Thermal characterization data of PBS, PBTDG and PBSPBTDGt copolymers.

polymer	$T_{5\% \text{ w.loss}}$ (°C)	$T_{\max}$ (°C)	1 <sup>st</sup> Scan				2 <sup>nd</sup> Scan					
			$T_g$ (°C)	$\Delta C_p$ (J/°C g)	$T_m$ (°C)	$\Delta H_m$ (J/g)	$T_g$ (°C)	$\Delta C_p$ (J/°C g)	$T_c$ (°C)	$\Delta H_c$ (J/g)	$T_m$ (°C)	$\Delta H_m$ (J/g)
PBS	360	395	-32	0.101	115	81	-34	0.105	/	/	116	64
PBTDG	331	366	-48	0.561	/	/	-48	0.577	/	/	/	/
PBSPBTDG10	327	381	-40	0.340	113	33	-40	0.348	/	/	113	30
PBSPBTDG45	331	374	-40	0.482	100	30	-41	0.526	/	/	99	29
PBSPBTDG120	327	380	-41	0.454	79	29	-42	0.423	/	/	79	29
PBSPBTDG180	331	376	-41	0.510	58	28	-43	0.604	30	4	64	5
PBSPBTDG240	322	379	-41	0.483	50	25	-44	0.628	/	/	/	/

Concerning the melting phenomenon from Figure 4.36, it can be noted that the endothermic process became broader and its peak shifts to lower temperature as the mixing time increased. Because PBS crystallizes quite quickly, whereas PBTDG is completely amorphous under the experimental conditions adopted, the melting peaks observed in the copolymers can be attributed to the fusion of the crystalline phase of PBS. Therefore, the

decrement of the block length induces the formation of crystals with a low degree of perfection and a wide distribution of dimensions. In fact, the very long blocks of PBS present in PBSPBTDG10 seem to favour the formation of crystals with a good level of perfection (the  $T_m$  value ( $113^\circ\text{C}$ ) is in fact very close to that characteristic of the homopolymer ( $116^\circ\text{C}$ )). As far as the heat of fusion is concerned, the estimated enthalpy of fusion, after normalization for the butylene succinate unit content, corresponds to 33, 30, 29, 28 and 25% of crystallinity for PBSPBTDG10, PBSPBTDG45, PBSPBTDG120, PBSPBTDG180 and PBSPBTDG240, respectively, assuming  $200\text{ J/g}$  as the heat of fusion of perfectly crystalline PBS (Hexig *et al.*, 2005). Taking into account that PBS homopolymer is characterized by a crystallinity degree of 41%, the presence of non-crystallizable blocks of PBTGD influences the total crystallinity degree of PBS, which crystallizes in the copolymers in minor percentage than in the pure state. Moreover, in the case of copolymers with short BS block length (PBSPBTDG45, PBSPBTDG120 and PBSPBTDG180) and the random copolymer (PBSPBTDG240), multiple melting endotherms are evident, due to melt-recrystallization processes occurring during the DSC scan (section 4.3.3).

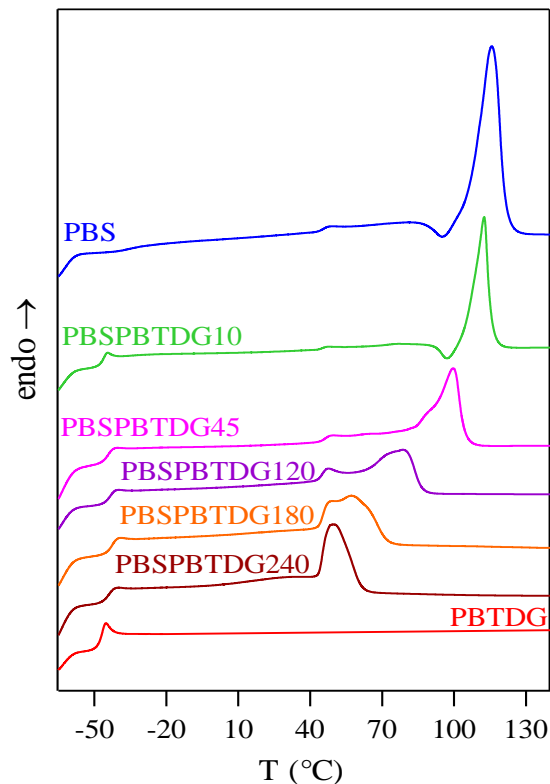


**Figure 4.36**  
Calorimetric  
curves of PBS,  
PBTGD and their  
copolymers (1<sup>st</sup>  
scan).

In order to investigate more deeply the nature of the crystalline phase in the polymers under investigation, X-ray analysis was performed. The X-ray diffraction profiles for PBS and PBSPTDGSt copolymers are reported in Figure 4.37. All the samples showed the reflections in the angular position characteristic of the  $\alpha$ -PBS crystal phase (Yasuniwa *et al.*, 2002): no extra peaks were present, proving the presence of a unique crystal phase. In the sample PBSPBTDG45, and in PBSPBTDG240, even though only slightly, the intensities of the reflections 020 and 021 were over expressed because of a preferential orientation of the  $0k0$  planes parallel to the sample holder. Unfortunately, XRD analysis carried out in Bragg-Brentano reflection geometry are often affected by this aberration. Lastly, the overall width of the peaks and the relative area of the halo due the amorphous material increased as the transesterification reactions proceeded. Consequently, we can state that the main effect of copolymerization process is an overall worsening of the ordered domains as shown by the decrease of both the crystallinity and the mean crystal size (Table 4.17).

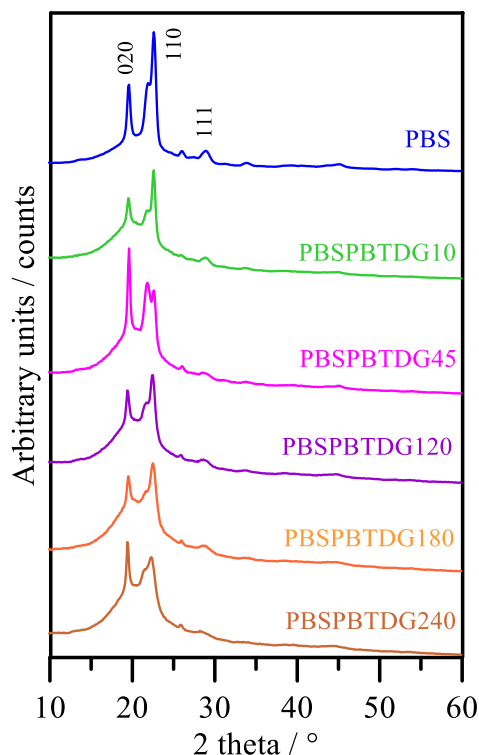


**Figure 4.37** X-ray diffraction patterns of PBS, and PBSPBTDGt copolymers; the indexes of the three main peaks of  $\alpha$ -PBS are reported.

**Table 4.17** Crystal sizes in the direction perpendicular to 1 1 0 planes ( $L_{110}$ ) and crystallinity indexes ( $\chi_c$ ).

polymer	$L_{110}$ (nm)*	$\chi_c$ (%)	$T_{cc}$ (°C)
PBS	$21 \pm 1$	$41 \pm 4$	78
PBSPBTDG10	$22 \pm 1$	$33 \pm 3$	74
PBSPBTDG45	$22 \pm 1$	$31 \pm 3$	53
PBSPBTDG120	$18 \pm 1$	$24 \pm 3$	35
PBSPBTDG180	$13 \pm 1$	$20 \pm 3$	6
PBSPBTDG240	$12 \pm 1$	$21 \pm 3$	/

\* calculated from the reflection at  $19.3^\circ$  ( $2\theta$ )

The miscibility and the crystallization capacity of PBSPBTDGt samples have been investigated on the samples quenched from the melt (2<sup>nd</sup> scan). The corresponding DSC traces are shown in Figure 4.38: as it can be seen, the calorimetric traces of PBS, PBSPBTDG10, PBSPBTDG45 and PBSPBTDG120 were characterized by a glass transition followed by a conspicuous melting endotherm.

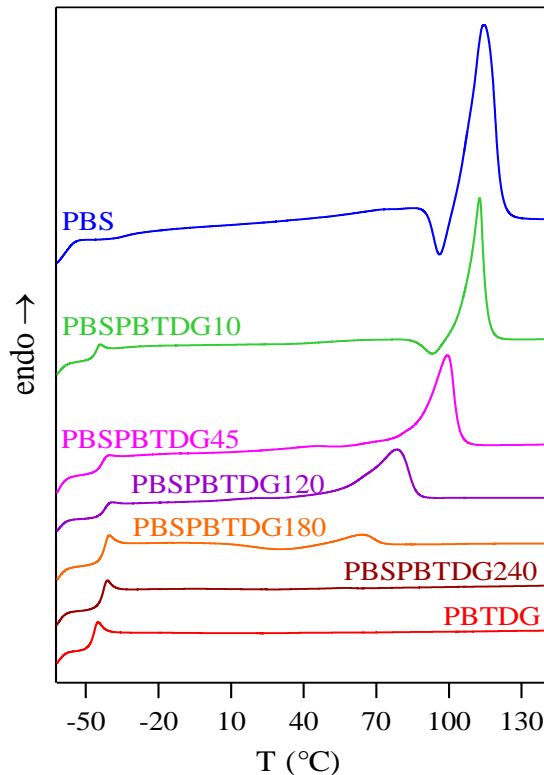


**Figure 4.38**  
Calorimetric curves of PBS, PBTDG and PBSPBTDGt copolymers after melt quenching (2<sup>nd</sup> scan).

The DSC curve of PBSPBTDG180 shows a glass transition followed by an exothermal “cold crystallization” peak and a melting endotherm at a higher temperature. In particular, the enthalpy of crystallization well compares with the corresponding heat of fusion, indicating that this polymer is completely amorphous.

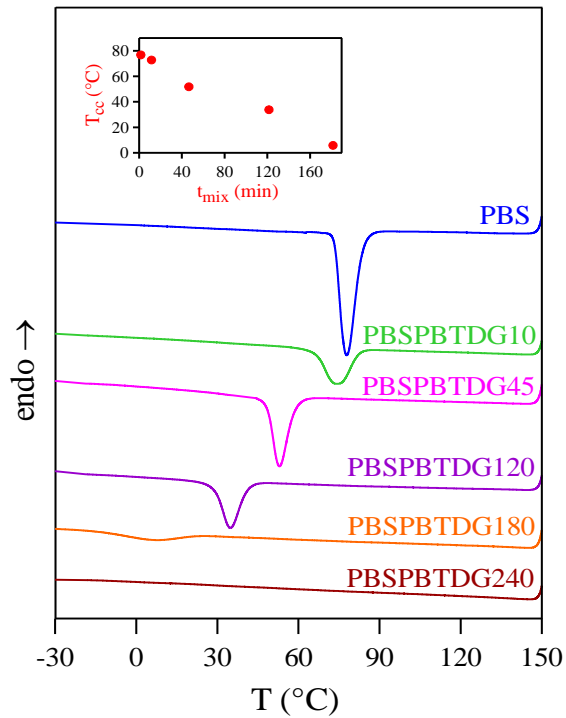
As regards the calorimetric curves of PBSPBTDG240 and pure PBTDG, only an intense endothermal baseline deviation associated with the glass transition is observed. Therefore, the phase behaviour of PBSPBTDGt copolymers appeared to depend on the mixing time (therefore on the block length): as a matter of fact, after melt quenching, completely amorphous samples can be exclusively obtained at long mixing times.

Regarding the glass transition phenomenon, in all cases only one glass transition was evident, analogously to the first scan, confirming the presence of a single homogeneous amorphous phase. In particular, the PBSPBDGt copolymers obtained at  $t_{\text{mix}} \geq 180$  min, which, as mentioned above, are completely amorphous after melt quenching, showed a glass transition ranging from  $-43$  to  $-44^\circ\text{C}$ , which well agrees with the value of  $-44^\circ\text{C}$  predicted by the Fox equation, valid for random copolymers and/or miscible polymer blends (with  $T_g$  values of  $-39$  and  $-48^\circ\text{C}$  for PBS and PBTDG, respectively). In the case of copolymers obtained at  $10 \leq t_{\text{mix}} \leq 120$  min slightly higher values of  $T_g$  are found (Table 4.16). This result can be explained on the basis of the higher crystallinity present in these samples.

As far as the melting phenomenon is concerned, an analogous trend to that observed in the first scan was found: the melting point decreased with increasing the mixing time, due to the formation of less perfect crystals; moreover the width of the endothermic peak increased as the mixing time was increased because of the presence of a larger distribution of crystallites with different degree of perfection. Lastly, a decrement of the heat of fusion of the copolymers with respect to that of homopolymer PBS was observed.

To confirm that in the copolymers the tendency of PBS to crystallize decreases, non-isothermal experiments were carried out, subjecting the samples to a controlled cooling rate from the melt. The exothermic crystallization peaks of the samples under investigation are displayed in Figure 4.39 and the  $T_{\text{cc}}$  values reported in Table 4.17: as it can be seen, the copolymers obtained at mixing times longer than 180 min are not able to crystallize even though cooled from the melt at very low rate ( $1^\circ\text{C}/\text{min}$ ). From the inset of Figure 4.39, where the  $T_{\text{cc}}$  values are reported as a function of mixing time, it can be observed that the temperature corresponding to the maximum of the exothermal crystallization peak regularly decreases as the mixing time is increased.

**Figure 4.39.** DSC crystallization exotherms of PBS and PBSPBTDGt copolymers cooled from the melt at 5°C/min. In the inset:  $T_{cc}$  as a function mixing time.



This result indicates that the crystallization process becomes more and more difficult as the BS blocks become progressively shorter and the copolymer tends toward a random distribution of the sequences. Such trend is due to the effect of the PBTDG phase, which limits the transport of the PBS chains on the crystal surface and act as a defect during chain folding. Therefore, in block copolymers, a decrement of the crystallization rate with a reduction of the block length is evident.

#### 4.4.5 PBSPBTDGt copolymers mechanical characterization

Taking into account that mechanical properties affect stem cells biology, these were investigated for PBSPBTDGt copolymers. The tensile behavior of the investigated polymers, together with that of PBS added for comparison, is shown in Figure 4.40 that plots, as an example, the stress as a function of strain for PBSPBTDG120. Table 4.18 reports the corresponding mechanical characteristics (elastic modulus,  $E$ ; stress at break,  $\sigma_b$ , and deformation at break,  $\epsilon_b$ ), together with those of PBS, and some of the copolymers PBSPBDGt previously investigated (section 4.3.4).

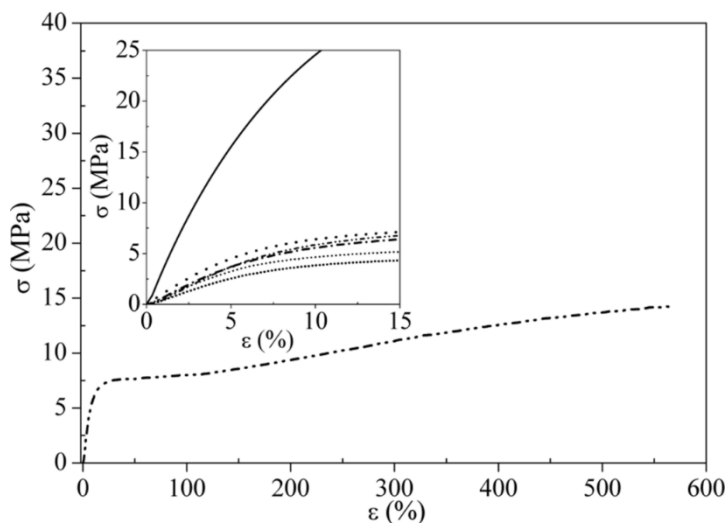


**Figure 4.40** Stress-strain curve of PBSPBTDG120. In the inset: enlarged zone of the initial linear portion of the stress-strain curve: solid line PBS; dot PBSPBTDG10; dash dot PBSPBTDG45; dash dot dot PBSPBTDG120; short dash PBSPBTDG180; short dot PBSPBTDG240.

As it can be seen, all the copolymers were characterized by a lower elastic modulus and therefore were less strong in comparison with PBS. Moreover, elastic modulus and elongation to break respectively decreased and increased as the block length decreased. Since all the investigated polymers displayed a soft amorphous phase ( $T_g$  values are in all cases well below RT), the observed trend can be ascribed to the decrease in crystallinity degree (Table 4.17).

The copolymers PBSPBTDGt obtained at  $t_{\text{mix}} \geq 45$  min were characterized by an elastomeric behaviour, which is particularly important in the context of soft tissue engineering applications. Quite interesting is the comparison with the PBSPBDGt copolymers previously investigated. PBSPBDG5, PBSPBDG90 and PBSPBDG180 are characterized by practically same block length and by the same crystallinity degree compared to PBSPBTDG10, PBSPBTDGS180 and PBSPBTDG240, respectively. Nevertheless, the sulphur-containing copolymers are less rigid than the corresponding ether oxygen-atom containing samples ( $E$  decreases of 25% and  $\epsilon_b$  increases of 20%). This result can be correlated to the higher chain flexibility of PBSPBTDGt copolymers on respect to PBSPBDGt ones, due to the presence along the polymeric chain of C-S bonds longer than the C-O ones and to weaker interchain interactions because of the lower electronegativity of sulphur atoms with respect to oxygen ones.

**Table 4.18** Mechanical data of PBS, PBSPBTDGt and PBSPBDGt copolymers.

polymers	E (MPa)	$\epsilon_b$ (%)	$\sigma_b$ (MPa)
PBS	337 ± 26	24 ± 4	31 ± 2
PBSPBTDG10	160 ± 15	95 ± 4	18 ± 1
PBSPBTDG45	87 ± 8	464 ± 82	12 ± 2
PBSPBTDG120	86 ± 2	510 ± 95	13 ± 2
PBSPBTDG180	75 ± 5	610 ± 16	11 ± 1
PBSPBTDG240	61 ± 4	713 ± 51	7 ± 1
PBSPBDG5	229 ± 20	17 ± 1	18 ± 1.5
PBSPBDG90	101 ± 8	773 ± 24	16 ± 1
PBSPBDG180	83 ± 7	883 ± 72	16 ± 2.5

#### 4.4.6 Electrospinning of PBSPBDG and PBSPBTDG copolymers

In order to obtain 3-D scaffolds to be used in tissue engineering, some of the PBSPBDG and PBSPBTDG polyesters investigated have been subjected to electrospinning (ES). In particular, the two blends (PBSPBDG5 and PBSPBTDG10), and the two long block copolymers (PBSPBDG20 and PBSPBTDG45) have been considered. PBS has been also electrospun for sake of comparison. Experiments have been carried out according to the procedure previously described (section 3.5).

ES conditions parameters were optimized in order to obtain defect-free fibres by evaluating fiber morphology by SEM. The optimization study was carried out for each polymer; the approach to optimize ES parameters was always a “trial-and-error” procedure as follows.

First, given the importance of solution parameters, different polymer concentrations and several solvent systems were investigated to address their influence on fibre morphology. In fact, as it is well known, solution concentration and kind of solvent impact on polymer viscoelastic and electrical properties and on solution surface tension. Once a proper polymer solution was selected, instrumental parameters were then optimized in order to obtain bead-free fibers (section 1.3.1.1).

In Figure 4.41 SEM micrographs, fiber dimensions and fiber distribution of the obtained scaffolds are reported. The scaffolds appeared to be highly porous mats with microscale interstitial pores. All the polymers yielded fibers free of beads defects, randomly oriented and possessing submicrometric diameters, with the exception of PBSPBDG5, whose fiber

dimensions were slightly higher ( $1080 \pm 260$  nm). In the case of PBSPBDG20, two different fiber diameters have been obtained:  $890 \pm 410$  nm and  $410 \pm 160$  nm.

ES fibres were characterized by TGA and DSC (sections 3.7.1. and 3.7.2). TGA did not reveal residual solvents in the ES fibres under study and confirmed that ES process did not affect polymer thermal degradation behavior. DSC was used to investigate the thermal transitions in electrospun mats. From DSC analysis did not emerged significant differences between polymeric films and the corresponding electrospun mats.

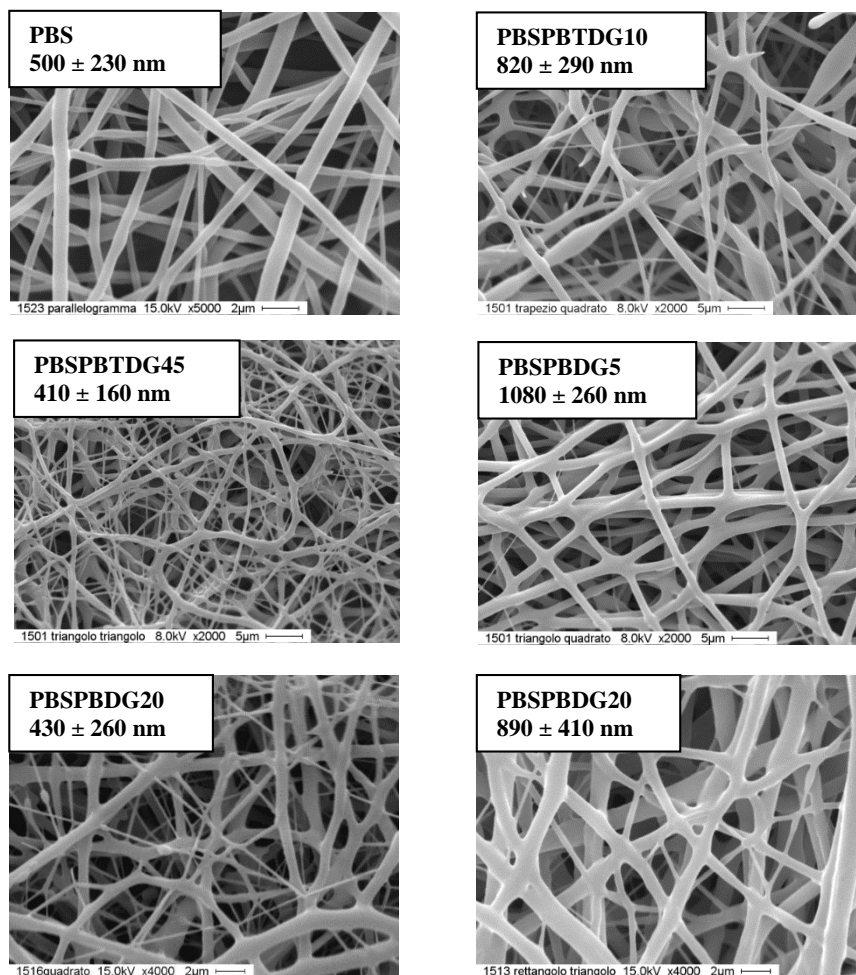


**Figure 4.41** SEM micrographs of PBS, PBSPBDG5, PBSPBDG20, PBSPBDG10 and PBSPBDG45 electrospun scaffolds. Fiber dimensions and distributions are also reported.

In order to investigate the relative hydrophilicity of the scaffolds under study, water contact angle measurements were performed. Unfortunately, due to the high porosity of the electrospun mats, water droplets were instantaneously absorbed by the material making the measure of the surface wettability not possible.

Therefore, WCA analysis were performed on hot-pressed films, providing the following results:  $WCA_{\text{PBS}} = 96 \pm 1^\circ$ ;  $WCA_{\text{PBSPBDG5}} = 75 \pm 2^\circ$ ;  $WCA_{\text{PBSPBDG20}} = 80 \pm 3^\circ$ ;

$WCA_{\text{PBSPBTDG10}} = 81 \pm 2^\circ$ ;  $WCA_{\text{PBSPBTDG45}} = 79 \pm 4^\circ$ . As previously reported (sections 4.1.1 and 4.2.3), the introduction of highly electronegative atoms (O and S) along the PBS polymeric chain increased the surface wettability of the final material.

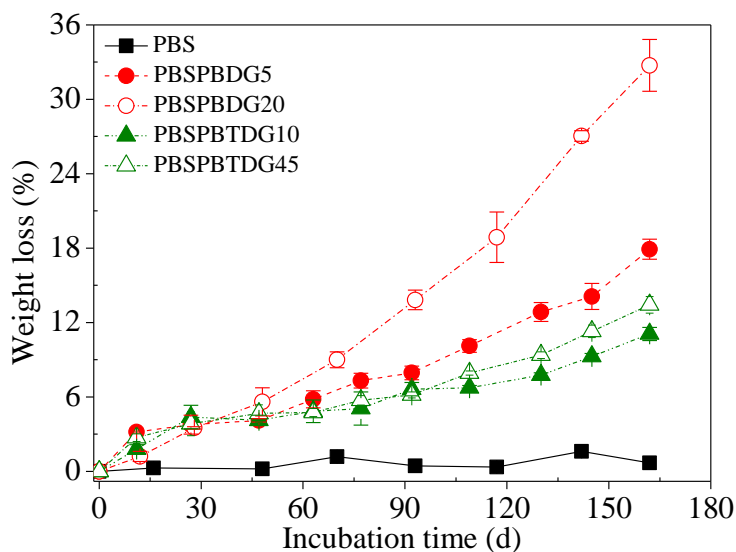
#### 4.4.7 Hydrolytic degradation

Hydrolytic degradation experiments were performed under physiological conditions (section 3.11) on the electrospun mats in order to evaluate the effect of the following factors on the hydrolysis rate:

- introduction of hydrophilic BDG and BTDG co-units in the PBS macromolecular chain;
- kind of etheroatom (O or S) introduced;
- different molecular architecture (blend or block copolymer).

Weight losses are reported in Figure 4.42 as a function of incubation time.

**Figure 4.42**  
Weight loss of  
PBS,  
PBSPBDG5,  
PBSPBDG20,  
PBSPBTDG10  
and  
PBSPBTDG45  
scaffolds as a  
function of  
incubation time.



As it can be evicted form Figure 4.42, weight losses were strongly affected by the factors mentioned above: as a matter of fact after 162 days of incubation PBS practically did not lose weight, whereas polymer blends and block copolymers appreciably degraded. In particular, ether-oxygen containing polyesters showed a higher degradation rate with respect to sulphur containing ones.

Moreover, block copolymers degraded faster than blends. The trend was particularly evident if we consider PBSPBDG5 and PBSPBDG20: the weight losses were 17% and

33%, respectively. On the contrary, only a small difference has been displayed in the case of PBSPBTDG10 and PBSPBTDG45, the weight losses being 11% and 13%, respectively. The percentage of residual number average molecular weight for PBS, PBSPBDG20 and PBSPBTDG45 ( $M_n$  res%) is reported in Figure 4.43 as a function of incubation time. The three samples, including PBS, underwent a decrease of  $M_n$  with time: it is in fact well known (section 1.1.4.1) that in the first stages of hydrolytic degradation substantial decrease in molecular weight occurs, even if weight losses are still negligible.

PBS was less affected by this phenomenon in the time scale explored, due to its high crystallinity degree, high crystal perfection and hydrophobicity, while in the case of copolymers, the change of molecular weight was more evident and it seemed to be affected by the type of polymer investigated; the residual molecular weight was in fact equal to 38% and 23% for PBSPBDG20 and PBSPBTDG45, respectively.

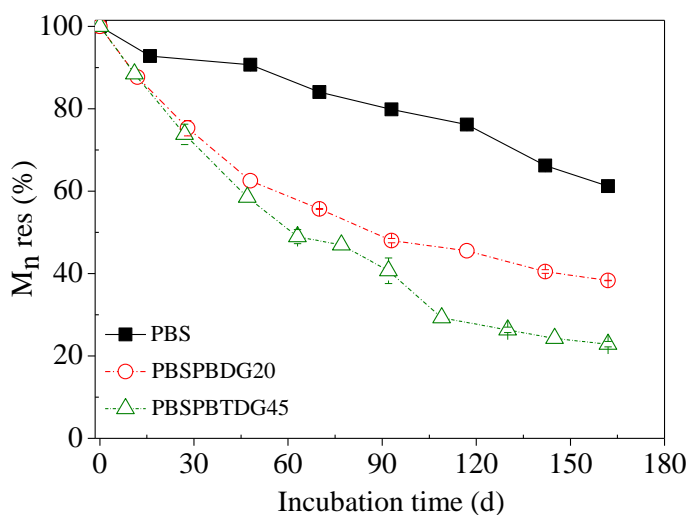


**Figure 4.43**  
Residual number molecular weight of PBS, PBSPBDG20 and PBSPBTDG45 scaffolds as a function of incubation time.

As far as the two blends are concerned, the calculation of the number average molecular weight was not possible because the GPC traces of the analyzed polymers revealed a bump since the very beginning of the incubation period. With the increasing of incubation time, a second peak was detectable (Figure 4.44 reports as an example the GPC traces of PBSPBDG5 as a function of incubation time). Therefore, to monitor the degradation process, the peak molecular weight of both peaks ( $M_p$ , 1 and  $M_p$ , 2) was calculated and reported in Table 4.19.

**Figure 4.44** GPC traces of PBSPBDG5 as a function of incubation time.

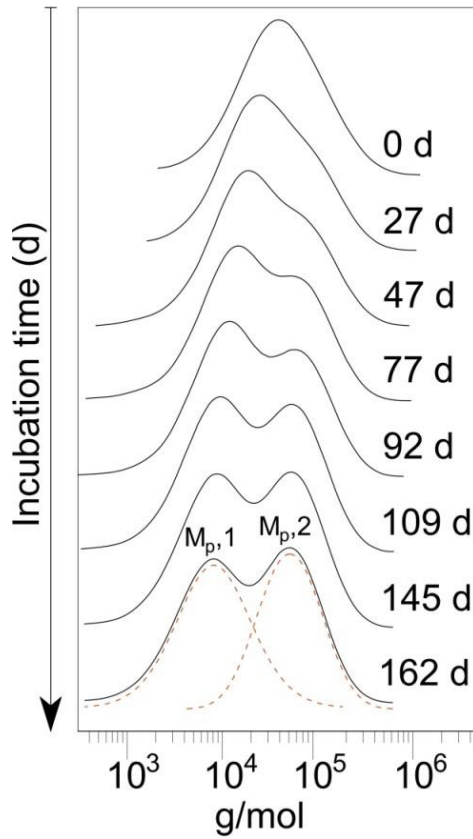


**Table 4.19** Peak molecular weight as a function of incubation time for PBSPBDG5 and PBSPBTDG10.

Incubation time (d)	PBSPBDG5		PBSPBTDG10	
	$M_{p,1}$	$M_{p,2}$	$M_{p,1}$	$M_{p,2}$
0	40600	/	51400	/
27	24700	58800	37900	/
47	18500	58600	32000	59300
77	14200	58600	26100	59400
92	12000	58100	18800	59000
109	10700	56600	12500	57500
145	8200	51100	9700	52100
162	5400	50900	8700	51000

As expected, in both PBSPBDG5 and PBSPBTDG10, the PBS phase remained practically undegraded ( $M_{p,2}$ ), while  $M_{p,1}$  remarkably decreased with the increasing of incubation

time, demonstrating that the PBDG and PBDTG phases underwent a substantial hydrolytic degradation.

In order to gain a better understanding of the hydrolysis mechanism of the copolymers, <sup>1</sup>H-NMR measurements were performed on degraded retrieved samples. Figure 4.45 reports the content of BS units in mol% as a function of degradation time.

In all samples, an evident increase of BS content (therefore a decrease in the BDG and BTDG content) was observed during degradation. The copolymer composition change was more consistent for ether-oxygen containing samples. In particular, after 162 days of water exposure, the amount of BDG units decreased from the initial 50 mol% of the non-degraded samples down to 41% and 29% for PBSPBDG5 and PBSPBDG20, respectively. In the case of PBSPBDTG10 and PBSOBTDG45, the BTDG content decreased in both cases from 50% to 44%.

Hydrolytic degradation of the samples under investigation can be interpreted on the basis of two different factors: crystallinity degree and surface hydrophilicity. The first is the most important parameter governing the degradation rate of a polymer (section 1.1.4.3); in particular, the higher the crystallinity degree, the lower the degradation rate. As regards the second parameter, the higher the hydrophilicity, the higher the degradation rate.

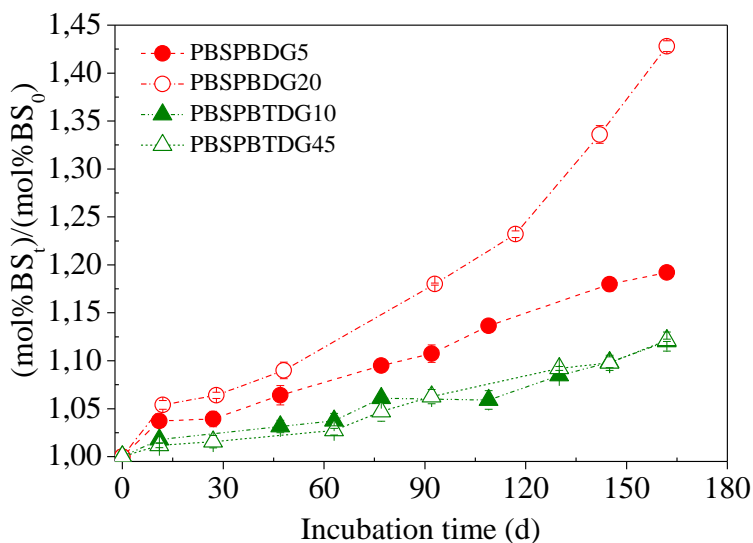
As a matter of fact, PBSPBDG20, the less crystalline material, degraded to the highest extent; as regards the two blends, the higher degradation rate of PBSPBDG5 with respect to PBSPBDTG10 is due to the higher hydrophilicity of the first polymer, being the crystallinity degree comparable for the two samples (Table 4.12 and Table 4.17).

Sulphur containing polymers underwent a similar degradation profile because both crystallinity degree and hydrophilicity were comparable.

The change in chemical composition (Figure 4.43) showed that a higher increase of BS unit content corresponded to a higher weight loss.

Consequently, ester cleavage preferentially occurred on etheroatom containing chain segments, which, due to their hydrophilic nature, were easily solubilized in water. Moreover, as expected, ether-oxygen containing sequences demonstrated higher solubility in water with respect to sulphur containing ones: the lower decrease in molecular weight and the contemporary higher degradation rate of PBSPBDG5 with respect to PBSPBDTG10, indicated that the longer sequences of BDG were solubilized in water generating a more pronounced weight loss and more marked decrease in BDG mol%.

**Figure 4.45**  
Increase in BS  
mol% content in  
PBSPBDG5,  
PBSPBDG10,  
PBSPBTDG10  
and  
PBSPBTDG45  
scaffolds as a  
function of  
degradation time.



A confirmation that the amorphous regions of a polymer are degraded more quickly than the crystalline ones, was obtained by subjecting the partially degraded copolymer samples to a heating calorimetric scan (20°C/min). All the calorimetric traces were found to be characterized by an endothermic peak associated with the fusion process of crystalline portion of the material (data not shown). The corresponding heat of fusion was normalized respect to the heat of fusion of non-degraded sample ( $\Delta H_t/\Delta H_0$ ). The results obtained are reported in Figure 4.46.

In all the polymers under investigation the normalized heat of fusion regularly increased with incubation time, with the exception of PBS, whose crystallinity degree was not significantly affected.

It is worth remembering that the increment of the crystalline/amorphous ratio can be also due to an additional process occurring when a polymer is placed at a temperature comprised between its glass transition and its melting temperature (as it is 37°C for this class of polyesters). This phenomenon, called annealing, consists of an increase and improvement of the crystalline phase with time.

The curves showed in Figure 4.46 can therefore be considered as the sum of two contributions: 1) preferential attack by water of the amorphous region of a polymer with respect to crystalline one during degradation and 2) annealing.

In block copolymers the annealing process played a greater role than in the blends because of the lower crystallization rate of the first ones, as previously reported in both PBSPBDG and PBDPBDG copolymer systems (section 4.3.3 and 4.4.4, respectively). As a matter

of fact, the crystallization process becomes more difficult as the BS blocks become shorter due to the effect of the second phase (PBDG or PBDTG), which limits the transport of the PBS chains on the crystal surface and acts as a defect during chain folding.

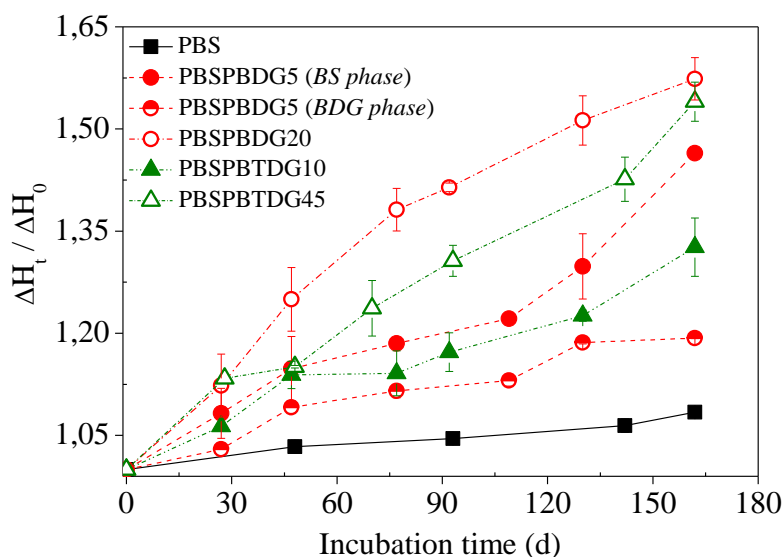


**Figure 4.46** Normalized heat of fusion as a function of incubation time for PBSPBDG5, PBSPBDG10, PBSPBTDG10 and PBSPBTDG45 scaffolds as a function of degradation time.

In the light of the above information, the more pronounced increase in the heat of fusion of PBSPBTDG45 with respect to PBSPBTDG10, which showed a comparable degradation rate, is not surprising.

From a comparison between ether-oxygen containing polymers and sulphur containing ones, the higher increase in the heat of fusion can be on the contrary explained on the basis of the higher degradation rate.

Lastly, the slight increase in the heat of fusion of the pure PBDG phase present in the PBSPBDG5 sample can be related to the contemporary attack by water of amorphous and PBDG crystalline phases, this latter showing a lower packing density and degree of perfection with respect to the PBS one, as already reported in the case of PBSPTDGS copolymers (section 4.1.5).

#### 4.4.8 Cell morphology and viability

According to the different fibre dimensions of the prepared scaffolds, different comparison, presented in Figure 4.47, are possible for the cell culture experiments, which

are being performed by using Human Mesenchymal Stem Cells treated with chondrogenic medium, osteogenic medium and basic medium.

Four different effects are under investigation:

- introduction of a different comonomeric unit (either BDG or BTDG) in the PBS polymeric chain;
- introduction of a different component (either PBDG or PBTDG) in a PBS based physical blend;
- fiber diameter;
- macromolecular architecture (physical blending versus copolymerization).

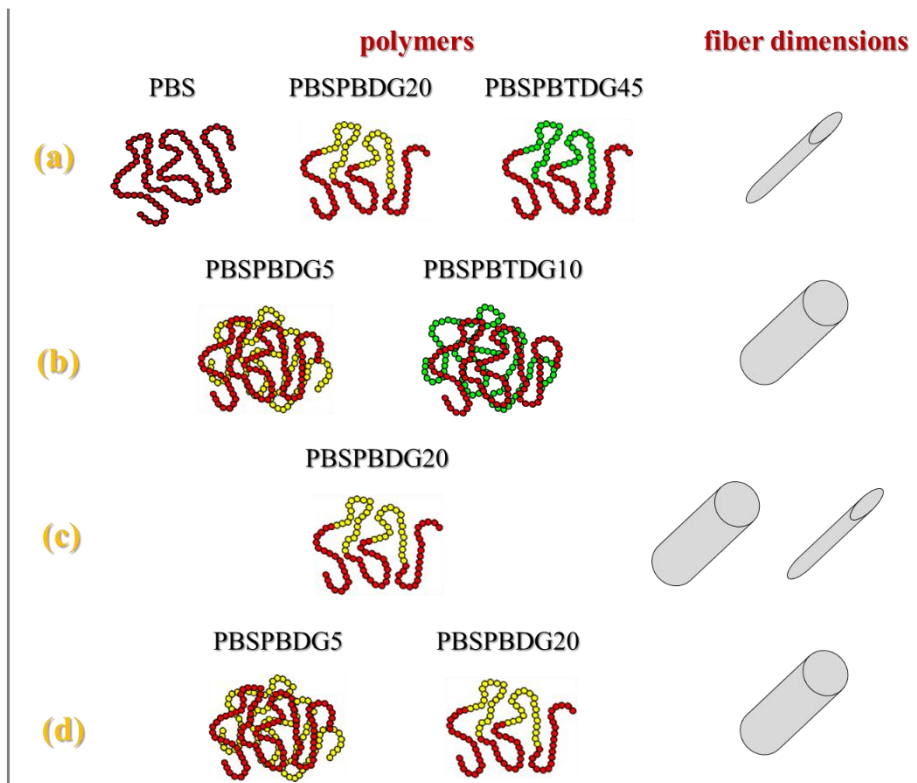


**Figure 4.47**  
Comparisons  
among  
electrospun  
scaffolds.

Detection of cell morphology by SEM will be performed and tissue differentiation will be analysed by PCR for bone related (bone sialoprotein, collagen type I, osteopontin, and osteocalcin) and cartilage related (sox-9, aggrecan, collagen type II) gene expression.

Unfortunately, the experiments are still on-going in the laboratories of the Institute for Biomedical Technology and Technical Medicine of the University of Twente, therefore no data are yet available.

## 4.5 Novel random copolyesters of poly(butylene succinate) containing ether-linkages

In the present work random copolymers with different composition of PBS and poly(butylene diglycolate) (PBDG), previously synthesized in our laboratories (section 4.3), were prepared by copolycondensation. The aim of the research was to investigate the effect of chemical structure and composition on the thermal and mechanical properties of these new materials in order to obtain structure-properties relationships which open up the possibility of controlled modification and optimization of polymer properties.

The copolyesters here presented will be indicated as P(BS<sub>x</sub>BDG<sub>y</sub>) where x and y are mol % of butylene succinate and butylene diglycolate units, respectively.

### 4.5.1 P(BS<sub>x</sub>BDG<sub>y</sub>) synthesis and molecular characterization

At room temperature P(BS<sub>x</sub>BDG<sub>y</sub>) copolymers appeared as semicrystalline light yellow solids. Prior to characterization, the copolymers were kept at room temperature for 1 month. The polymers are listed in Table 4.20, which also collects the data of molecular characterization.

**Table 4.20** Molecular characterization data of P(BS<sub>x</sub>BDG<sub>y</sub>) copolymers, together with those of the parent homopolymers added for sake of comparison.

polymer	BS (mol %) <sup>1</sup> H-NMR	$M_n$	<i>b</i>	$L_{BS}$	$L_{BDG}$
PBS	100	51200	/	/	/
P(BS90BDG10)	89.8	51500	0.97	10.1	1.1
P(BS80BDG20)	80.9	53900	1.04	5.2	1.2
P(BS70BDG30)	72.1	50600	0.96	3.7	1.5
P(BS60BDG40)	61.1	48000	1.02	2.5	1.6
P(BS50BDG50)	51.6	47300	1.02	2.0	2.0
P(BS40BDG60)	38.6	38300	0.94	1.8	2.7
P(BS30BDG70)	29.9	47900	0.99	1.5	3.4
P(BS20BDG80)	17.5	46200	0.97	1.3	5.7
P(BS10BDG90)	9.7	51200	0.95	1.2	10.8
PBDG	0	28100	/	/	/

As it can be noted from Table 4.20 all the samples are characterized by relatively high molecular weights, indicating that appropriate synthesis conditions and a good

polymerization control were obtained. The chemical structure of all polyesters was confirmed by means of  $^1\text{H-NMR}$  spectroscopy as well as the real copolymer composition which turned out very close to feed one (section 4.3.1 – 4.3.2).

Table 4.20 lists the value of  $b$  obtained for all samples investigated. In all cases, the degree of randomness was found closed to 1, indicating the random nature of the copolyesters synthesized.

#### 4.5.2 $P(\text{BSxBDGy})$ thermal characterization

The copolyesters were afterwards examined by thermogravimetric analysis and differential scanning calorimetry. The investigation on the thermal stability was carried out under dry nitrogen atmosphere. Analogously to parent homopolymers (section 4.3.1) the temperature corresponding to 5% weight loss ( $T_{5\% \text{ w.loss}}$ ) and the temperature corresponding to the maximum weight loss rate ( $T_{\text{max}}$ ) were determined from the thermogravimetric curves and collected in Table 4.21.

**Table 4.21** Thermogravimetric and calorimetric data of  $P(\text{BSxBDGy})$  random copolymers and of the parent homopolymers for comparison.

polymer	$T_{5\% \text{ w.loss}}$ (°C)	$T_{\text{max}}$ (°C)	1 <sup>st</sup> scan			2 <sup>nd</sup> scan						$\chi_c$ (%)
			$T_m$ (°C)	$\Delta H_m$ (J/g)	$T_g$ (°C)	$\Delta C_p$ (J/°C g)	$T_c$ (°C)	$\Delta H_c$ (J/g)	$T_m$ (°C)	$\Delta H_m$ (J/g)	$T_{cc}$ (°C)	
PBS	305	395	115	85	-34	0.105	/	/	115	76	78	$41 \pm 4$
P(BS90BDG10)	328	394	109	78	-33	0.211	/	/	107	63	63	$39 \pm 3$
P(BS80BDG20)	321	393	96	62	-34	0.194	/	/	96	53	40	$35 \pm 3$
P(BS70BDG30)	322	396	86	52	-34	0.422	11	19	86	45	30	$30 \pm 4$
P(BS60BDG40)	324	390	72	46	-34	0.685	35	17	72	17	24	$27 \pm 3$
P(BS50BDG50)	315	388	59	36	-33	0.734	/	/	/	/	/	$21 \pm 3$
P(BS40BDG60)	328	386	46	15	-32	0.825	/	/	/	/	/	$17 \pm 3$
P(BS30BDG70)	328	384	46	9	-30	0.716	/	/	/	/	/	$17 \pm 3$
P(BS20BDG80)	328	384	50	41	-29	0.736	/	/	/	/	/	$28 \pm 3$
P(BS10BDG90)	328	378	54	46	-28	0.664	/	/	/	/	/	$29 \pm 3$
PBDG	330	380	66	55	-27	0.672	/	/	/	/	/	$34 \pm 4$

As far as the thermal stability of all the copolymers synthesized is concerned, it was found good and similar to that of parent homopolymers ( $T_{\text{max}}$  ranging from 380 to 395 °C, see Table 4.21).

DSC traces of samples kept at room temperature for 1 month to provide them the same heat treatment, are reported in Figure 4.48 and the data obtained in Table 4.21.

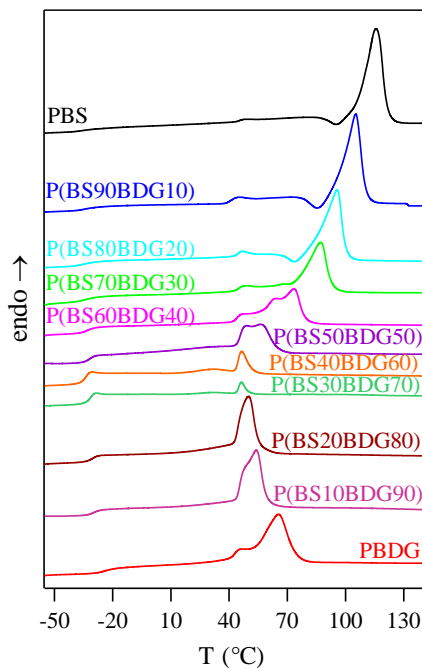


**Figure 4.48**  
Calorimetric curves of random copolymers (1<sup>st</sup> scan). PBS and PBDG calorimetric curves have been added for comparison.

In all cases, a glass transition and a melting endotherm were evident. In the copolymers, peak location appeared to depend on composition; furthermore, the increase in the amount of comonomer added to PBS or PBDG chain, led to a reduction of the heat of fusion, indicating a reduced level of crystallinity in the copolymers with respect to the homopolymers. The  $\Delta H_m$  and  $T_m$  values are plotted in Figure 4.49 as a function of BS unit content.

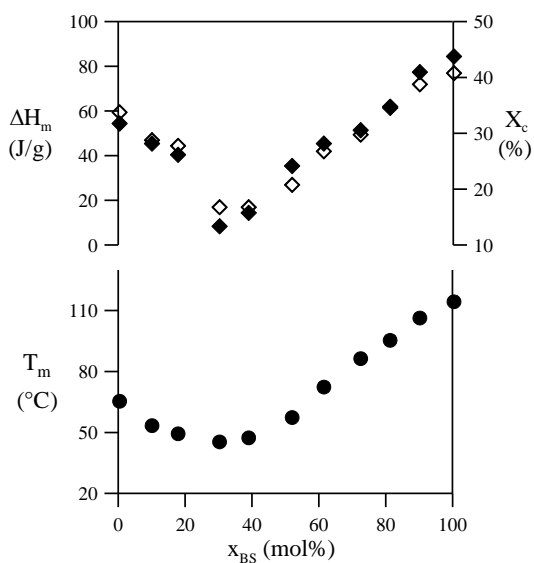
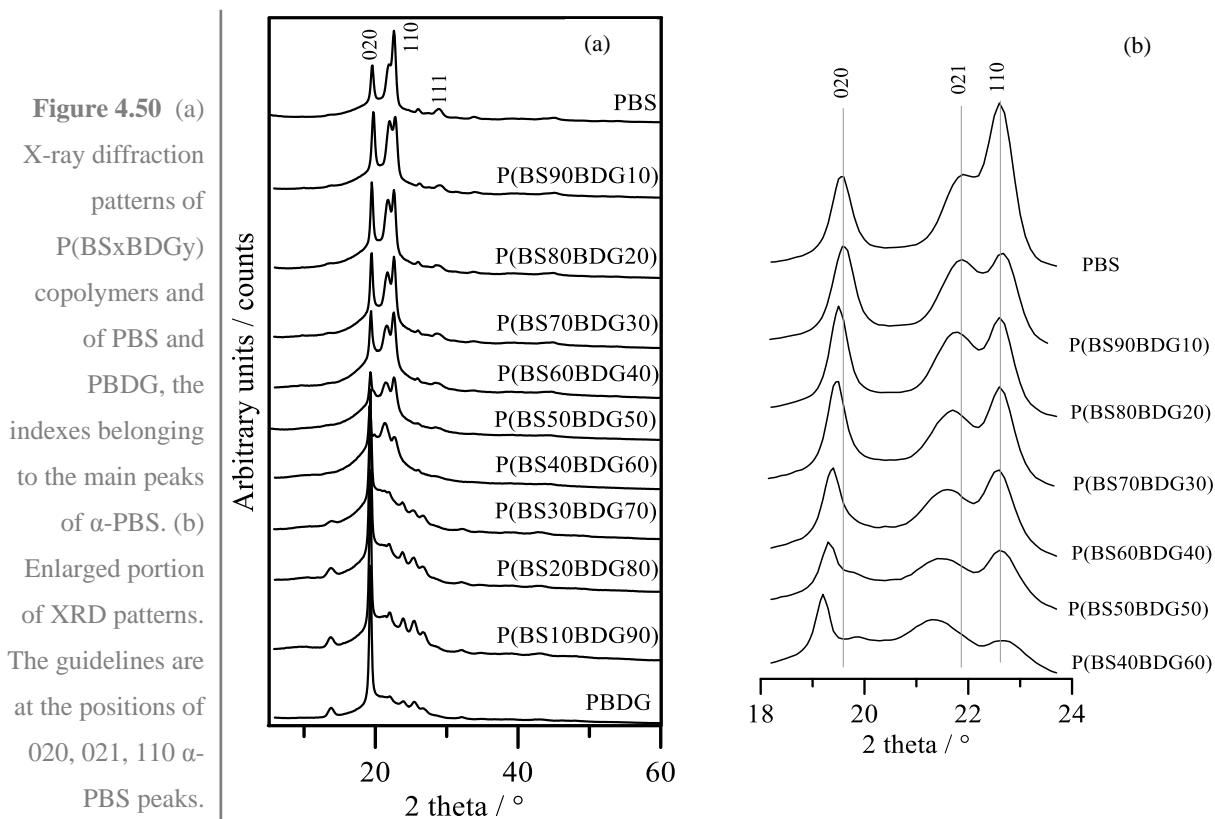


**Figure 4.49**  
Composition dependence of  $T_m$  (●),  $\Delta H_m$  (◆) and  $X_c$  (◇) for P(BS<sub>x</sub>BDG<sub>y</sub>) random copolymers.

Both the minimum in the heat of fusion and the melting point-composition dependence are typical of random copolymers, where both comonomers are able to crystallize, regardless of the fact that the comonomeric units present in minor amount are completely rejected or not from the crystalline phase (Mandelkern, 1954; 1989).

In order to clarify the nature and purity of the crystalline phase present in the polymers under investigation, the structural characterization of P(BS<sub>x</sub>BDG<sub>y</sub>) copolymers was carried out by wide angle X-ray diffraction. The X-ray diffraction patterns of P(BS<sub>x</sub>BDG<sub>y</sub>) copolymers are reported in Figure 4.50a, together with those of PBS, PBDG added for sake of comparison.



As it can be seen, the WAXD patterns of copolymers appear to be characterized by relatively intense diffraction peaks over the whole composition range. Moreover, considering the profile shapes, it can be deduced that only one crystalline phase is present in each sample. The patterns can be divided into two groups, according to the BS unit content: the samples containing from 40 up to 90 mol % of BS units show the three main  $\alpha$ -PBS peaks 020, 110, 111 and, even if the intensities are slightly modified, the crystal structure which developed in these copolymers has the characteristics of PBS lattice. On

the contrary, the copolymers containing up to 30% BS units crystallize assuming the lattice of PBDG.

The structural modifications induced by the copolymerization in PBS-type samples are evident looking at the enlarged patterns shown in Figure 4.50b.

As can be seen, the reflections 020 and 021 of the PBS-type samples shifted towards small angle (bigger distances) as the content of BDG units increased, while the reflection 110 remained constant at  $22.6^\circ$  ( $2\theta$ ). The interplanar distances calculated from peak positions are reported in Figure 4.51 as a function of composition: it is evident that the expansion of 021 plane is bigger than 020 one.

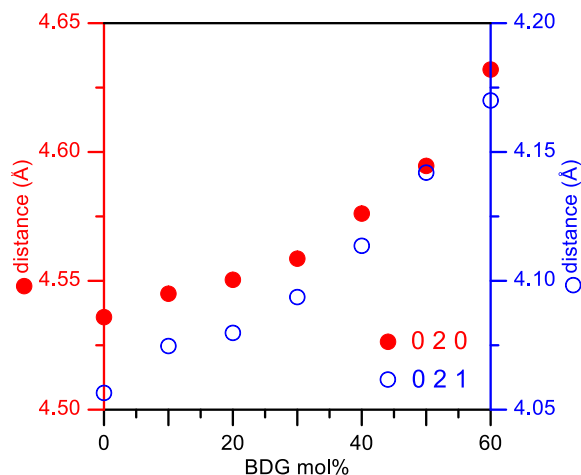


**Figure 4.51** 020 and 021 interlayer distances as a function of composition in PBS-type samples.

These expansions indicates that the  $b$  and  $c$  axes of the unit cell expand with the increment of BDG content; on the contrary the constancy of 110 reflection means that the  $a$ -axis remains constant. In the  $\alpha$ -PBS structure the polymer chain is oriented along the  $c$ -axis and consequently the reflections with a contribution in the  $l$ -index ( $hkl$  with  $l \neq 0$ ) could be influenced by a substitution of BS unit with the longer BDG ones. In particular, the insertion of an oxygen atom in the repeating unit of PBS would increase its length of about 1.1-1.4 Å. Consequently, the  $c$ -axis, almost parallel to the molecular chain, would be varied of a similar amount. The maximum values of the expansion, observed in P(BS40BDG60) sample, resulted on the contrary only of 0.09 Å for 020 peak and 0.12 Å for 021 peak. Therefore, these values can be considered a clear indication of a distortion of the unit cell, confirmed also by a variation of the relative intensities of the reflections, but exclude the possibility of cocrystallization. The patterns of the samples belonging to the PBDG-type structure seem to be less influenced by the presence of comonomer BS, both because of the limited range of samples and the fact that the shorter BS units can

replace the longer BDG ones without distortion of PBDG crystal lattice. For all the copolymers under investigation, the crystallinity degree appreciably decreased as the composition is far from the parent homopolymers, in agreement with calorimetric results (Table 4.21 and Figure 4.48).

In addition, the values of the mean crystal sizes, as calculated by the width of the 020 peak for PBS-type samples and from the peak at  $19.3^\circ$  ( $2\theta$ ) in PBDG-type samples, are in the range 18-25 nm and seem not to be affected by composition. As far as the samples crystallizing in PBS crystal lattice are concerned, the width of the peaks 021 and 110 seems to increase as the content of BDG increases: however, no conclusions can be drawn, the results being affected by the peak shift and by the variation of amorphous band.

In order to confirm X-ray results, the applicability of the equations proposed in the literature to describe the dependence of  $T_m$  on composition was checked.

Several theories have been developed to explain copolymer crystallization (section 1.2.1). On the basis of Baur equation, the  $T_{m,co}$ 's were reciprocally plotted against  $-\ln x_C - 2x_C(1-x_C)$  in Figure 4.52 and the equilibrium melting temperature and the heat of fusion for the completely crystalline PBS were extrapolated.

As can be noted, the plot shows a good linearity and this result can be considered a further proof of the random nature of the copolymers investigated as well as of the exclusion of the co-units from the crystalline lattice of PBS. The estimated  $T_m^\circ$  and  $\Delta H_m^\circ$  were found to be  $132^\circ\text{C}$  and  $107 \text{ J/g}$  respectively, in excellent agreement with the values found previously (Ren *et al.*, 2005; Soccio *et al.*, 2009). In conclusion, the results appeared to be in perfect agreement with those obtained by means of X-ray diffraction measurements.

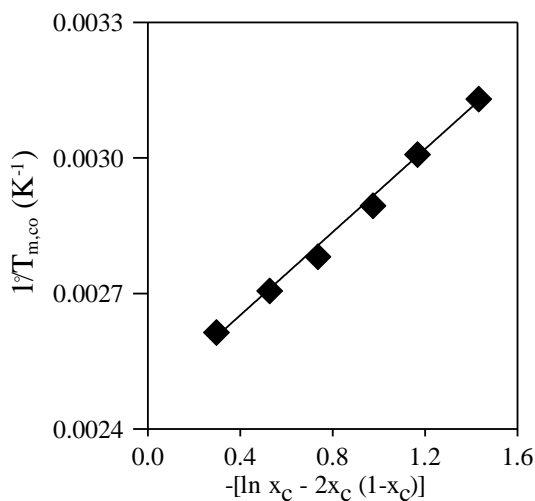


**Figure 4.52**  
 $1/T_{m,co}$ -  
 composition plot  
 according to  
 Baur's equation.

To confirm that in the copolymers the tendency of PBS to crystallize decreases as the content of BDG co-units is increased, non-isothermal experiments were carried out.

The exothermic crystallization peaks of the samples under investigation are shown in Figure 4.53. PBDG and the copolymers containing from 10 to 50 mol % of BS units were not able to crystallize even though cooled from the melt at low rate (1°C/min).

Such behaviour indicates that in these copolymers the crystallization rate of PBS is significantly decreased by the presence of BDG comonomeric units. In particular, an amount of BDG units of 40 mol% is sufficient to completely depress the crystallisation process of PBS under the adopted experimental conditions. Moreover, it can be observed, as also shown in the inset, reporting  $T_{cc}$  values as a function of composition, that the temperature of the maximum of the exothermal crystallization peak regularly decreases as the BDG unit content is increased. This fact indicates a decrement of the overall crystallization rate of PBS, due to the presence of co-units which act as obstacles in the regular packing of polymer chains.

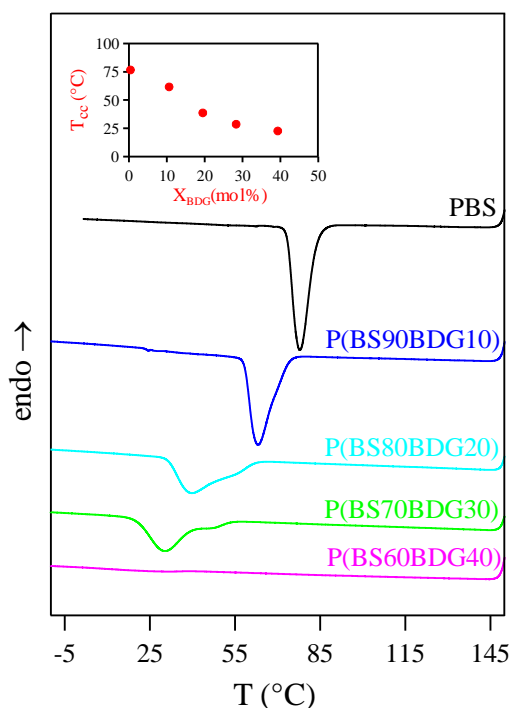
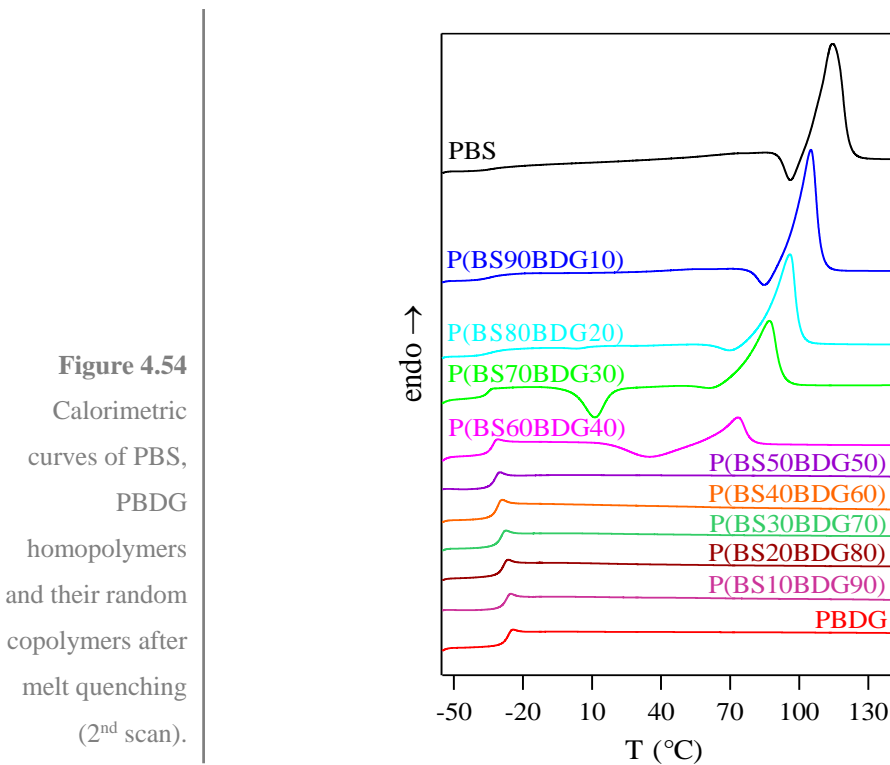


**Figure 4.53** DSC crystallization exotherms of PBS and P(BS $x$ BDG $y$ ) random copolymers cooled from the melt at 5°C/min. In the inset:  $T_{cc}$  as a function of BDG unit content.

It is well known that a partially crystalline material usually exhibits a different glass transition behavior than the completely amorphous analogous. In fact, although some conflicting results are reported in the literature (Boyer, 1963), crystallinity usually acts

like crosslinking and raises  $T_g$  through its restrictive effect on the segmental motion of amorphous polymer chains. Therefore, in order to study the influence of chemical structure on the glass transition of random copolymers, the phenomenon should be examined in the total absence of crystallinity. In this view, all the samples under investigation were subjected to rapid cooling (quenching) from the melt. The DSC curves after melt quenching are shown in Figure 4.54: the calorimetric traces of PBS and P(BSxBDGy) copolymers containing up to 20 mol % of BDG units showed a melting endotherm phenomenon, indicating the partially crystalline nature of these samples. Copolymers containing 30 and 40 mol % of BDG units, showed a glass transition followed by an exothermal “cold crystallization” peak and a melting endotherm at higher temperature.

As concern P(BS70BDG30) the enthalpy associated with the crystallization phenomenon is lower than that of the fusion endotherm, indicating that this sample cannot be frozen into a completely amorphous state by quenching. The DSC curve of such sample is therefore typical of partially crystalline polymer.



In the case of P(BS60BDG40) the enthalpy of crystallization very well compared with the corresponding heat of fusion, indicating that this copolymer is completely amorphous. As regards the calorimetric curves of pure PBDG and the copolymers containing from 50 to

90 mol % of BDG units, only an intense endothermal baseline deviation associated with the glass transition was observed. Therefore, the DSC scans indicate a quite different thermal behavior of PBDG and PBS homopolymers: in fact, the former is completely amorphous, whereas the latter is partially crystalline. Moreover, the phase behavior of P(BS $x$ BDG $y$ ) copolymers depends on composition: as a matter of fact, after melt quenching, semicrystalline samples are exclusively obtained at high BS content.

As can be seen in Figure 4.54 and from the data collected in Table 4.21, the glass transition temperature is influenced by the amount of BDG units in the chain. The values of  $T_g$  are plotted in Figure 4.55 as a function of BDG unit content.

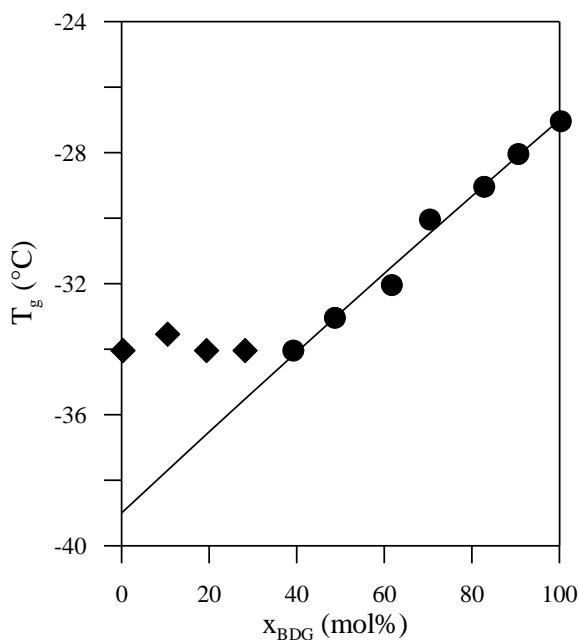


**Figure 4.55** Composition dependence of  $T_g$  for P(BS $x$ BDG $y$ ) random copolymers (◆ semicrystalline samples; ● amorphous samples); solid line represents the best fitting of  $T_g$  data of completely amorphous samples according to a Fox-type equation.

The values of  $T_g$  of partially crystalline PBS and P(BS $x$ BDG $y$ ) copolymers containing from 10 to 30 mol % of BDG units do not follow the same composition dependence as that of the amorphous samples: in fact, the measured glass transition temperature value is higher than expected, the crystallites hindering the motion of the amorphous chains. As far as the trend of the glass transition temperature with the composition is concerned, it can be observed that  $T_g$  values increase as BDG unit content is increased; such results can

be explained on the basis of interchain interactions among PBDG macromolecular chains, due to the electronegativity of ether-oxygen atoms (Eisenberg, 1984).

In order to determine  $T_g$  value of completely amorphous PBS, the experimental data of the completely amorphous copolymers were fitted by a Fox-type equation (Fox, 1956) (Figure 4.54), using for PBDG the glass transition temperature experimentally measured by us. The value obtained for PBS is  $-39^\circ\text{C}$ .

#### 4.5.3 *P(BS<sub>x</sub>BDG<sub>y</sub>) copolymers mechanical characterization*

Lastly, the mechanical properties of *P(BS<sub>x</sub>BDG<sub>y</sub>)* copolymers were investigated subjecting the samples to stress-strain measurements. Their tensile behaviour, together with that of PBS and PBDG added for comparison, is shown in Figure 4.56, that plots the stress as a function of strain. Table 4.22 reports the corresponding mechanical data (elastic modulus,  $E$ ; stress at break,  $\sigma_b$ , and deformation at break,  $\varepsilon_b$ ) of PBS, PBDG and some copolymers *P(BS<sub>x</sub>BDG<sub>y</sub>)*.

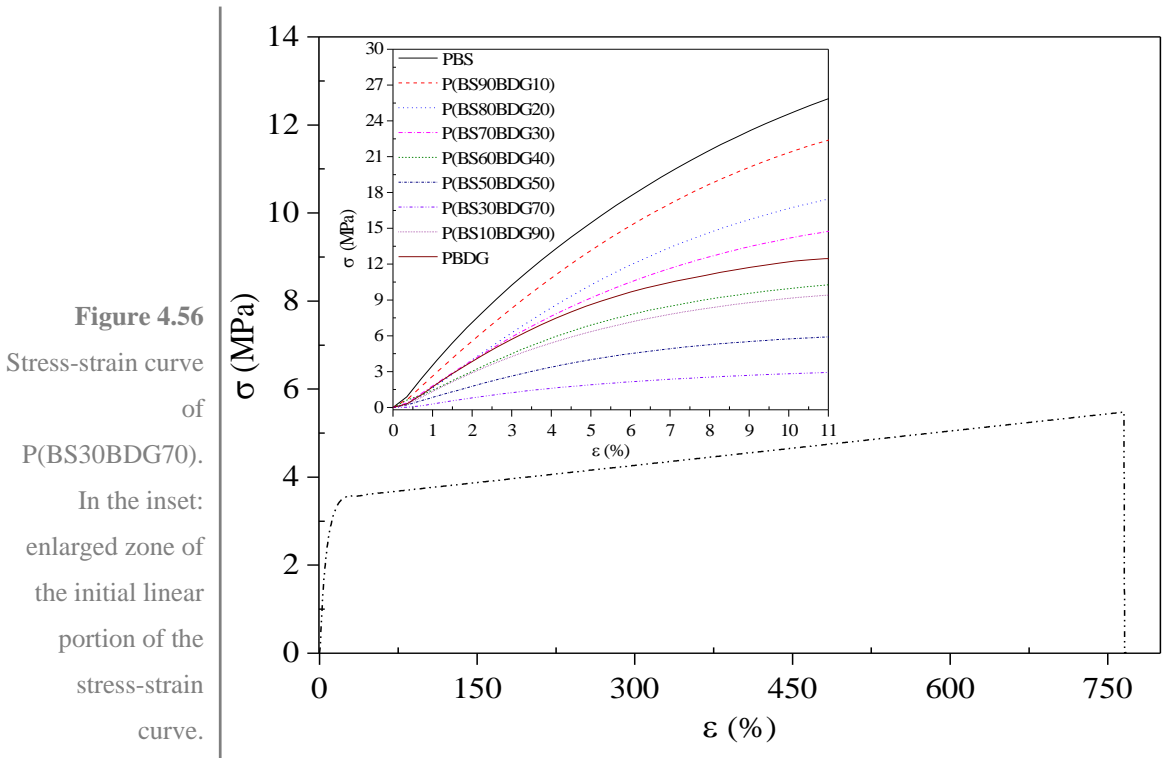


**Table 4.22** Mechanical data of PBS, PBDG and their random copolymers.

Polymers	E (MPa)	$\epsilon_b$ (%)	$\sigma_b$ (MPa)
PBS	337 ± 27	24 ± 4	31 ± 2
P(BS90BDG10)	304 ± 22	45 ± 8	28 ± 2
P(BS80BDG20)	225 ± 13	285 ± 31	23 ± 1
P(BS70BDG30)	195 ± 7	948 ± 26	26 ± 3
P(BS60BDG40)	144 ± 3	1064 ± 68	21 ± 1
P(BS50BDG50)	83 ± 6	883 ± 72	16 ± 3
P(BS30BDG70)	40 ± 6	759 ± 50	16 ± 1
P(BS10BDG90)	134 ± 11	556 ± 22	26 ± 1
PBDG	147 ± 21	427 ± 33	23 ± 2

Copolymer elastic modulus regularly decreased as BDG unit content was increased, up to 70 mol% of BDG units, whereas increased in the range 70-90 mol%.

Since all the investigated polymers display a soft amorphous phase ( $T_g$  values are in all cases well below RT), the observed trend can be ascribed to two effects: changing in composition and in crystallinity degree (see Table 4.21). Moreover, it has to be emphasized that the copolymers with a BDG unit content ranging from 30 to 60 mol%, are characterized by an elastomeric behaviour.

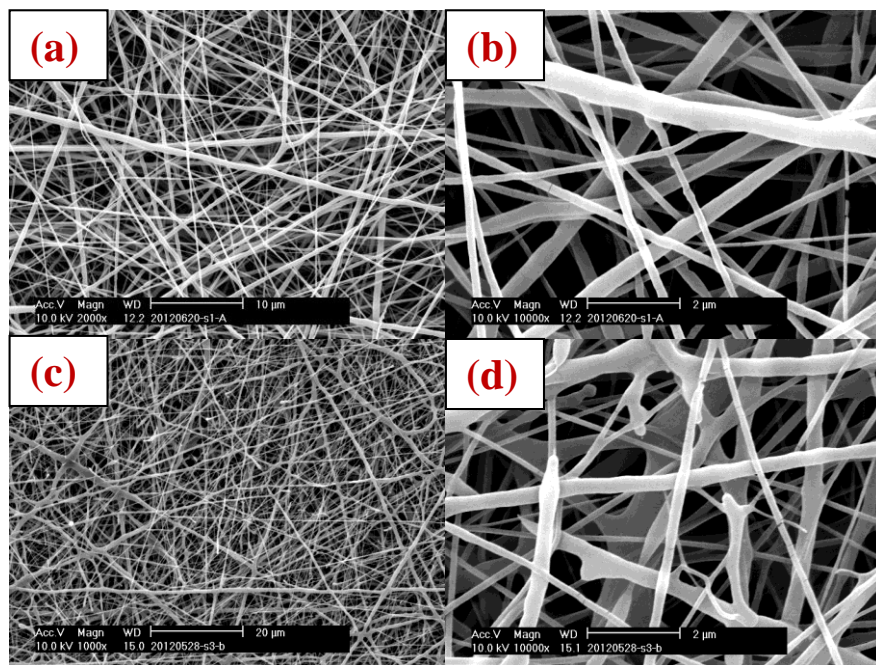
#### 4.5.4 Electrospinning of PBS and P(BS80BDG20)

P(BS80BDG20) has been electrospun to obtain engineered 3-D scaffold for tissue engineering applications. PBS has been also considered for sake of comparison.

ES conditions parameters were optimized in order to obtain defect-free fibres by evaluating fiber morphology by SEM according to the procedure previously described (section 4.4.6).

In Figure 4.50 SEM micrographs of the scaffolds under investigation are reported. The scaffolds appeared to be highly porous mats with microscale interstitial pores. Both polymers yielded fibers free of beads defects, randomly oriented and possessing very close submicrometric diameters:  $237 \pm 81$  nm and  $245 \pm 127$  nm for PBS and P(BS80BDG20), respectively.

**Figure 4.57** SEM micrographs of:  
 (a) PBS 1000x,  
 (b) PBS 10000x,  
 (c) P(BS80BDG20) 1000x, (d) P(BS80BDG20) 10000x.



#### 4.5.5 Characterization of PBS and P(BS80BDG20) scaffolds

ES fibres were characterized by TGA and DSC. As in the previous case (section 4.4.6), TGA did not reveal residual solvents in the ES fibres and confirmed that ES process did not contribute to decrease the thermal stability of the polymers. DSC analysis evidenced negligible differences in the thermal behavior between polymeric films and the corresponding electrospun fibers.

In order to investigate the relative hydrophilicity of the scaffolds under study, water contact angle measurements were performed. As in the previous case (section 4.4.6), the high porosity of the electrospun mats prevented the direct measure on the scaffolds. Therefore, WCA analysis were performed on hot-pressed films providing the following results:  $WCA_{\text{PBS}} = 96 \pm 1^\circ$ ;  $WCA_{\text{P(BS80BDG20)}} = 92 \pm 2^\circ$ . The introduction of ether-oxygen containing BDG co-units in the PBS macromolecular chain increased its surface wettability, even if to a smaller extent as compared to the block copolymers (section 4.4.6), due to the lower amount of BDG units (20 mol% with respect to 50 mol%) and the different molecular architecture (random distribution of sequences instead of block one). Due to the possible application in tissue engineering, the evaluation of the mechanical properties of the scaffolds are of crucial interest. Therefore, PBS and P(BS80BDG20) electrospun mats were subjected to stress-strain measurements. Their tensile behaviour is

shown in Figure 4.58, that plots the stress as a function of strain, and in Table 4.23, that reports their corresponding mechanical data (elastic modulus,  $E$ ; stress at break,  $\sigma_b$ , and deformation at break,  $\varepsilon_b$ ).

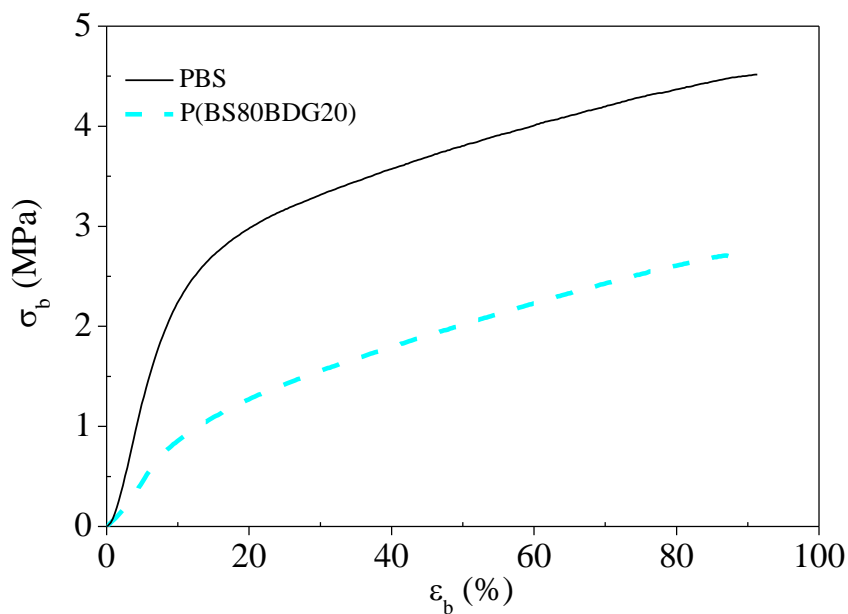


**Figure 4.58** Stress-strain curve of PBS and P(BS80BDG20) scaffolds.

The results obtained for elastic modulus and stress at break confirmed those reported in the case of thin films (section 4.5.3): PBS showed higher  $E$  and  $\sigma_b$  with respect to P(BS80BDG20). As underlined above (section 4.5.3), they can be ascribed to the changing in composition and in crystallinity degree.

On the contrary, no improvement was observed in the elongation at break of the copolymer with respect to PBS homopolymer.

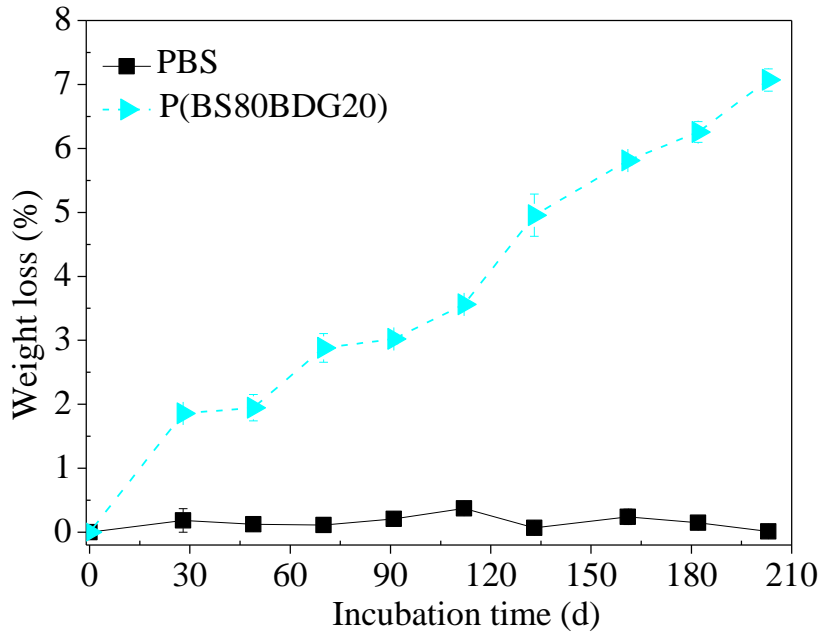
**Table 4.23** Mechanical data of PBS and P(BS80BDG20) scaffolds.

polymer	$E$ (MPa)	$\varepsilon_b$ (%)	$\sigma_b$ (MPa)
PBS	$18 \pm 7$	$93 \pm 15$	$4 \pm 1$
P(BS80BDG20)	$6 \pm 2$	$90 \pm 12$	$1.6 \pm 0.4$

#### 4.5.6 Hydrolytic degradation

Hydrolytic degradation experiments were performed under physiological conditions (section 3.11) on the electrospun mats in order to evaluate hydrolysis rate. Weight losses are reported in Figure 4.59 as a function of incubation time.

**Figure 4.59**  
Weight loss of  
PBS and  
P(BS80BDG20)  
scaffolds as a  
function of  
incubation time.



As it can be evicted form Figure 4.59, after 203 days of incubation PBS weight loss was almost negligible; on the contrary P(BS80BDG20) scaffold degraded to a higher extent, reaching weight loss of about 7%.

The results confirmed the trend observed in the previous case (section 4.4.7): as a matter of fact copolymerization of PBS with BDG co-unit enhanced its degradability, mainly because of the decreased crystallinity degree and the increased hydrophilicity.

In addition, from a comparison between the PBSPBDG5, PBSPBDG20 and P(BS80PBDG20), it can be evicted that this latter displayed a lower degradation rate with respect to the others, due to its higher crystallinity degree and hydrophobicity.

The percentage of residual number average molecular weight ( $M_n$  res%) is reported in Figure 4.60 as a function of incubation time. As expected (section 1.1.4.1), both samples underwent a decrease of  $M_n$  with time. The results confirmed the trend observed for weight loss analysis and those obtained in the previous case (section 4.4.7).

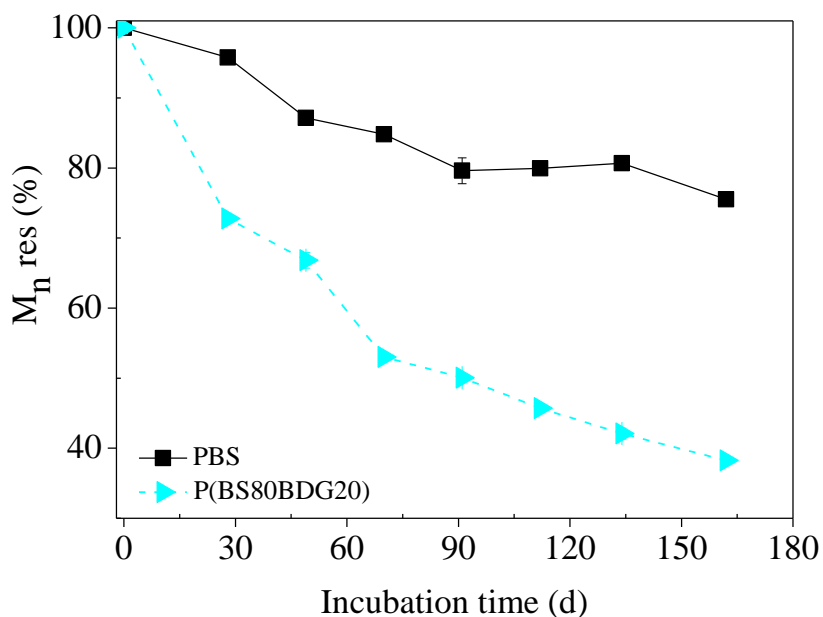


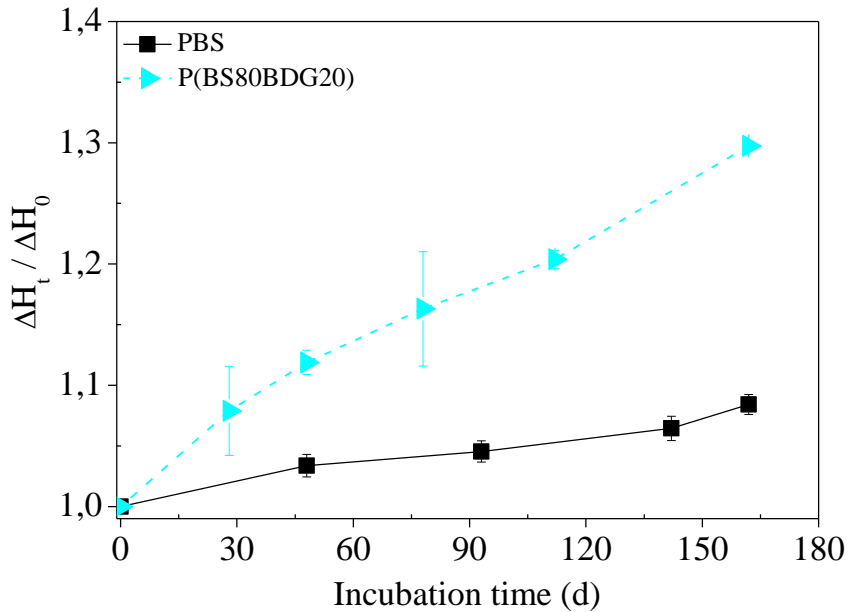
**Figure 4.60**  
Residual molecular weight of PBS and P(BS80BDG20) scaffolds as a function of incubation time.

A confirmation that the amorphous regions of a polymer are degraded more quickly than the crystalline ones, was obtained by subjecting the partially degraded copolymer samples to a heating calorimetric scan (20°C/min). All the calorimetric traces were found to be characterized by an endothermic peak associated with the fusion process of crystalline portion of the material (data not shown). The corresponding heat of fusion was normalized respect to the heat of fusion of non-degraded sample ( $\Delta H_t/\Delta H_0$ ). The results obtained are reported in Figure 4.61.

As highlighted in the previous section (section 4.4.7), the increment of the crystalline/amorphous ratio can be due also to the annealing process. Taking this into consideration, all the copolymers under study have been incubated at 37°C under nitrogen atmosphere (to prevent any possible degradation process) and subjected to DSC measurements. Interestingly, after 45 days an increment in the normalized heat of fusion was found for both polymers under investigation. Moreover, this increment coincided with that observed for hydrolytically degraded samples.

Therefore, after 45 days of incubation the trend observed in Figure 4.61 can only be ascribed to the annealing contribution. Annealing studies are still in progress, consequently up to now further evaluations cannot be made. In particular, at present nothing can be established for longer incubation times, when the degradation process is more relevant.

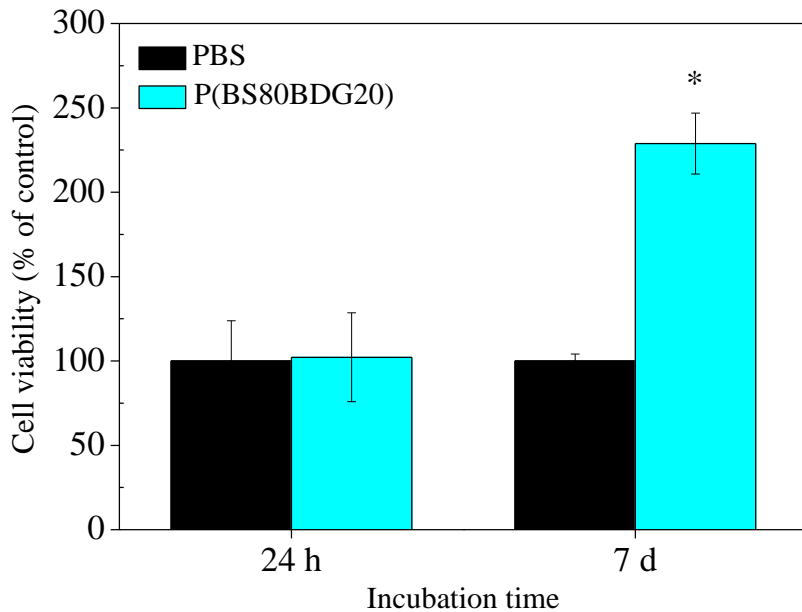
**Figure 4.61**  
Normalized heat of fusion as a function of incubation time for PBS and P(BS80BDG20) scaffolds as a function of incubation time.



#### 4.5.7 Biocompatibility assay

Biocompatibility studies have been conducted according to the procedure previously described (section 3.19.3). Figures 4.62 shows the viability data obtained by incubating C2C12 cells on PBS and P(BS80BDG20) scaffolds after appropriate sterilization.

**Figure 4.62**  
Percentage of C2C12 viability on PBS and P(BS80BDG20) scaffolds after 24h and 7 days.



Data were expressed as percentage of cell viability  $\pm$  SD onto P(BS80BDG20) electrospun mats relative to PBS control film (set at 100%). The statistical differences between scaffolds were evaluated by independent two-sample t-test with significance level  $p = 0.05$ .  $*p < 0.05$  compared to PBS at 7 days.

Cell viability was measured at 24h and 7 days to characterize C2C12 attachment and proliferation.

At 24h, the cell density on the electrospun P(BS80BDG20) was similar to that on PBS. On the contrary, after a week of culture, cell density was found significantly greater on the copolymer ( $*p < 0.05$ ). In particular, cell viability reached a value of about 230% with respect to the control.

The results showed that the cell adhesion and proliferation are greatly enhanced on P(BS80BDG20) scaffolds.

## **4.6 Random copolyesters based on poly(butylene 1,4-cyclohexanedicarboxylate) containing ether-oxygen atoms**

In the present study random copolymers based on 1,4-trans-cyclohexanedicarboxylic acid and diglycolic acid (P(BCEmBDGn)) have been prepared by melt polycondensation in the whole range of composition. The two parent homopolymers, poly(butylene cyclohexanedicarboxylate) (PBCE) and poly(butylene diglycolate) (PBDG) have been also synthesized for sake of comparison.

The thermal and structural properties, wettability and mechanical properties of the synthesized polymers were investigated and correlated to polymer chain microstructure.

In addition, this work aimed to assess the versatility of this class of fully aliphatic polyesters to be used both for biomedical and environmental applications. Therefore, to verify the applicability in food-packaging, barrier properties to different gases (oxygen and carbon dioxide) were evaluated. On the other hand, to analyse the possible use of P(BCEmBDGn) as drug carriers, enzymatic degradation studies in the presence of hog pancreas lipase have been conducted and *in vitro* drug release and cell culture experiments were performed.

#### 4.6.1 Synthesis, molecular and thermal characterization

At room temperature all the synthesized polyesters appeared as semicrystalline light yellow solids. The polymers are listed in Table 4.24, which also collects the data of molecular characterization.

As far as the two homopolymers are concerned, both PBCE and PBDG were characterized by relatively high and comparable molecular weights (Table 4.24), indicating that appropriate synthesis conditions and a good polymerization control were achieved. In order to have an understanding into their chemical structure, the  $^1\text{H-NMR}$  investigation was performed on both homopolymers. Their spectra were found to be consistent with the expected structure (Figure 4.63).

All the copolyesters were also characterized by relatively high and similar molecular weights, comparable to those of parent homopolymers.  $^1\text{H-NMR}$  analysis confirmed the awaited structures (see as an example the  $^1\text{H-NMR}$  spectrum of P(BCE55BDG45) shown in Figure 4.63).

The copolymer composition, calculated from the relative areas of the  $^1\text{H-NMR}$  resonance peak of the **1** aliphatic protons in *trans* configuration of the cyclohexanedicarboxylic subunit located at 2.28 ppm and of the **5** protons of the methylene groups of the diglycolic subunit at 4.24 ppm, was found close to the feed one (Table 4.24).

**Table 4.24** Molecular characterization data of PBCE, PBDG and P(BCEmBDGn).

polymer	$M_n^a)$	$PDI^b)$	$BDG (mol\%)$ ( $^1\text{H-NMR}$ )	$L_{BCE}^c)$	$L_{BDG}^d)$	$b^e)$	Thickness ( $\mu\text{m}$ )
PBCE	38500	2.0	0	-	-	-	$152.00 \pm 0.82$
P(BCE90BDG10)	31700	2.1	10.6	7.4	1.1	0.97	$151.33 \pm 0.47$
P(BCE80BDG20)	38700	2.3	18.1	5.5	1.2	1.07	$187.67 \pm 1.25$
P(BCE70BDG30)	32300	2.3	29.9	3.2	1.4	1.04	$177.33 \pm 1.70$
P(BCE55BDG45)	39000	2.2	45.2	2.1	2.0	0.98	$214.33 \pm 2.05$
P(BCE40BDG60)	33600	2.2	60.7	1.7	2.5	1.00	$237.00 \pm 2.94$
P(BCE25BDG75)	32000	2.1	72.9	1.4	3.6	1.02	$174.57 \pm 12.55$
P(BCE5BDG95)	31300	2.3	93.2	1.1	19.4	0.96	$263.67 \pm 0.94$
PBDG	46700	2.3	100	-	-	-	$228.00 \pm 2.16$

<sup>a)</sup> number average molecular weight calculated by GPC analysis

<sup>b)</sup> polydispersity index calculated by GPC analysis

<sup>c)</sup> butylene cyclohexanedicarboxylate block length calculated by  $^1\text{H-NMR}$

<sup>d)</sup> butylene diglycolate block length calculated by  $^1\text{H-NMR}$

<sup>e)</sup> degree of randomness calculated by  $^{13}\text{C-NMR}$

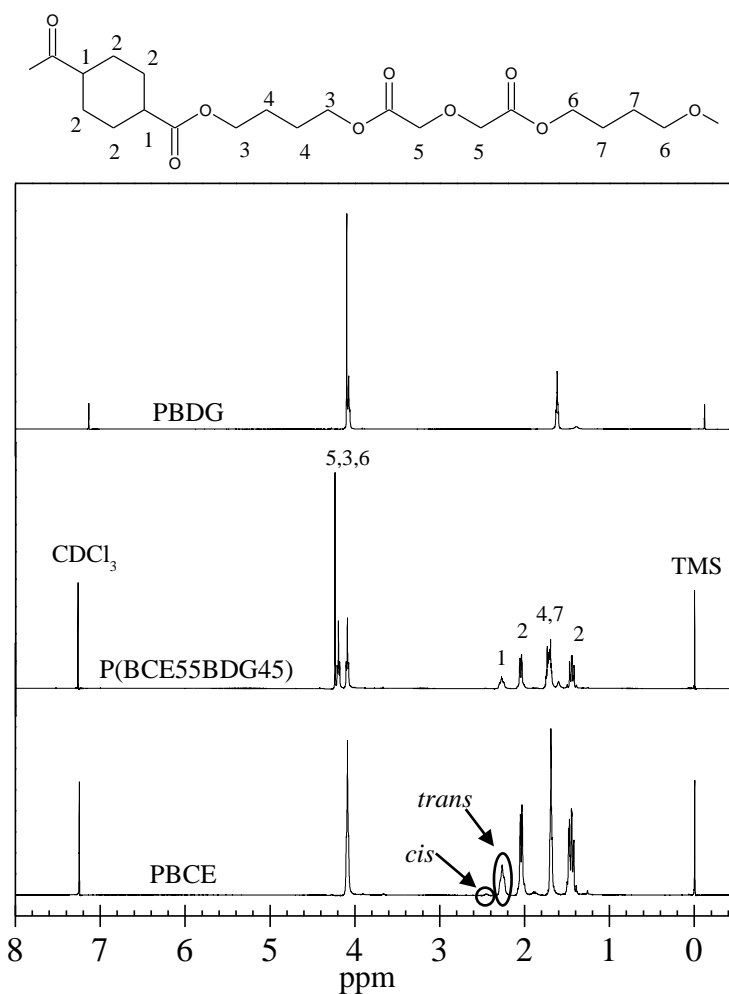


**Figure 4.63**  $^1\text{H}$ -NMR spectra of PBDG, P(BCE55BDG45) and PBCE with resonance assignments.

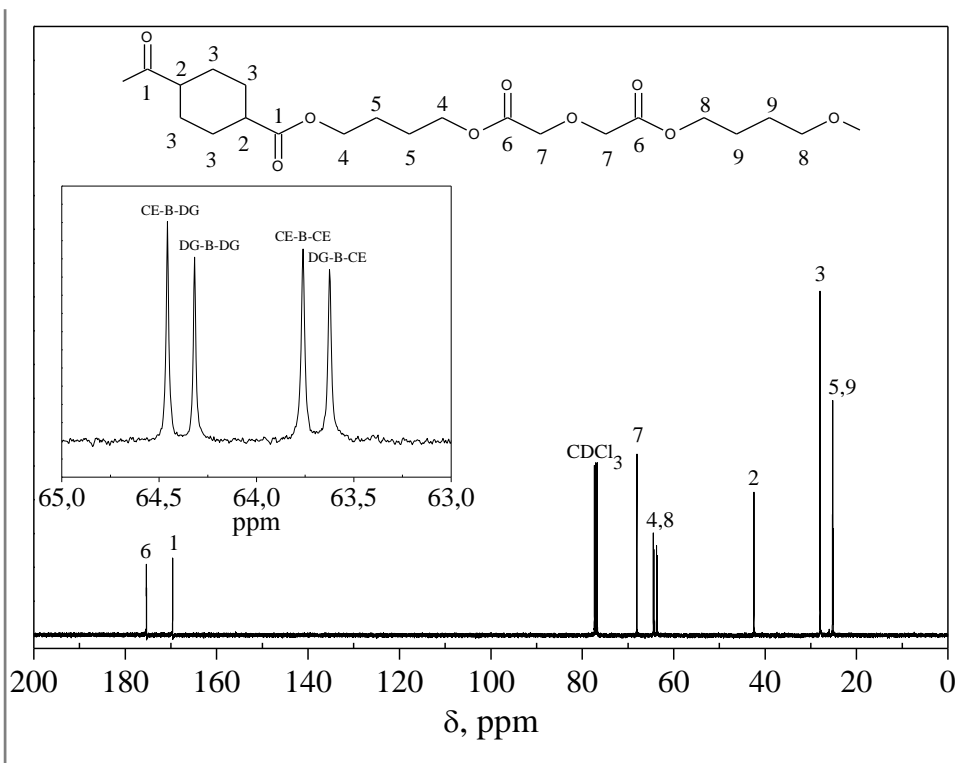
Previous studies (Berti *et al.*, 2008; Colonna *et al.*, 2011) reported that the 1,4-cyclohexylene ring present in DMCE can isomerize during polymer synthesis or thermal treatments carried out at temperature higher than 260°C for longer than 1h, moving toward the thermodynamically stable *cis/trans* ratio of 34-66%. Therefore,  $^1\text{H}$ -NMR analysis was used to calculate the *trans* percentage in the polymers under study. The ratio of the areas of the signals centred at 2.28 ppm (*trans* isomer) and 2.44 ppm (*cis* isomer) has been considered (Figure 4.63). From these data it can be evicted that isomerization from the *trans* form to the *cis* one occurred only to small extent during polymerization, being the *cis* content in all cases less than 3%.

Information on the arrangement of the comonomeric units in the chain can be deduced by the degree of randomness  $b$ , which in this case has been determined by  $^{13}\text{C}$ -NMR spectroscopy, according to the procedure described elsewhere (section 3.6.1). In particular, the region between  $\delta = 63.4$  and  $\delta = 64.8$  ppm (where the signals due to the

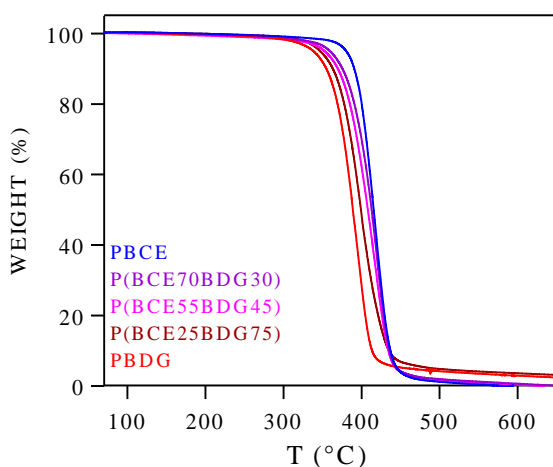
carbon atoms of the 1,4-butanediol glycol subunit are located) has been considered to evaluate the degree of randomness (Figure 4.64).

Table 4.24 lists the value of  $b$  obtained for all samples investigated: as it can be seen, the degree of randomness was found closed to 1, indicating the random nature of the copolyesters synthesized.

**Figure 4.64**  $^{13}\text{C}$ -NMR spectrum of P(BCE55BDG45) and resonance assignments with expansion of region between 63.4 and 64.8 ppm.



Subsequently, the polymers were subjected to thermogravimetric analysis and the temperature corresponding to 5% weight loss ( $T_{5\% \text{ w. loss}}$ ) has been determined and collected in Table 4.25. As evidenced in Figure 4.65 reported in the following, where the thermogravimetric curves of the parent homopolymers and of some of the synthesized copolyesters are reported as an example, the weight loss took place in all cases practically in one-step. From the comparison between the two TGA curves of PBCE and PBDG, it can be seen that the former is more thermally stable than the latter. The result can be attributed to different factors: 1) the introduction of etheroatoms along the polymeric chain reduces the thermal stability of a polymer because it favours thermo-oxidative processes; 2) the presence in the main chain of PBCE of bulky and thermally stable cyclohexylene groups (Sun & Wang, 1999). As reported in the literature (Berti *et al.*, 2008), the fully aliphatic ring renders the polymer even more thermally stable than the corresponding aromatic polyester, i.e. PBT.



**Figure 4.65**  
Thermogravimetric curves of PBCE, PBDG, P(BCE70PBDG30), P(BCE55PBDG45) and P(BCE25PBDG75) under nitrogen atmosphere (heating rate: 10 °C/min).

As regards the copolyesters, it is worth noting that they are characterized by a good thermal stability ( $T_{5\% \text{ w.loss}}$  ranging from 341 to 376 °C) which is however strictly dependent on the composition (Table 4.25): as a matter of fact, the thermal stability regularly decreased with the increase of mol% of BDG co-unit.

In order to provide the same heat treatments to all the samples investigated, prior to thermal analysis each film was kept at room temperature for two weeks. DSC traces of so-treated samples are reported in Figure 4.66a and the data obtained in Table 4.25.

**Table 4.25** Thermal and diffractometric characterization data and water contact angles for PBCE, PBDG and their random copolymers.

polymer	$T_{5\% \text{ w.loss}}$ (°C)	1 <sup>st</sup> scan					2 <sup>nd</sup> scan					WCA (°)
		$T_m$ (°C)	$\Delta H_m$ (J/g)	$T_g$ (°C)	$\Delta C_p$ (J/°C g)	$T_c$ (°C)	$\Delta H_c$ (J/g)	$T_m$ (°C)	$\Delta H_m$ (J/g)	$T_{cc}$ (°C)	$X_c$ (%)	
PBCE	380	166	33	12	0.065	-	-	167	31	144	42 ± 3	110 ± 2
P(BCE90BDG10)	376	155	30	-1	0.062	-	-	155	29	135	43 ± 4	107 ± 1
P(BCE80BDG20)	371	141	25	-12	0.144	-	-	141	24	115	42 ± 3	96 ± 1
P(BCE70BDG30)	360	120	24	-15	0.237	-	-	121	22	97	39 ± 3	92 ± 2
P(BCE55BDG45)	353	93	17	-21	0.350	29	4	93	19	60	32 ± 3	87 ± 3
P(BCE40BDG60)	350	42	10	-25	0.511	-	-	-	-	-	19 ± 3	85 ± 1
P(BCE25BDG75)	347	40	20	-26	0.538	-	-	-	-	-	12 ± 2	82 ± 1
P(BCE5BDG95)	341	45	42	-27	0.640	-	-	-	-	-	31 ± 3	78 ± 2
PBDG	338	58	48	-27	0.678	-	-	-	-	-	38 ± 3	76 ± 2

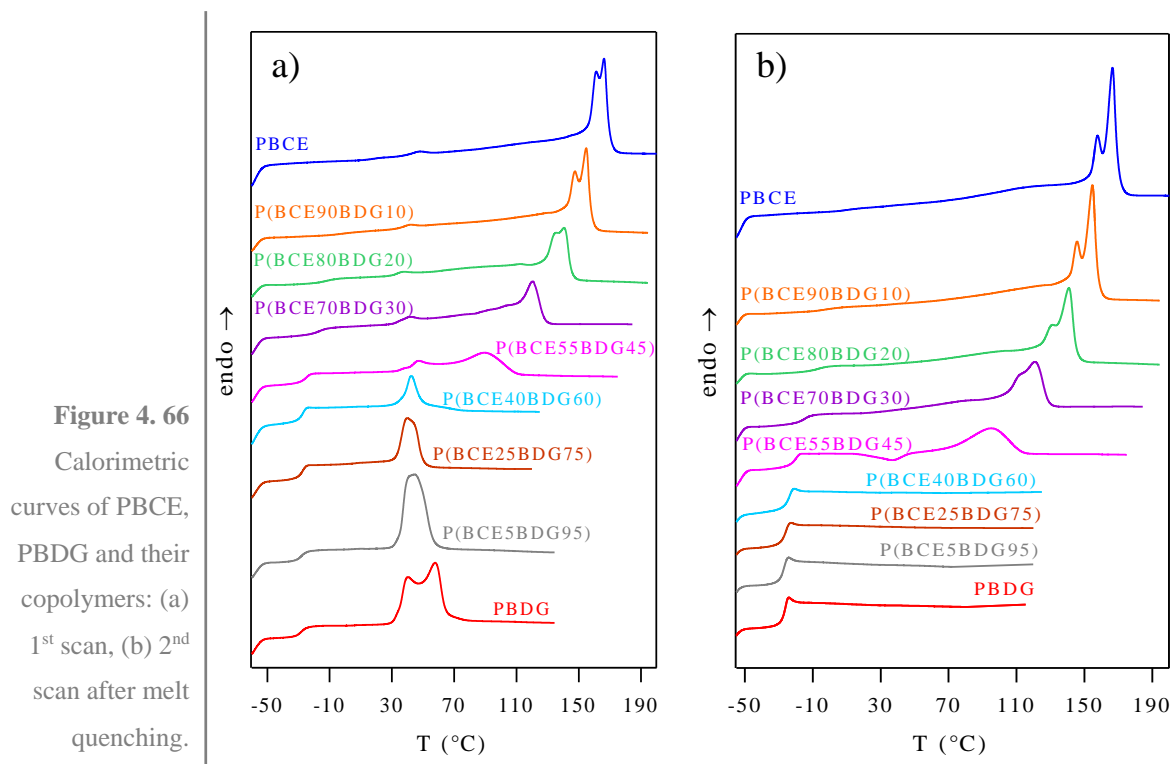


**Figure 4.66**  
Calorimetric curves of PBCE, PBDG and their copolymers: (a) 1<sup>st</sup> scan, (b) 2<sup>nd</sup> scan after melt quenching.

The phase behaviour of the two parent homopolymers is similar: both are semicrystalline, being the corresponding calorimetric traces characterized by a conspicuous melting endotherm (see Table 2): the  $T_m$  of PBDG ( $T_m = 58^\circ\text{C}$ ) is anyway significantly lower than that of PBCE ( $T_m = 166^\circ\text{C}$ ).

As a matter of fact, the perfection of crystalline phase is strongly influenced by the symmetry of the polymeric chain, this latter being drastically reduced in PBDG by the introduction of ether-oxygen atoms along the polymer chains (the van der Waals radius of oxygen atom ( $1.4\text{ \AA}$ ) is indeed significantly lower than that of the neighbor  $-\text{CH}_2$  groups ( $2.0\text{ \AA}$ )). Moreover, it is worth remembering that the aliphatic rings present in PBCE are practically all in *trans* configuration: in such configuration the polymeric chain assumes a “stretched” form and is characterized by a high symmetry and, as it is well known, both these conditions are favourable to the chain packing (Berti *et al.*, 2008).

As evidenced by the calorimetric curves shown in Figure 4.66a, both the endothermic process of PBDG and PBCE were characterized by a double melting peak, but the significant differences between the two maxima observed in PBDG confirmed the presence in this polyester of a crystalline phase with a lower degree of perfection, which melts and recrystallize in a more perfect form during the heating scan. After melt quenching (Figure 4.66b), the phase behaviour of the two polymers becomes opposite:

PBCE is semicrystalline, whereas PBDG is completely amorphous, indicating that the crystallization ability of PBCE is significantly higher than that of PBDG. The higher crystallization rate of PBCE can be related to the higher symmetry of PBCE polymer chain on respect PBDG one.

The glass transition temperature of PBCE ( $T_g = 12^\circ\text{C}$ ) turns out to be much higher than that of PBDG ( $T_g = -27^\circ\text{C}$ ); this result can be explained on the basis of the enhanced polymer chain flexibility given by the presence of methylene groups in PBDG with respect to the aliphatic ring of PBCE. In the case of PBCE the endothermal shift of baseline related to the glass transition phenomenon is not well observable in the Figure 4.66, due to the high crystallinity of this sample. The high  $T_g$  value of this aliphatic polyester can be explained as due to the presence of the aliphatic ring, which creates numerous impediments to chain mobility in the amorphous phase (Berti *et al.*, 2008).

As far as the P(BCEmBDGn) copolymers are concerned, in all cases a glass transition and a melting endotherm are present (Figure 4.66a). In copolymers with mol% of BCE units higher than 70%, the glass transition phenomenon is less evident due to the high amount of crystalline phase present in these samples.

As to the melting process, the samples, similarly to parent homopolymers, showed multiple melting peaks, which can be ascribed to melt-recrystallization processes occurring during the DSC scan in polyesters (Berti *et al.*, 2008).

The peak location appears to depend on copolymer composition and the increase in the amount of comonomer added to PBCE or PBDG chain leads to a reduction of the heat of fusion, indicating a reduced level of crystallinity in the copolymers with respect to the homopolymers (Table 4.25).

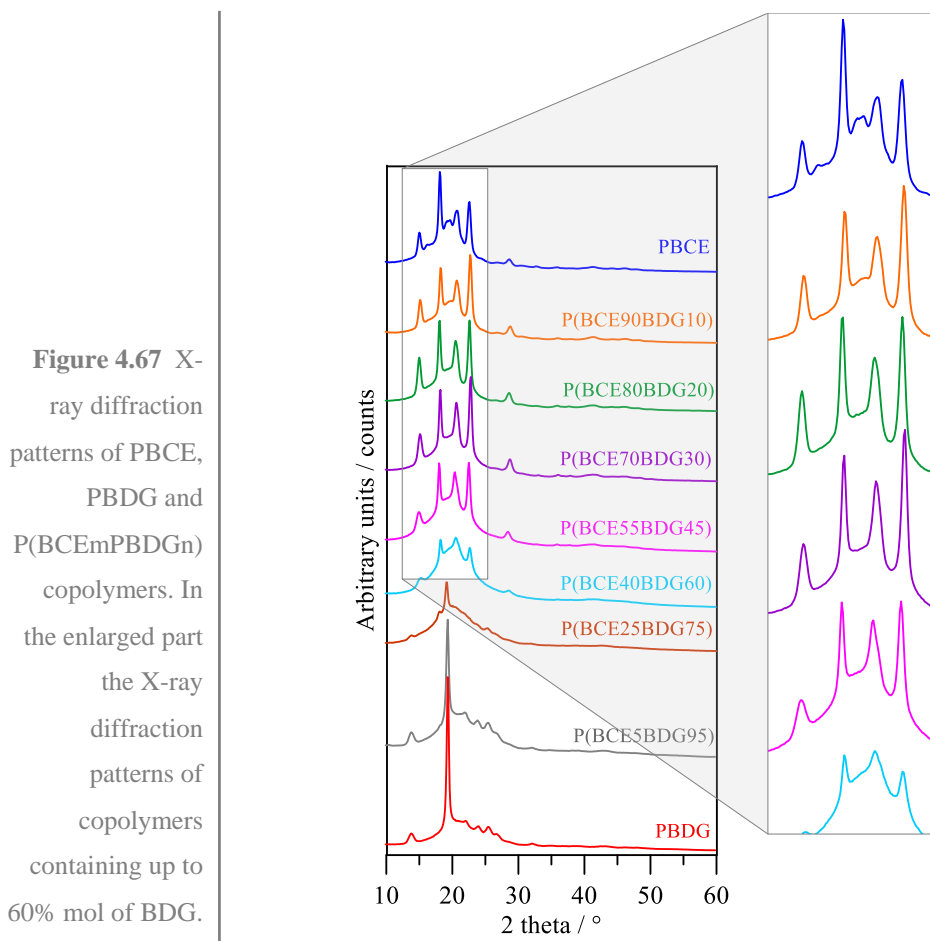
Both the minimum in the heat of fusion and the melting point-composition dependence are typical of random copolymers, where both comonomers are able to crystallize, regardless of the fact that the comonomeric units present in minor amount are completely rejected or not from the crystalline phase (Mandelkern, 1954; 1989).

To better understand the nature of the crystalline phase present in the polymers under investigation, the structural characterization of P(BCEmBDGn) copolymers was carried out by X-ray diffraction. The patterns are reported in Figure 4.67, together with those of PBCE and PBDG added for sake of comparison.

As it can be seen, the XRD profiles of copolymers appear to be characterized by relatively intense diffraction peaks over the whole composition range. Based on their shapes they can be divided into two groups, according to the BCE unit content: *i*) the samples containing from 40 up to 90 mol % of BCE units are characterized by the PBCE pattern

with the four most intense peaks positioned at the angles  $15.0^\circ$ ,  $18.1^\circ$ ,  $20.7^\circ$ ,  $22.6^\circ$  ( $2\theta$ ), even if the intensities are slightly modified; *ii*) the samples containing up to 25% BCE units show the PBDG lattice, with a very intense peak at  $19.4^\circ$ . It can't be excluded the presence of a little amount of PBDG crystalline phase in the sample P(BCE40BDG60) due to the small bump between the peaks at  $18.1^\circ$  and  $20.7^\circ$ .

The presence of two low intense and broad reflections at  $16.2^\circ$  and  $19.4^\circ$  in the PBCE pattern, but not in the copolymers, could suggest the presence of a low amount of a second polymorphic phase whose crystallization is not favoured if other co-units are present in the chain.



The overall width of the peaks and the relative area of the halo due to the amorphous material increased as the co-unit mol% increased. Consequently, the values of the crystallinity degree decreased (Table 4.25). Interestingly, copolymers having up to 20% mol of BDG, showed practically the same crystallinity degree of PBCE, indicating that the crystallizing

ability is not influenced by the presence of BDG co-unit. Lastly, the position of the reflections was not affected by composition, indicating that a complete rejection of the “foreign” units (BDG or BCE) from the crystal lattice occurred. This result is not surprising taking into account that the two comonomeric units have significantly different chemical structures and the two parent homopolymers are characterized by different crystal structures.

In order to confirm X-ray results, the applicability of the equations proposed in the literature to describe the dependence of  $T_m$  on composition (section 1.2.1) has been checked. As it can be evinced from Figure 4.68a, the  $T_m$  of copolymers under study regularly decrease with the increase of BDG mol%.

In order to study the influence of chemical structure on the glass transition of random copolymers, all the samples under investigation were subjected to rapid cooling (quenching) from the melt. The DSC curves after melt quenching are shown in Figure 4.66b: the calorimetric traces of PBCE and P(BCEmBDGn) copolymers containing up to 30 mol % of BDG units show a melting endotherm phenomenon, indicating the partially crystalline nature of these samples.

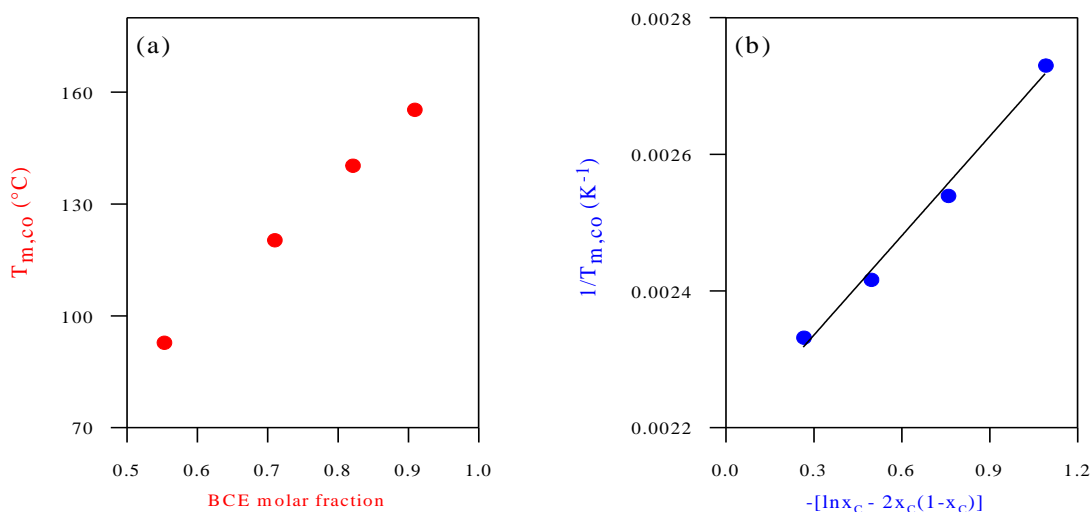


**Figure 4.68** (a)  $T_{m,co}$  – BCE molar fraction plot and (b)  $1/T_{m,co}$  – composition plot according to Baur’s equation.

P(BCE55BDG45) displays a glass transition followed by an exothermal “cold crystallization” peak and a melting endotherm at higher temperature. The enthalpy associated with the crystallization phenomenon is lower than that of the fusion endotherm,

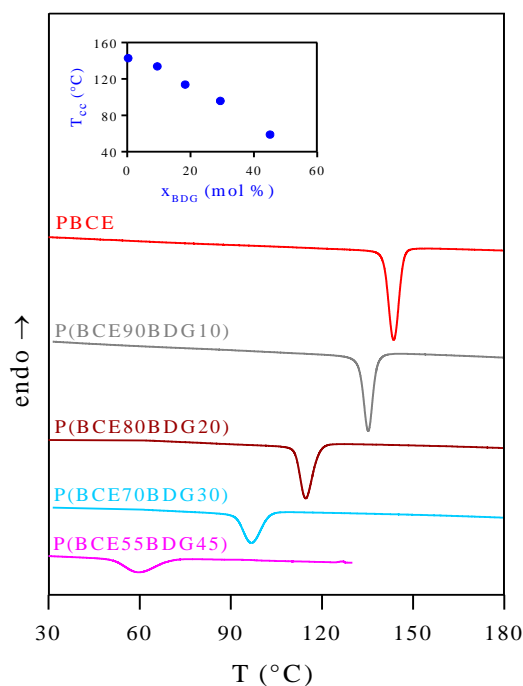
indicating that this sample cannot be frozen into a completely amorphous state by quenching. The DSC curve of such sample is therefore typical of partially crystalline polymer.

As regards the calorimetric curves of the copolymers containing from 60 to 95 mol% of BDG units, only an intense endothermic baseline deviation associated with the glass transition is observed. Therefore, the phase behaviour of P(BCEmBDGn) copolymers depends on composition: as a matter of fact, after melt quenching, semicrystalline samples are exclusively obtained at high BCE content.

As can be seen in Figure 4.66b and from the data collected in Table 4.25, the glass transition temperature is influenced by the amount of BDG units in the chain. It can be observed that  $T_g$  values decrease as BDG unit content is increased; as reported above, this result can be explained on the basis of the enhanced flexibility given by the presence of  $-\text{CH}_2\text{-O-CH}_2-$  group in PBDG with respect to the rigid aliphatic ring of PBCE.

To confirm that in the copolymers the tendency of PBCE to crystallize decreases as the content of BDG co-units is increased, non-isothermal experiments were carried out, subjecting the samples to a controlled cooling rate from the melt. The exothermic crystallization peaks of the samples under investigation are shown in Figure 4.69.

**Figure 4.69** DSC crystallization exotherms of PBCE and P(BCEmBDGn) random copolymers cooled from the melt at  $5^\circ\text{C}/\text{min}$ . In the inset:  $T_{cc}$  as a function of BCE unit content.



PBDG and the copolymers containing from 5 to 40 mol% of BCE units are not able to crystallize even though cooled from the melt at low rate ( $1^{\circ}\text{C}/\text{min}$ ). Such behaviour is a clear evidence of the significant decrease of the crystallization rate of PBCE due to the presence of BDG comonomeric units. In particular, an amount of BDG units of 60 mol% is sufficient to depress completely the crystallization process of PBCE under the adopted experimental conditions.

Moreover, it can be observed that the temperature of the maximum of the exothermal crystallization peak regularly decreases as the BDG unit content is increased, as also shown in the inset of Figure 4.69. This fact indicates a decrement of the overall crystallization rate of PBCE, due to the presence of co-units which act as obstacles in the regular packing of polymer chains.

In order to investigate the relative hydrophilicity of PBCE, PBDG and P(BCEmBDGn) films, water contact angle (WCA) measurements were performed. Table 4.25 reports the contact angle values for each polymer. Data showed that PBCE was the most hydrophobic material ( $\text{WCA} = 110^{\circ}$ ) while PBDG displayed the highest hydrophilicity ( $\text{WCA} = 76^{\circ}$ ): this result can be explained on the basis of the the presence along the polymeric chain of PBDG of highly electronegative ether-oxygen atoms.

The P(BCEmBDGn) samples wettability is remarkably affected by the copolymer composition: as expected, hydrophilicity regularly increased with the increasing of the BDG mol%. In Figure 4.70 the water drops deposited on some of the polymeric films under study are reported as an example.

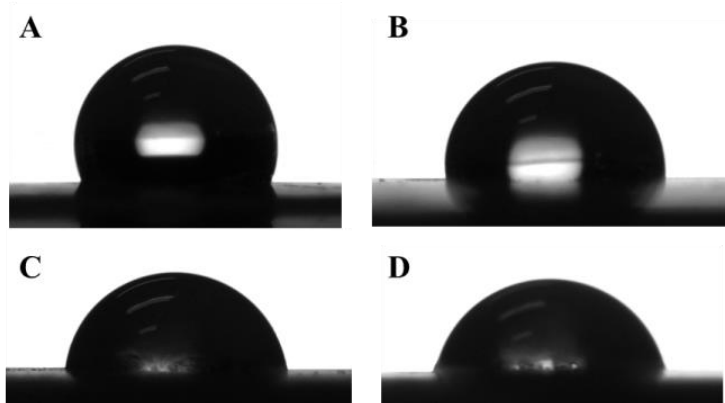


**Figure 4.70** Water drops on the polymeric film surface of: a) PBCE, b) P(BCE70BDG30), c) P(BCE25BDG75), d) PBDG.

#### 4.6.2 Mechanical characterization

Taking into account the different possible applications of the polymers under study (e.g. food packaging) in this work, the study of mechanical properties is of crucial interest. The mechanical properties of PBCE, PBDG and P(BCEmBDGn) copolymers were investigated subjecting the samples to stress-strain measurements. Table 4.26 reports their corresponding mechanical data (elastic modulus,  $E$ , stress at break,  $\sigma_b$ , and deformation at break,  $\varepsilon_b$ ).

**Table 4.26** Mechanical characterization data of P(BCEmBDGn) copolymers.

polymer	$E$ (MPa)	$\sigma_b$ (MPa)	$\varepsilon_b$ (%)
PBCE	$459 \pm 11$	$33 \pm 1$	$31 \pm 11$
P(BCE90BDG10)	$358 \pm 22$	$28 \pm 2$	$40 \pm 5$
P(BCE80BDG20)	$286 \pm 21$	$19 \pm 4$	$375 \pm 45$
P(BCE70BDG30)	$192 \pm 10$	$15 \pm 3$	$458 \pm 8$
P(BCE55BDG45)	$81 \pm 5$	$7 \pm 1$	$536 \pm 32$
P(BCE40BDG60)	$13 \pm 1$	$3 \pm 1$	$635 \pm 23$
P(BCE25BDG75)	$15 \pm 4$	$2 \pm 1$	$649 \pm 15$
P(BCE5BDG95)	$123 \pm 13$	$21 \pm 3$	$538 \pm 43$
PBDG	$137 \pm 21$	$23 \pm 2$	$445 \pm 33$

As it can be seen, the two homopolymers are characterized by a completely different behaviour. PBCE displays a higher elastic modulus and a very poor deformation at break typical of brittle materials. PBDG elastic modulus is on the contrary about 3 times lower than that of PBCE and PBDG elongation to break is almost 15 times higher than that of PBCE being, however, PBDG crystallinity degree only slightly lower than that of PBCE. Therefore, the results obtained can be ascribed to the high chain rigidity of PBCE given by the aliphatic ring; on the contrary, PBDG is much more flexible because of the presence of ether-oxygen atoms.

As concerns copolymers, elastic modulus regularly decreases as BDG unit content is increased, up to 60 mol % of BDG units, whereas it increases in the range 75-95 mol%; an opposite trend is observed for the elongation to break, which increases for copolymers containing up to 75% of BDG mol%, and then decreases (Figure 4.71).

Since all the investigated polymers display a soft amorphous phase ( $T_g$  values are in all cases well below room temperature), the observed trend can be ascribed to two effects:

changes in copolymer composition and in crystallinity degree (Table 4.25). Moreover, it is worth emphasizing that the copolymers with a BDG unit content ranging from 45 to 75 mol%, are characterized by an elastomeric behaviour, being therefore promising materials to fabricate for example wrapping films.

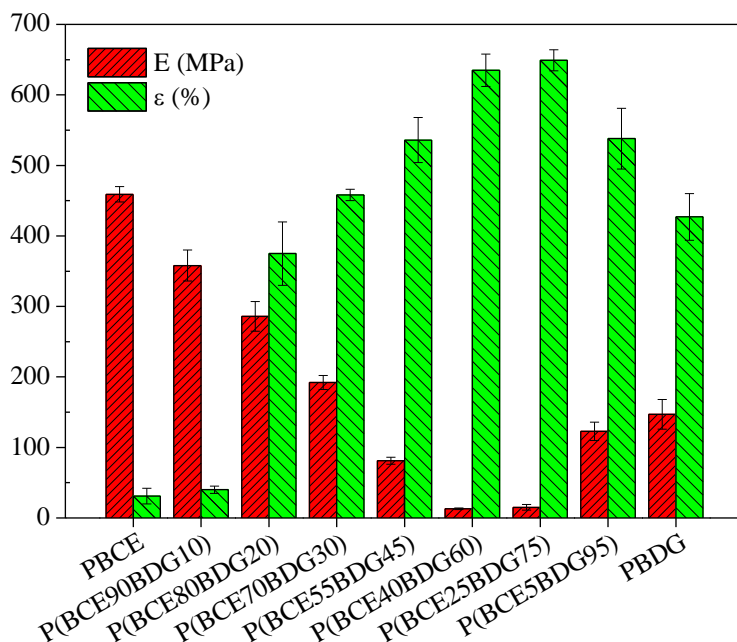


**Figure 4.71** Elastic modulus ( $E$ ) and deformation to break ( $\epsilon_b$ ) as a function of copolymer composition.

#### 4.6.3 Barrier properties

Carbon dioxide and oxygen are the main permeating agents studied in packaging applications because they may transfer from or to the environment through the polymer package wall, continuously influencing the product quality and durability. Permeability measurements were carried out on the polymeric films of a measured thickness. GTR,  $t_L$ , S and D, reported in Table 4.27 and 4.28, are well described on literature (Robertson, 1993, Mrkic *et al.*, 2006; Lee *et al.*, 2008): GTR gives an indication of the material gas permeability, the S parameter expresses the volume solubility of the gas dissolved in one volume of polymer material, the D parameter gives information on how the gas molecules diffuse through the material and the  $t_L$  parameter represents the time required by the diffusion process to reach the steady-state. Another interesting parameter is the permeability ratio (also called selectivity ratio) between  $O_2$  and  $CO_2$  gases which is already known for several polymers (Van Krevelen, 1997). It permits to determine the permeability on respect to a gas knowing the permeability behavior on respect to the other one under the same experimental conditions.

Although molecular size of permeating species could affect the transmission speed, in the case of O<sub>2</sub> and CO<sub>2</sub> there is no relationship between gas molecular size and permeability behavior. In fact, CO<sub>2</sub> is more permeable with respect to O<sub>2</sub>, despite its molecular diameter (3.4 Å) is greater than that of oxygen molecules (3.1 Å).

*GTR* values, together with *t<sub>L</sub>*, *S* and *D* of the tested gases are reported in Table 4.27 and Table 4.28 for O<sub>2</sub> and CO<sub>2</sub> pure gas respectively.

As it can be seen, highly crystalline samples showed low permeability to both gases, demonstrating a very high dependence of the permeability behavior on the crystalline/amorphous ratio. In addition, a relation between the selectivity ratio and the *T<sub>g</sub>* can be observed: in copolymers the *T<sub>g</sub>* decreased while the CO<sub>2</sub>/O<sub>2</sub> ratio (reported on Table 4.28) increased with the increasing of the BDG unit content. This result can be explained on the basis of the enhanced mobility of the polymeric chain, with consequently easier crossing of the CO<sub>2</sub> molecules through the polymeric film. CO<sub>2</sub> molecules move faster than O<sub>2</sub> ones: this is demonstrated by the fact that in all cases the O<sub>2</sub> *GTR* was found lower than the CO<sub>2</sub> *GTR* value.

**Table 4.27** *t<sub>L</sub>*, *GTR*, *D* and *S* for O<sub>2</sub> gas.

polymer	<i>t<sub>L</sub></i> (s)	<i>GTR</i> (cm <sup>3</sup> m <sup>2</sup> d <sup>-1</sup> bar <sup>-1</sup> )	<i>S</i> (cm <sup>3</sup> cm <sup>-2</sup> bar <sup>-1</sup> )	<i>D</i> (cm <sup>2</sup> sec <sup>-1</sup> )
PBCE	1128.67 ± 1.70	56.20 ± 0.22	2.84·10 <sup>-2</sup> ± 4.19·10 <sup>-4</sup>	3.42·10 <sup>-8</sup> ± 2.49·10 <sup>-10</sup>
P(BCE90BDG10)	923.33 ± 1.25	65.30 ± 0.08	2.73·10 <sup>-2</sup> ± 3.30·10 <sup>-4</sup>	4.12·10 <sup>-8</sup> ± 4.71·10 <sup>-11</sup>
P(BCE80BDG20)	764.67 ± 0.47	58.43 ± 0.12	1.66·10 <sup>-2</sup> ± 3.40·10 <sup>-4</sup>	7.70·10 <sup>-8</sup> ± 8.60·10 <sup>-10</sup>
P(BCE70BDG30)	573.33 ± 0.47	81.80 ± 0.08	1.82·10 <sup>-2</sup> ± 1.63·10 <sup>-4</sup>	9.31·10 <sup>-8</sup> ± 1.63·10 <sup>-10</sup>
P(BCE55BDG45)	1146.00 ± 2.45	94.73 ± 0.17	3.52·10 <sup>-2</sup> ± 2.05·10 <sup>-4</sup>	6.67·10 <sup>-8</sup> ± 1.25·10 <sup>-10</sup>
P(BCE40BDG60)	61.33 ± 1.25	184.57 ± 0.42	3.27·10 <sup>-3</sup> ± 3.86·10 <sup>-5</sup>	1.57·10 <sup>-6</sup> ± 1.63·10 <sup>-8</sup>
P(BCE25BDG75)	143.33 ± 1.25	131.17 ± 0.46	7.43·10 <sup>-3</sup> ± 1.25·10 <sup>-5</sup>	3.59·10 <sup>-7</sup> ± 2.94·10 <sup>-9</sup>
P(BCE5BDG95)	n.a.	30.8 ± 0.16	n.a.	n.a.
PBDG	228.33 ± 1.25	22.37 ± 0.40	1.54·10 <sup>-3</sup> ± 3.56·10 <sup>-5</sup>	3.81·10 <sup>-7</sup> ± 4.97·10 <sup>-9</sup>
PLA*	/	487.67 ± 2.52	/	/

\*from Siracusa *et al.*, 2012

As it can be seen from the thermal characterization data, P(BCE40BDG60) displayed the lowest crystallinity degree and, consequently, showed the highest O<sub>2</sub> and CO<sub>2</sub> *GTR* values.

The  $t_L$  value was found higher in the case of CO<sub>2</sub> for all polymers, with the exception of P(BCE55BDG45). This means that the carbon dioxide molecules spent more time to distribute on the polymer film surface than O<sub>2</sub> ones due to their faster and very chaotic motion. As a matter of fact, the oxygen molecules are characterized by a slowly and organized motion.

The Diffusion coefficient, correlated to kinetic parameters, showed a similar value for all polymers under investigation, indicating that the gas diffusion process into the polymeric matrix is the same regardless of the gas used. As it can be seen from the data reported in Table 4 and Table 5, for copolymers containing from 70 to 100 mol% of BCE units the O<sub>2</sub> D values were slightly higher than the CO<sub>2</sub> D ones, as expected on the basis of the lower permeability of this gas. In the case of P(BCE55BDG45), CO<sub>2</sub> D value was about 40 times greater than O<sub>2</sub> D value because the faster motion of CO<sub>2</sub> with respect to O<sub>2</sub> on the polymer surface, permitted the earlier starting of the permeation process.

P(BCE40BDG60) showed the lowest barrier value and the highest diffusion coefficient. This result can be well explained by the correlation between GTR and crystalline/amorphous ratio reported above.

As regards the solubility parameter, an opposite trend was displayed: CO<sub>2</sub> solubility was higher than that of O<sub>2</sub>. These results confirmed that, despite the molecule size, CO<sub>2</sub> was more soluble into the polymeric matrix, as well explained by the GTR data. For both the analysed gases, the solubility was not influenced by the chemical composition of the polymers, remaining practically constant.

Lastly, as far as the selectivity ratio between the two gases is concerned, it increased with the increasing of BDG mol% (see Table 4.28). The presence of the aliphatic ring of PBCE acted as an obstacle to the gas crossing.

Permeability results here presented are of particular relevance if we compare the permeability of the P(BCEmBDGn) copolymers with that of PLA films obtained under the same conditions (Siracusa *et al.*, 2012). As reported in Table 4.27 and Table 4.28, the copolyesters under investigation showed lower permeability, and therefore improved barrier properties, to both CO<sub>2</sub> and O<sub>2</sub> gases with respect to polylactide. It is worth remembering that this latter is the most extensively used polyester in the production of biodegradable packaging films.

**Table 4.28**  $t_L$ , GTR, D, S for CO<sub>2</sub> gas and selectivity ratio CO<sub>2</sub>/O<sub>2</sub>.

polymer	$t_L$ (s)	GTR (cm <sup>3</sup> m <sup>-2</sup> d <sup>-1</sup> bar <sup>-1</sup> )	S (cm <sup>3</sup> cm <sup>-2</sup> bar <sup>-1</sup> )	D (cm <sup>2</sup> sec <sup>-1</sup> )	CO <sub>2</sub> /O <sub>2</sub>
PBCE	2939.00 ± 1.25	318.33 ± 2.05	4.30 <sup>-1</sup> ± 2.49·10 <sup>-3</sup>	1.31·10 <sup>-8</sup> ± 1.41·10 <sup>-10</sup>	5.66
P(BCE90BDG10)	2691.30 ± 1.25	450.00 ± 0.82	5.57·10 <sup>-1</sup> ± 8.16·10 <sup>-4</sup>	1.41·10 <sup>-8</sup> ± 1.18·10 <sup>-11</sup>	6.89
P(BCE80BDG20)	1634.33 ± 0.94	404.67 ± 1.25	2.44·10 <sup>-1</sup> ± 8.16·10 <sup>-4</sup>	3.64·10 <sup>-8</sup> ± 4.71·10 <sup>-10</sup>	6.93
P(BCE70BDG30)	2538.33 ± 0.82	709.43 ± 4.92	6.92·10 <sup>-1</sup> ± 5.25·10 <sup>-3</sup>	2.15·10 <sup>-8</sup> ± 4.01·10 <sup>-10</sup>	8.67
P(BCE55BDG45)	318.66 ± 0.82	806.00 ± 0.82	8.33·10 <sup>-2</sup> ± 5.00·10 <sup>-5</sup>	2.40·10 <sup>-7</sup> ± 3.54·10 <sup>-9</sup>	8.51
P(BCE40BDG60)	492.00 ± 1.63	1880.33 ± 0.47	2.71·10 <sup>-1</sup> ± 8.16·10 <sup>-4</sup>	1.93·10 <sup>-7</sup> ± 3.54·10 <sup>-10</sup>	10.19
P(BCE25BDG75)	3246.00 ± 1.63	1370.33 ± 0.47	1.74 ± 3.86·10 <sup>-2</sup>	1.59·10 <sup>-8</sup> ± 7.07·10 <sup>-11</sup>	10.46
P(BCE5BDG95)	8111.00 ± 1.71	309.00 ± 0.82	7.06·10 <sup>-1</sup> ± 1.70·10 <sup>-3</sup>	1.34·10 <sup>-8</sup> ± 1.25·10 <sup>-10</sup>	10.03
PBDG	7089.00 ± 1.70	270.00 ± 0.82	5.78·10 <sup>-1</sup> ± 1.25·10 <sup>-3</sup>	1.24·10 <sup>-8</sup> ± 2.59·10 <sup>-10</sup>	12.07
PLA*	/	1201.00 ± 1.73	/	/	2.46

\*from Siracusa *et al.*, 2012

#### 4.6.4 Enzymatic and hydrolytic degradation studies

In order to evaluate the potentialities of these new polyesters in the biomedical field, in particular for constructing drug delivery systems, more specific studies have been conducted on three different copolymers: P(BCE70BDG30), P(BCE55BDG45) and P(BCE40BDG60). PBCE has also been considered for sake of comparison.

The biodegradability under physiological conditions (37°C, pH 7.4) has been tested both in the presence of 50U/ml of hog pancreas lipase and in buffer solution without enzyme addition. As previously reported (section 4.1.3), the enzyme solution was weekly replaced in order to avoid incubation in the presence of significantly reduced enzyme activity.

In Figure 4.72 and 4.73, weight losses of the copolymers under study in the presence of hog pancreas lipase and in absence of enzyme, respectively are reported.

In the time scale explored, PBCE did not lose any weight (data not shown), whereas all copolymers appreciably degraded in both experimental conditions. As it can be seen from Figure 4.72 and Figure 4.73, the degradation rate appeared strongly dependent on the copolymer composition; as a matter of fact the higher the BDG mol%, the higher the degradation rate.

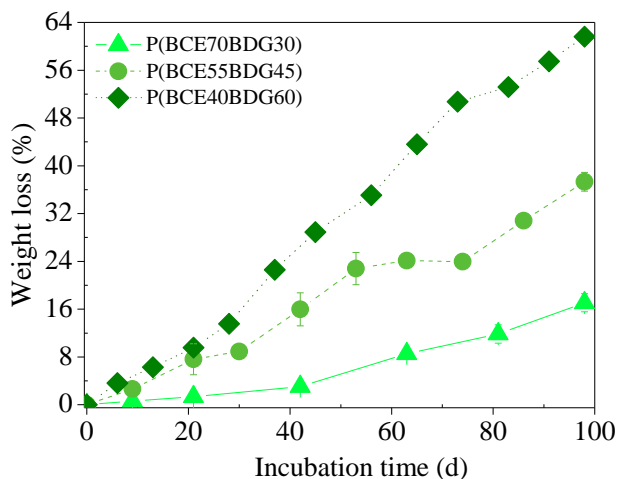


**Figure 4.72** Weight loss (%) as a function of incubation time for P(BCE70BDG30), P(BCE55BDG45) and P(BCE40BDG60) in the presence of 50U/ml of hog pancreas lipase.

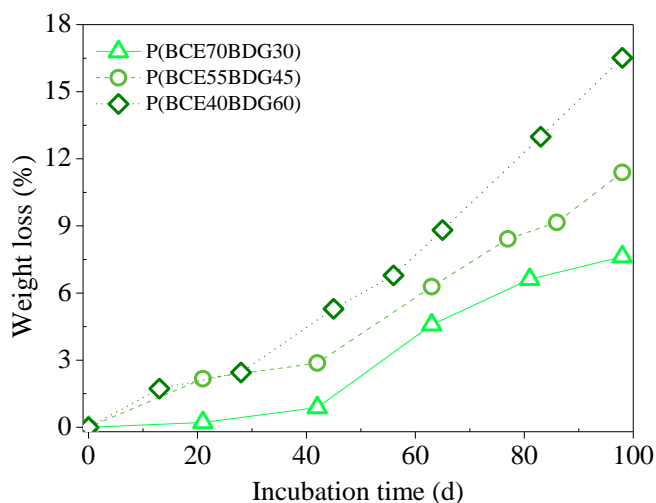


**Figure 4.73** Hydrolytic degradation weight losses (%) as a function of incubation time for P(BCE70BDG30), P(BCE55BDG45) and P(BCE40BDG60).

After 98 days, P(BCE40BDG60) lost over 60% of its initial weight if incubated in the presence of the pancreatic lipase and 17% in the presence of water without enzyme. The slowest degradation rate was on the contrary displayed by P(BCE70BDG30), which residual weights at the end of the experiments were 92% and 84% for the enzymatic and hydrolytic degradation, respectively.

The results obtained can be explained on the basis of different factors affecting the biodegradation rate of a polymer; among all, crystallinity degree, crystal perfection and hydrophilicity (section 1.1.4.3).

PBCE did not undergo any degradation due to its high crystallinity degree and crystal perfection and its marked hydrophobicity (Table 4.25).

On the other hand, the presence of BDG co-units along the PBCE polymeric chain, resulted in an enhanced hydrophilicity and reduced crystallinity degree and crystal perfection. Hydrophilicity regularly increased whereas crystallinity degree and crystal perfection regularly decreased with the increase of BDG mol% (Table 4.25). Therefore, the increased biodegradation rate of the copolymers with respect to the homopolymer and the different degradation profiles among the copolymers are readily clear.

As regards P(BCE70BDG30), its higher degradability with respect to PBCE can be ascribed only to the lower perfection of its crystal phase and to its higher hydrophilicity, being its crystallinity degree comparable to that of PBCE.

Lastly, a confirmation of the catalytic effect of lipases in the degradation of polyesters has been given by the significantly higher degradation rate shown by the samples incubated in the presence of the hog pancreas lipase with respect to the mere hydrolysis.

A confirmation that the amorphous regions of a polymer are degraded more quickly than the crystalline ones, was obtained by subjecting the partially degraded copolymer samples to a heating calorimetric scan (20°C/min). All the calorimetric traces were found to be characterized by an endothermic peak associated with the fusion process of crystalline portion of the material (data not shown). The corresponding heat of fusion was normalized respect to the heat of fusion of non-degraded sample ( $\Delta H_f/\Delta H_0$ ). The results obtained are reported in Figure 4.74.

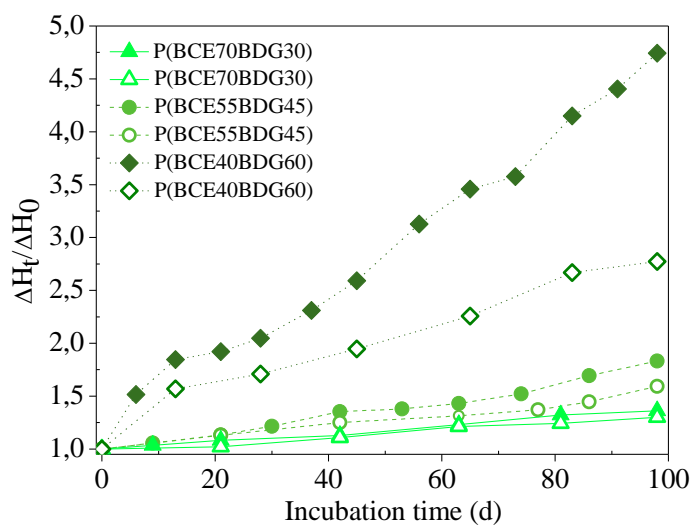


**Figure 4.74** Normalized heat of fusion as a function of incubation time for P(BCE70BDG30), P(BCE55BDG45) and P(BCE40BDG60). Solid symbols: enzymatic degradation, open symbols: hydrolytic degradation.

In all the copolymers the normalized heat of fusion regularly increased with incubation time for both enzymatic and hydrolytic degradation. Moreover, it can be observed that the higher the degradation rate, the higher the increase in the crystalline/amorphous ratio. As a matter of fact, P(BCE40BDG60) displayed the highest increase in the normalized heat of fusion, while P(BCE30BDG70) the lowest.

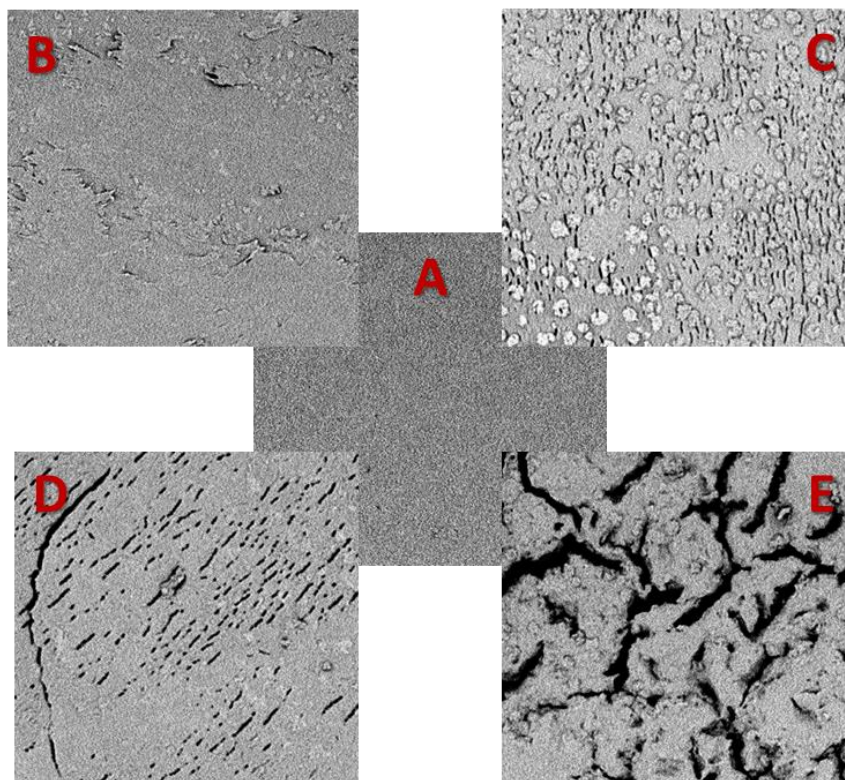
However, the increment of the crystalline/amorphous ratio can be also due to the annealing process previously described (section 4.4.7). Taking this into consideration, all the copolymers under study have been incubated at 37°C under nitrogen atmosphere (to prevent any possible degradation process) and subjected to DSC measurements after 98 days. Interestingly, an increment in the normalized heat of fusion equal to 40%, 60% and 80% for P(BCE70BDG30), P(BCE55BDG45) and P(BCE40BDG60) was respectively found.

In conclusion, the trend observed in Figure 4.74 is due to the sum of two different contributions: 1) preferential attack by water of the amorphous region of a polymer with respect to crystalline one during biodegradation and 2) annealing.

The morphology of the polymeric film surface after enzymatic degradation was analysed using SEM; micrographs of the copolymers at the end of the incubation period are presented in Figure 4.75. In addition, the micrograph of P(BCE55BDG45) prior to incubation has been added for sake of comparison.

The micrographs of all samples under investigation prior to enzyme exposure revealed a homogeneous and smooth surface. On the contrary, after enzyme exposure surface irregularities appeared, whose intensity depended on the degree of degradation. P(BCE55BDG45) surface displayed holes and cracks (Figure 4.75d), while in the case of P(BCE40BDG60) many channels were clearly evident (Figure 4.75e). In conclusion, SEM analyses confirmed the trend shown by weight loss measurements.

**Figure 13** SEM micrographs of partially degraded copolymers, 1000X. A: P(BCE55BDG45) prior to incubation; B: PBCE, C: P(BCE70BDG30), D: P(BCE55BDG45) and E: P(BCE40BDG60) after 98 days of incubation in the presence of hog pancreas lipase.



#### 4.6.5 *In vitro* fluorescein isothiocyanate (FITC) release

In the present study FITC was used as a model molecule (molecular weight = 389.38 g/mol, water solubility < 0.1 mg/ml) to evaluate how the different copolyesters can assist the sustained release of small drugs according to polymer matrix properties. Figure 4.76 shows the percentage of FITC cumulative release as a function of time for PBCE, P(BCE70BDG30), P(BCE55BDG45) and P(BCE40BDG60).

All materials exhibited a typical diffusion-driven release profile, with a fast FITC release within the first 7 hours followed by a slower release. However, the ability to retain FITC and release it in a sustainable manner over time was significantly different for the investigated materials. During the burst stage, PBCE matrix lost only 2% of FITC, whereas all the copolymers lost a much higher amount of FITC: 21%, 32% and 44% in the case of P(BCE70BDG30), P(BCE55BDG45) and P(BCE40BDG60), respectively.

After more than 9 days in phosphate buffer, PBCE film lost only 11% of the total FITC whereas the amount of FITC released by P(BCE70BDG30) reached 66%, very close to that released from P(BCE55BDG45) and P(BCE40BDG60), 67 and 71%, respectively.

In the present case, where the FITC release is primarily driven by its diffusion out of the polymer matrix, material hydrophilicity and chain mobility, both ruling water uptake and FITC extraction, are of primary importance in defining release kinetics.

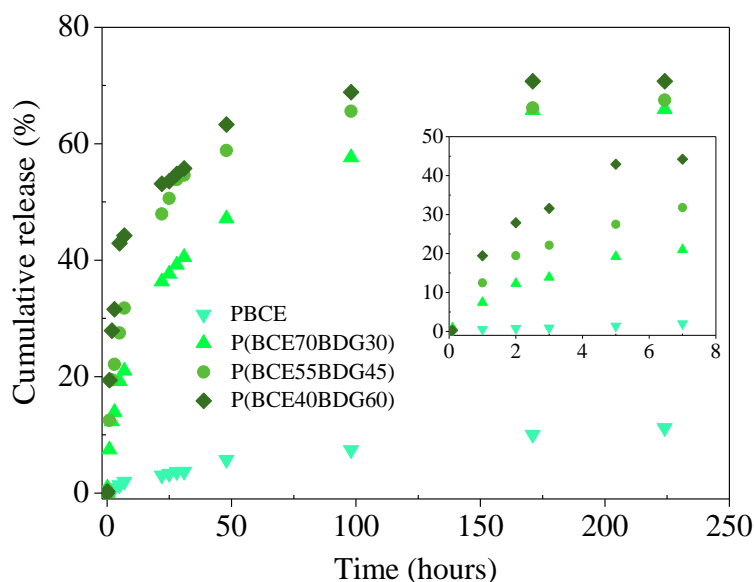


**Figure 4.76**  
Percentage of FITC cumulative release as a function of time from PBCE, P(BCE70BDG30), P(BCE55BDG45) and P(BCE40BDG60) at 37°C in phosphate buffer.

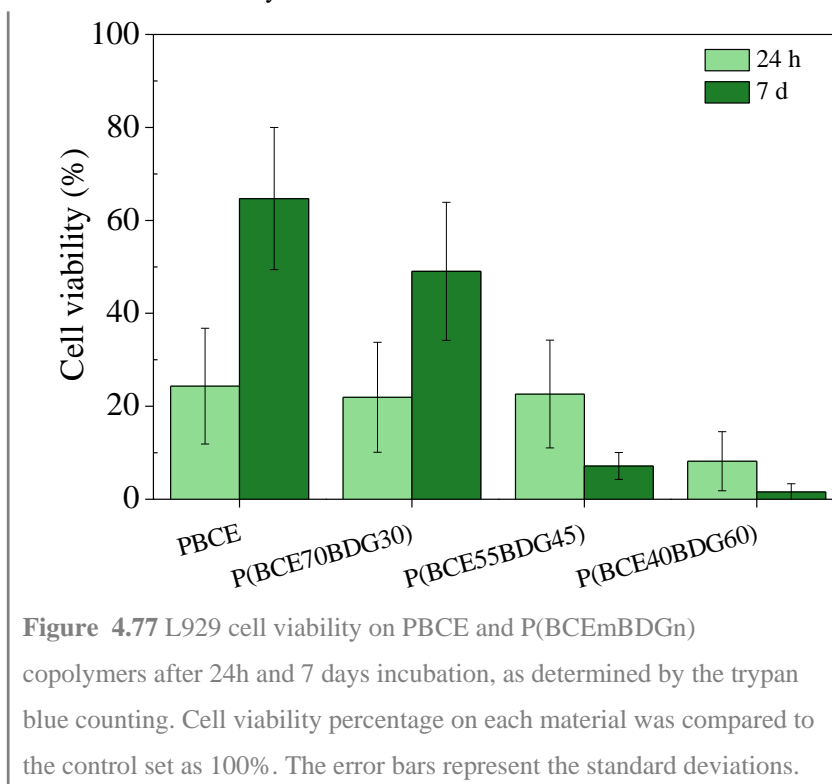
Accordingly, PBCE, the most hydrophobic material among those investigated, showed the slowest FITC release. The addition of BDG co-units, regardless of the mol%, in the PBCE macromolecular chain increased material hydrophilicity with a consequent faster FITC release with respect to homopolymer. The sustained release profile of the copolymers depended on the copolymer composition; the higher the mol% of BDG units, the faster the release of FITC. The trend observed can be explained on the basis of the different crystallinity degree and crystal perfection. As previously found (Jeong *et al.*, 2003; Karavelidis *et al.*, 2011; Gualandi *et al.*, 2012) crystal lamellae probably act as a barrier, delaying FITC diffusion during the initial burst stage. As mentioned above (section 4.6.1 and Table 4.25), the crystallinity degree and the crystal perfection regularly decreased as the BDG content was increased, thus the fastest release for P(BCE40BDG60). At longer time, however, the amount of FITC released by the copolymers was very close. A switching from a diffusion-controlled mechanism to an erosion-controlled one could be hypothesized.

In conclusion, among the investigated materials, PBCE displays the most promising features to allow a sustained drug release over several weeks, while copolymers result more suitable when a faster release of the drug is required.

#### 4.6.6 Biocompatibility assay

Biocompatibility studies have been conducted according to the procedure previously described (section 3.19.1). Figures 4.77 and 4.78 show the viability data obtained by incubating L929 cells (Figure 4.77) or INS-1 (Figure 4.78) with each polymer under study after appropriate sterilization.

Data are represented as survival percentage of L929 or INS-1 cells grown onto tissue culture plate. In addition, experiments were performed at two incubation times for both cell lines: 24 hours and 7 days.



With regards to the viability data for the L929 (Figure 4.77), after 24 hours of incubation, a cell adhesion between 20-25% was observed if compared to cells seeded on tissue culture plate. An exception was represented by P(BCE40BDG60) that showed very low cell adhesion. The vitality data obtained at 7 days and compared to cells deposited on tissue culture plate exhibited a trend slightly different: the homopolymer PBCE and the sample P(BCE70BDG30) showed the highest value of viability, 65 and 50%, respectively, while both samples P(BCE55BDG45) and P(BCE40BDG60) displayed a very low value, below 10%.

In summary, it seems that after 24 hours the effect due to the increase of BDG mol% in the material causes a reduction in cell adhesion. After 7 days, the trend is quite similar: the cell proliferation is elevated, but appears to decrease with increasing the BDG unit content if compared to the homopolymer.

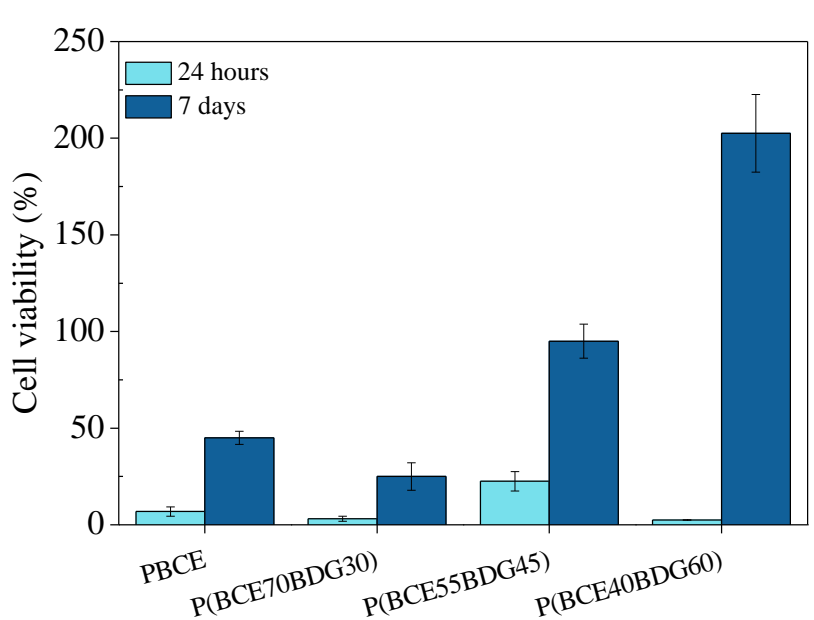


**Figure 4.78** INS-1 cell viability on PBCE and P(BCEmBDGn) copolymers after 24h and 7 days incubation, as determined by the trypan blue counting. Cell viability percentage on each material was compared to the control set as 100%. The error bars represent the standard deviations.

As far as the vitality data for INS-1 are concerned (Figure 8b), after 24 hours of incubation cell adhesion was low for all the samples under investigation. The proliferative data at 7 days, if compared to cells seeded on tissue culture plate, exhibited a different trend: the homopolymer and the sample P(BCE70BDG30) showed the lowest values of vitality (ranging from 25 to 45%), while both P(BCE55BDG45) and P(BCE40BDG60) displayed the highest values, about 100 and 200%, respectively. In this case, it would seem that at 24 hours the increase in the mol% of BDG does not influence cell adhesion, which is lower for all materials with respect to L929 cell line. On the contrary, after 7 days the cell proliferation increased with the increasing content of BDG, differently from L929 cell line.

In conclusion, the two cell lines showed a different behavior on the tested materials; this could be also dictated by the different cell morphology, respectively fibroblast-like for L929 and round-shape for INS-1.

Unfortunately, due to technical problems, the observation on CLSM of adhesion of INS-1 to the materials at the given incubation times was not possible. Figure 4.79 shows, therefore, only the confocal images for the adhesion and proliferation of L929.

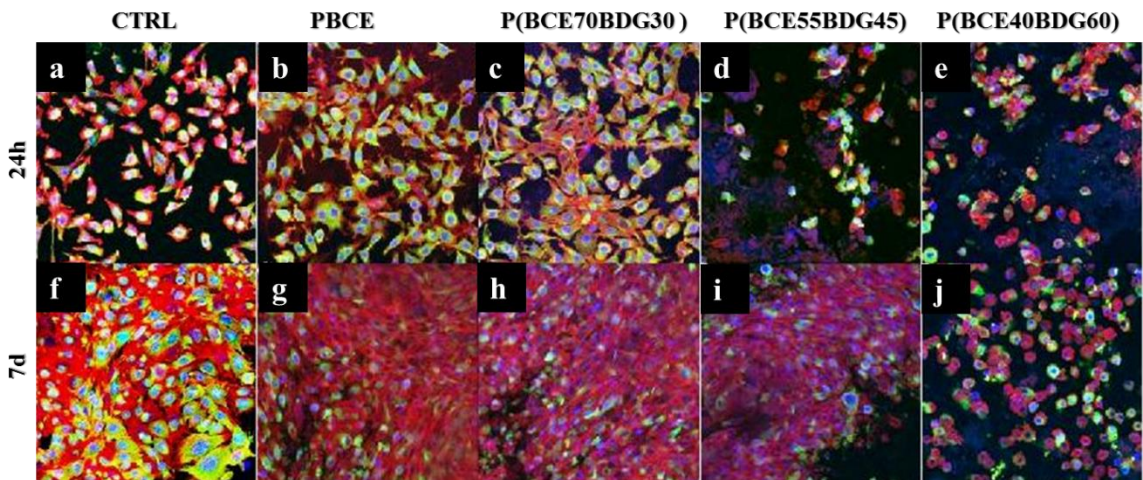


**Figure 4.79** CLSM images of L929 cell adhesion (24 h) and longer incubation time (7 days) onto all tested materials. After incubation cells were fixed and stained as indicated in section 3.19.1.3. Nuclei are stained with DAPI (in blue); F-actin is stained with phalloidin–tetram-ethylrhodamine isothiocyanate (TRITC, in red), and alfa-tubulin is stained with FITC-conjugated mouse anti-tubulin.

The images of the L929 cells adhering to glass coverlips (controls) were also reported. As observed by CLSM, L929 adhered and grew on the surface of all materials with some differences. As to PBCE, P(BCE70BDG30) and P(BCE55BDG45), fibroblasts cultivated on the surface of the materials exhibited a flat, elongated cell morphology and a relatively smooth surface at 24h of incubation. A typical surface features of fibroblasts, such as long processes at the cell periphery and slender filopodia connecting the cells to the substrate were observed. Furthermore, a confluent cell monolayer of fibroblast cells was observed after 7 days onto the different materials, despite the vitality data. The situation was completely different for sample P(BCE40BDG60) either at 24h or 7 days of incubation: the confocal images of this material confirmed the quantitative data.

## 4.7 Random PBCE-based copolyesters containing PEG-like subunit

In the present study, the effect on solid-state properties of PBCE due to the random insertion along its macromolecular chain of triethylenecyclohexanedicarboxylate (TECE) co-units has been explored. Five (P(BCE $m$ TECE $n$ )) copolymers (with different composition) have been prepared by melt polycondensation. The thermal and structural properties, wettability and mechanical properties of the synthesized polymers were investigated and correlated to polymer chain microstructure.

To analyse the feasibility of employing these copolyesters for environmental applications, their biodegradability has been studied under composting conditions and in soil burial experiments. Moreover, ecotoxicity assessment of the reagents used for the syntheses was evaluated by the plant growth test. Lastly, barrier properties to different gases (oxygen and carbon dioxide) were investigated.

On the other hand, as regards the biomedical field, electrospun scaffold have been prepared in order to evaluate their possible utilization in tissue engineering. In addition, hydrolytic degradation studies have been conducted under physiological conditions and cell culture experiments have been performed.

### 4.7.1 Synthesis, molecular and thermal characterization

At room temperature all the synthesized polyesters appeared as semicrystalline light yellow solids. The polymers are listed in Table 4.28, which also collects the data of molecular characterization.

The polymers were characterized by relatively high and comparable molecular weights (Table 4.28), indicating that appropriate synthesis conditions and a good polymerization control were achieved. In order to have an understanding into their chemical structure, the  $^1\text{H-NMR}$  investigation was performed. The analysis confirmed the awaited structures (see as an example the  $^1\text{H-NMR}$  spectrum of P(BCE70TECE30) shown in Figure 4.80).

The copolymer composition, calculated from the relative areas of the  $^1\text{H-NMR}$  resonance peak of the **4** aliphatic protons butandiol subunit located at 4.10 ppm and of the **5** protons of the triethylene diol subunit at 4.23 ppm, was found to be close to the feed one (Table 4.28).

As previously reported (section 4.6.1),  $^1\text{H-NMR}$  analysis was used to calculate also the *trans* percentage in the polymers under study because of the possible isomerization of cyclohexanedicarboxylic acid from the *trans* form to the *cis* one occurring during high

temperature polycondensations. Also in the present case, the isomerization was very limited, being the *cis* content in all cases less than 3%.

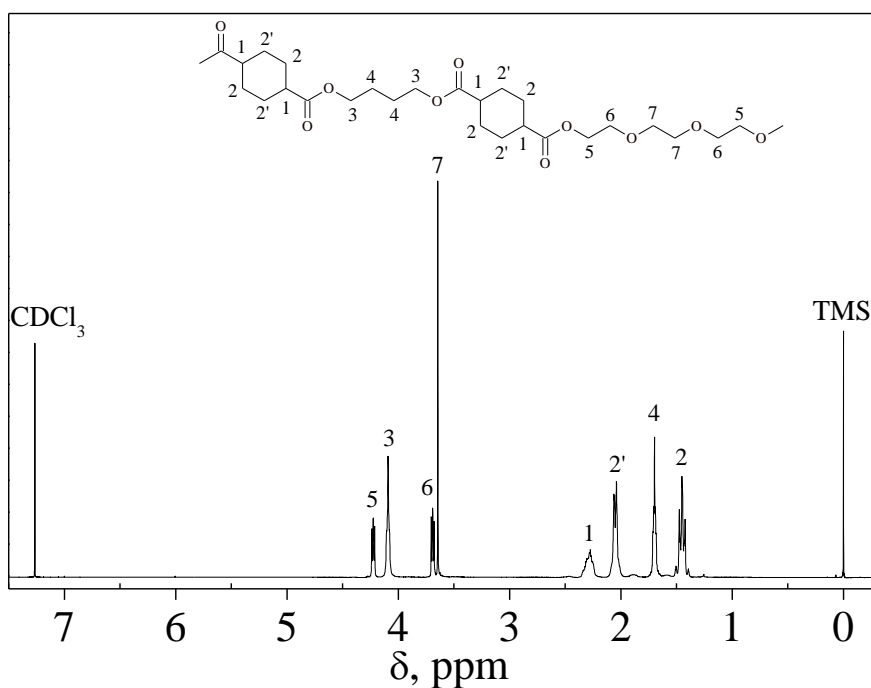
**Table 4.28** Molecular characterization data of PBCE and P(BCEmTECEn) copolymers.

polymer	$M_n^a$	PDI <sup>b</sup>	PTECE (mol %) <sup>1</sup> H-NMR
PBCE	38500	2.0	0
P(BCE90TECE10)	38250	2.1	10.2
P(BCE80TECE20)	41000	2.0	20.8
P(BCE70TECE30)	39300	2.0	33.3
P(BCE60TECE40)	36000	2.0	40.7
P(BCE50TECE50)	38900	2.2	49.2

<sup>a</sup>) number average molecular weight calculated by GPC analysis

<sup>b</sup>) polydispersity index calculated by GPC analysis

**Figure 4.80** <sup>1</sup>H-NMR spectra of P(BCE70TECE30) with resonance assignments.



Because of the high temperature involved in the polycondensation process and of the catalyst employed ( $\text{Ti}(\text{OBU})_4$ ), which both favour the transesterification reactions, the arrangement of the comonomeric units along the chain follows a random distribution.

Subsequently, the polymers were subjected to thermogravimetric analysis and the temperature corresponding to 5% weight loss ( $T_{5\% \text{ w.loss}}$ ) has been determined and collected in Table 4.29.

As evidenced in Figure 4.81 reported in the following, where the thermogravimetric curves of the synthesized copolyesters are reported, the weight loss took place in all cases in one-step.

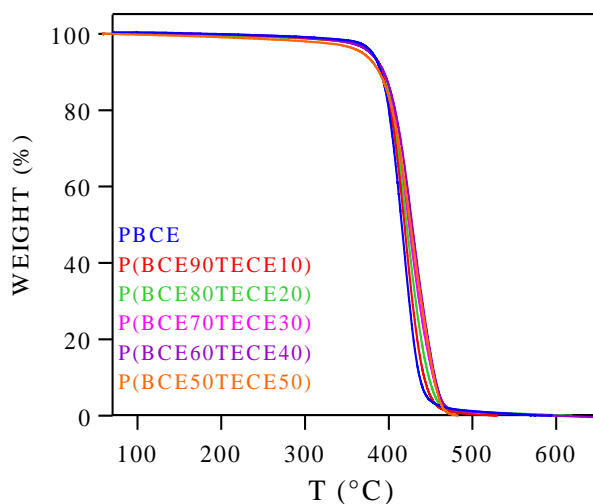


**Figure 4.81**  
Thermogravimetric curves of PBCE and P(BCEmTECEn) copolymers under nitrogen atmosphere (heating rate: 10 °C/min).

**Table 4.29** Thermal and diffractometric characterization data and water contact angles for PBCE and P(BCEmTECEn) copolymers.

polymer	$T_{5\% \text{ w.loss}}$ (°C)	1 <sup>st</sup> scan				2 <sup>nd</sup> scan						WCA (°)
		$T_m$ (°C)	$\Delta H_m$ (J/g)	$T_g$ (°C)	$\Delta C_p$ (J/°C g)	$T_c$ (°C)	$\Delta H_c$ (J/g)	$T_m$ (°C)	$\Delta H_m$ (J/g)	$T_{cc}$ (°C)	$X_c$ (%)	
PBCE	380	166	33	12	0.065	/	/	167	31	144	42 ± 4	110 ± 2
P(BCE90TECE10)	380	153	25	0	0.110	/	/	153	25	129	41 ± 3	107 ± 4
P(BCE80TECE20)	380	131	22	-7	0.187	/	/	131	22	113	40 ± 3	98 ± 3
P(BCE70TECE30)	379	112	19	-12	0.197	/	/	112	19	86	33 ± 3	89 ± 3
P(BCE60TECE40)	378	104	17	-16	0.242	/	/	103	17	82	34 ± 3	88 ± 4
P(BCE50TECE50)	368	78	15	-17	0.384	40	11	78	14	47	27 ± 3	80 ± 1

All the copolyesters, showed a high thermal stability, comparable with that of PBCE with the exception of P(BCE50TECE) that displayed a slightly lower  $T_{5\% \text{ w.loss}}$  (Table 4.29). The result demonstrated that the introduction of TECE co-units along the PBCE macromolecular chain did not have any detrimental effect up to 40 mol%; over this value,

the presence of ether-oxygen atoms reduces the thermal stability of the parent homopolymer, as previously reported (section 4.6.1).

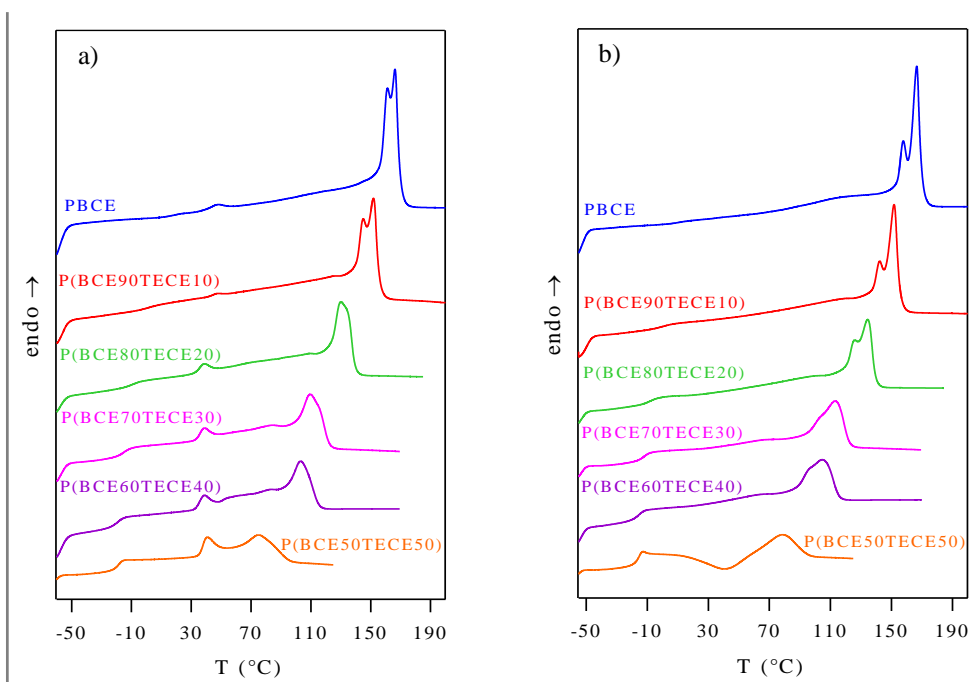
In order to provide the same heat treatments to all the samples investigated, prior to thermal analysis each film, obtained by compression moulding, was kept at room temperature for two weeks. DSC traces of so-treated samples are reported in Figure 4.82a and the data obtained in Table 4.29.

All P(BCEmBDGn) copolymers presented a glass transition and a melting endotherm. In copolymers with mol% of BCE co-units higher than 70%, the glass transition phenomenon is less evident due to the high amount of crystalline phase present in these samples.

As to the melting process, the samples, similarly to parent homopolymer, showed multiple melting peaks, which can be ascribed to melt-recrystallization processes occurring during the DSC scan in polyesters (Berti *et al.*, 2008).

The peak location appears to depend on copolymer composition and the increase in the amount of comonomer added to PBCE leads to a reduction of the heat of fusion, indicating a reduced level of crystallinity in the copolymers with respect to the parent homopolymer (Table 4.29).

**Figure 4.82**  
Calorimetric curves  
of PBCE and  
P(BCEmTECEn)  
copolymers: (a) 1<sup>st</sup>  
scan, (b) 2<sup>nd</sup> scan  
after melt  
quenching.



Both the minimum in the heat of fusion and the melting point-composition dependence are typical of random copolymers (Mandelkern, 1954; 1989).

To better understand the nature of the crystalline phase present in the polymers under investigation, the structural characterization of P(BCEmBTECEn) copolymers was carried out by X-ray diffraction (XRD). The patterns are reported in Figure 4.83, together with that of PBCE added for sake of comparison.

As it can be seen, the XRD profiles of copolymers appear to be characterized by relatively intense diffraction peaks over the whole composition range. The samples are characterized by the PBCE pattern with the four most intense peaks positioned at the angles  $15.0^\circ$ ,  $18.1^\circ$ ,  $20.7^\circ$ ,  $22.6^\circ$  ( $2\theta$ ); only a modest decrease of the relative intensity of the peak at  $22.6^\circ$  ( $2\theta$ ) is observed with the increasing of the TECE co-unit content.

Interestingly, copolymers having up to 20% mol of TECE, showed practically the same crystallinity degree of PBCE, indicating that the crystallizing ability is not influenced by the presence of TECE co-unit (Table 4.29). On the other hand, the presence of an higher amount of TECE units increased the overall disorder in the structure since a decrease in the crystallinity degree was observed (Table 4.29).

Lastly, the position of the reflections is not affected by composition, indicating that a complete rejection of the TECE from the crystal lattice occurred, with the only exception of P(BCE50TECE50), which displayed a moderate increase of the width of the peak at  $15.1^\circ$  (results not shown).

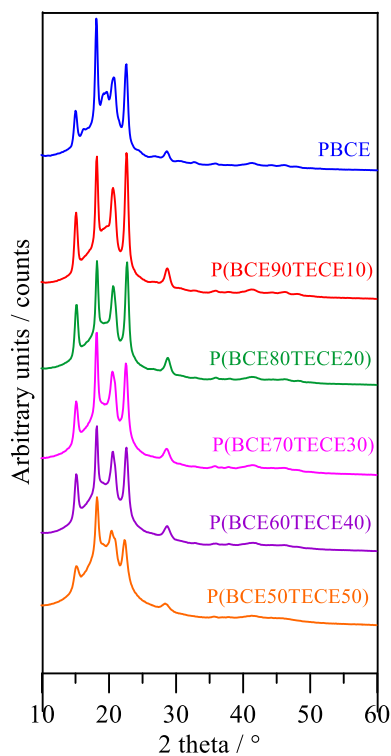


**Figure 4.29** X-ray diffraction patterns of PBCE and P(BCEmPTECEn) copolymers.

In order to confirm X-ray results, the applicability of the equations proposed in the literature to describe the dependence of  $T_m$  on composition (section 1.2.1) has been verified.

The melting temperatures of copolymers containing from 50 to 90 mol% of TECE units are plotted as a function of BCE molar fraction in Figure 4.30a, together with the melting points-composition data concerning P(BCEmBDGn) copolymers (section 4.6.1). As it can be seen,  $T_m$  decreased with the increasing of the co-unit content. Moreover, the  $T_m$  data of both the copolymeric systems examined appeared to lie on the same curve. As  $T_m$  depends exclusively on the molar fraction of BCE and not on the specific chemical characteristics of the co-units, the total exclusion of these last from the crystalline lattice of PBCE is confirmed, as well as the random nature of the copolymers investigated, with the only exception of P(BCE50TECE50) (purple square), as already observed in the XRD patterns.

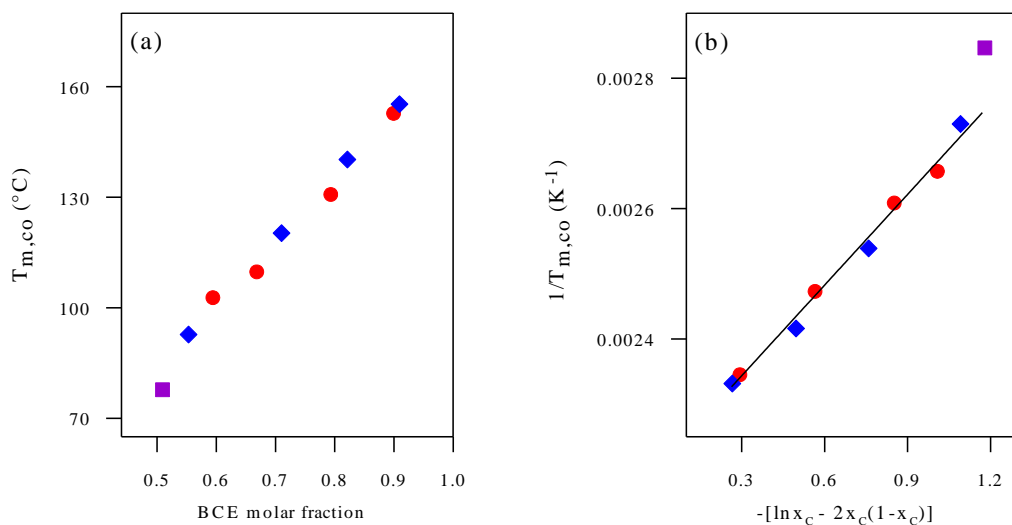


**Figure 4.30** (a)  $T_{m,co}$  – BCE molar fraction plot and (b)  $1/T_{m,co}$  – composition plot according to Baur's equation. Red circles: P(BCEmTECEn) copolymers, purple square: P(BCE50TECE50), blue rhombs: P(BCEmBDGn) copolymers.

On the basis of Baur's equation (section 1.2.1), which is applicable in the case of comonomer exclusion, the  $T_{m,co}$  were reciprocally plotted against  $-(\ln x_c - 2x_c(1-x_c))$  in Figure 4.30b and the equilibrium melting temperature and the heat of fusion for the completely crystalline PBCE were extrapolated. As it can be noted, the plot shows a good linearity and this result can be considered a further proof of the random nature of the copolymers investigated as well as of the exclusion of the co-units from the crystalline lattice of PBCE. The estimated  $T_m^\circ$  and  $\Delta H_m^\circ$  were found to be  $182^\circ\text{C}$  and  $82 \text{ J/g}$

respectively, in excellent agreement with the values reported in the literature (Celli *et al.*, 2011).

In order to study the influence of chemical structure on the glass transition of random copolymers, all the samples under investigation were subjected to rapid cooling (quenching) from the melt. The DSC curves after melt quenching are shown in Figure 4.82b: the calorimetric traces of PBCE and P(BCEmTECEn) copolymers containing up to 40 mol % of BDG units showed a melting endotherm phenomenon, indicating the partially crystalline nature of these samples.

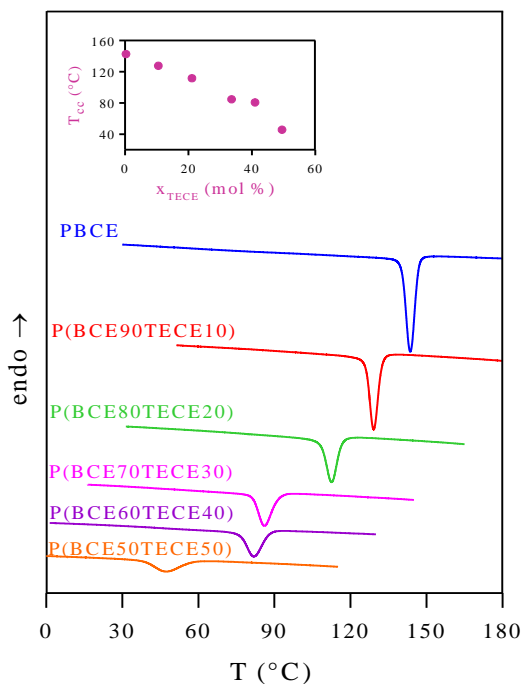
P(BCE50TECE50) displayed a glass transition followed by an exothermal “cold crystallization” peak and a melting endotherm at higher temperature. The enthalpy associated with the crystallization phenomenon is lower than that of the fusion endotherm, indicating that this sample cannot be frozen into a completely amorphous state by quenching. The DSC curve of such sample is therefore typical of partially crystalline polymer.

Therefore, in the range of composition investigated, the phase behaviour of P(BCEmTECEn) copolymers is not affected composition: as a matter of fact, after melt quenching, semicrystalline samples are obtained.

As can be seen in Figure 4.82b and from the data collected in Table 2.29, the glass transition temperature is influenced by the amount of TECE units in the chain. It can be observed that  $T_g$  values decreased as TECE unit content was increased: this result can be explained on the basis of the enhanced flexibility given by the triethylene glycol subunit, which is characterized by the presence of two additional ether-oxygen atoms and methylene groups with respect to the butandiol one. To confirm that in the copolymers the tendency of PBCE to crystallize decreases as the content of TECE co-units is increased, non-isothermal experiments were carried out, subjecting the samples to a controlled cooling rate from the melt. The exothermic crystallization peaks of the samples under investigation are shown in Figure 4.83.

As it can be observed, the temperature of the maximum of the exothermal crystallization peak regularly decreased as the TECE unit content was increased, as also shown in the inset of Figure 4.83. This fact indicates a decrement of the overall crystallization rate of PBCE, due to the presence of co-units which act as obstacles in the regular packing of polymer chains.

**Figure 4.83** DSC crystallization exotherms of PBCE and P(BCEmBDGn) random copolymers cooled from the melt at 5°C/min. In the inset:  $T_{cc}$  as a function of TECE unit content.



In order to investigate the relative hydrophilicity of PBCE and P(BCEmTECEn) films, water contact angle (WCA) measurements were performed. Table 4.29 reports the contact angle values for each polymer. Once more, data showed that the surface wettability is remarkably affected by the copolymer composition: as expected, hydrophilicity regularly increased with the increasing of the TECE mol%, due to the PEG-like portion.

#### 4.7.2 Mechanical characterization

The mechanical properties of PBCE and P(BCEmBDGn) copolymers were investigated subjecting the samples to stress-strain measurements. In Table 4.30 their corresponding mechanical data (elastic modulus,  $E$ , stress at break,  $\sigma_b$ , and deformation at break,  $\varepsilon_b$ ) are shown.

As it can be seen, the elastic modulus regularly decreased as TECE unit content was increased; on the contrary, the elongation to break, increased with the increasing of the molar amount of TECE co-unit.

Since all the investigated polymers display a soft amorphous phase ( $T_g$  values are in all cases well below room temperature), the observed trend can be ascribed to two effects: changes in copolymer composition and in crystallinity degree (Table 2.29). Moreover, it

is worth emphasizing that the copolymers containing more than 70 mol% of TECE are characterized by an elastomeric behaviour.

**Table 4.30** Mechanical characterization data of PBCE and P(BCEmTECEn) copolymers.

polymer	E (MPa)	$\sigma_b$ (MPa)	$\epsilon_b$ (%)
PBCE	459 ± 11	33 ± 1	31 ± 11
P(BCE90TECE10)	383 ± 17	26 ± 1	28 ± 2
P(BCE80TECE20)	264 ± 9	12 ± 1	236 ± 12
P(BCE70TECE30)	155 ± 5	13 ± 1	363 ± 34
P(BCE60TECE40)	136 ± 6	12 ± 2	412 ± 25
P(BCE50TECE50)	56 ± 2	7 ± 1	573 ± 41

### 4.7.3 Barrier properties

*GTR* values, together with  $t_L$ , *S* and *D* of the tested gases are reported in Table 4.31 and Table 4.32 for O<sub>2</sub> and CO<sub>2</sub> pure gas, respectively.

As it can be seen, highly crystalline samples showed low permeability to both gases, demonstrating a very high dependence of the permeability behavior on the crystalline/amorphous ratio. In addition, a relation between the selectivity ratio and the  $T_g$  can be observed: in copolymers the  $T_g$  decreased while the CO<sub>2</sub>/O<sub>2</sub> ratio (reported on Table 4.32) increased with the increasing of the TECE unit content. This result can be explained on the basis of the enhanced mobility of the polymeric chain, with consequently easier crossing of the CO<sub>2</sub> molecules through the polymeric film. CO<sub>2</sub> molecules move faster than O<sub>2</sub> ones: this is demonstrated by the fact that in all cases the O<sub>2</sub> *GTR* was found lower than the CO<sub>2</sub> *GTR* value.

The dependence of the *GRT* data on sample crystallinity is more evident for the CO<sub>2</sub> gas, whose values are in the range of 318-3740 cm<sup>3</sup> m<sup>-2</sup> d<sup>-1</sup> bar<sup>-1</sup>. On the contrary, as regards O<sub>2</sub>, *GTR* values are between 56 and 357 cm<sup>3</sup> m<sup>-2</sup> d<sup>-1</sup> bar<sup>-1</sup>, confirming that the CO<sub>2</sub> molecules move faster than the O<sub>2</sub> ones, despite the morphological structure of the sample.

The  $t_L$  value was found higher in the case of CO<sub>2</sub> for all polymers, meaning that the carbon dioxide molecules spent more time to distribute on the polymer film surface than

O<sub>2</sub> ones due to their faster and very chaotic motion. As a matter of fact, the oxygen molecules are characterized by a slowly and organized motion.

**Table 4.31**  $t_L$ ,  $GTR$ ,  $D$  and  $S$  for O<sub>2</sub> gas of P(BCEmTECEn) copolymers.

polymer	$t_L$ (s)	$GTR$ (cm <sup>3</sup> ·m <sup>-2</sup> ·d <sup>-1</sup> ·bar <sup>-1</sup> )	$S$ (cm <sup>3</sup> cm <sup>-2</sup> ·bar <sup>-1</sup> )	$D$ (cm <sup>2</sup> ·sec <sup>-1</sup> )
PBCE	1128.67 ± 1.70	56.20 ± 0.22	2.84·10 <sup>-2</sup> ± 4.19·10 <sup>-4</sup>	3.42·10 <sup>-8</sup> ± 2.49·10 <sup>-10</sup>
P(BCE90TECE10)	1721.68 ± 2.62	107.00 ± 0.82	8.27·10 <sup>-2</sup> ± 4.50·10 <sup>-4</sup>	2.33·10 <sup>-8</sup> ± 2.49·10 <sup>-10</sup>
P(BCE80TECE20)	304.67 ± 2.05	126.33 ± 1.25	1.58·10 <sup>-2</sup> ± 2.05·10 <sup>-4</sup>	1.56·10 <sup>-7</sup> ± 1.25·10 <sup>-9</sup>
(PBCE70TECE30)	371.67 ± 1.25	169.33 ± 1.25	2.59·10 <sup>-2</sup> ± 4.71·10 <sup>-5</sup>	1.28·10 <sup>-7</sup> ± 1.25·10 <sup>-9</sup>
P(BCE60TECE40)	n.a.	258.67 ± 0.47	n.a.	n.a.
P(BCE50TECE50)	187.00 ± 0.82	357.00 ± 0.82	2.61·10 <sup>-2</sup> ± 1.25·10 <sup>-4</sup>	2.81·10 <sup>-7</sup> ± 8.16·10 <sup>-10</sup>
PLA*	/	487.67 ± 2.52	/	/

\*from Siracusa *et al.*, 2012

As far as the diffusion coefficient is concerned, different trends have been observed. The PBCE and P(BCE90TECE10) showed a comparable value for O<sub>2</sub> and CO<sub>2</sub>, in both cases the lowest among the polymers under investigation. Not surprisingly, they displayed the highest  $t_L$ . It means that the diffusion process, i.e. the number of gas molecules crossing speed through the polymer wall, is low, resulting in a low permeability. With the increase of the TECE mol%, both diffusion coefficient and  $GTR$  values increased and accordingly  $t_L$  decreased. In addition, as it can be noted from Table 4.31 and Table 4.32, the CO<sub>2</sub>  $D$  value increased much faster than the O<sub>2</sub> one with the increase of TECE content, reaching in the case of P(BCE50TECE50) a value over 25 times higher for CO<sub>2</sub> with respect to O<sub>2</sub>.

**Table 4.32**  $t_L$ ,  $GTR$ ,  $D$ ,  $S$  for CO<sub>2</sub> gas and selectivity ratio CO<sub>2</sub>/O<sub>2</sub>.

polymer	$t_L$ (s)	$GTR /$ (cm <sup>3</sup> ·m <sup>-2</sup> ·d <sup>-1</sup> ·bar <sup>-1</sup> )	$S$ (cm <sup>3</sup> ·cm <sup>-2</sup> ·bar <sup>-1</sup> )	$D$ (cm <sup>2</sup> ·sec <sup>-1</sup> )	CO <sub>2</sub> /O <sub>2</sub>
PBCE	2939.00 ± 1.25	318.33 ± 2.05	4.30 <sup>-1</sup> ± 2.49·10 <sup>-3</sup>	1.31·10 <sup>-8</sup> ± 1.41·10 <sup>-10</sup>	5.66
P(BCE90TECE10)	3280.30 ± 1.86	761.33 ± 1.25	1.13 ± 1.25·10 <sup>-2</sup>	1.22·10 <sup>-8</sup> ± 1.65·10 <sup>-10</sup>	7.11
P(BCE80TECE20)	1884.33 ± 1.70	1009.30 ± 0.82	7.82·10 <sup>-1</sup> ± 8.16·10 <sup>-4</sup>	2.53·10 <sup>-8</sup> ± 1.41·10 <sup>-10</sup>	7.99
(PBCE70TECE30)	1430.33 ± 1.70	1600.67 ± 0.94	9.42·10 <sup>-1</sup> ± 8.16·10 <sup>-4</sup>	3.32·10 <sup>-8</sup> ± 4.71 10 <sup>-11</sup>	9.45
P(BCE60TECE40)	754.67 ± 1.25	2661.33 ± 1.25	1.44 ± 8.16·10 <sup>-3</sup>	2.07·10 <sup>-8</sup> ± 4.71·10 <sup>-11</sup>	10.29
P(BCE50TECE50)	726.33 ± 1.25	3740.33 ± 0.47	1.06 ± 8.16·10 <sup>-3</sup>	7.27·10 <sup>-8</sup> ± 7.07·10 <sup>-11</sup>	10.48
PLA*	/	1201.00 ± 1.73	/	/	2.46

\*from Siracusa *et al.*, 2012

As regards the solubility parameter, an opposite trend is displayed: CO<sub>2</sub> solubility was higher than that of O<sub>2</sub>. These results confirmed that, despite the molecule size, CO<sub>2</sub> was more soluble into the polymeric matrix, as well explained by the GTR data. For both the analysed gases, the solubility was not influenced by the chemical composition of the polymers, remaining practically constant in all the composition range.

Lastly, as far as the selectivity ratio between the two gases is concerned, it increased with the increasing of TECE mol% (Table 4.32). This result can be explained on the basis of the enhanced mobility of the polymeric chain ( $T_g$  decreased with the increasing of TECE content, Table 4.29), thus easier crossing of the CO<sub>2</sub> molecules through the polymer matrix.

If we compare the permeability data here obtained with those of P(BCEmBDGn) copolymers previously investigated (4.6.3), it can be noted that the GTR values increased for both gases of about 2-4 times in the case of P(BCEmTECEn) polyesters, which therefore possess inferior barrier properties to O<sub>2</sub> and CO<sub>2</sub>.

As previously reported (sections 4.6.1 and 4.7.2), both copolymeric systems display a soft amorphous phase ( $T_g$  values are in all cases well below room temperature).

However, the presence of the CE subunit in both the comonomeric units of P(BCEmTECEn) samples hampers the chain mobility because of the considerable steric hindrance of the aliphatic rings (see chemical structures in section 3.3.1).

In addition, P(BCEmBDGn) samples possess higher crystallinity degree with respect to P(BCEmTECEn) copolymers of comparable molar fraction of BCE.

Therefore, both the higher mobility and the higher crystallinity degree of P(BCEmBDGn) copolyesters contribute to the improved barrier properties.

Permeability results here presented are of particular relevance if we compare the permeability of the P(BCEmTECEn) copolymers with that of PLA films obtained under the same conditions (Siracusa *et al.*, 2012). As reported in Table 4.31 and Table 4.32, all the copolyesters under investigation showed lower permeability, and therefore improved barrier properties, to O<sub>2</sub> gas with respect to polylactide. As regards CO<sub>2</sub>, only copolymers with TECE mol% lower than 30% displayed better barrier properties compared to those of PLA. In conclusion, it has been possible to modulate the barrier properties of P(BCEmTECEn) copolymers, by simply varying their chemical composition.

#### 4.7.4 Soil burial and composting studies

The biodegradability of P(BCEmTECEn) copolymers was monitored by subjecting them to soil burial (section 3.13) and composting (section 3.14).

Aiming to utilize the polymers under study for environmental applications such as packaging or mulching films, both tests can well represent different fates of these plastics at the end of their useful life. Soil burial mimics the degradation of polymers when they are thrown away in the environment or left in landfills directly after use. On the other hand, composting is a particularly useful technique to biodegrade a polymeric material which has been contaminated by organic matter (section 1.4).

Biodegradation rate was investigated by weight loss measurements.

As regards soil burial, after 162 days of incubation highest weight loss value was of 2.5%, measured for P(BCE50TECE50), while PBCE remained practically undegraded. Degradation rate was found dependent on composition: the higher the TECE content, the higher the weight loss. Experiments are still running to evaluate the biodegradation of the polymers for longer exposure times.

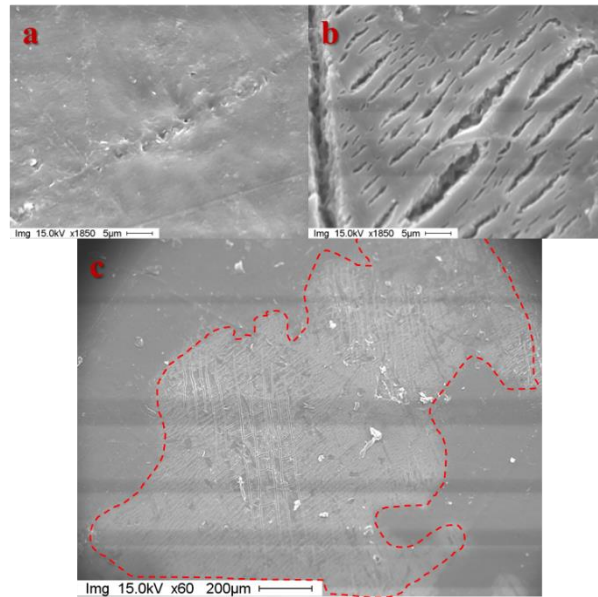


**Figure 4.84** SEM micrographs of PBCE and P(BCE50TECE50) after 162 days of soil burial: a) PBCE, 1850x magnification, b) P(BCE50TECE50), 1850x magnification, c) P(BCE50TECE50), 60x magnification. Red line is an eye-guide which delimits a damaged area of the sample.

The morphology of the polymer films was analysed by SEM. Micrographs of PBCE and P(BCE50TECE50) films taken after 162 days of soil burial are reported in Figure 8. As it can be seen, results are in perfect agreement with weight loss measurements: PBCE surface appeared smooth and homogeneous (Figure 4.84a), while in the copolymer large damaged areas (about 30 – 40% of the total surface, Figure 4.84c) appeared. As it can be seen, these latter are characterized by numerous cracks and channels (Figure 4.84b).

On the other hand, as far as the composting process is concerned, two different steps can be highlighted: the first occurred at higher temperature (about 70°C) and lasted for 14 days, while the second one, of about 23 days, was conducted at lower temperature (starting from 70°C down to about 40°C at the end of the process). During both steps, a constant air flux was supplied from the bottom of the composting biotunnel by forced ventilation. In this view, two samplings have been considered: one after 14 days and the second at the end of the biotransformation (day 37). In Figure 4.85 the retrieved samples are displayed.

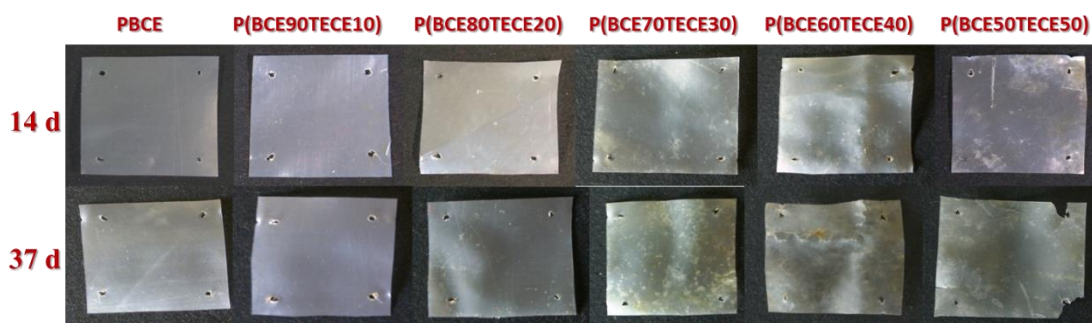


**Figure 4.85** PBCE and P(BCE<sub>m</sub>TECE<sub>n</sub>) copolymers after 14 and 37 days of incubation in compost.

After 14 days of incubation negligible weight losses were measured for all polymers, but the film surface underwent considerable changes. As it can be seen from the picture (Figure 4.85), PBCE and P(BCE90TECE10) surface remained smooth and homogeneous as prior to degradation (data not shown). With the increasing of TECE mol%, wider surface irregularities formed. In the P(BCE50TECE50) a crack is also visible. At the end of the composting process, PBCE and P(BCE90TECE10) did not undergo any degradation, while other copolymers degraded, even if to a different extent, reaching a maximum of about 3% in the case of P(BCE50TECE50). Accordingly, film surfaces irregularities of copolymers with a molar content of TECE higher than 30% notably increased with respect to the first sampling.

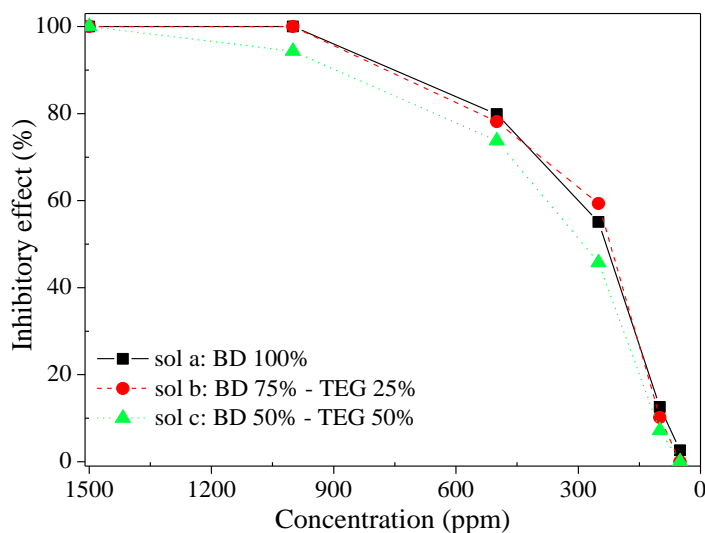
#### 4.7.5 Ecotoxicity assessment

The *Lepidium sativum* ecotoxicity test was performed for three stock solutions represented by a mixture of DMCED, BD and TEG monomers for a total concentration of 2000 ppm (section 3.18). The three monomers were used to simulate the impact of the possible products released during the biodegradation process of P(BCEmTECEn) copolymers on the *Lepidium sativum* growth.

The three solutions differed from each other in the mutual ratio between BD and TEG (**a**: 100% BD, **b**: 75% BD – 25% TEG, **c**: 50% BD – 50% TEG), while the DMCED amount was kept constant.

As reported in Figure 4.86, very similar inhibitory effect of the seed's germination was observed among all three solutions, with an average  $EC_{50}$  of 281 ppm.

**Figure 4.86**  
Inhibitory effect of monomers employed in the P(BCEmTECEn) synthesis on the *Lepidium sativum* growth.



The concentration of monomers used in the tests was much higher than that expectable in real environment. As reported in literature (Witt *et al.*, 2001), taking into account various assumptions, estimations of the concentration of substances in the soil originating from Ecoflex® composting assume a maximum value of about 130 ppm directly after the application of the compost.

As it can be seen from Figure 4.86, at the concentration of 130 ppm, an inhibitory effect ranging from 18% in the case of solution **c** to 22% for solution **a** is observable.

In summary, it can be stated that under practical conditions no toxic effect can be expected from composting P(BCEmTECEn) copolyesters.

#### 4.7.6 Electrospinning of *P(BCEmTECEn)* copolymers

PBCE, P(BCE80TECE20) and P(BCE70TECE30) have been subjected to electrospinning to obtain engineered 3-D scaffold for tissue engineering applications. Two different fiber morphologies have been considered: random and aligned fibres. Moreover, two different series of aligned fibres, characterized by different dimensions, micrometric and submicrometric, were considered.

**Table 4.33** PBCE, P(BCE80TECE20) and P(BCE70TECE30) fiber diameter distribution.

scaffold	fiber diameter distribution (nm)
PBCE, random fibers	500 ± 190 nm
PBCE, aligned submicrometric fibers	510 ± 210 nm
PBCE, aligned micrometric fibers	940 ± 230 nm
P(BCE80TECE20), random fibers	400 ± 140 nm
P(BCE80TECE20), aligned submicrometric fibers	430 ± 110 nm
P(BCE80TECE20), aligned micrometric fibers	830 ± 350 nm
P(BCE70TECE30), random fibers	580 ± 160 nm
P(BCE70TECE30), aligned submicrometric fibers	430 ± 120 nm
P(BCE70TECE30), aligned micrometric fibers	740 ± 270 nm

ES conditions parameters were optimized in order to obtain defect-free fibres by evaluating fiber morphology by SEM according to the procedure previously described (section 4.4.6).

In Figure 4.87 SEM micrographs of the scaffolds under investigation are reported. The scaffolds appeared to be highly porous mats with microscale interstitial pores. All polymers yielded fibers free of beads defects and possessing the diameters reported in Table 4.33.

ES fibres were characterized by TGA and DSC. As in the previous case (section 4.4.6), TGA did not reveal residual solvents in the ES fibres and confirmed that ES process did not contribute to decrease the thermal stability of the polymers. DSC analysis evidenced negligible differences in the thermal behavior between polymeric films and the corresponding electrospun fibers.

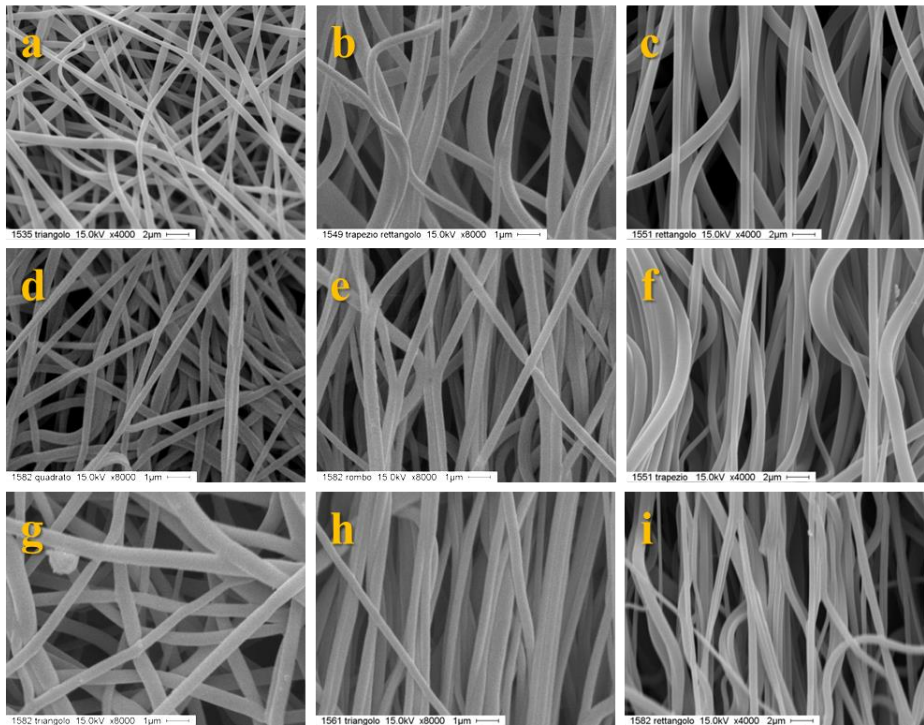


**Figure 4.87** SEM micrographs of: (a) PBCE random fibres, 4000x; (b) PBCE aligned submicrometric fibres, 4000x; (c) PBCE aligned micrometric fibres, 4000x; (d) P(BCE80TECE20) random fibres, 8000x; (e) P(BCE80TECE20) aligned submicrometric fibres, 8000x; (f) P(BCE80TECE20) aligned micrometric fibres, 4000x; ; (g) P(BCE70TECE30) random fibres, 8000x; (h) P(BCE70TECE30) aligned submicrometric fibres, 8000x; (i) P(BCE70TECE30) aligned micrometric fibres, 4000x.

#### 4.7.7 Hydrolytic degradation

Hydrolytic degradation experiments were performed under physiological conditions on the randomly oriented electrospun mats in order to evaluate hydrolysis rate. As a matter of fact, analogous results are expected for aligned fibres.

After 162 days of incubation weight losses were negligible for all the polymers under study. Therefore, as previously reported (section 4.4.7), the study of molecular weight

decrease is of crucial interest to monitor the first stages of hydrolytic degradation process when weight losses are not relevant.

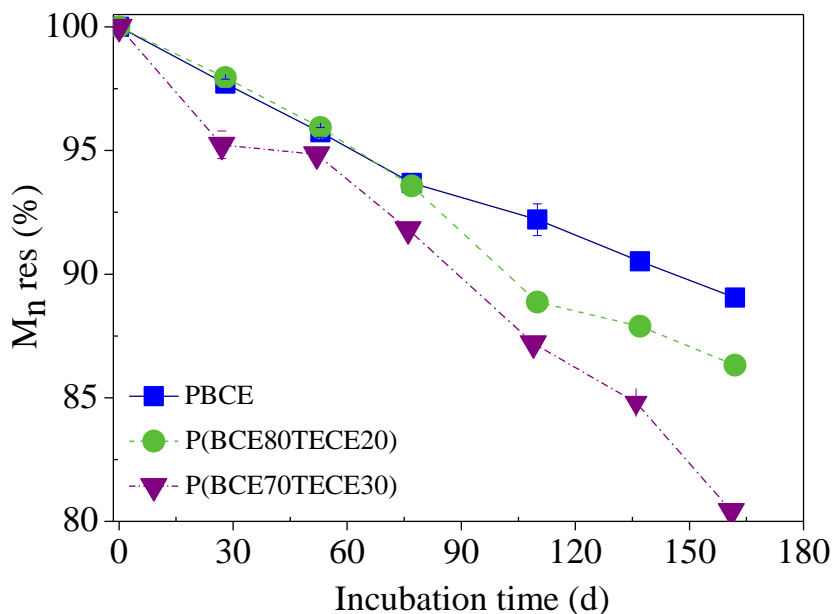


**Figure 4.88**

Residual molecular weight of PBCE, P(BCE70TECE30) and P(BCE80TECE20) scaffolds as a function of incubation time.

The percentage of residual number average molecular weight ( $M_n$  res%) is reported in Figure 4.88 as a function of incubation time. All samples underwent a decrease of  $M_n$  with time. The molecular weight decrement appeared more evident with the increase of the TECE mol%. As reported also in the previous sections (section 4.4.7 and section 4.5.6), this result can be explained on the basis of the reduced crystallinity degree and increased hydrophilicity of copolymers with respect to PBCE homopolymer.

#### 4.7.8 Biocompatibility

Biocompatibility studies have been conducted according to the procedure previously described (section 3.19.2).

The attachment and proliferation of C2C12 cultured on polymeric fiber scaffolds after 24 h and 7 days is shown in Figure 4.89.

Data were expressed as percentage of cell seeded  $\pm$  SD onto different scaffolds. The statistical differences between all different scaffolds were evaluated by independent two-sample t-test with significance level  $p = 0.05$ . \* $p < 0.05$  vs PBCE *a* micro; \*\* $p < 0.05$  vs P(BCE70TECE30) *a* micro; \*\*\* $p < 0.05$  vs P(BCE80TECE20) *a* micro; # $p < 0.05$  vs PBCE *a* submicro; ## $p < 0.05$  vs P(BCE70TECE30) *a* submicro; ###  $p < 0.05$  vs P(BCE80TECE20) *a* submicro.

The results showed that, independently of material types, the cells were able to adhere at 24h, and increased their proliferation after 7 days. However, some significant differences were observed among materials. After 24h, a decrease in cell adhesion was observed in all polymer scaffolds, with the exception of PBCE scaffold with aligned micrometric fibers, that showed the highest number of attached cells. After 7 days of culture, PBCE and P(BCE70TECE30) displayed a significant increment in cell proliferation, whereas P(BCE80TECE20) did not show a much greater increase in cell proliferation if compared to 24h cell incubation.

Moreover, the results demonstrated that the fiber size and alignment affected cell adhesion and cell viability. Cell density was found significantly greater on micrometric fibers of PBCE ( $*p < 0.05$ ) at both time of analysis. A higher cell viability was observed on scaffolds composed of micrometric rather than submicrometric fibers at 24h ( $**p < 0.05$ ) and 7 days on P(BCE70TECE30) and at 7 days on P(BCE80TECE20) ( $***p < 0.05$ ).

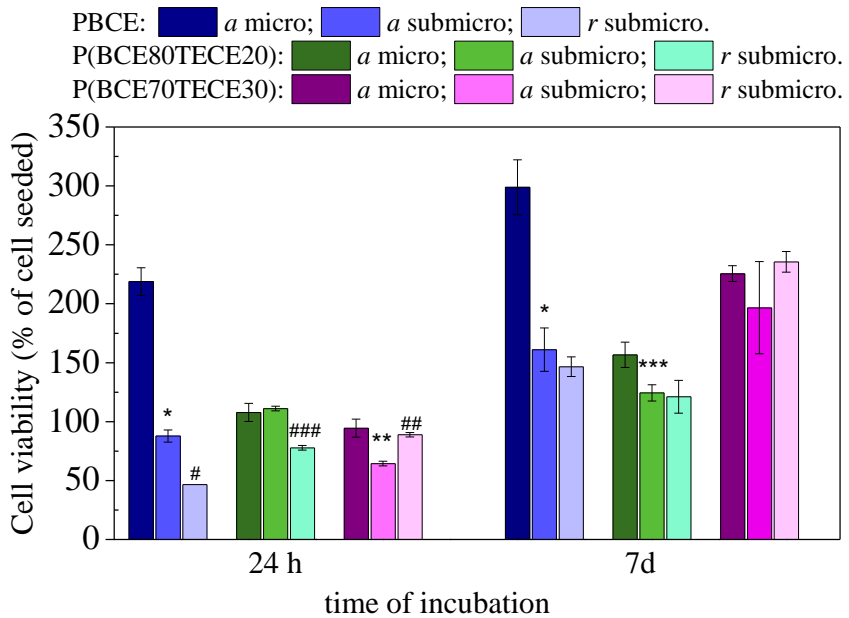


**Figure 4.89** Percentage of C2C12 viability on scaffolds with fibres differently sized and orientated after 24h and 7 days from cell seeding.

Coding: *a* = aligned fibers; *r* = random fibers; micro = micrometric fibers; submicro = submicrometric fibers.

By the observation of the effect of fibers alignment, it can be noted that after 24h it was obtained a significantly higher viability on aligned than on random submicrometric fibers of PBCE ( $\#p < 0.05$ ) and P(BCE80TECE20) ( $\###p < 0.05$ ), which was not observed after 7 days of culture. On the contrary, opposite results were found on submicrometric fibers of P(BCE70TECE30) scaffold ( $\##p < 0.05$ ).

In conclusion, from these data emerge that: a) the scaffolds with micrometric and aligned fibers may be more suitable for *in vitro* cell adhesion; b) the effect of fibers size as well as of alignment on cell proliferation are strictly correlated to the type of materials. Further studies will be performed to evaluate if fiber size and alignment can influence the differentiation of C2C12 cells.

5.

Conclusions

The present PhD Thesis confirmed that aliphatic polyesters are really promising for many applications requiring elimination or biorecycling after temporary use.

The versatility of etheroatom containing PBS and PBCE-based copolymers has been well proved: as a matter of fact these polymers can be exploited both for biomedical and ecological applications.

As far as the biomedical field is concerned, feasibility of 3D electrospun scaffolds has been investigated for different copolymeric systems; biocompatibility studies and controlled release of a model molecule showed good responses.

On the other hand, as regards ecological applications, barrier properties and ecotoxicological assessments have been conducted with outstanding results.

The ability of the synthesized polyesters to undergo both hydrolytic and enzymatic degradation has been demonstrated under physiological and environmental conditions.

Moreover, as we attempted to show, solid-state properties and biodegradation rate can be tailored acting on chemical composition or molecular architecture: the type and amount of comonomeric units and the sequence distribution deeply affect the material final properties owing, among all, to the hydrophobic/hydrophilic ratio and to the different ability of the polymer to crystallize.

The results presented in this work highlighted that both copolymerization and reactive blending represent a winning strategy to modulate the polymer performances according to the desired application: in particular, both approaches are simple, versatile and cost-effective synthetic strategies to obtain a wide range of materials.

Unfortunately, although many people consider biodegradable polymers very attractive and necessary for the co-existence of the human society with the nature, global production of biodegradable polymers is not as large as expected. The major reason for this seems to be not their poor properties as materials but their high production costs. Consumers do not want to pay much for conventional daily products even if they are urgently required to keep our environments both inside and outside the human body safe and clean. The largest challenge to polymer scientists is to manufacture at a reasonably low cost biodegradable polymers having well-balanced biodegradability and mechanical properties.

In this view, aliphatic polyesters, and above all those here presented, are industrially very appealing; as a matter of fact they are currently obtained from fossil carbon sources at an acceptable cost. In addition, their monomers can be also prepared from renewable resources (Bechthold *et al.*, 2008; Colonna *et al.*, 2011a; 2011b; Luckachan & Pillai,

2011); therefore, when monomers from renewable resources will become economically more convenient, these polymers may be mass produced and marketed simply varying the origin of raw materials, without the need to change technology and production plants.

Last but not least, we strongly believe that etheroatom containing PBS and PBCE-based copolymers can represent a valid alternative to PLA and its copolymers, both in biomedical and environmental fields.

Of course, the results obtained only represent a starting point towards a real application of the polyesters here presented; upscalability of the synthesis process has to be verified and deeper investigations on the polymers are necessary, especially for the biomedical field (e.g. *in vivo* tests).



## References

- Abe H., Doi Y.; *Int. J. Biol. Macromol.*, **1999**, 25: 185.
- Adomaviciute E., Rimvydas M.; *Fibers. Text. East. Eur.*, **2007**; 15: 64.
- Albertsson A.C., Varma I.K.; *Advances in Polymer Science*, Springer-Verlag Berlin Heidelberg, Vol. 157, **2002**.
- Albertsson A.C., Srivastava R.K.; *Advanced Drug Delivery Reviews*, **2008**, 60: 1077.
- Allegra G., Marchessault R.H., Bloembergen S.J.; *Polym. Sci., Part B: Polym. Phys.*, **1992**, 30: 809.
- Agarwal P., Srivastava P.; *Intern. J. Biom. Research*, **2011**, 3: 181.
- Arvanitoyannis I.S.; *Journal of Macromolecular Science - Reviews in Macromolecular Chemistry and Physics*, **1999**, C39(2): 205.
- Asfari M., Janjic D., Meda P., Li G., Halban P.A., Wollheim C.B.; *Endocrinology*, **1992**, 130: 167.
- Atala A.; *Rejuvenation Res*, **2004**, 7: 15.
- Babensee J.E., et al.; *Adv. Drug Del. Rev.*, **1998**, 33: 111.
- Bajpai A.K., Shukla S.K., Bhanu S., Kankane S.; *Progress in Polymer Science*, **2008**, 33: 1088.
- Barker M., Safford R.; *Home Grown Cereals Authority (HGCA)*, **2009**.
- Barnes D.K.A., Galgani F., Thompson R.C., Barlaz M.; *Phil. Trans. R. Soc. B*, **2009**, 364: 1985.
- Baur V.H.; *Makromol. Chem.*, **1966**, 98: 297.
- Bechthold I., Bretz K., Kabasci S., Kopitzky R., Springer A.; *Chem. Eng. Technol.*, **2008**, 31, 5: 647.
- Berti C., Binassi E., Celli A., Colonna M., Fiorini M., Marchese P., Marianucci E., Gazzano M., Di Credico F., Brunelle D.J.; *Journal of Polymer Science Part B: Polymer Physics*, **2008**, 46, 6: 619. (a)
- Berti C., Celli A., Marchese P., Marianucci E., Barbiroli G., Di Credico F.; *Macromolecular Chemistry and Physics*, **2008**, 209, 13: 1333. (b)
- Berti C., Celli A., Marchese P., Marianucci E., Sullalti S., Barbiroli G.; *Macromolecular Chemistry and Physics*, **2010**, 211, 14: 1559.
- BioIntelligence Service, **2011**.
- Bloembergen S., Marchessault R.H.; *Macromolecules*; **1986**, 19: 2685.
- Bonassar L.J., Vacanti C.A.; *J Cell Biochem Suppl*, **1998**, 30-31: 29.
- Boyer R.F.; *Rub. Chem. Tech.*, **1963**, 36: 1303.
- Briassoulis D.; *J Polym Environ*, **2004**, 12(2): 65.
- Briassoulis D., Dejean C.; *J. Polym. Environ.*, **2010**, 18: 384.
- Brown B.N., et al.; *Biomaterials*, **2009**, 30 (8): 1482.
- Burns A. E.; *J. Foot Ankle Surg.*, **1995**, 34: 276.
- Celli A., Marchese P., Sullalti S., Berti C., Barbiroli B.; *Macromolecular Chemistry and Physics*, **2011**, 212, 14: 1524.

- Clough G.H., Reed G.L.; *Proc Natl Agr Plastics Congr*, **1989**, 21: 42.
- Colonna M., Berti C., Binassi E., Celli A., Fiorini M., Marchese P., Messori M., Brunelle D.J.; *Polymer International*, **2011**, 60, 11: 1607. (a)
- Colonna M., Berti C., Fiorini M., Binassi E., Mazzacurati M., Vannini M. and Karanam S.; *Green Chem.*, **2011**, 13: 2543. (b)
- Conn J., Oyasu R., Welsh Beal M.; *J. M. Am. J. Surg.*, **1974**, 128: 19.
- Conn R.E., Kolstad J.J., Borzelleca J.F., Dixler D.S., Filer Jr. L.J., LaDu Jr. B.N., *et al.*; *Food and Chemical Toxicology*, **1995**, 33(4): 273.
- Cook W.J., Cameron J.A., Bell J.P., Huang S.J.; *J. Polym. Sci. Polym. Lett. Ed.*, **1981**, 19: 159.
- Coulembier O., Degee P., Hedrick J., Dubois P.; *Prog. Polym. Sci.*, **2006**, 31: 723.
- Darney P.D., Monroe S.E., Klaisle C.M., Alvarado A.; *Am. J. Obstet. Gynecol.*, **1989**, 160: 1292.
- Davidson G.W.R., Peppas N.A.; *J Control Release*, **1986**, 3: 243.
- Davis G., Song J. H.; *Ind. Crop. Prod.*, **2006**, 23: 147.
- Di Marzio E.A., Gibbs J.H.; *J. Polymer Sci.*, **1959**, 40: 121.
- Doi Y.; *Microbial Polyesters*, Wiley-VCH, Weinheim, Germany, **1990**.
- Duda A., Kowalski A., Penczek S., Uyama H., Kobayashi S.; *Macromolecules*, **2002**, 35: 4266.
- Duda A., Penczek S.; *Biopolymers*, Wiley-VCH, Weinheim, Germany, Vol. 3b, Ch. 12, **2002**.
- Eisenberg A.; *Physical properties of polymers*, ACS, Washington, **1984**.
- Feuilloley P.; *La Recherche*, **2004**, 374: 52.
- Feuilloley P., Cesar L., Benguigui L., Grohens Y., Pillin I., Bewa H., Lefaux S., Jamal M.; *J Polym Environ*, **2005**, 13: 349.
- Flory P.J.; *J. Am. Chem. Soc.*, **1936**, 58: 1877.
- Flory P.J.; *J. Am. Chem. Soc.*, **1939**, 61: 3334.
- Flory P.J.; *J. Am. Chem. Soc.*, **1942**, 64: 2205.
- Flory P.J.; *J. Chem. Phys.* **1947**, 15: 684.
- Flory P.J.; *Principles of Polymer Chemistry*, Ithaca, NY, **1953**.
- Folkman J., Long D.M.; *Surg. Res.*, **1964**, 4: 139.
- Fox G.; *Bull. Am. Phys. Soc.*, **1956**, 1: 123.
- Fritz J.; *Macromol Symp*, **2003**, 197: 397.
- Göpferich A.; *Biomaterials*, **1996**, 17: 103.
- Gordon M., Taylor J.S.; *J. Appl. Chem.*, **1952**, 2: 493.
- Greer L., Dole J.M.; *HoriTechnol*, **2003**, 13: 276.
- Grigat E., Koch R., Timmermann R.; *Polym. Degrad. Stab.*; **1998**; 59: 223.
- Grima S., Bellon-Maurel V., Feuilloley P., Silvestre F.; *Journal of Polymers and the Environment*, **2002**, 8, 4: 183.
- Grinsted R.A., Clark K., Koenig J.L.; *Macromolecules*, **1992**, 25: 1235.
- Gross R.A., Kalra B.; *Science*, **2002**, 297: 803.
- Gross R.A., Ganesh M., Lu W.; *Trends in Biotechnology*, **2010**, 28: 435.

- Gualandi C., Soccio M., Saino E., Focarete M.L., Lotti N., Munari A., Moroni L., Visai L.; *Soft Matter*, **2012**, 8: 5466.
- Guilbert S., Gontard N.; *Innovations in food packaging*, Elsevier, Amsterdam, **2005**.
- Gunatillake P., Mayadunne R., Adhikari R.; *Biotechnol. Annu. Rev.*, **2006**, 12: 301.
- Halek G.W.; *American Chemical Society*, **1988**, 16: 195.
- Helfland E., Lauritzen J.I.; *Macromolecules*, **1973**, 6: 631.
- Hexig B., Alata H., Asakawa N., Inoue Y.; *J Polym Sci Part B: Polym Phys*, **2005**, 43: 368.
- Hiskakis M., Briassoulis D.; *World Congress of Agricultural Engineering*, Bonn, Germany, **2006**.
- Hoffman A.S.; *Journal of Controlled Release*, **2008**, 132: 153.
- Hollister S.J., *Biofabrication*, **2009**, 1: 012001.
- Hopewell J., Dvorak R., Kosior E.; *Phil. Trans. R. Soc. B*, **2009**, 364: 2115.
- Hutmacher D.W., et al.; *Biomaterials.*, **2000**, 21: 2529.
- Ikada Y., Tsuji H.; *Macromol. Rapid Commun.*, **2000**, 21: 117.
- Ichikawa Y., Kondo H., Igarashi Y., Noguchi K., Okuyama K., Washiyama J.; *Polymer*, **2000**, 41:4719; *corrigendum Polymer*, **2001**, 42: 847.
- Ingold C.K.; *Structure and Mechanisms in Organic Chemistry*, Ithaca, N.Y.: Cornell University Press., **1969**.
- Jalil R., Nixon J.R.; *J. Microencapsulation*, **1990**, 7- 3: 297.
- Jeong J.C., Lee J., Cho K.; *J. Controlled Release*, **2003**, 92: 249.
- Jérôme C., Lecomte P.; *Advanced Drug Delivery Reviews*, **2008**, 60: 1056.
- Jiang H.L., Fang D.F., Hsiao B.J., Chu B.J., Chen W.L.; *J. Biomat. Sci.*, **2004**; 15: 279.
- Johnson H.; *Proc Natl Agr Plastics Congr*, **1989**, 21: 1.
- Karavelidis V., Karavas E., Papadimitriou S., Bikiaris D.; *Int. J. Nanomed.*, **2011**, 6: 3021.
- Kasirajan S., Ngouajio M.; *Agron. Sustain. Dev.*, **2012**, 32: 501.
- Kats A.R., Turner R.; *J. Surg. Gynecol. Obstet.*, **1970**, 131: 701.
- Kilian H.G.; *Kolloid-Z. Polym. Z.*, **1965**, 202: 97.
- Kyrikou I., Briassoulis D.; *J Polym Environ*, **2007**, 15(2): 125.
- Ko H.C., et al.; *Eur Cell Mater.*, **2007**, 14: 1.
- Korshak V.V., Vinogradova S.V.; *Polyesters* Pergamon Press: Oxford, Ch. 6, **1965**.
- Kostewicz S.R., Stall W.M.; *Proc Natl Agr Plastics Congr*, **1989**, 21: 17.
- Kwon I.K., Kidoaki S., Matsuda T.; *Biomaterials* **2005**, 26: 3929.
- Lamont W.J., Marr C.W.; *Proc Natl Agr Plastics Congr*, **1990**, 22: 33.
- Langer R.; *Acc Chem Res*, **2000**, 33: 94.
- Laeger T., Metges C.C., Kuhla B.; *Appetite* **2010**, 54: 450.
- Lee D.S., Yam K.L., Piergiovanni L.; *Food Packaging Science and Tecnology*, CRC Taylor & Francis Group, LLC, **2008**.
- Legras R., Dekoninck J.M., Vanzielegem A., Mercier J.P., Nield E.; *Polymer*; **1986**, 27: 109.
- Lensen D., Breukelen K.V., Vriezema D.M., Hest J.C.M.V.; *Macromol. Biosci.*, **2010**, 10: 475.
- Li D., Xia Y.N.; *Advanced Materials*, **2004**; 16: 1151.

- Li S.; *Scaffolding in Tissue Engineering*, Taylor & Francis Group, Boca Raton, Ch. 23, **2006**.
- Liu Z.; *Innovations in food packaging*, Elsevier, Amsterdam, pp 318, **2005**.
- Lucas N., Bienaime C., Belloy C., Queneudec M., Silvestre F., Nava-Saucedo J.E.; *Chemosphere*, **2008**, 73: 429.
- Luckachan G.E., Pillai C.K.S.; *J Polym Environ*, **2011**, 19: 637.
- Lunt J.; *Polym. Degrad. Stab.*, **1998**, 59: 145.
- Lloyd A.W.; *Med. Device Technol.*, **2002**, 13: 18.
- Lyons F., Al-Munajjeda A.A., Kierana S.M., Tonere M.E., Murphya C.M., Duffya G.P., O'Brien F. J.; *Biomaterials*, **2010**, 31(35): 9232.
- Mandelkern L.; *Crystallization of Polymers*, McGraw-Hill, New York, **1954**.
- Mandelkern L., *Comprehensive polymer science*, Pergamon Press, Oxford, Vol. 2, Ch. 11, **1989**.
- Mark H., Whitby G. S.; *Interscience*, New York, **1940**.
- Martín-Closas L., Soler J., Pelacho A.M.; *Biodegradable materials and natural fiber composites*, KTBL Darmstadt Schrift, **2003**, 414: 78.
- Martin I., Wendt D., Heberer M.; *Trends Biotechnol*, **2004**, 22: 80.
- Maurus P.B., Kaeding C.C.; *Oper. Techn. Sports Med.*, **2004**, 12: 158.
- Middleton J.C., Tipton A.; *J. Biomaterials*, **2000**, 21: 2335.
- Mochizuki M., Hirami M.; *Polym. Adv. Technol.*, **1997**, 8: 203.
- Mrkic S., Galic K., Ivankovic M., Hamin S., Cikovic N.; *J Appl Polym Sci*, **2006**, 99: 1590.
- Mukai K., Yamada K., Doi Y.; *Int. J. Biol. Macromol.*, **1993**, 15: 361.
- Müller A.J., Balsamo V., Arnal M.L.; *Adv. Polym. Sci.* **2005**, 190: 1
- Müller A.J., Balsamo V., Arnal M.L.; *Lect. Notes Phys.*, **2007**, 714: 229
- Murphy C.M., Haugh M.G., O'Brien F.G.; *Biomaterials*, **2010**, 31-3: 461. (a)
- Murphy C.M., O'Brien F.J.; *Cell Adh Migr*, **2010**, 4: 377. (b)
- Nair L.S., Laurencin C.T.; *Prog. Polym. Sci.*, **2007**, 32: 762.
- Nayak P.L.; *Rev Macromol Chem Phys*, **1999**, 39: 481.
- Noh H.K., Lee S.W., Kim J.M., Oh J.E., Kim K.H., Chung C.P., Choi S.C., Park W.H., Min B.M.; *Biomaterials*, **2006**, 27: 3934.
- O'Brien F.J., et al.; *Biomaterials*, **2005**, 26: 433.
- O'Brien F.J.; *Materials Today*, **2011**, 14: 1.
- Okada M.; *Prog. Polym. Sci.*, **2002**, 27: 87.
- Papageorgiou G.Z., Bikiaris D.N.; *Biomacromolecules*, **2007**, 8: 2437.
- Patlolla A., Collins G., Arinzech T.L.; *Acta Biomater*, **2010**, 6: 90.
- Phelps E.A., et al.; *Regen Med*, **2009**, 4: 65.
- Plastics Europe: The Facts, **2012**.
- Potts J.E., Clendinning R.A., Ackart W.B., Niegish W.D.; *Polym. Sci. Technol.*, **1973**, 3: 61.
- Rabinovitch E.; *Trans. Faraday Soc.*, **1937**, 33: 1225.
- Reed T. M.; *J. Foot Ankle Surg*, **1999**, 38: 14.

- Ren M., Song J., Song C., Zhang H., Sun X., Chen Q., Zhang H., Mo Z.; *J. Polym. Sci.*, **2005**, 43: 3231.
- Reneker D.H., Chun I.; *Nanotechnology*, **1996**; 7: 216.
- Reneker D.H., Yarin A.L., Fong H., Koombhongse S.; *J. Appl. Phys.*, **2000**, 87: 4531.
- Rizzarelli P., Puglisi C., Montaudo G.; *Polym. Degrad. Stab.*, **2004**, 85: 855.
- Rizzarelli P., Impallomeni G.; *Biomacromolecules*, **2004**, 5: 433.
- Robertson G.L.; *Food Packaging: Principles and Practice*, CRC, Taylor & Francis Group LLC, **1993**.
- Saino E., Focarete M.L., Gualandi C., Emanuele E., Cornaglia A.I., Imbriani M., Visai L.; *Biomacromolecules*, **2011**, 12: 1900.
- Sanchez I.C., Eby R.K.; *Journal of research of the Notional Bureau of Standards - A. Physics and Chemistry*, **1973**, Vol. 77A, 3: 353.
- Sanchez I.C., Eby, R.K.; *Macromolecules*, **1975**, 8: 638.
- Sanders D.C., Prince C.A., David P.P.; *Proc Natl Agr Plastics Congr*, **1989**, 21: 11.
- Schwarz K., Epple M.; *Macromol. Chem. Phys.*, **1999**, 200: 2221.
- Scott G., Gilead D.; *Degradable polymers: Principles and applications*, Chapman & Hall, Ch. 13, **1995**.
- Scott G.; *Polymer Degradation and Stability*, **2000**; 68: 1.
- Shah A.A., Hasan F., Hameed A., Ahmed S.; *Biotechnol Adv*, **2008**, 26(3): 246.
- Simha R., Boyer R. F.; *J. Chem. Phys.*, **1962**, 37: 1003.
- Siracusa V., Rocculi P., Romani S., Dalla Rosa M.; *Trends in Food Science & Technology*, **2008**; 19: 634.
- Siracusa V., Blanco I., Romani S., Tylewicz U., Rocculi P., Dalla Rosa M.; *Journal of Applied Polymer Science*, **2012**, Vol. 125, E390.
- Soccio M., Lotti N., Finelli L., Gazzano M., Munari A.; *European Polymer Journal*, **2008**, 44: 1722.
- Soccio M., Lotti N., Finelli L., Munari A.; *Eur. Polym. J.*, **2009**, 45: 171.
- Soccio M., Lotti N., Gazzano M., Govoni M., Giordano E., Munari A.; *Reactive & Functional Polymers*, **2012**, 72: 856.
- Song J.H., Murphy R.J., Narayan R., Davies G.B.H.; *Phil. Trans. R. Soc. B*, **2009**, 364: 2127.
- Spyros A., Kimmich R., Briese B.H., Jendrosseck D.; *Macromolecules*, **1997**, 30: 8218.
- Staab H.A.; *Chem. Ber.*, **1957**, 90: 1326.
- Steinbüchel A.; *Biomaterials: Novel Materials from Biological Sources*, Stockton, New York, **1991**, 123–124.
- Stevens M.M., George J.H.; *Science*, **2005**, 310: 1135.
- Shukla S., Bajpai A.K., Bajpai J.; *Macromol Res*, **2003**, 11: 273.
- Sun Y.M., Wang C.S.; *European Polymer Journal*, **1999**, 35: 1087.
- Suuronen R., Pohjonen T., Hietanen J., Lindqvist C.; *J. Oral Maxillofac. Surg.*, **1998**, 56: 604.
- Taylor G.I.; *roc.R.Soc.Lond.*, **1969**, 313: 453.
- Theron S.A., Zussman E., Yarin A.L.; *Polymer*, **2004**, 45: 2017.

- Timmins M.R., Gilmore D.F., Lotti N., Scandola M., Fuller R.C., Lenz R.W.; *J. Environ. Polym. Degrad.*, **1997**, 5: 1.
- Tokiwa Y., Ando T., Suzuki T.; *J. Ferment. Technol.*, **1976**, 54: 603.
- Tokiwa Y., Suzuki T.; *Nature*, **1977**, 270: 76.
- Thompson R.C., Moore C.J., vomSaal F.S., Swan S.H.; *Phil. Trans. R. Soc. B*, **2009**, 364: 2153.
- Tserki V., Matzinos P., Pavlidou E., Vachliotis D., Panayiotou C.; *Polymer Degradation and Stability*, **2006**, 91: 367.
- Tudorachi C.N., Cascaval M., Rusu M., Pruteanu M.; *Polymer Test*, **2000**, 19(7): 785.
- Ueda H., Tabata Y.; *Adv. Drug Deliv. Rev.*, **2003**, 55: 501.
- Ulery B.D., Lakshimi S.N., Cato T.L.; *J. Polym. Sci. Part B: Polymer Physics*, **2011**, 49: 832.
- Van Krevelen D.W.; *Properties of polymers*, Elsevier: Amsterdam, Netherlands, p. 898, **1997**.
- Van Natta F.J., Hill J.W., Carothers W.H.; *J. Am. Chem. Soc.*, **1934**, 57: 455.
- Varma I.K., Albertsson A.C., Rajkhowa R., Srivastava R.K.; *Prog. Polym. Sci.*, **2005**, 30: 949.
- Vert M.; *Biomacromolecules*, **2005**, 6: 538.
- Vert M.; *J Mater Sci: Mater Med*, **2009**, 20: 437.
- Von Burkersroda F., Schedl L., Göpferich A.; *Biomaterials*, **2002**, 23: 4221.
- Wang X.L., Yang K.K., Wang Y.Z.; *J Macromol Sci Pol Rev*, **2003**, 43: 385.
- Walter T., Augusta J., Müller R.J., Widdecke H., Klein J.; *Enzyme Microb. Technol.*; **1995**, 17: 218.
- Webster T.J., Schadler L.S., Siegel R.W., Bizios R.; *Tissue Engineering* **2001**, 7: 291.
- Wendling J., Suter U. W.; *Macromolecules*, **1998**, 31: 2509.
- Windle A.H., Golombok C., Donald A.M., Mitchell G.R.; *Faraday Discuss., Chem. Soc.*, **1985**, 79: 55.
- Witt U., Yamamoto M., Seeliger U., Muller R.J., Warzelhan V.; *Angew. Chem. Int. Ed.*, **1999**, 38: 1438.
- Woodings C.; *NF New Fibres*, **2001** ([www.technica.net/NF](http://www.technica.net/NF)).
- Yamamoto M., Witt U., Skupin G., Beimborn D., Muller R.J.; *Biopolymers Polyesters*, A. Steinbüchel, Y. Doi, Eds., Wiley-VCH, Weinheim, Germany, Vol. 4, Ch. 3, **2002**.
- Yang J., Tian W., Li Q., Cao A.; *Biomacromolecules*, **2004**, 5: 2258.
- Yannas I.V., *et al.*; *PNAS*, **1989**, 86: 933.
- Yarin A.L., Koombhongse S., Reneker D.H.; *J. Appl. Phys.*, **2001**, 89: 3018.
- Yasuniwa M., Tsubakihara S., Satou T., Iura K.J.; *J Polym Sci Polym Phys*, **2002**, 40: 2411.
- Yoo E., Im S.S.; *J Polym Sci Polym Phys*, **1999**, 37: 1357.
- Yoshie N., Inoue, Y., You H. Y., Okui N.; *Polymer*, **1994**, 35: 1931.
- Zhijiang C., Zhihong W.; *J. Mater. Sci.*, **2007**, 42: 5886.
- Zielhuis S.W., Nijssen J.F.W., Seppenwoolde J.H., Bakker C.J.G., Krijger G.C., Dullens H.F.J., Zonnenberg B.A., Rijk P.P.V., Hennink W.E., Schip A.D.V.; *Biomaterials*, **2007**, 28: 4591.
- Zimmermann H.; *Degradation and stabilization of polyesters*, Applied Science Publishers, New York, Ch. 3, **1984**.

## Publications

- 1) M. Soccio, A. Negroni, M. Gigli, G. Zanaroli, N. Lotti, A. Munari “Enzymatic degradation of novel etheroatom-containing copolyesters based on poly(butylene succinate)” IBS 2010. *Journal of Biotechnology* **150**, 201 (2010).
- 2) N. Lotti , M. Soccio, M. Gigli, M. Gazzano, L. Finelli, A. Munari “Poly(butylene/diethylene succinate) block copolymers: correlation between block length and miscibility and cristallization capacity” IBS 2010. *Journal of Biotechnology* **150**, 198-199 (2010).
- 3) M. Gigli, N. Lotti, M. Gazzano, L. Finelli, A. Munari, “Macromolecular design of novel sulphur-containing copolyesters with promising mechanical properties for soft tissue engineering”. *J. Appl Polym Sci* **126**, 686-696 (2012).
- 4) M. Gigli, N. Lotti, M. Gazzano, L. Finelli, A. Munari, “Novel eco-friendly random copolyesters of poly(butylene succinate) containing ether-linkages”. *React Funct Polym* **72**, 303-310 (2012).
- 5) M. Soccio, N. Lotti, M. Gigli, L. Finelli, M. Gazzano and A. Munari “Reactive blending of poly(butylene succinate) and poly(triethylene succinate): characterization of the copolymers obtained”. *Polym Int* **61**, 1163-1169 (2012).
- 6) M. Gigli, A. Negroni, M. Soccio, G. Zanaroli, N. Lotti, F. Fava and A. Munari, “Influence of chemical and architectural modifications on the enzymatic hydrolysis of poly(butylene succinate)”. *Green Chemistry* **14**, 2885-2893 (2012).
- 7) M. Gigli, N. Lotti, A. Munari, A. Negroni, G. Zanaroli, F. Fava. “Poly(Butylene/Triethylene Succinate): Effect Of Block Length On Mechanical Properties And Biodegradability”. *Environmental Engineering and Management Journal* **11**, 3, Supplement, S89-S98 (2012).

8) M. Gigli, N. Lotti, M. Gazzano, L. Finelli, A. Munari “Synthesis and characterization of novel Poly(butylene succinate)-based Copolyesters designed as potential candidates for soft tissue engineering”. *Polym Eng Sci* **53**, 491-501 (2013).

9) M. Gigli, A Negroni, M. Soccio, G Zanaroli, N. Lotti, F. Fava A. Munari, “Enzymatic hydrolysis studies on novel eco-friendly aliphatic thiocopolyesters”. *Polym Degr Stab* DOI: 10.1016/j.polymdegradstab.2013.02.019.

10) M. Gigli, A Negroni, G Zanaroli, N. Lotti, F. Fava A. Munari, “Environmentally friendly PBS-based copolyesters containing PEG-like subunit: effect of block length on solid-state properties and enzymatic degradation”. Accepted on *React Funct Polym*.

## **Scientific contributions to national and international congresses**

1) M. Gigli, M. Soccio, N. Lotti, A. Munari, G. Zanaroli, A. Negroni, F. Fava “Biodegradability Of Novel Copolyesters Of Poly(Butylene Succinate) Containing Sulphur Atoms.” In: Proceedings of EUPOC 2011: Biobased Polymers and related biomaterials. Gargnano (Italy), May, 29<sup>th</sup> – June, 3<sup>rd</sup>, 2011.

2) M. Gigli, C. Gualandi, M. Soccio, M.L. Focarete, N. Lotti, A. Munari, L. Visai “Poly(Butylene/Triethylene Succinate) Multiblock Copolyesters From Reactive Blending For Soft Tissue Engineering”. In: Proceedings Of Eupoc 2011: Biobased Polymers And Related Biomaterials. Gargnano (Italy), May, 29<sup>th</sup> – June, 3<sup>rd</sup>, 2011.

3) M. Gigli, M. Soccio, N. Lotti, A. Munari, A Negroni, G Zanaroli, F. Fava. “Enzymatic degradation of novel ethero-oxygen atom-containing copolyesters based on Poly(butylene succinate)”. In: EPF2011, XII GEP Congress. Granada (Spain), June, 26<sup>th</sup> – July, 1<sup>st</sup>, 2011.

4) A. Munari, M. Gigli, N. Lotti, M. Gazzano, E. Giordano, M. Govoni. “Poly(Butylene/Thiodiethylene Succinate) Multiblock Copolyesters From Reactive Blending For Soft Tissue Engineering”. VIII Congresso dell'Associazione Italiana di Chimica per l'Ingegneria, Catania (Italy), 16<sup>th</sup> – 19<sup>th</sup> September, 2012.

5) M. Gigli, N. Lotti, A. Munari, A. Negroni, G. Zanaroli, F. Fava. “Novel Eco-Friendly Multiblock Copolymers Poly(Butylene/Triethylene Succinate): Effect Of Block Length On Mechanical Properties And Biodegradability”. VIII Congresso dell'Associazione Italiana di Chimica per l'Ingegneria, Catania (Italy), 16<sup>th</sup> – 19<sup>th</sup> September, 2012.

### **Participation to Congresses**

- 1) 11th European Symposium on Controlled Drug Delivery, Egmond Aan Zee (Netherland), April, 7<sup>th</sup> - 9<sup>th</sup>, 2010.
- 2) IBS2010, “Biotechnology for the Sustainability of Human Society”, Rimini (Italy), September, 14<sup>th</sup> -18<sup>th</sup>, 2010.
- 3) EUPOC 2011: Biobased Polymers and related biomaterials. Gargnano (Italy), May, 29<sup>th</sup> – June, 3<sup>rd</sup>, 2011
- 4) EPF2011, XII GEP Congress. Granada (Spain), June, 26<sup>th</sup> – July, 1<sup>st</sup>, 2011.
- 5) EMB2012, “In the frame of the knowledge-based Bio & Green Economy”, Bologna (Italy), April, 10<sup>th</sup> – 12<sup>th</sup>, 2012.
- 6) XXXIII Convegno-Scuola “Mario Farina” – “Sintesi di materiali polimerici”, Gargnano (Italy), May, 21<sup>th</sup> – 25<sup>th</sup>, 2012.

### **Experiences abroad**

Advanced Materials and System Research Center, BASF, Ludwigshafen (Germany), September, 2011 – February, 2012).

## Acknowledgments

Finally, here I am to the last paragraph of my Thesis which is, in my opinion, by far the most difficult.

Besides thanks, I surely have to apologize to everybody...I made many mistakes, but you know, I'm too impulsive, and sometimes, as my dad always says, I move before thinking...Sorry!

I think it's really difficult to thank people using words...everybody knows how much he/her contributed to the realization of this important step of my life...my thank is therefore the Thesis itself, I realized with your constant support.

Anyway, I still want to spend a few words, starting from the beginning...

Of course first come dad, mum, Ugo Andrea, Paolo and Davide (which I consider part of the family), thank you for supporting me from any point of view...an additional thanks goes to the "editor" Ugo Andrea, for creating the gorgeous layout of the Thesis and for helping me with the paging.

Then, all the people who have been part of my everyday life during these wonderful three years:

...Prof. Munari for giving me the chance to start a PhD in his group...

...Prof. Fava for getting me in touch with prof. Munari, and for giving me the opportunity to spend six months in BASF...

...Paola and all the professors and researchers from the Polymer Group...

..."zia" Michi, my first teacher and confident...

...the “colleagues”, which I prefer to call friends: Simone, Ciccio, Letizia, Tommy and Alessandro who already left the Department and Grazia, Micaela, Andrea and Fra “Di Credico” who are still here...

...all the students: Gabriele, Giulia, Veronica, Ernesto, Giulia, Carlotta, Francesco, Asja and Maria...great job!

...both the new PhD students: Laura and Martina, for helping me in the last crazy months...

...the DICAM staff, above all Vilma, in my opinion the most helpful person I’ve ever met.

Thanks to prof. Agathos and prof. Verney because they kindly accepted to review my Thesis and to prof. Kowalczuk who agreed to be part of the judging commission.

How not to mention also all the people I met in BASF during my fruitful permanence in Germany, starting from Kian and Robert for their kindness and continuous scientific exchange of views, and ending to Manuela, Martin, Petra and my roommates Simon and Malte, who made me feel at home and tried, unfortunately without success, to teach me some German words!

A special thanks goes to Nadia...there are no other words to thank you, but saying that you have been not only a perfect tutor, but also a second mum...

Finally, I’ll never end to thank all of you because, through this experience, I could meet Nena, who makes every day sweeter ...